

MAX-PLANCK-INSTITUT FÜR POLYMERFORSCHUNG IN MAINZ

Reversible Stimuli Responsive Radicals and Their EPR Spectroscopic Characterization

Dissertation Zur Erlangung des Grades

“Doktor der Naturwissenschaften”

am Fachbereich Chemie, Pharmazie und Geowissenschaften

der Johannes Gutenberg-Universität in Mainz

Di Wang

Geboren in Anhui Province, China

Mainz im Jahr 2018

Dekan: Prof. Dr.

1. Berichterstatter: Prof. Dr.

2. Berichterstatter: Prof. Dr.

Tag der mündlichen Prüfung:

Die vorliegende Arbeit wurde in der Zeit von Okt 2013 bis Apr 2018 im Max-Planck-Institut für Polymerforschung in Mainz unter der Betreuung von Prof. Dr. Martin Baumgarten durchgeführt.

Ich danke Prof. Dr. Martin Baumgarten für seine wissenschaftliche und persönliche Unterstützung sowie für seine ständige Diskussionsbereitschaft.

For My Parents

*“Science cannot solve the ultimate mystery of nature.
And that is because, in the last analysis,
we ourselves are a part of the mystery that we are trying to solve.”*

— Max Planck



Table of Contents

Index of Symbols and Abbreviations.....	IV
1 Introduction	1
1.1 General Background	1
1.2 Overview of Organic radicals	2
1.2.1 Carbon Based Radicals	3
1.2.2 Nitroxide Radicals (Mono-, Bi- and Multi-radicals).....	5
1.2.3 Nitrogen Based Radicals (Radical Ions)	6
1.3 Spin and Magnetism	7
1.4 Stimuli Responsive Radical (SRR) Systems.....	11
1.4.1 Temperature Stimuli Responsive Radicals	11
1.4.2 Redox Stimuli Responsive Radicals.....	13
1.4.3 Photo Stimuli Responsive Radicals	15
1.4.4 Pressure Stimuli Responsive Spin Molecules	18
1.5 Applications of Magnetic Materials and SRR Systems	19
1.6 Motivation and Objectives.....	22
1.7 References.....	26
2 Instrument, Measurement and Spectroscopy of EPR	33
2.1 Introduction.....	33
2.2 Discription of EPR Instrument.....	34
2.3 EPR Measurement and Interpretation of EPR Spectroscopy	35
2.3.1 Performance of Unpaired Electron or Spin in Magnetic Field (Zeeman Effect).....	35
2.3.2 Principle of Hyperfine Splitting.....	38
2.3.3 Analysis of the EPR Signal Splitting Pattern.....	39
2.3.4 Spin Systems with More Than One Unpaired Electron ($S \geq 1$) and Zero-Field Splitting (zfs)	41
2.3.5 The Signals of EPR Measurements Influenced by External Factors	42
2.4 Application of Quantitative EPR	43
2.5 Expectation of EPR.....	43
2.6 EPR-Related Books and References	44
3 Temperature Stimuli Responsive Spin Coupling Interactions of Nitronyl Nitroxide Diradicals	46
3.1 Introduction.....	47
3.2 Synthesis of Temperature Stimuli Responsive Radicals.....	48

3.3.	Optical Properties.....	50
3.4.	EPR Measurements and Analysis	52
3.4.1.	<i>EPR spectra of GBN1 and GBN2 at rt</i>	52
3.4.2.	<i>The Deduction of EPR Spectrum of GBN1 (The Relative Intensity of Every Splitting).....</i>	53
3.4.3.	<i>Temperature Dependent EPR Spectra of GBN1 in 5 Pure Solvents.....</i>	54
3.4.4.	<i>EPR Spectra of GBN1 in Mixed Solvents</i>	58
3.4.5.	<i>EPR Spectrum of Solid State of GBN1</i>	59
3.5.	Analysis and Deduction of New Model: Two-Comformational Model	60
3.5.1.	<i>Analysis and Deduction of Two-Comformational Model</i>	60
3.5.2.	<i>The Relationships Among Thermodynamic Parameters, Temperature and EPR Data</i>	62
3.6.	Magnetic Measurements	64
3.7.	Analysis of Additional Plots	65
3.8.	Conclusions.....	67
3.9.	References.....	67
4	Redox Stimuli Spin Responsive Systems with The Formation of Cation-Radical Diradicals	72
4.1.	Introduction.....	72
4.2.	Synthesis of Cation-Radical Diradicals	74
4.3.	Optical Properties.....	79
4.3.1.	<i>UV-Vis Absorption Spectra Radicals with Phenothiazine and Phenoxazin.....</i>	79
4.3.2.	<i>UV-Vis Absorption of Redox Stimuli Responsive Process and Cation Radicals</i>	81
4.4.	Cyclic Voltammetry Measurements	87
4.5.	EPR Measurements and Properties.....	91
4.5.1.	<i>EPR Spectra of Contrast Molecules and The Oxidation Process.....</i>	91
4.5.2.	<i>EPR Spectra of Redox Stimuli Responsive Process.....</i>	93
4.5.3.	<i>Fitting of Simulated EPR with New Signal Pattern of Experimental EPR Spectra</i>	95
4.5.4.	<i>EPR Spectra of Bidirectional Oxidation-Reduction Process (Reversibly Stimuli Responsive System)</i>	98
4.6.	DFT Calculations of Redox Stimuli Responsive System (Spin Distribution and Orbital Energy Level).....	99
4.7.	Conclusions.....	102
4.8.	References.....	102
5	Photo Induced Spin Responsive Systems Studied by EPR	107
5.1.	Introduction.....	107
5.2.	Photo Induced Radical or Spin Species Activated Systems in Photocatalysis Reaction	107

5.2.1.	<i>Radical and Spin Analysis of Photo Induced Reaction through Hydrophobic-Hydrophilic Switchable Photocatalyst.....</i>	109
5.2.2.	<i>Radical and Spin Analysis of Photo Induced Reaction about [2 + 2] Cycloaddition of Styrene Derivatives.....</i>	112
5.2.3.	<i>Radical and Spin Analysis of Photo Induced Reaction about α-Alkylation of Aldehyde Derivatives</i>	116
5.2.4.	<i>Radical and Spin Analysis of Photo Induced Reaction about Cycloaddition of Diphenylphosphine Oxide Derivatives and Alkynes Derivativees.....</i>	118
5.3.	Conclusions.....	122
5.4.	References.....	123
6	Redox Spin Active Systems of Aromatic Hydrocarbons Studied by EPR.....	125
6.1.	Introduction.....	125
6.2.	Redox Spin Switch of Aromatic Hydrocarbons.....	126
6.2.1.	<i>Back Ground Knowledge about Redox Processes in Triphenylene and Corolene</i>	126
6.2.2.	<i>EPR Measurement of Spiro-HBC and Mono-HBC in Different Valence State</i>	127
6.2.3.	<i>DFT Calculations about Spiro-HBC and Mono-HBC in Different Valence State.....</i>	132
6.2.4.	<i>The DFT Calculations about Spiro-HBC and Mono-HBC in Dication State through Broken Symmetry Method.....</i>	136
6.3.	Conclusions.....	138
6.4.	References.....	138
7	Experimental Section	144
	List of Publications.....	159
	Acknowledgement	161
	Curriculum Vitae	163

Index of Symbols and Abbreviations

Symbols

\AA	Angstrom
a_{ij}	hyperfine coupling constant (between two spin centers: i and j)
a_{iso}	isotropic hyperfine splitting
a_{H}	nucleus of hydrogen hyperfine splitting constant
a_{N}	nucleus of nitrogen hyperfine splitting constant
a_{P}	nucleus of nitrogen hyperfine splitting constant
B_o	applied external magnetic field tensor
B_r	central magnetic field in spectrum
C_m	Curie constant
d	distance
D	parameter of zero-field splitting (axial)
E	parameter of zero-field splitting (rhombic)
E^{η}	activation energy of viscosity
ΔE	difference in energy
g_e	g factor of free electron
g	g factor of radicals
h	Planck constant
H	spin Hamiltonian
ΔH	enthalpy changes
I	nucleus spin quantum number
J	spin exchange coupling constant
k	reaction rate constant

K	chemical equilibrium constant
M	magnetization
M_s	magnetic quantum number
S	spin quantum number
ΔS	entropy changes
ϵ	dielectric constant
δ	ligand field strength
Π	electrons pairing energy
μ_B	Bohr magneton
μ	effective magnetic moment
ν	frequency
χ	magnetic susceptibility
χ_{mol}	molar magnetic susceptibility
τ	average lifetime

Abbreviations

BHA	2,3-dimethyl-2,3-bis(hydroxylamino)-butane
BSC	broken symmetry calculation
CV	cyclic voltammetry
CW	continuous wave
DCM	dichloromethane
DFT	density functional theory
DMF	<i>N,N</i> -dimethylformamide
DMSO	dimethylsulfoxide
DMPO	5,5-dimethyl-pyrroline- <i>N</i> -oxide

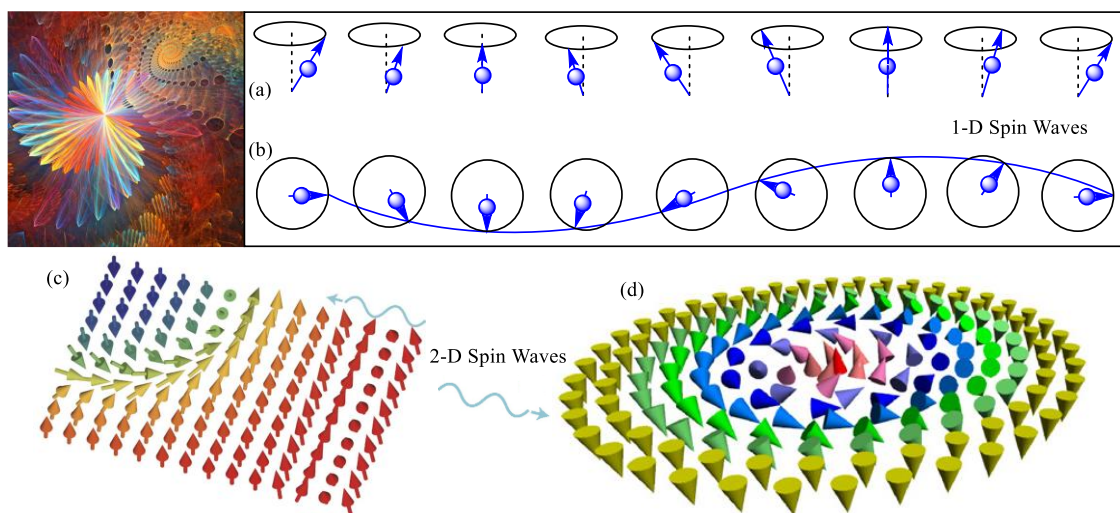
DPPH	<i>N,N'</i> -Diphenyl- <i>N'</i> -picrylhydrazyl
EPR	electron paramagnetic resonance
ESR	electron spin resonance
FD-MS	field desorption mass spectrometry
HBC	hexa- <i>peri</i> -hexabenzocoronenes
HF	Hartree-Fock
<i>hfc</i>	hyperfine coupling constant
HOMO	highest occupied molecular orbital
IN	imino nitroxide
LUMO	lowest unoccupied molecular orbital
NBS	<i>N</i> -bromosuccinimide
NMR	nuclear magnetic resonance
NN	nitronyl nitroxide
OS - CS	open shell – close shell
PBN	<i>N-tert</i> -butyl- σ -phenylnitron
PL	photoluminescence
QC	quantum computer
QIP	quantum information processing
QY	relative quantum yield
SOMO	singly occupied molecular orbital
SQUID	superconducting quantum interference device
SRR	stimuli responsive radicals
S-HBC	spiro - hexa- <i>peri</i> -hexabenzocoronenes
TEMP	2,2,6,6-tetramethylpiperidine
TEMPO	2,2,6,6-tetramethylpiperidinyloxyl

THF	tetrahydrofuran
TLC	thin layer chromatography
TMEDA	tetramethylethylenediamine
TRESR	time resolved electron spin resonance
UV-Vis	ultraviolet-visible spectroscopy
<i>zfs</i>	zero field splitting

Chapter 1 Introduction

1.1 General Background

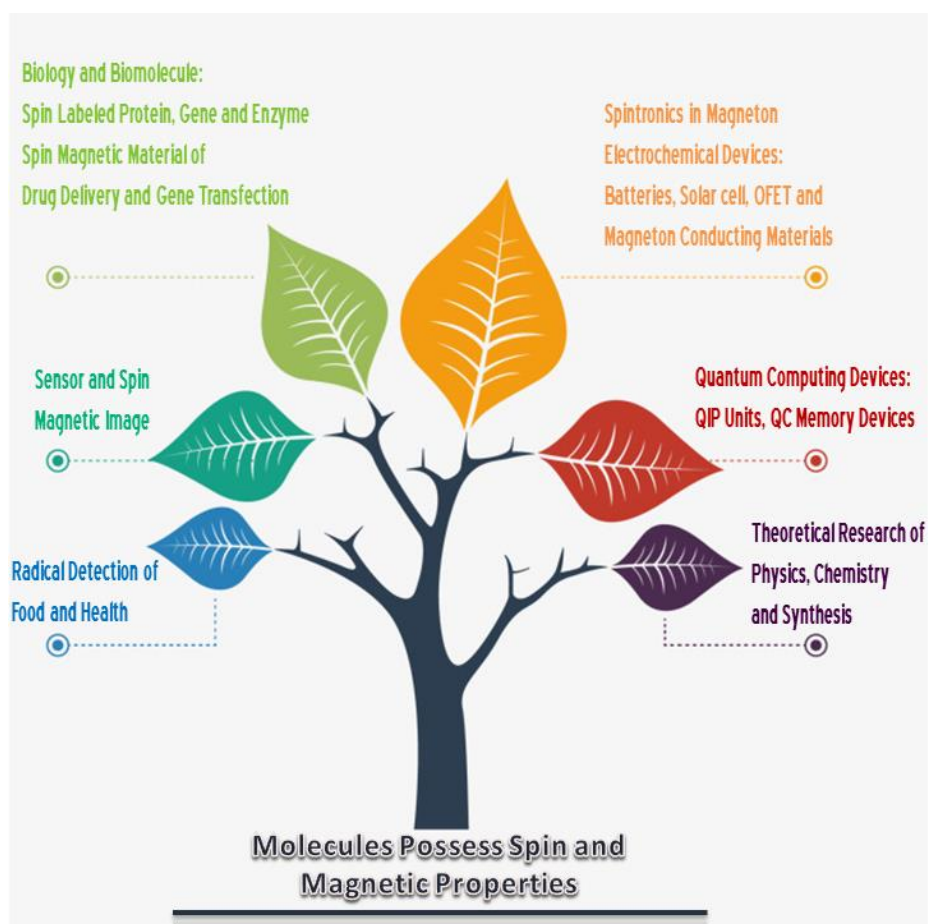
Magnetics and electrics form a specific symmetrical esthetics in the objective world or physical theorem. The symmetry comes from the reciprocal transformation of electromagnetic wave and reciprocal generation of electromagnetic field. If we trace to its source, all the magnetic matters and properties are root from the spin of electron, and with a specific aggregation or arrangement of electron spin, macroscopic magnetic properties and behaviors appear. Spin properties of electrons actually are intrinsic properties, and every unpaired electron with a certain spin vector resemble a tiny magnetic field. They would affect and have exchange interaction with each other nearby. So a concept spin wave which was first put forward by F. Bloch¹ is used to depict the process about macroscopic performance of spin and magnetic interactions with the specific wave properties of nearby reciprocal interactions and periodicity.²⁻⁴ When one of the spin centers was disturbed in a certain spin systems, the transmission of exchange interaction would start from the magnetic turbulence, due to the field of nearby spin centers.⁵⁻⁸ As shown in the scheme 1-1, (a) and (b) represent the exchange interaction of linear one dimensional spin waves from lateral and above perspective respectively. In addition, (c) and (d) represent the exchange interaction of two dimensional spin waves.



Scheme 1-1. The sketch of the propagating disturbances of spin waves or magnons in 1-D or 2-D magnetic materials

The history of application about magnetic materials for human beings could retrospect to more than one thousand years ago. The first utilization of magnetic materials which was recorded is the compass which is made by a natural magnet with ferromagnetic property. In

contemporary era, a great variety of magnetic materials were discovered, from inorganic metal to organic molecules and even organic-inorganic composites.⁹⁻¹¹ They have great potential uses in every aspect of life, as shown in scheme 1-2, from the theoretical research of physics and chemistry, the computer science especially quantum computer science¹²⁻¹⁵ (just as the quantum computer (QC) memory devices and quantum information processing (QIP) units or devices) to the aspect of spintronics and electrochemical devices, such as batteries, solar cells, organic field-effect transistors (OFET) and magneton conducting materials;¹⁶⁻²⁶ and from the field of biology and biomolecule, for instance spin labeled proteins, genes and enzymes, the spin magnetic materials of drug delivery and gene transfection to the aspect of sensors or spin magnetic image and even the aspect of applications in radical detection of food and health.²⁷⁻³⁰ So molecules or materials which possess spin and magnetic properties will play more and more important roles in science, especially in the aspects of organic radicals which are very popular in recent decades.³¹⁻³³



Scheme 1-2. The research and application domains of spin molecules and magnetic materials

1.2. Overview of Organic Radicals

1.2.1. Carbon Based Radicals

Carbon based radicals are one category of organic radicals which refer to the open-shell molecules where the unpaired electron is located on a carbon atom. Generally, this category of radicals generally is not stable and has relatively high reactivity. So for a long time, they do not have practical application although the first radical which is carbon based radical (triphenylmethyl) was synthesized more than one hundred years ago. During the development of carbon based radical systems, various structures with the unpaired electron located on alkanes, cyclanes or conjugated structure possessed Kekulé type and non-Kekulé type appear. We chose some typical representative structures for each kinds of carbon based radicals in the following text.

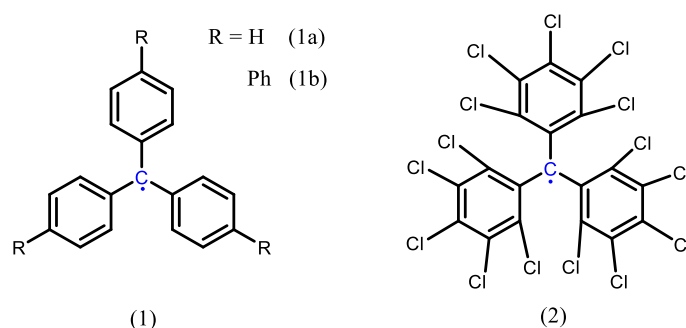


Figure 1-1. The structures of two classical carbon based monoradicals

Triphenylmethyl (1a) was the first carbon radical that was mentioned long time ago among this category, as shown in figure 1-1.³⁴ But due to the instability and quick oxidation, it did not draw so much attention. Later on, tris(4-biphenyl)methyl (1b) was synthesized and the problem of sensitive property was solved,³⁵ carbon based radicals bring back researchers interests. Synthesis of organic spin-magnetic materials become a vital scientific topic. With huge efforts that organic scientist made, a new triphenylmethyl structure that possess extremely high stability was acquired, namely polychlorotriphenylmethyl (PTM, 2) which the structure contains fifteen chlorides can stabilize the unpaired electron on carbon.³⁶ Because of the electron withdrawing chloride atoms, the electron cloud density of the central carbon was decreased and much more dispersed.

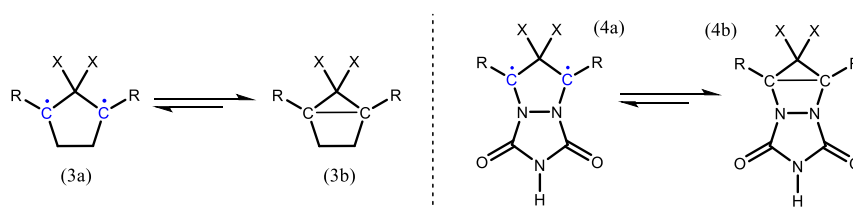


Figure 1-2. The structures of two carbon based biradicals in cyclopentane groups

Organic radical molecules with the unpaired electrons existed on cyclanes, like cyclobutane or cyclopentane is shown in figure 1-2.^{37,38} They normally appear in the form of two unpaired electrons and exhibit singlet interaction state for the biradicals. In addition, they are generally localized carbon diradicals and are more stable than alkane chain radicals. The radicals were generated from photochemical reactions and existed as intermediates. One way that has possibility to isolate the intermediates-state radicals is under low temperature conditions. The effect of different substituents at C1, C2 and C3 in cyclopentane could change the spin multiplicity of ground state and also the stability of the whole open shell structure. The substituents could be, X or R = H, MeO, OH or Ph.

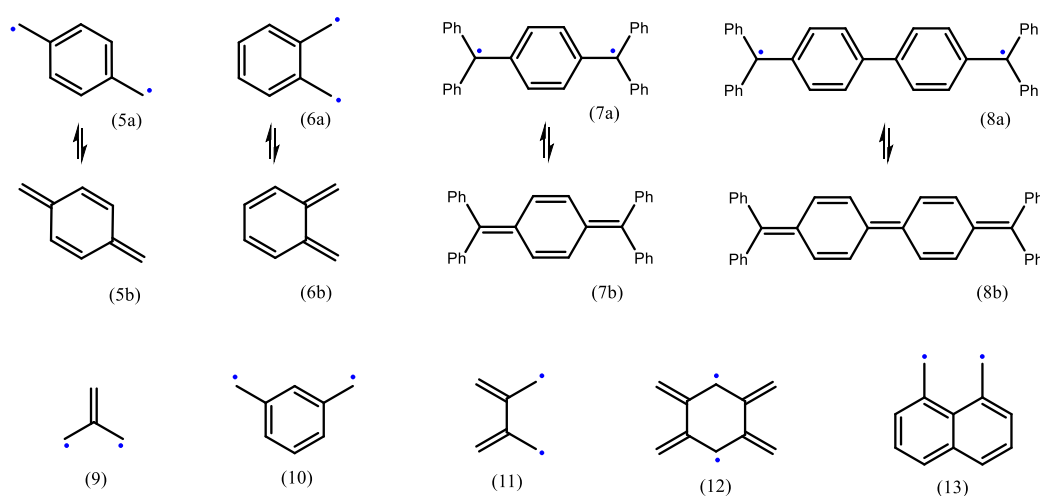


Figure 1-3. The classical structures of Kekulé type and Non-Kekulé type radicals

Another important category for carbon radicals is the radicals on conjugated structures. Phenylene composed structures are usually used to explain this spin category which is normally divided into two parts: Kekulé type and non-Kekulé type.³⁹⁻⁴¹ Generally, for a couple of radicals, the para and ortho position connection would lead to antiferromagnetic coupling (singlet ground state) and the meta position connection would lead to ferromagnetic coupling (triplet ground state) due to the rule that spin up and spin down exist alternately. For Kekulé type radicals, para-quinodiamethanes (5a) and ortho-quinodimethanes (6a) with the spin multiplicity of singlet state are shown in figure 1-3. The structure could resonantly exchange to a quinoide structure in equilibrium. In addition, the extension of π conjugated structure (7a and 8a) would enhance the stability of radical molecule and make the isolation much easier. The classical representative non-Kekulé type radicals are the molecules which still possess fully conjugated structures but contain two carbon atoms with unpaired electrons which are not π -bond connected with main conjugated structure. That means they could not be drawn as the quinoide structures. Typical representative structures are trimethylenemethanes

(9) as shown in figure 1-3, meta-quinodimethane (10), tetramethylenemethane (11), tetramethylenbenzene (12) and 1,8-naphthoquinodimethane (13). The two radicals in non-Kekulé structure are disjoint, while the radicals with the structure of Kekulé type joint to each other.

1.2.2. Nitroxide Radicals

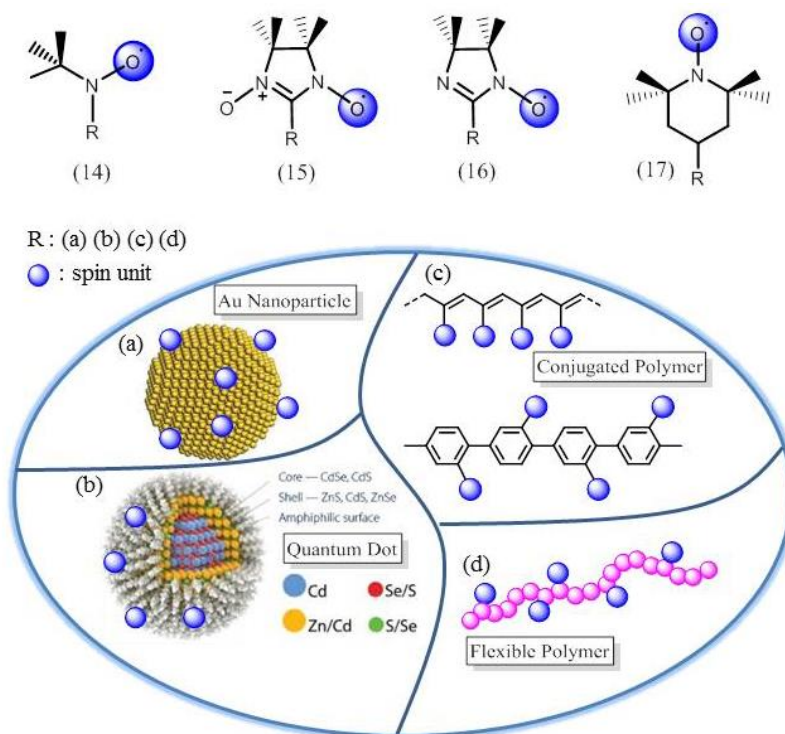


Figure 1-4. The classical nitroxide radicals

Up to now, nitroxide radicals are the most popular used and most stable organic radicals that were widely applied in scientific research and future promising materials.⁴²⁻⁴⁴ Just as shown in figure 1-4 that the unpaired electron was drawn and located at oxygen atom, but actually the spin densities are located at nitrogen and oxygen and the surroundings. For example the nitronyl nitroxide (NN) radical group (15), the spin density is distributed on O-N=C-N-O' structure fragment which contain several atom. There are four main nitroxide radicals that can represent this category of organic radicals. They are tert-butyl nitroxide (14), α -nitronyl nitroxide (15), α -imino nitroxide (IN) (16) and (2,2,6,6-tetramethylpiperidin-1-yl)oxidanyl (17), commonly known as TEMPO. The tert-butyl group in (14) and two pairs of methyl groups in (15), (16) and (17) which take large space and block the attacks from other active centers could stabilize the unpaired electron from radical cancellation reaction and make the life time of radical much longer. The synthesis of these four nitroxide radicals follow multi-step reactions. For tert-butyl nitroxide (14), generally, the protocol 2-methyl-2-

nitrosopropane (t-BuNO) dimer was used to provide hydroxylamine group. Then further oxidation step with the oxidized agent Ag₂O can transform the hydroxylamine group to nitroxide radical group. For the synthesis of NN and IN, the most important step among all is the condensation of protocol aldehyde which would undergo ring closure. But the further oxidation step is different. NN is much easier than IN to acquire by oxidation in the cases of (15) and (16). For all the four radical structures contain nitrogen (the nuclear spin angular momentum $I=1$ for ¹⁴N), the hyperfine splitting peaks should not less than triplet peaks. For (14) and (17), this hyperfine splitting leads to a three line pattern. The hyperfine splitting of (15) leads to a quintet pattern and (16) is heptet pattern (details are explained in chapter 2). All these four typical nitroxide radical groups have the ability to be functionalized to other structures or materials through N-R and C-R bond, as shown in the picture above.

There are many nitroxide radical molecules have already been published in recent few years. Stiff conjugated carbon backbone and flexible σ -bond connected carbon backbone based multi-nitroxide radicals polymers give new methods to prepare functional multi-radical materials with multi-spin centers which are shown in Figure 1-4.¹⁶ It is worth to mention that the nitroxide radicals which are decorated on gold nano-particles and quantum dots are part of novel concepts to combine two or three unique physical properties together as materials for sensors, bio-imaging, drug delivery and therapy. For example, the NN radicals which were decorated on the surface of gold nano particles are good representatives for the combination of spin technique and nanogold labelling technique. Quantum dots are known for their excellent photoluminescence property. The decoration of quantum dots with NN radicals would also perform a double response (they are spin and fluorescence response) for bio or vivo imaging and detection.⁴⁵⁻⁴⁸

1.2.3. Nitrogen Based Radical Cations

Open shell organic ions with tertiary amine structures are one of the important classes of radicals, electron donor structures which have one or several relative low oxidation potentials would easily form cations with unpaired electron owing to electron transfer under oxidizing conditions. Generally, the donor structures are prone to stabilize cation radicals and the distribution of spin density delocalized over the whole donor. Till to now, most open shell structures about cation radicals which acquired under different oxidation conditions are based on conjugated tertiary amine structures like triphenylamine system or phenothiazine, as shown in figure 1-5.

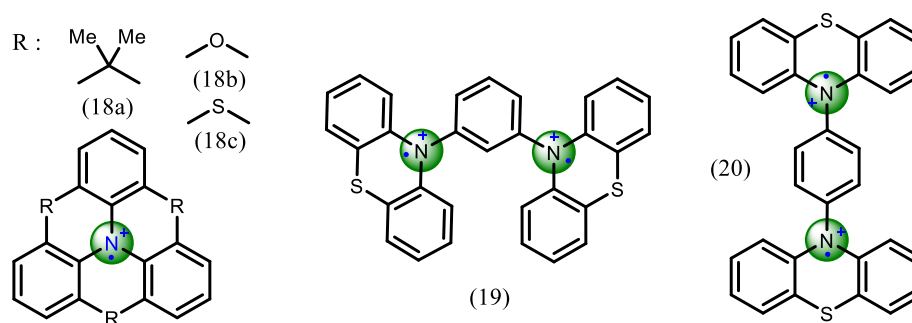


Figure 1-5. The structures of several nitrogen based cation radicals

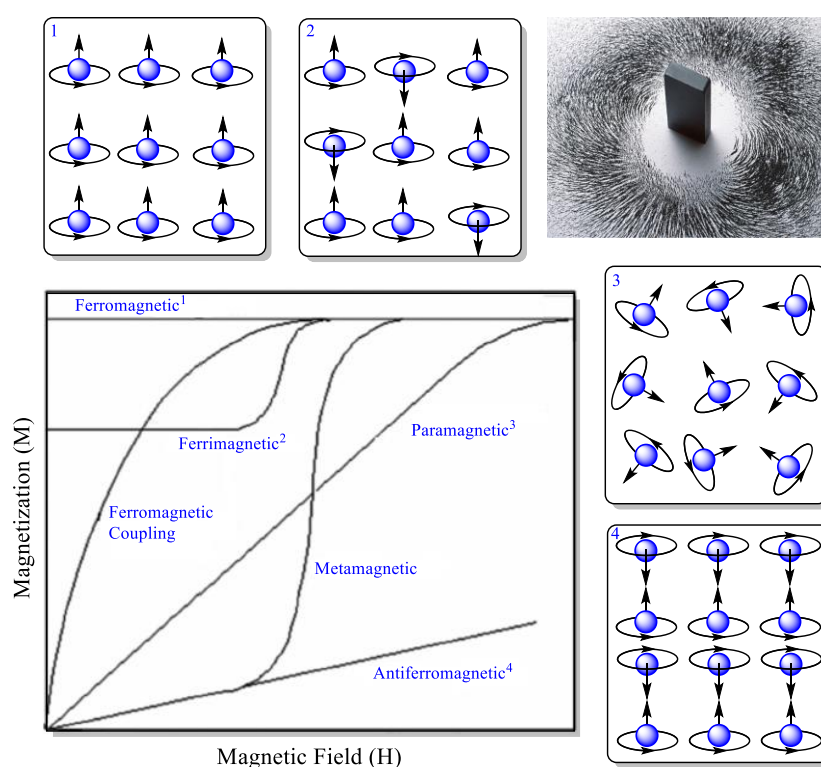
Triphenylamines which contain tertiary amine undergo oxidation and it transform to mono cation radical. Two typical structures based on that are dimethylmethylene bridged or oxygen bridged triphenylamine, as (18a) and (18b) respectively. The spin density would delocalize over the whole framework when cation radical are generated by oxidation of lead tetraacetate (solved in trifluoroacetic acid) or sulfuric acid. This work was reported by Wang, X. P. et al.⁴⁹ Further progress of synthesis based on triphenylamine is sulfur bridged structure (18c). Most of them are mono nitrogen cation radicals.

K. Okada and coworkers synthesized a series of phenothiazine based radical cations, including mono-cation radical and dication diradicals.^{50,51} For dication diradicals systems, two phenothiazine groups which are connected with para and meta position of phenylene respectively were synthesized and reported with ferromagnetic and antiferromagnetic spin-spin coupling interaction respectively, as shown in figure 1-5 (19) and (20). This new concept also provided a foundation to synthesize and investigate the mixed spin systems with neutral stable radicals and cation radical spin units.

1.3. Spin and Magnetism

Spin and the spin quantum properties originate from unpaired electrons in orbitals. The direction of spin of unpaired electron on single occupied orbital would not counteract by another electron. The first-row of atoms which can be used as magnets are some transition metals (Fe, Co, and Ni) and their oxides. The unpaired electron spins are residing in d-orbitals. Later on, magnets based on rare earth metals where the unpaired electron resides in f-orbitals were published. But for novel molecular magnets, the unpaired electron located on p-orbitals

always attracted large interests of scientist, especially organic chemists who are looking for soft materials-magnets. The first organic radical based magnet was alluded in 1960's by conceptual perspective, while the experimental realization achieved till 1980's. $[\text{Fe}(\text{C}_5\text{Me}_5)_2]^+[\text{TCNE}]^-$, (TCNE is tetracyanoethylene), which can be dissolved in conventional organic solvents and has unpaired electron in p-orbitals, exhibits magnetic hysteresis and magnetic ordering temperature $T_c = 4.8 \text{ K}$.⁵² The first pure organic radical reported in 1991, is para-nitrophenyl nitronyl nitroxide radical which has a magnetic order below 0.6 K or a cation radical salts $[\text{C60}]^+[\text{TDAE}]^-$ (TDAE is tetrakis(dimethylamino)ethylene) with a ferromagnetic order at 16 K .^{53,54}



Scheme 1-3. The magnetization behaviors of different types of magnetic materials and the arrangement of their spin units

For the concept of magnetic materials and molecular magnets, one thing must be noted that the ferromagnetic or antiferromagnetic couplings are completely different from the ferromagnetism or antiferromagnetism. The ferromagnetic or antiferromagnetic couplings actually refers to the spin coupling, which means the interactions between two spin units based on two unpaired electrons. While for ferromagnetism or antiferromagnetism, they are used to depict a substance that has this magnetic physical property. But the concepts have immanent relationships with each other, if materials are below magnetically order temperature T_c .

We can divide magnetic materials into several classes by the arrangement of every spin units in a certain range at bulk or solid state.⁵⁵ They have different trends of magnetization (M), when the materials are placed in a changeable applied magnetic field (H), as shown in scheme 1-3. While the spin units are all in the same direction in a certain range, it would lead to long range ferromagnetic ordering. If they are in contradict direction, and the intensity are different which means the whole spin could not be offset in all range of magnetic domain, the whole materials would display ferromagnetic. The magnetization would have a certain value even without the external magnetic field in these two situations. The difference is that M value of a perfect ferromagnetic materials would never change no matter whether there is an external H or not, but for ferrimagnetic materials, because of the partial magnetic order in structure, the M value would quickly enhance to another M value when the H increased to a certain value. In contrary, the magnetic spins do not have interaction with each other and display paramagnetic behavior where the orientations of spin are random and fluctuate. For antiferromagnetic coupling, the spins are all in the pair of opposite direction interaction. The magnetization increased very slowly during the increase of applied magnetic field, which actually means the magnetic susceptibility is very low when below the Curie temperature.

Some other classes are diamagnetism, spin glass, cluster glass, metamagnet and superparamagnet.⁵⁵ Diamagnetism describes a magnetic phenomenon with an opposite magnetization created by an external magnetic field. This unique magnetic property is completely different from the normal magnetic phenomena described above. Spin glass refers to a random orientation of frozen spin orientations in an amorphous material which is similar to a paramagnet. However, it is a broad distribution of time constant with spin fluctuate during whole process. Cluster glass means the spin orientations lock in small clusters with magnetic order, but there is no magnetic order between the clusters. The concept of cluster here is different from magnetic domain. The cluster is much larger than magnetic domain. The size of magnetic domain depends on different category and geometry. For example, one magnetic domain of the cubic Fe_3O_4 has 3.65×10^5 repeat units while spherical iron owns 1.5×10^5 iron atom. Metamagnets refer to the magnetic materials which possess a low magnetization but transformed to relatively high magnetization, induced by the external magnetic field. A typically example is the transition from antiferromagnetic state to ferromagnetic state caused by external magnetic field. Superparamagnet can be regard as big paramagnet with higher magnetic susceptibility. The reason is that the superparamagnet is

composed by many small ferromagnetic particles, which the size is at critical point that sustain the single magnetic domain ferromagnetic structure.

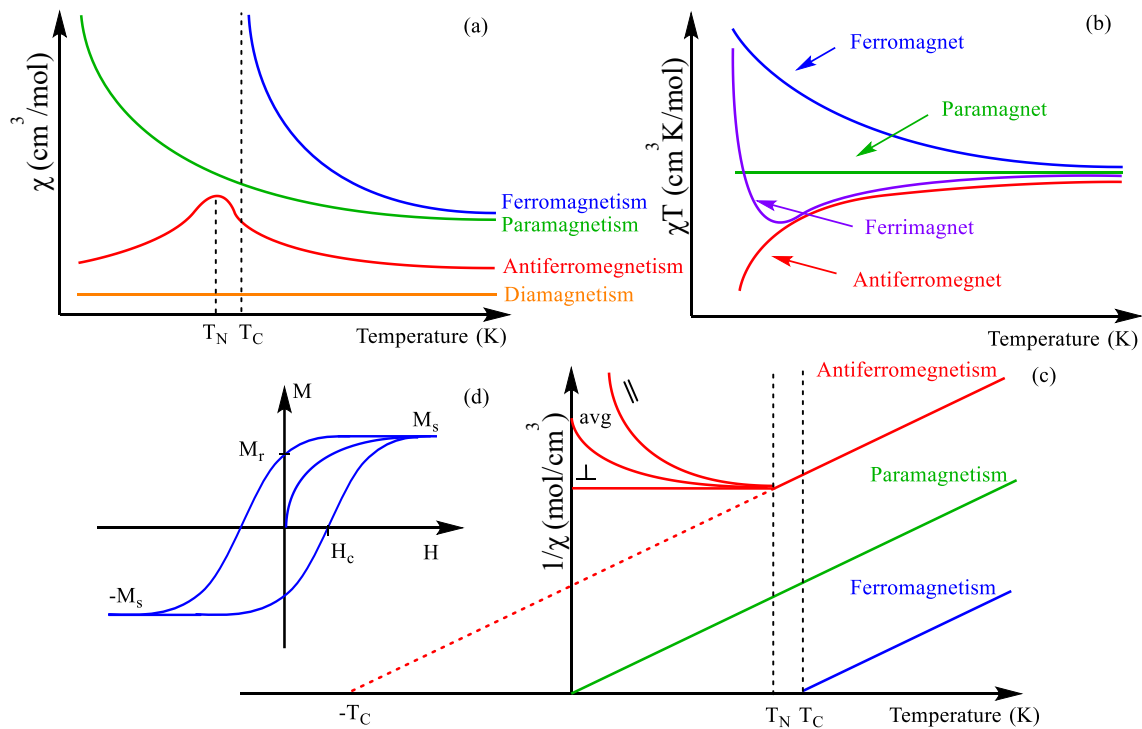


Figure 1-6. The relationships of χ , χT and $1/\chi$ with T for (a), (b) and (c), (d) the plot of hysteretic magnetic behavior

Magnetic susceptibility χ is the most important parameter to identify magnetic behavior. The concept of χ is the degree of magnetization which is divided by a certain applied magnetic field (M/H or dM/dH). For paramagnetism, the relationships between χ and T should obey Curie law which is shown in equation (a) below, while for ferromagnetism and antiferromagnetism, it should obey Curie-Weiss law shown in equation (b). Generally, three different forms of plots were used to depict the tendency of magnetic susceptibility with the changing value T . They are χ , χT and $1/\chi$ with T , respectively, as shown in figure 1-6 (a), (b) and (c). Curie temperature T_C for ferromagnets and Neel temperature T_N for antiferromagnets can be acquired from figure 1-6 (a) and (c). The magnetic ordering in long range no matter ferromagnetic or antiferromagnetic ordering only occurs below critical temperature. The Weiss constant θ which can be acquired from the intercept of T , when $1/\chi = 0$. $T = 0$ is for the situation of paramagnet, $T > 0$ is for the situation of ferromagnet (T_C , sometimes could be written as θ_w Curie Weiss temperature) and $T < 0$ is for an antiferromagnet (the intercept is $-\theta_N$ minus Neel temperature) from figure 1-6 (c). (d) is the plot of magnetic behavior figure about hysteresis of $M(H)$, where ferromagnets and

ferrimagnets are both suited for this pattern. M_s and $-M_s$ are saturation magnetization, in addition, M_r is remanent magnetization.

$$\text{Curie Law : } \chi = C / T \quad (\text{a})$$

$$\text{Curie-Weiss Law : } \chi = C / (T - \theta) \quad (\text{b})$$

1.4. External-Stimuli Responsive Radical (SRR) Systems

The stimuli responsive materials⁵⁶ (SRMs) which are usually called "smart" materials draw more and more attentions, because of the potential applications in many fields, including organic inorganic devices in electronic engineering and memory, sensors, nano-technology of biochemistry and biomedicine, theoretical research of physical chemistry and so on. The concept of SRMs normally means a kind of materials that have significantly change in their physical and chemical properties such as optical, electrical and magnetic properties, or mechanical, shape and state with an external variation on temperature (thermal), photo, pH, pressure, redox condition, enzymes, ultrasonic field and electric field.⁵⁷⁻⁶¹ Among the stimuli responsive systems, two key points are: 1. the responsive should be at better bidirectional or reversible; 2. the whole switch process should be repeated as many times as possible. Although remarkable advances about SRMs upon various types of external stimuli has already been made during the past decade, the open-shell organic structures (SRR) especially nitronyl nitroxide radicals based spin stimuli responsive systems still need further investigations.⁶² The responsive of magnetic properties including monoradicals-biradicals transform, radical-spin coupling interactions, and magnetism under different external stimuli are valuable and magnificent topics. We focus on exhibiting four kinds of external factors stimuli responsive radical systems in this thesis: temperature (thermal) stimuli, photo stimuli, pressure stimuli and redox condition stimuli.

1.4.1. Temperature Stimuli Responsive Radicals

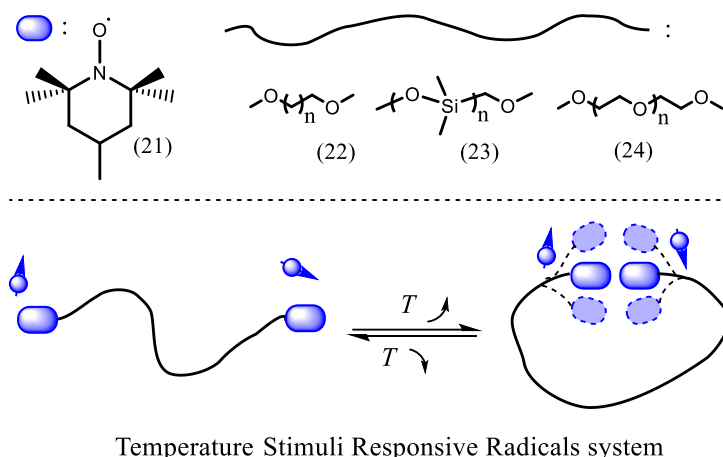


Figure 1-7. Several examples of radicals systems with temperature stimuli responsible property

At first glance, temperature-dependent stimuli responsive magnetic properties describe the relationships between magnetic ordering of condensed or bulk materials and temperature. Actually, the temperature stimuli responsive radicals here is the topic that discuss the spin interaction between two spin centers in single molecule in solution state just as the figure 1-7 shown above. Two important questions should be mainly considered: how do the features of spin coupling interaction transform intramolecularly during the change of T , and the characterizations of biradical features and spin interactions upon the stimuli responsive process. The recent publications about this research field are engaged in synthesis of flexible bridged two nitroxide radicals-end capped molecule. The flexible bridged structure made the molecule much easier to move in solution state (which also means much more conformations exist and fast exchange). The rotation of various C-C σ bonds, O-Si σ bonds or C-O σ bonds on the bridge give the possibility of the two end capped nitroxide groups stay close. When T goes up, the molecule displays a biradical feature where the two spin centers have strong spin interaction, whereas the T goes down, the two radical end-capped molecule exhibits mono-radical feature. Actually, V. N. Parmon et al. have already given some results about mechanism (some thermodynamic parameters about this spin-switch system were deduced) of spin exchange of nitroxide biradicals in long-chain and put forward a three conformation model to explain this kind of phenomenon that is affected by different temperature and solvents thirty years ago.^{63,64} Parmon's model gave some explanations to this system, but some problems still remain and are not clear to all the T stimuli responsive radicals systems. For example, the nitroxide radicals they used are tempo radicals which are one of the easy situations, that the hyperfine splitting is three lines pattern, to all kinds of cases as shown in figure 1-7 (21) as end capped radicals, and (22, 23) as flexible bridge. So it could not explain other more complicated cases which hyperfine splitting could be five lines pattern or nine

lines pattern displayed on EPR spectra. In addition, the three conformations model has a concept of solvent cage which is not so clearly understood. The distinguish between two conformations in the solvent cage which have spin interaction or haven't is not obvious from the perspective of spatial topology in this model.

Later on, A. I. Kokorin's research group also synthesized a series of ethylene glycol bridged tempo.⁶⁵ The bridges with different length as shown in figure 1-7 (24) became an important factor and was discussed the relationships with spin coupling interaction in different viscosity of solvents. A parameter of lifetime τ was used to describe the process. Every conformation has its own lifetime during the whole process. The different relative lifetime τ changed which could be acquired from EPR spectra and deduced relationships with thermodynamic parameters enthalpy ΔH , entropy ΔS , in different solvents upon the change of temperature.

1.4.2. Redox Stimuli Responsive Radicals

Redox stimuli responsive radicals system means a series of molecule have a response of spin property or form new spin centers upon the stimuli of external redox conditions. The system could be divided into two main parts as shown in the figure 1-8 (top left corner). One is the transformation from close shell structure to open shell structure which contains ion spin centers. The other one is the transformation which combine ion spin species and stable radical groups. The spin coupling interaction between stable radical spin and new formed ion spin species under the redox condition should be under consideration.

A famous carbon material example is fullerene. The newly formed radical or spin center on carbon based open-shell structure, as shown in figure 1-8 (25a) and (25b) was published in 1993 by M. Baumgarten. et al.⁶⁶ They used a THF/K reduction condition to obtain anion radical fullerene which possesses special threefold degenerate LUMOs that may lead to high spin state, like as quartet state upon three electrons transfer to every fullerene molecule. Clear EPR spectrum of zero field splitting illustrate the formation of a diradical dianion spin species. In addition, several situations of reduction states of fullerene in different reduction conditions were provided and discussed. That is to say, the stimuli responsive property of spin center (appear or disappear) could be fulfilled under the change of oxidation and reduction conditions. Another series example for this part are phenothiazine and its derivatives. The first mention of application was in 1880 for medical and biological use. The property of color change which is due to electron transfer from the core structure tertiary

amine of phenothiazine could be used in electronic devices, such as organic light emitting diodes and dye sensitized solar cells. Later on, scientists discovered that radical cation was formed during the redox sensitive process. The redox-spin stimuli responsive system was emerged from the oxidized process which is also reversible by using specific reducing agents. An orthogonally linked phenothiazine transformed to dication diradical species with triplet ground state by the oxidation of antimony pentachloride (SbCl_5) was reported, as shown in figure 1-8 (26a) and (26b).⁶⁷ Moreover, many similar works with a series of phenothiazine based structure that use different redox conditions to prepare radical cations, including mono-cation radical and di-cations di-radicals, have also been done by K. Okada's group and T. Sugawara et al.^{68,69} The key point of the redox stimuli responsive system is that the molecular structure should carry a potential spin species, such as phenothiazine, phenoxazine and triphenylamine.

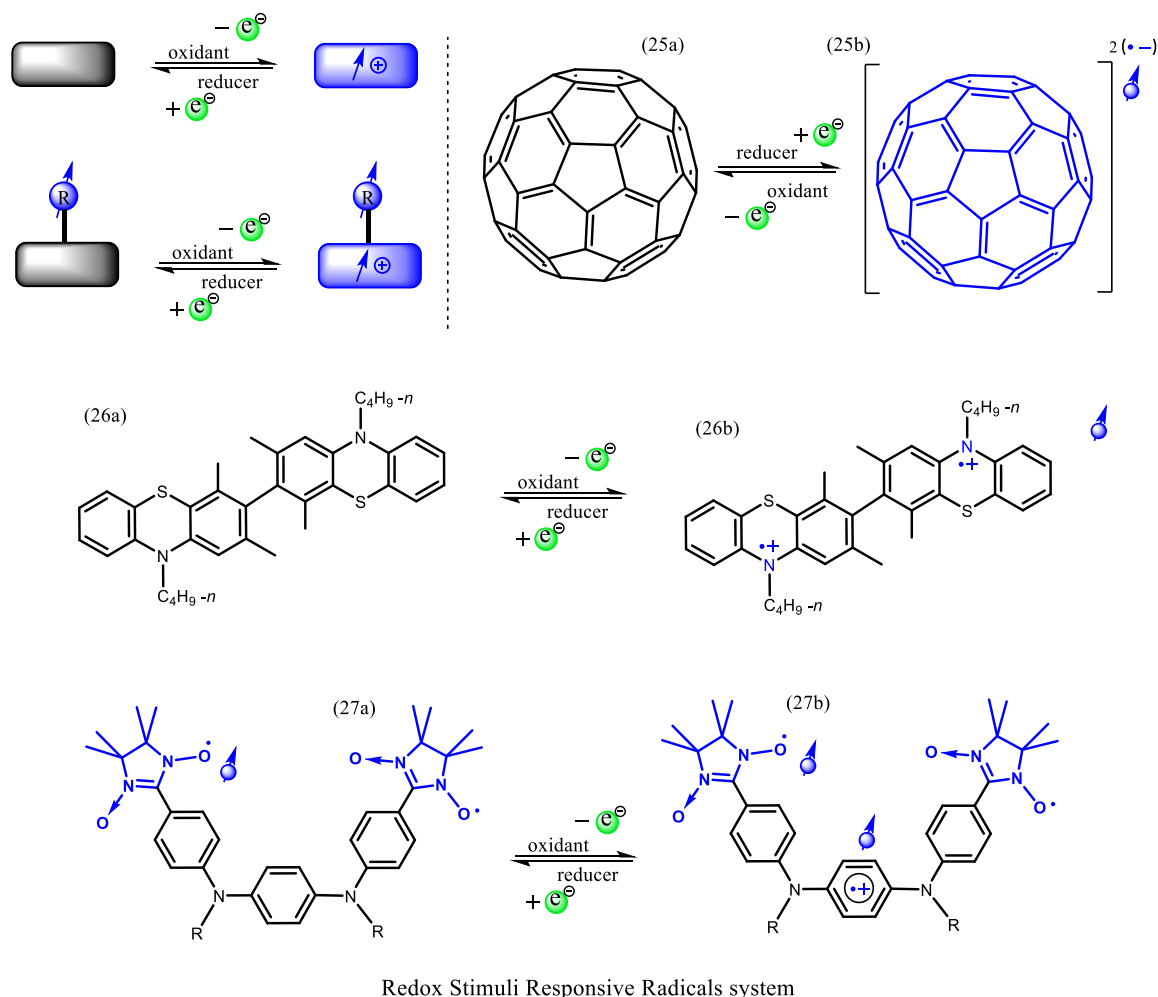


Figure 1-8. Several examples of radicals systems with redox stimuli responsible property

The other category belongs to redox stimuli responsive radical system is a new cation radical field that attract researchers' interests recently. A stable nitroxide radical, such as

nitronyl nitroxide would be combined to the redox sensitive unit. That is to say, the nitroxide radical should be inert to the redox stimuli reaction during the whole process no matter whether it is oxidation or reduction. Spin coupling interaction performed between existing stable NN which is the localized spin center and new formed delocalized cation radical spin center by the responsive property of redox sensitive unit. A persuasive work which was devoted by Kazuyoshi Tanaka's group exhibited a redox sensitive unit para-phenylenediamine as a bridge to connect two NN radical groups at both ends of the structure,⁷⁰ as shown in figure 1-8 (27a) and (27b). Through one electron oxidation by magic blue, the molecule which carried two NN radicals with paramagnetic spin properties at beginning shift to three spin centers coupling interactions that possessed high spin state (ferromagnetic spin coupling interactions). It is also can be called redox-excited quartet state ($S = 3/2$) spin species from low spin state. The new spin characteristics were detected by EPR measurement. Moreover, cyclic voltammetry (CV) and UV-vis-NIR absorption measurement were also used to supplementarily testify the new phenomenon. The phenomenon of responsive spin interaction switch is fulfilled by electron transference in variant external redox conditions. K. Tanaka also gave a forecast about these molecules, that the spin transfer property in the stimuli responsive system has tremendous potential applications in electronic-magnetic devices. But the researchers didn't give a further investigation about whether the redox stimuli responsive process is reversible or not.

1.4.3. Photo Stimuli Responsive Radicals

Photo stimuli responsive radical systems are very popular research field of stimuli responsive system recently. Structures containing photo sensitive properties plays an important role in these spin responsive system.⁷¹ Depending on this design idea, the molecules should have both photo sensitive units and spin units. And the spin units should be ensured stable under the photo triggering.⁷² Nitronyl nitroxide and imino nitroxide have already been proved stable under normal light (the wave length of light should be not less than 250 nm) in the past. So two stable nitroxide radicals at two ends which are bridged by photo stimuli responsive units are usually seen in these fields. Two main categories can be concluded in this stimuli responsive system (as shown in figure 1-9 at top left corner). The first one is the radicals have no spin coupling interaction which means totally individual and paramagnetic before stimuli, but correspondingly changed to ferromagnetic ($\uparrow\uparrow$) which called triplet state or antiferromagnetic spin interaction ($\uparrow\downarrow$) which called singlet state, through specific photo

stimuli. The second one is the reversible transformation between the two spin coupling interaction states, the singlet state ($\uparrow\downarrow$) and the triplet state ($\uparrow\uparrow$), through light stimuli responsive unit.

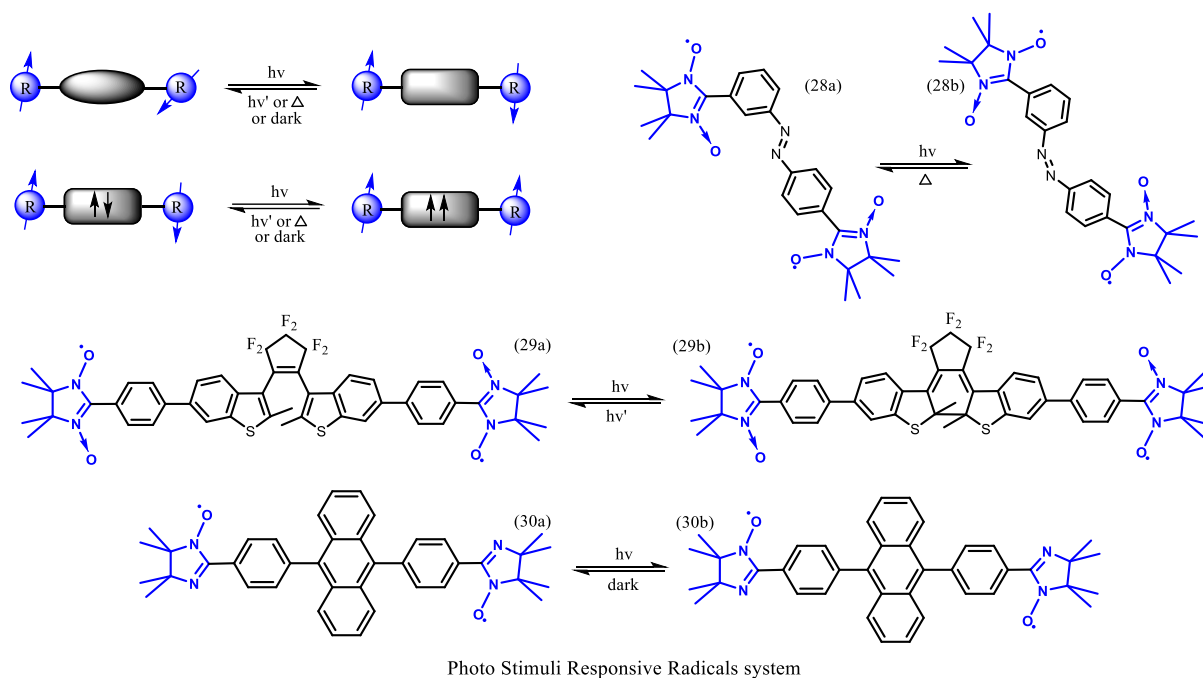


Figure 1-9. Several examples of radicals systems with photo stimuli responsive property

Several classical organic radicals with light stimuli responsive properties which exhibit intramolecular spin and magnetic properties shift will be discussed in this part. The first example is an azobenzene derivative which is a well-known photo sensitive unit that can undergo isomerization by photo irradiation in the range of 345-415 nm light,⁷³ as shown in figure 1-9 (28a) and (28b). The substituents, two NN radicals were connected through this specific light sensitive bridge showed a magnetic property change due to the change of trans-isomer to cis-isomer by external stimuli. Although the conversion between trans and cis isomers are not complete, the difference in EPR spectra was observed at certain temperature and solvent that can prove the alteration of spin properties. Some other similar publications also showed some different stable radicals, such as Imino nitroxide and verdazyl which were carried out to investigate the process of photoinduced switch of magnetic properties.⁷¹ But these publications focused on the aspect of theoretical calculation of the magnetic switch. They investigate the photo stimuli responsive systems through broken symmetry approach in the framework of density functional theory (DFT). The theoretical calculation results gave some proves of crossover from antiferromagnetic interaction to ferromagnetic interaction in photo stimuli.

The second example is an organic biradical molecule with a photo sensitive unit diarylethene. The light switching structure could undergo a transition between conjugated connection and non-conjugated connection due to the chemical ring opening and closure of structure in different photo irradiation. K. Matsuda and M. Irie synthesized a series of these kinds of molecules that have the properties of photoswitchable intramolecular magnetic interaction.^{74,75} A bridge with photo sensitive unit diarylethene and two phenylene space is a good example as a representative in this series, as shown in Figure 1-9 (29a) and (29b). We know the principle that the delivery of electron interaction on single C-C σ bond and C-C double bond that contain π bond are completely different. So the spin exchange interactions which were located at the two end position would also change owing to the structure transition of photo sensitive bridge. For the bridge only containing photo sensitive group diarylethene, the spin coupling exchange constant J , which is intramolecular antiferromagnetic interaction at ring opened isomer (non-conjugated connection state), is about -2.2 K ($2J/k_B$), while $2J/k_B = -11.6$ K at ring closed isomer (conjugated connection state) situation.

The last example of photo stimuli responsive spin system is a type that comprised of organic di-imino nitroxide (IN) radicals and bridged with anthracene unit, which was published by Teki et al., as shown in Figure 1-9 (30a) and (30b).⁷⁶ The switchable magnetic characteristics is that the two IN radicals are antiferromagnetic spin coupling before photo irradiation (or put in the dark for some while), while excited to ferromagnetic spin coupling (high spin with spin multiplicity of quintet $S = 2$) after photo irradiation. The measurement of detecting the shift is using time-resolved ESR which is short for TRESR. The spin coupler 9, 10-diphenylanthracene which can be excited to high spin state under photo irradiation played an important role in this photo-stimuli spin-responsive process. Another similar structure but not symmetry is 9-phenylanthracene with mono IN radical. The excited high spin state is quartet ($S = 3/2$) state. An interesting phenomenon is that, for a same diphenylanthracene bridge, the different topological connections also affect the spin alignment in excited states. For example a different meta-position connection with the same diphenylanthracene bridge could not exhibit high spin state when excited by photo irradiation. This is completely different from the para-position connection depicted above. So we could draw a conclusion by this point that isomers with different topological connection bridge directly influence the magnetic properties and spin states no matter they stay in the ground state or excited state during the photo stimuli responsive process.

1.4.4. Pressure Stimuli Responsive Spin Molecules

Among all the external stimuli responsive systems, only pressure of atmosphere stimuli factor is not only a mono stimuli responsive external factor. The spin systems that possessing pressure stimuli responsive properties usually undergo corresponding respond upon other external stimuli factors, such as temperature, light irradiation and mechanical force. There are two examples exhibiting in this section to depict double external stimuli (pressure and temperature) responsive systems as shown in figure 1-10.

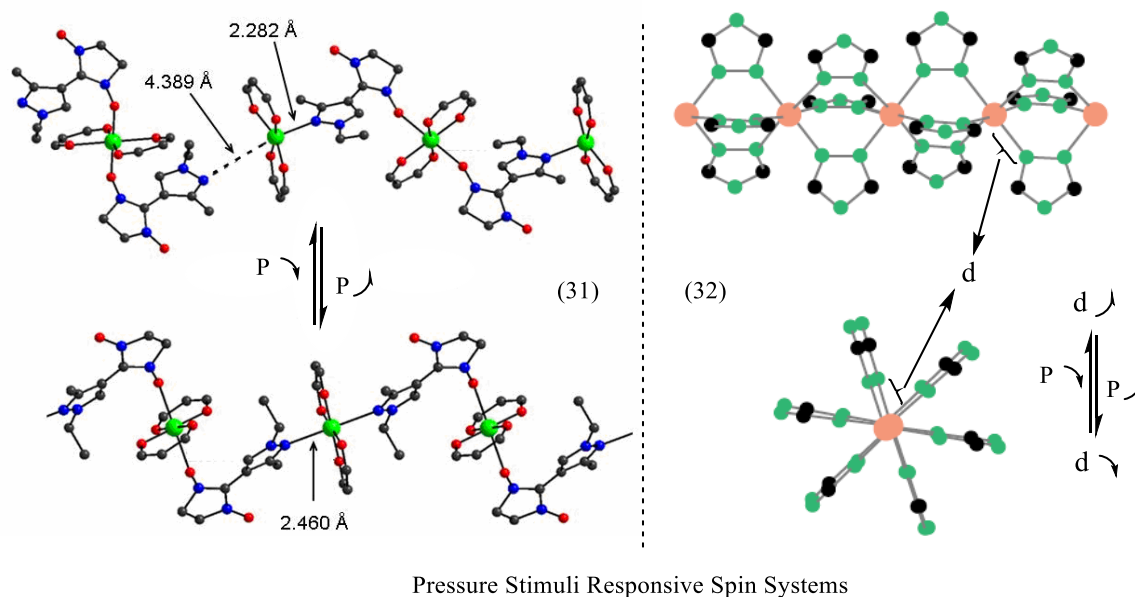


Figure 1-10. Several examples of radicals systems with pressure stimuli responsible property

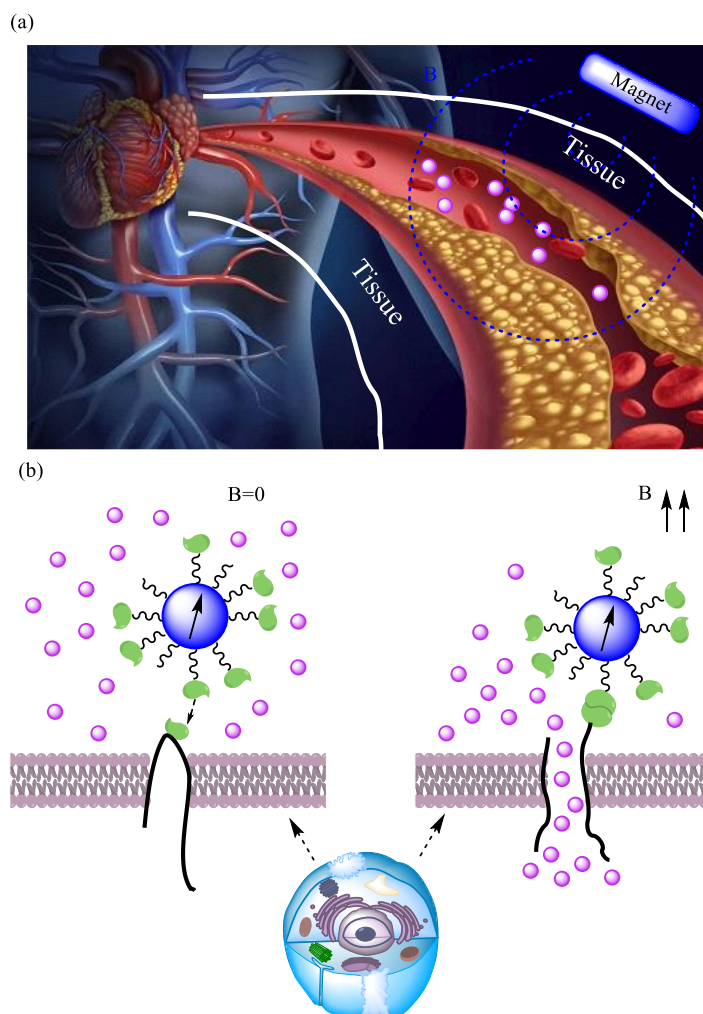
The two examples are both molecules containing organic groups and also coordinated with metal atoms, while the first one is copper (+2) hexafluoroacetylacetonates coordinated with pyrazole mono-substituted NN radical, which was synthesized by group of V. Ovcharenko et al.,⁷⁷ as shown in figure 1-10 (31). Except temperature factor, the variation of external pressure factor change the magnetic properties of the compound obviously by analyzing the change of effective magnetic moment. There are two main different value of effective magnetic moment during the change of external pressure process. This is mainly because there are two stages of crystal structures states existing (the different distance between copper atom and the nitrogen atom of pyrazole) by the change of pressure. When the external pressure increased to a certain critical value, the distance between copper atom and the nitrogen atom of pyrazole would be close to about 2.46 Å, while the pressure decreased to another relative low critical value, the distance would be to about 4.39 Å. They also give a

funny name to the special crystals, the "breathing crystals" for that phenomenon described above.

The second example which is shown in figure 1-10 (32), represent a series of compounds that transition metal Fe complexed with triazole groups synthesized by O. Kahn et al. An important article that published in science in 1998 announced these organic and inorganic ligands compounds possess pressure-spin stimuli responsive properties.⁷⁸ For a Fe^{2+} ion, the number of electron in 3d orbitals (five orbitals totally) is six. Then Fe ion contained complex acquired high spin state and low spin state transition upon external stimuli, when considered by crystal field theory, because of the five orbitals of 3d divided into two groups with two different energy levels (two higher energy level orbitals e_g and three lower energy level orbitals t_{2g}). The high spin state is quintet ($S = 2$) state with four unpaired electron on the same direction ($e_g^2 t_{2g}^4$), while the low spin state is singlet ($S = 0$) state with three pairs of coupled electrons (t_{2g}^6). The change of external pressure directly affects the distance between Fe^{2+} ion and the three nitrogen atoms of triazole. And the distance further influence the energy distinction between the two groups of orbitals which give the opportunity to the outermost electrons rearrange in 3d orbitals. This transition between two spin states is also according to the relative value of ligand field strength δ and electrons pairing energy Π . When $\delta > \Pi$, the arrangement of electrons would chose low spin state, while $\delta < \Pi$, it would chose high spin state. So when the external pressure increased to a certain value, the metal ligands distance would decrease. And this outer stimuli factor would give the tendency to high spin state, vice versa.

1.5. Applications of Magnetic Materials and SRR Systems

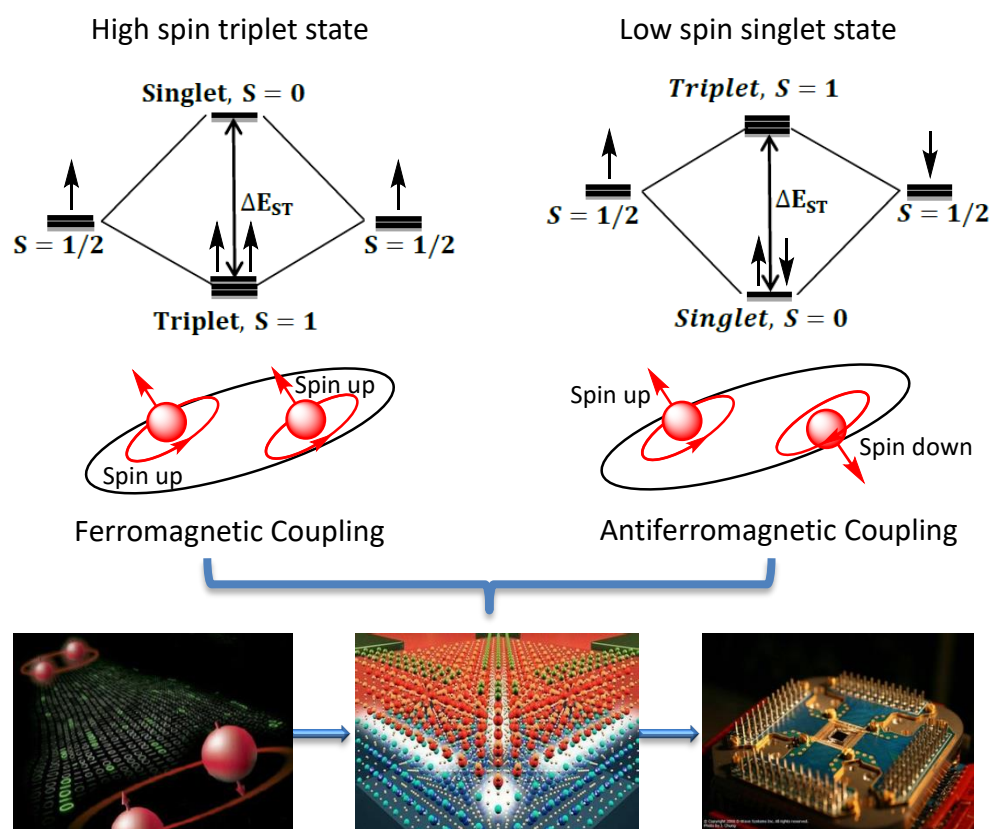
The applications of spin and magnetic materials including organic SRR systems are widely spread out to various walks of life, as shown in scheme 1-2. Recently, a meaningful and promising application of spin and magnetic material (magnetic nanoparticles) was used in biomedicine research field which can represent new technology for magnetic materials, as shown in scheme 1-4.⁷⁹⁻⁸³



Scheme 1-4. The applications of spin and magnetic materials in the research field of biomedicine

The non-specific of medical chemotherapies is the most troublesome disadvantage that the chemotherapist wanted to conquer. The non-specific would lead to side effect which means it could also attack normal or healthy cells during medicine treatment. However, if the process could be specified and localized, the medical treatment would be much more effective and healthy. The magnetic nanoparticles which own special physical property that could have interaction with external magnetic field could be used as promising biocompatible carrier to deliver the drugs to some specific tissue. The scheme 1-4 (a) shows an intravenous treatment, which ferromagnetic nanoparticles as a drug carriers were injected to blood vessel. The external magnetic field can locate at the target tissue in advance (generally cancer tumours). Depending on the attractive interaction between the ferromagnetic nanoparticles and external magnetic field, the drug will accumulate to the specific tissue and acquire a better drug therapy. Another good example that present the application in biomedicine is the usage of magnetic nanoparticles in cell therapy, as shown in scheme 1-4 (b). By coating the molecules which can bind to special protein (such as integrin receptors or antibodies) at the surface of

cytomembrane, the magnetic micro or nanoparticles could twist and pull the cell membrane in a gradient magnetic field where the intensity and direction could be easily changed. The force is strong enough to open or activate the channel on the membrane, sometimes the two directions of forces can combine together to give a better mechanical motion on the surface of cell. The figure shows the whole process of cellular uptake through magnetic interaction. At first, the magnetic nanoparticles were attached directly to one type of ion channel through specific binding of antibodies at the absence of external magnetic field. The ion channel was opened and the ions were absorbed when exposing upon an external magnetic field with high gradient. So the cell uptake, the control of channel and cytomembrane by magnetic force were achieved. The novel magnetic way provides a new perspective to investigate the cellular mechanical properties and the specific chemotherapies.



Scheme 1-5. The sketch of SRR systems applied in QIP unit or QC memory devices

For the application of SRR systems, the stimuli responsive switchable magnetic property plays an important role and have substantial potential prospect in various research field. Actually the magnetic properties we often mentioned are root from the properties of molecular spin. The spin in magnetic materials or spintronics both come from unpaired electron. So the electron with charge properties and spin properties should be both

considered.⁸⁴⁻⁸⁶ The microelectronic devices which possessed SRR systems have a very prosperous future in quantum computer (QIP unit or QC memory devices). It is universally known that, no matter an information process unit or a memory device in computer logic gates is binary system, namely “0” and “1” two states in logic gates for computer. Fortunately, the highly similar properties that the electron spins also possessed are two spin states i.e. spin up and spin down. And for a normal molecule with two electron spin centers, the spin magnetic state also can display two states i.e. high spin state and low spin state. For every electron spin or every molecule owns two quantum states, the density and ability of information process and storage is quite suit for quantum concept of computer science. These interesting phenomena and properties give the spin magnetic molecule high possibility to apply to QIP unit or QC memory devices, as shown in scheme 1-5.

Here comes out another important issue, namely, how to switch the two electron spin states in quantum level or molecular level reversibly to suit the requirements of quantum computer device that should be erasable and alterable. So creating spin magnetic materials with reversibly stimuli responsive properties become essential and urgent. The scheme 1-5 presents the relationship between electron spin state and molecule spin state. A molecule that contains two unpaired electron spin center presents two states in different situations. One is the two electron spin directions are the same (both are spin up or spin down), this lead to ground state triplet, in other word is the molecule possess high spin state. Another situation vice versa and the molecule possess low spin state. The molecules were arranged at a proper logic gate to a device, and then searching a proper external factor to stimuli the change of spin state to satisfy the conditions of quantum computer devices. The organic molecules which can combine so many stimuli responsive units to radical spin structures and with their own excellent structure-modified properties provide a novel perspective to conquer these issues.

1.6. Motivation and Objectives

For quite some time, the magnetic materials (including the most common ferromagnetic or ferrimagnetic materials) are composed of inorganic elements of iron group (like as Fe, Co and Ni) or rare earth elements and their alloy or oxidized compounds. These inorganic magnetic materials have excellent strong magnetic interactions but the disadvantage is also very obvious, namely the density is too high and it is difficult to processing. Later on, organic magnetic materials or organic-inorganic complex magnetic materials appear and draw

a lot of attentions of material scientist. They are soft and flexible, light and easy to process, especially the organic molecule could finely regulate their chemical structures by just functionalizing some organic group to suit the new requirements of magnetic properties. These new classes of magnetic materials solve some problems and disadvantages that inorganic materials have, but meanwhile they also bring new problems to these magnetic materials, i.e. Curie temperature (T_c the critical point temperature of magnetic ordered phase shift) of these organic magnetic materials is too low. For a general benzene ring connected nitronyl nitroxide spin molecule, the T_c is low to about 1 K. And most T_c of organic magnetic molecules are around the range from 1 K to 10 K. Many organic chemists and material scientists have put in a lot of effort for finding a new organic molecule where the T_c could stay around rt. That would be a huge and great advantage. If the target were fulfilled, many electronic magnetic devices would confront revolutionary change. In addition, the principles and relationships between magnetic properties of organic molecules and their aggregation or crystallization are still not perfect and need further investigation.

Another huge motivation is the urge to control and switch the spin magnetic materials among different magnetic or spin states, especially the procedure of change is reversible and repeatable. Depending on advantages of organic or organic-inorganic composite magnetic molecules are obvious comparing to the typical inorganic magnetic materials. Till to now, the typical pure inorganic molecules don't have possibility to control and switch the spin states at molecule level. And the requirements in different kinds of application field (such as QC memory devices, biology, chemotherapies, sensors or theoretical research) are the ability to control and switch the spin and magnetic states. So seeking a proper external stimuli factor to change the spin magnetic states of molecules or synthesizing a new organic radical structure which can respond to external condition's change is indispensable. The external perturbations in recent study about tunable or switchable spin molecules refer to thermal factor, pressure, photo, chemical redox conditions or mechanical force and so on. Some researchers believed that principle of the transitions of spin states could be explained by the concept of entropy driven process.^{62,71} As reviewed all above and based on molecular design and the application of spin magnetic materials, our research group is trying to synthesize novel organic spin magnetic molecule combine with stimuli responsive functional group to achieve our target. Meanwhile the spin magnetic properties and the reversibly tunable or switchable abilities are also under investigated by several characterized. This dissertation mainly display the novel SRR systems from three parts (1. temperature dependent spin coupling interactions responsive systems with organic diradicals. 2. redox stimuli spin responsive systems with the formation

of cation-radical diradicals. 3. photo induced spin responsive systems in organic catalytic reaction) which represent the most promising external stimulation factors respectively and also described some new methods of EPR to characterize and analyze spin magnetic molecules.

During the recent two decades, nitroxide radicals, as typical spin structure, have been used to synthesize spins materials with excellent stability which can exist even in 330 K and tolerant oxygen and water vapor. It gives a vital tool to investigate the spin coupling interactions in different situations. For example, the intramolecular spin interactions and intermolecular interactions, the spin interactions through chemical bond or through space, the switch of spin properties through external induced factors, and so on.

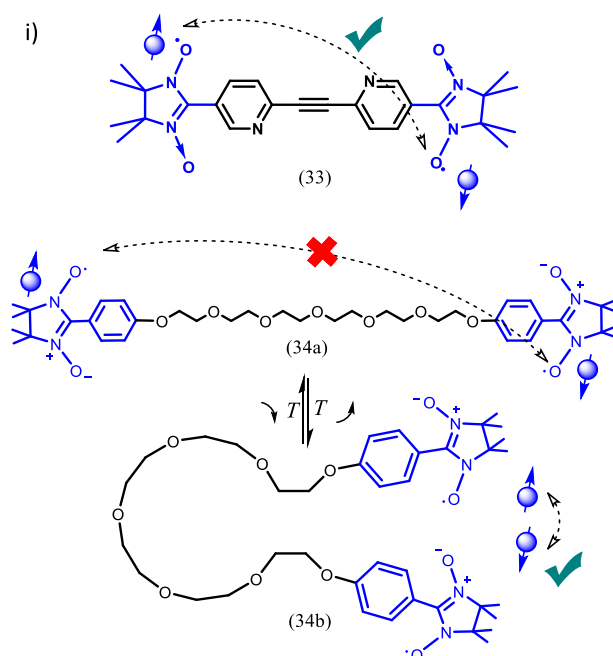


Figure 1-11. The distance between two spin units was turned by temperature

i) The conjugated bridges which mean all range π -bond connected could supply good channel for radicals intramolecular spin coupling interactions, like as alkyne, alkene, pyridine, phenylene, naphthaline, anthracene, pyrene and other heterocyclic aromatic ring or different assemble of them. A representative diradical structure coupling with conjugated bond synthesized by our research group, which is shown in figure 1-11 (33), can describe spin interaction case clearly. It is composed of two pyridines and one yne group as bridge. Two NN were connected in para-position. The results showed that these two NN radical have an antiferromagnetic J_{exp} nearly from -5.3 K to - 5.6 K. But an interesting question arised, what about the spin interactions of two NN radicals which bridged by unconjugated chemical bond

or how about the spin coupling performance through space. So we designed a biradical system consisting of two nitronyl nitroxide (NN) radicals bridged by diphenyl-hexa ethylene glycol chain [phenyl-O-(CH₂CH₂O)₆-phenyl] as shown in figure 1-11 (34a) which is a flexible amphiphilic polymer chain was synthesized. In this case, no possibility for this structure can acquire spin coupling interaction through chemical bond. The long range carbon carbon σ bond could not provide a way to transport electron. But due to the large hyperfine splitting signals and the spin coupling interactions which were found in EPR measurements, we could investigate whether the strong spin interaction was formed by the two NN through space. The flexible chain bend gives the chance for two NN end groups close enough for performing a spin coupling interaction, as shown in figure 1-11 (34b). The two conformations are two extreme structures which represent two different mutual exchangeable situations in this through-space system. One is stretched conformation and the other one is bent conformation. Our group use two conformational model which are representatives of countless conformation cases during the whole process to depict the T reversibly stimuli responsive system. The temperature stimuli responsive property comes from the changeable ratio between the two extreme conformations which directly influenced by the increase or decrease of T. Higher T has more tendency to impel the equilibrium to bent conformation. That means the quantity of molecule with bent conformations is becoming higher, (In other words, the interval time between bent conformations becomes shorter.) vice versa.

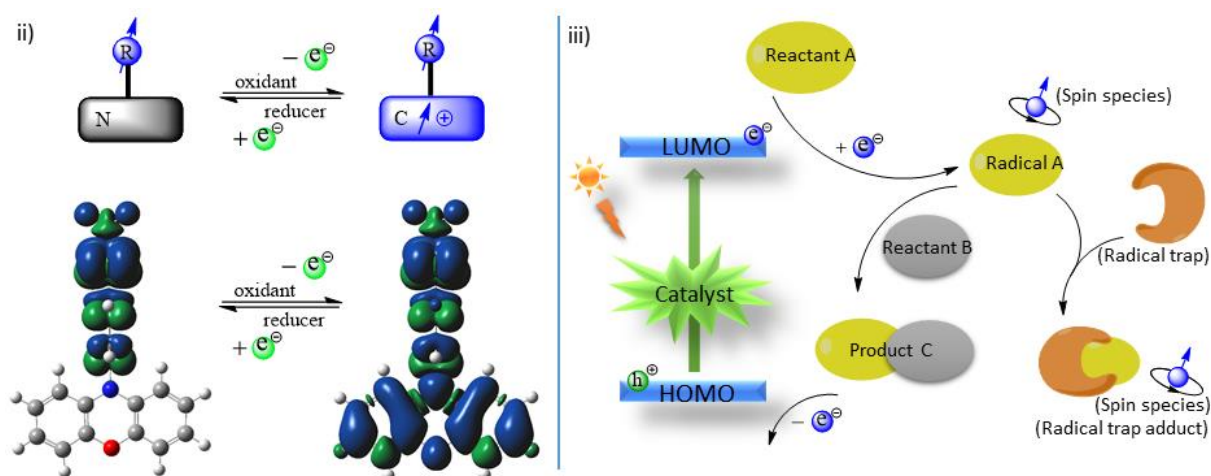


Figure 1-12. The transition of spin species through redox and photo

ii) As the introduction of 1.4.2 discussed, the investigation of transforms of spin species and the spin exchange interactions through redox factor is indispensable and has broad prospect of application. The electron transfer lead to the switching of spin properties and the

energy differences between close-shell structure and open-shell structure by oxidation and reduction reactions. We used the design philosophy to synthesize a NN radical group bridge to phenoxazin or phenothiazine with a para-position connected phenylene, as shown in figure 1-12 left. By using oxidant SbCl_5 and reducer Zn, the reversible transition with or without the diradical spin coupling interaction was discovered through EPR measurements. Three different stages emerged successively during the redox stimuli responsive process. The EPR spectrum which got seven lines pattern signal (suit for the simulation of EPR results) illustrate a new intermediate state containing diradical features. The seven lines pattern signal originated from the hyperfine splitting of three nitrogen nucleus. Two of them are the equivalent nitrogen nucleus in NN stable radical, another nitrogen nucleus is rooted from the new formed tertiary amine cation radical. The total spin-density distribution of molecule completely changed during the switching process.

iii) For the photo induced spin responsive systems, our objective is engaged in characterizing and analyzing the new formed intermediate spin species which are induced by external stimuli factor: visible light. Four different kinds of photo-catalytic reaction were under consideration. They are 1) photo oxidation, 2) [2 + 2] cycloaddition reactions about styrene derivatives, 3) α -alkylation of aldehyde derivatives and 4) cycloaddition of diphenylphosphine oxide derivatives and alkynes derivatives. The questions in photo induced spin responsive systems (what are the roles or functions of these intermediate spin species in the photo catalytic reactions, and how are the reactions mechanism triggered) are still not completely clear and need further investigation. Photocatalyst was excited by visible light, meanwhile the electron which belongs to the photocatalyst was active in LUMO and take part in the formation of intermediate spin species of catalytic reaction. Radical traps were used to “catch” the unstable intermediate spin species and transformed to stable radical trap adducts which also exhibited spin properties and are much easier to detect, as shown in figure 1-12 right. These processes can wholly be traced and be characterized by EPR measurements.

1.7. References

(1) Bloch, F. Zur Theorie des Ferromagnetismus (The Theory of Ferromagnetism). *Zeitschrift für Physik* **1930**, *61*, 206-219

- (2) Dyson, F. J. General Theory of Spin-Wave Interactions. *Phys. Rev.* **1956**, *102*, 1217-1230
- (3) Kubo, R. The Spin-Wave Theory of Antiferromagnetics. *Phys. Rev.* **1952**, *87*, 568-580
- (4) Seavey, M. H.; Tannenwald, P. E. Direct Observation of Spin-Wave Resonance. *Phys. Rev. Lett.* **1958**, *1*, 168-169
- (5) Rado, G. T.; Weertman, J. R. Spin-Wave Resonance in a Ferromagnetic Metal. *J. Phys. Chem. Solids* **1959**, *11*, 315-333
- (6) Cloizeaux, J.; Pearson, J. J. Spin-Wave Spectrum of the Antiferromagnetic Linear Chain. *Phys. Rev.* **1962**, *128*, 2131-2135
- (7) Kajiwara, Y.; Harii, K.; Takahashi, S.; Ohe, J.; Uchida, K.; Mizuguchi, M.; Umezawa, H.; Kawai, H.; Ando, K.; Takanashi, K.; Maekawa, S.; Saitoh, E. Transmission of Electrical Signals by Spin-Wave Interconversion in a Magnetic Insulator. *Nature* **2010**, *464*, 262-266
- (8) Qi, D. Z.; Kenaan, A.; Cui, D. X.; Song, J. Novel Insights into the Selection to Electron's Spin of Chiral Structure. *Nano Energy* **2018**, *52*, 142-152
- (9) Soria, J. F.; Vallejo, J.; Castellano, M.; Julve, M. Molecular Magnetism, Quo Vadis? A Historical Perspective from a Coordination Chemist Viewpoint. *Coord. Chem. Rev.* **2017**, *339*, 17-103
- (10) Su, Y. T.; Kinjo, R. Boron-Containing Radical Species. *Coord. Chem. Rev.* **2017**, *352*, 346-378
- (11) Fujita, W.; Awaga, K. Room-Temperature Magnetic Bistability in Organic Radical Crystals. *Science* **1999**, *286*, 261-262
- (12) Guzik, A. A.; Dutoi, D. A.; Love, P. J.; Gordon, M. H. Simulated Quantum Computation of Molecular Energies. *Science* **2005**, *309*, 1704-1707
- (13) Lloyd, S. A Potentially Realizable Quantum Computer. *Science* **1993**, *261*, 1569-1571
- (14) Affronte, M.; Troiani, F. Molecular Spins for Quantum Information Technologies. *Chem. Soc. Rev.* **2011**, *40*, 3119-3129
- (15) Aromi, G.; Aguila, D.; Gamez, P.; Luis, F.; Roubeau, O. Design of Magnetic Coordination Complexes for Quantum Computing. *Chem. Soc. Rev.* **2012**, *41*, 537-546
- (16) Suga, T.; Sugita, S.; Ohshiro, H.; Oyaizu, K.; Nishide, H. p- and n- Type Bipolar Redox-Active Radical Polymer: Toward Totally Organic Polymer-Based Rechargeable Devices with Variable Configuration. *Adv. Mater.* **2011**, *23*, 751-754
- (17) Morita, Y.; Nishida, S.; Murata, T.; Moriguchi, M.; Ueda, A.; Satoh, M.; Arifuku, K.; Sato, K.; Takui, T. Organic Tailored Batteries Materials Using Stable Open-Shell Molecules with Degenerate Frontier Orbitals. *Nat. Mater.* **2011**, *10*, 947-951

- (18) Janoschka, T.; Teichler, A.; Häupler, B.; Jähnert, T.; Hager, M. D.; Schubert, U. S. Reactive Inkjet Printing of Cathodes for Organic Radical Batteries. *Adv. Energy Mater.* **2013**, *3*, 1025-1028
- (19) Nakahara, K.; Oyaizu, K.; Nishide, H. Organic Radical Battery Approaching Practical Use. *Chem. Lett.* **2011**, *40*, 222-227
- (20) Nishide, H.; Oyaizu, K. Toward Flexible Batteries. *Science* **2008**, *319*, 737-738
- (21) Janoschka, T.; Hager, M. D.; Schubert, U. S. Powering up the Future: Radical Polymers for Battery Applications. *Adv. Mater.* **2012**, *24*, 6397-6409
- (22) Kato, F.; Kikuchi, A.; Okuyama, T.; Oyaizu, K.; Nishide, H. Nitroxide Radicals as Highly Reactive Redox Mediators in Dye-Sensitized Solar Cells. *Angew. Chem. Int. Ed.* **2012**, *124*, 10324-10327
- (23) Zhang, D.; Basel, T. P.; Gautam, B. R.; Yang, X. M.; Mascaro, D. J.; Liu, F.; Vardeny, Z. V. Spin-Enhanced Organic Bulk Heterojunction Photovoltaic Solar Cells. *Nat. Commun.* **2012**, *3*, 1043
- (24) Slota, M.; Keerthi, A.; Tretyakov, E.; Baumgarten, M.; Müllen, K.; Bogani, L. Magnetic Edge States and Coherent Manipulation of Graphene Nanoribbons. *Nature* **2018**, *557*, 691-695
- (25) Wang, Y.; Wang, H. M.; Liu, Y. Q.; Di, C. A.; Sun, Y. M.; Wu, W. P.; Yu, G.; Zhang, D. Q.; Zhu, D. B. 1-Imino Nitroxide Pyrene for High Performance Organic Field-Effect Transistors with Low Operating Voltage. *J. Am. Chem. Soc.* **2006**, *128*, 13058-13059
- (26) Aoki, K.; Akutsu, H.; Yamada, J.; Nakatsuji, S.; Kojima, T.; Yamashita, Y. The First Organic Radical Compounds Exhibiting n-Type FET Properties. *Chem. Lett.* **2009**, *38*, 112
- (27) Gomes, A.; Fernandes, E.; Lima, J. Fluorescence Probes Used for Detection of Reactive Oxygen Species. *J. Biochem. Biophys. Methods* **2005**, *65*, 45-80
- (28) Griffith, O. H.; Waggoner, A. S. Nitroxide Free Radicals: Spin Labels for Probing Biomolecular Structure. *Acc. Chem. Res.* **1969**, *2*, 17-24
- (29) Dizdaroglu, M.; Rodriguez, Henry. Free Radical-Induced Damage to DNA: Mechanisms and Measurement. *Free Radical Biology & Medicine* **2002**, *32*, 1102-1115
- (30) Iranmanesh, M.; Hulliger, J. Magnetic Separation: Its Application in Mining, Waste Purification, Medicine, Biochemistry and Chemistry. *Chem. Soc. Rev.* **2017**, *46*, 5925-5934
- (31) Ratera, I.; Veciana, J. Playing with Organic Radicals as Building Blocks for Functional Molecular Materials. *Chem. Soc. Rev.* **2012**, *41*, 303-349
- (32) Miller, J. S. Magnetically Ordered Molecule-Based Materials. *Chem. Soc. Rev.* **2011**, *40*, 3266-3296

- (33) Abe, M. Diradicals. *Chem. Rev.* **2013**, *113*, 7011-7088
- (34) Neumann, W. P.; Penenory, A.; Stewen, U.; Lehnig, M. Stabilization of Free Radicals by Substituents As Studied by Using Triphenylmethylys. *J. Am. Chem. Soc.* **1989**, *111*, 5845-5851
- (35) Neumann, W. P.; Uzick, W.; Zarkadis, A. K. Substituent-Dependent Stabilization of Para-Substituted Triphenylmethyl Radical. *J. Am. Chem. Soc.* **1986**, *108*, 3762-3770
- (36) Ballester, M. Inert Free Radicals (IFR): A Unique Trivalent Carbon Species. *Acc. Chem. Res.* **1985**, *18*, 380-387
- (37) Abe, M.; Ye, J. H.; Mishima, M. The Chemistry of Localized Singlet 1,3-Diradicals (Biradicals): from Putative Intermediates to Persistent Species and Unusual Molecules with a π -Single Bonded Character. *Chem. Soc. Rev.* **2012**, *41*, 3808-3820
- (38) Kita, F.; Adam, W.; Jordan, P.; Nau, W. M.; Wirz, J. 1,3-Cyclopentanediyyl Diradicals: Substituent and Temperature Dependence of Triplet-Singlet Intersystem Crossing. *J. Am. Chem. Soc.* **1999**, *121*, 9265-9275
- (39) Chandross, E. A. Bisgalvinoxyl, a Stable Triplet. *J. Am. Chem. Soc.* **1964**, *86*, 1263-1264
- (40) Bushby, R. J.; McGill, D. R.; Ng, K. M.; Taylor, N. Disjoint and Coextensive Diradical Diiions. *J. Chem. Soc. Perkin Trans.* **1997**, *2*, 1405-1414
- (41) Borden, W. T.; Davidson, E. R. Effects of Electron Repulsion in Conjugated Hydrocarbon Diradicals. *J. Am. Chem. Soc.* **1977**, *99*, 4587-4594
- (42) Dupeyre, E. M.; Lemaire, H.; Rassat, A. A Stable Biradical in the Nitroxide Series. *J. Am. Chem. Soc.* **1965**, *87*, 3771-3772
- (43) Blundell, S. J.; Pratt, F. L. Organic and Molecular Magnets. *J. Phys. Condens. Matter* **2004**, *16*, 771-828
- (44) Caneschi, A.; Gatteschi, D.; Rey, P. The Chemistry and Magnetic-Properties of Metal Nitronyl Nitroxide Complexes. *Prog. Inorg. Chem.* **1991**, *39*, 331-429
- (45) Benelli, C.; Gatteschi, D. Magnetism of Lanthanides in Molecular Materials with Transition-Metal Ions and Organic Radicals. *Chem. Rev.* **2002**, *102*, 2369-2387
- (46) Ipe, B. I.; Lehnig, M.; Niemeyer, C. M. On the Generation of Free Radical Species from Quantum Dots. *Small* **2005**, *1*, 706-709
- (47) Green, M.; Howman, E. Semiconductor Quantum Dots and Free Radical Induced DNA Nicking. *Chem. Commun.* **2005**, *0*, 121-123
- (48) Jiang, H.; Ju, H. X. Electrochemiluminescence Sensors for Scavengers of Hydroxyl Radical Based on Its Annihilation in CdSe Quantum Dots Film/Peroxide System. *Anal. Chem.* **2007**, *79*, 6690-6696

- (49) Zheng, X.; Wang, S. Y.; Qiu, Y. F.; Li, Y. T.; Zhou, C. K.; Sui, Y. X.; Ma, J.; Wang, X. P. One-Electron Oxidation of an Organic Molecule by $B(C_6F_5)_3$; Isolation and Structures of Stable Non-*para*-Substituted Triarylamine Cation Radical and Bis(triarylamine) Dication Diradicaloid. *J. Am. Chem. Soc.* **2013**, *135*, 14912-14915
- (50) Kuratsu, M.; Kozaki, M.; Okada, K. 2,2':6'2'':6'',6-Trioxotriphenylamine: Synthesis and Properties of the Radical Cation and Neutral Species. *Angew. Chem. Int. Ed.* **2005**, *44*, 4056-4058
- (51) Okada, K.; Imakura, T.; Oda, M.; Murai, H. 10,10'-(*m*- and *p*-Phenylene)diphenothiazine Dications: Violation of a Topology Rule in Heterocyclic High-Spin π -Systems. *J. Am. Chem. Soc.* **1996**, *118*, 3047-3048
- (52) Fritsche, L.; Weimert, B. First-Principles Theory of Ferromagnetic and Antiferromagnetic Order. *Phys. Stat. Sol.* **1998**, *208*, 287-337
- (53) Alberola, A.; Less, R. J.; Pask, C.M.; Rawson, J. M. A Thiazyl-Based Organic Ferromagnet. *Angew. Chem. Int. Ed.* **2003**, *42*, 4782-4785
- (54) Roessler, M. M.; Salvadori, E. Principles and Applications of EPR spectroscopy in the Chemical Sciences. *Chem. Soc. Rev.* **2018**, *47*, 2534-2553
- (55) Miller, J. S.; Epstein, A. J. Organic and Organometallic Molecular Magnetic Materials-Designer Magnets. *Angew. Chem. Int. Ed.* **1994**, *33*, 385-415
- (56) Meng, H.; Li, G. Q. A Review of Stimuli-Responsive Shape Memory Polymer Composites. *Polymer* **2013**, *54*, 2199-2221
- (57) Liu, F.; Urban, M. W. Recent Advances and Challenges in Designing Stimuli-Responsive Polymers. *Prog. Polym. Sci.* **2010**, *35*, 3-23
- (58) Roy, D.; Cambre, J. N.; Sumerlin, B. S. Future Perspectives and Recent Advances in Stimuli-Responsive Materials. *Prog. Polym. Sci.* **2010**, *35*, 278-301
- (59) Yan, X. Z.; Wang, F.; Zheng, B.; Huang, F. H. Stimuli-Responsive Supramolecular Polymeric Materials. *Chem. Soc. Rev.* **2012**, *41*, 6042-6065
- (60) Theato, P.; Sumerlin, B. S.; O'Reilly, R. K.; Epps, T. H. Stimuli Responsive Materials. *Chem. Soc. Rev.* **2013**, *42*, 7055
- (61) Mura, S.; Nicolas, J.; Couvreur, P. Stimuli-Responsive Nanocarriers for Drug Delivery. *Nature Materials* **2013**, *12*, 991-1003
- (62) Sato, O.; Tao, J.; Zhang, Y. Z. Control of Magnetic Properties through External Stimuli. *Angew. Chem. Int. Ed.* **2007**, *46*, 2152-2187
- (63) Parmon, V. N.; Kokorin, A. I.; Zhidomirov, G. M.; Zamaraev, K. I. On the Mechanism of Spin Exchange in Long-Chain Nitroxide Biradicals. *Mol. Phys.* **1975**, *30*, 695-701.

- (64) Parmon, V. N.; Kokorin, A. I.; Zhidomirov, G. M. Conformational Structure of Nitroxide Biradicals Use of Biradicals as Spin Probes. *J. Struct. Chem.* **1977**, *18*, 104-147.
- (65) Ionita, G.; Vorobieva, G. A.; Chechik, V.; Kokorin, A. I. Intramolecular Spin Exchange in Flexible Peg-Based Nitroxide Biradicals in Aqueous Solutions. *Appl. Magn. Res.* **2015**, *46*, 251-260.
- (66) Baumgarten, M.; Gügel, A. EPR and Optical Absorption Spectra of Reduced Buckminsterfullerene. *Adv. Mater.* **1993**, *5*, 458-461
- (67) Oka, H. Synthesis and Magnetic Properties of Orthogonally Linked Phenothiazine Cation Radical Dimer and Tetramer. *Org. Lett.* **2010**, *12*, 448-451
- (68) Okamoto, T.; Kuratsu, M.; Kozaki, M.; Okada, K. Remarkable Structure Deformation in Phenothiazine Trimer Radical Cation. *Org. Lett.* **2004**, *6*, 3493-3496
- (69) Sugawara, T.; Komatsu, H.; Suzuki, K. Interplay Between Magnetism and Conductivity Derived from Spin-Polarized Donor Radicals. *Chem. Soc. Rev.* **2011**, *40*, 3105-3118
- (70) Ito, A.; Kurata, R.; Sakamaki, D.; Yano, S.; Kono, Y.; Nakano, Y.; Furukawa, K.; Kato, T.; Tanaka, K. Redox Modulation of *para*-Phenylenediamine by Substituted Nitronyl Nitroxide Groups and Their Spin States. *J. Phys. Chem. A* **2013**, *117*, 12858-12867
- (71) Nakatsuji, S. Recent Progress toward the Exploitation of Organic Radical Compounds with Photo-Responsive Magnetic Properties. *Chem. Soc. Rev.* **2004**, *33*, 348-353
- (72) Skubi, K. L.; Blum, T. R.; Yoon, T. P. Dual Catalysis Strategies in Photochemical Synthesis. *Chem. Rev.* **2016**, *116*, 10035-10074
- (73) Hamachi, K.; Matsuda, K.; Itoh, T.; Iwamura, H. Synthesis of An Azobenzene Derivative Bearing Two Stable Nitronyl Nitroxide Radicals as Substituents and Its Magnetic Properties. *Bull. Chem. Soc. Jpn.* **1998**, *71*, 2937
- (74) Matsuda, K.; Irie, M. A Diarylethene with Two Nitronyl Nitroxides: Photoswitching of Intramolecular Magnetic Interaction. *J. Am. Chem. Soc.* **2000**, *122*, 7195-7201
- (75) Matsuda, K.; Irie, M. Photoswitching of Intramolecular Magnetic Interaction Using a Photochromic Spin Coupler: An ESR Study. *J. Am. Chem. Soc.* **2000**, *122*, 8309-8310
- (76) Teki, Y.; Miyamoto, S.; Nakatsuji, M.; Miura, Y. π -Topology and Spin Alignment Utilizing the Excited Molecular Field: Observation of the Excited High-Spin Quartet ($S = 3/2$) and Quintet ($S = 2$) States on Purely Organic π -Conjugated Spin Systems. *J. Am. Chem. Soc.* **2001**, *123*, 294-305
- (77) Veber, S. L.; Fedin, M. V.; Ovcharenko, V. I.; Bagryanskaya, E. G. High-Field EPR Reveals the Strongly Temperature-Dependent Exchange Interaction in “Breathing” Crystals $\text{Cu}(\text{hfac})_2\text{L}^{\text{R}}$. *J. Am. Chem. Soc.* **2008**, *130*, 2444-2445

- (78) Kahn, O.; Martinez, C. J. Spin-Transition Polymers: From Molecular Materials Toward Memory Devices. *Science* **1998**, *279*, 44-48
- (79) Soule, B. P.; Hyodo, F.; Matsumoto, K. I.; Simone, N. L.; Cook, J. A.; Krishna, M. C.; Mitchell, J. B. The Chemistry and Biology of Nitroxide Compounds. *Free Radical Biology & Medicine* **2007**, *42*, 1632-1650
- (80) Duan, M.; Shapter, J. G.; Qi, W.; Yang, S.; Gao, G. Recent Progress in Magnetic Nanoparticles: Synthesis, Properties, and Applications. *Nanotechnology* **2018**, *29*, 452001-452017
- (81) Dosev, D.; Nichkova, M.; Dumas, R. K.; Gee, S. J.; Hammock, B. D.; Liu, K.; Kennedy, I. M. Magnetic/Luminescent Core/Shell Particles Synthesized by Spray Pyrolysis and Their Application in Immunoassays with Internal Standard. *Nanotechnology* **2007**, *18*, 055102-055107
- (82) Kluchova, K.; Zboril, R.; Petridis, D. Superparamagnetic Maghemite Nanoparticles from Solid-State Synthesis – Their Functionalization towards Peroral MRI Contrast Agent and Magnetic Carrier for Trypsin Immobilization. *Biomaterials* **2009**, *30*, 2855-2863
- (83) Son, S. J.; Reichel, J.; He, B.; Schuchman, M.; Lee, S. B. Magnetic Nanotubes for Magnetic-Field-Assisted Bioseparation, Biointeraction, and Drug Delivery. *J. Am. Chem. Soc.* **2005**, *127*, 7316-7317
- (84) Ladd, T.D.; Jelezko, F.; Laflamme, R.; Nakamura, Y. Monroe, C. O'Brien, J. L. Quantum Computers. *Nature* **2010**, *464*, 45-53
- (85) Sato, K.; Nakazawa, S.; Takui, T. Molecular Electron-Spin Quantum Computers and Quantum Information Processing: Pulse-Based Electron Magnetic Resonance Spin Technology Applied to Matter Spin-Qubits. *J. Mater. Chem.* **2009**, *19*, 3739-3754
- (86) Leuenberger, M. N.; Loss, D. Quantum Computing in Molecular Magnets. *Nature* **2001**, *410*, 789-793

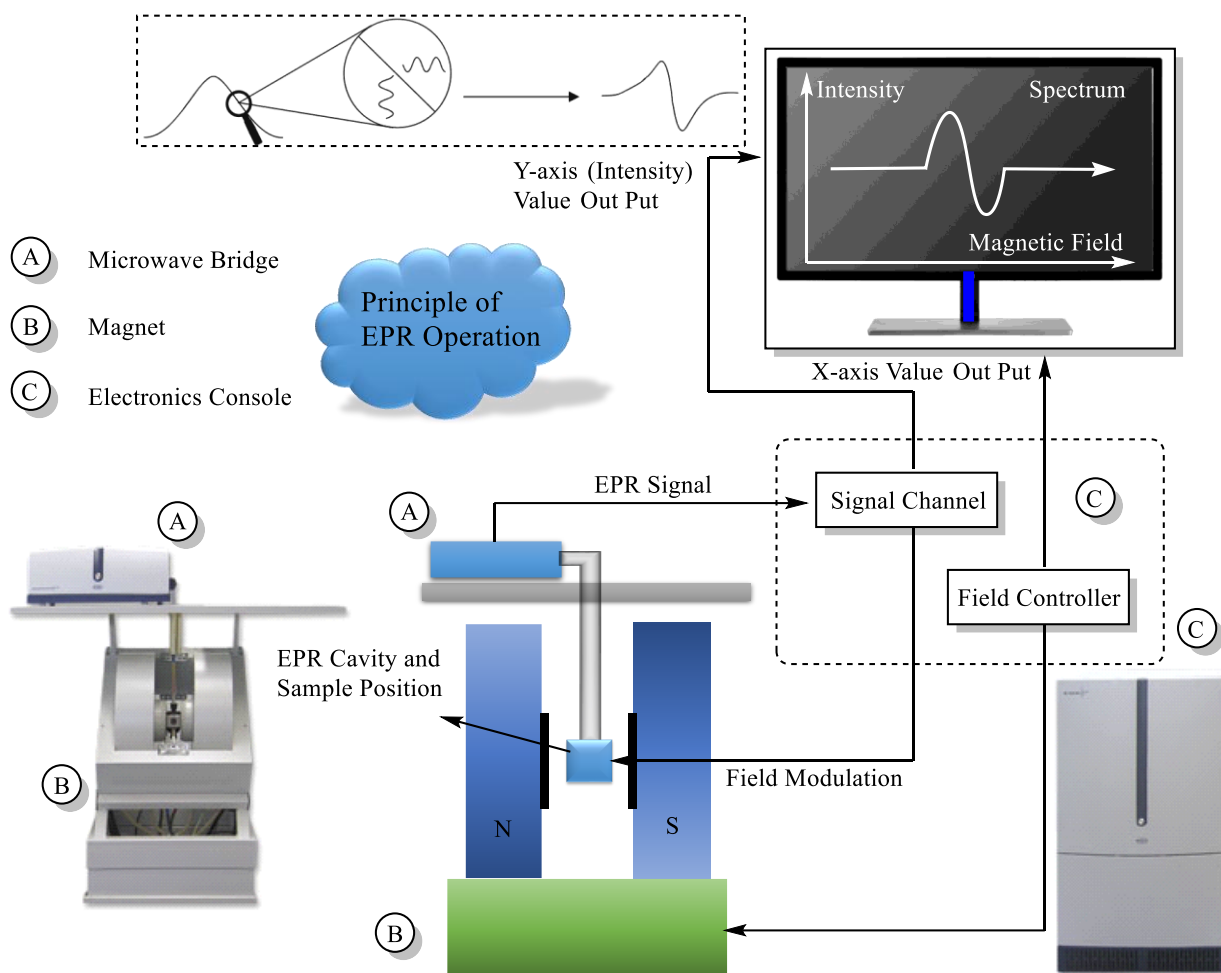
Chapter 2 EPR Measurements and Spectroscopic Details

2.1 Introduction

Electron paramagnetic resonance (EPR) no matter whether continuous wave (CW) or pulsed methods are playing more and more important roles in both industrial and academic research fields for increasing demands. It can be applied in several disciplines as: physics, chemistry, biology, materials science and medical or clinical science.¹ This chapter mainly discusses about the CW-EPR's measurements, applications and interpretation of EPR spectroscopy on quantitative level.²⁻¹⁶ In general, EPR is a spectroscopic technique that can detect the resonance signal of materials or samples with or containing unpaired electrons. These species include organic free radicals, various transition metal metal ions and their complexes. Normally, species with unpaired electrons are not stable and most of them have short lifetimes. So it is hard to characterize them for most of instrumental measurements. These external restrictions made EPR become a unique and the most important measurement for characterizing radical or spin species.

Here are sorted several issues which can be solved by interpretation of EPR spectroscopy: does the sample contain radical or spin center? What is the structure of the radical or the structure surrounding? How many spin centers every molecule has? What is the relative concentration of radical or spin center in a specific sample? And the questions concerning how do the spin interactions, molecular motion and relaxation times of the sample molecule display. The experimental data from EPR measurements which provide detailed information about radicals and spin centers can be subdivided into four categories. 1) The intensity height of EPR signal peaks I_d and the integrated intensity of EPR signal I_i belong to one category. These two parameters are very important information to acquire quantitative spin concentration of samples for monitor reaction or investigate the kinetics or mechanism of various reactions. 2) The g factor which is an identification of every radicals as the main parameter to distinguish the radicals or spin species. 3) The hyperfine splitting parameter " A_i " which is derived from the nucleus or surrounding nucleus hyperfine coupling offer the details about the structure of spin species. 4) The parameters D and E which are acquired from the zero field splitting for the situation of more than one unpaired electron ($S \geq 1$), could provide information about spin-spin interactions. The value of D can reflect the distance between two interacting spins, while the value of E can describe the deviation of electron density distribution from symmetry axis.

2.2. Description of EPR Instrument



Scheme 2-1. The diagram of continuous wave EPR instrumentations

The diagrammatic sketch of the components of EPR instrument and the operational principle is shown in scheme 2-1 above. EPR instrument is made up of three main parts: a microwave bridge (labeled "A"), an electromagnet component (labeled "B") and an electronics console (labeled "C"). The microwave bridge can radiate microwave upon the cavity where the sample measurement located in. The microwave bridge also contain a detector diode which can accept and deal with the microwave radiation reflected back from the cavity. Microwaves cast onto the cavity via a hole called iris which contain a screw to adjust the signal matching (it adjusts the power in cavity to obtain an optimized measurement position). The B component is a big electromagnet which could provide a tunable magnetic field. The magnetic field is derived from electric field. Generally, the electric and magnetic

components of the fields were associated and perpendicular to each other. And the direction of propagation and oscillate is in a narrow range with a specific frequency ν . The component electronics console labeled C is a composite platform, which is made up of signal channel and magnetic field controller, for analyzing and dealing with all the signals with a proper modulation amplitude, frequency and time constant to obtain an optimized EPR spectrum (the dependence of signal intensity and magnitude of magnetic field).

2.3. EPR Measurement and Interpretation of EPR Spectroscopy

2.3.1. Performance of Unpaired Electron or Spin in Magnetic Field (Zeeman Effect)

The intrinsic essence of EPR spectroscopy is the interaction between electromagnetic radiation and the sample's magnetic moments. Every electron has electron spin quantum state ($S = 1/2$) and owns the value of spin magnetic moments $9.274009 \times 10^{-24} \text{ JT}^{-1}$ (Bohr magneton). While molecule contain unpaired electrons, it becomes a spin active species. When the spin species in a magnetic field, it would exhibit Zeeman effect. That means the energy levels of unpaired electron splitted to two different energy states. The difference between the two energy states is also called electronic Zeeman energy ΔE , as shown in figure 2-1. The lower energy state of the spin species which owns $M_s = +1/2$ is aligned with or the magnetic field (parallel), while the higher energy state which owns $M_s = -1/2$ is aligned against to the magnetic field (antiparallel). The energy value are shown in equation (2-1, 2-2). The energy difference between the different spin states diverge linearly as the magnetic field increases. EPR could reflect the energy difference ΔE by offering an absorption which is usually derivative of spectrum. The value of g factor can be calculated by the equation of ΔE and the magnitude of magnetic field, namely the relationships of microwave frequency ν and magnitude of magnetic field B_0 , as shown in equation (2-3, 2-4 and 2-5). h and μ_B are Planck constant and the magnetic moment of unpaired electron belongs to sample respectively.

G factor of free electron which labeled g_e equals 2.00232. Generally, similar structures or categories lead to similar g factors. G factor would slightly shift by the influence of the nuclei the unpaired electron bonded and the total chemical structure around the spin species. So the difference of g factors of samples could be concluded as the equation (2-7, 2-8) compared to the g factor of free electron. Some different structures of radicals with different g factor range are taken as example, benzosemiquinones, which have most spin density on oxygens owns g factor around 2.004, while the category of nitroxide radicals which the most

spin distribution is around nitroxide group possess g factor around 2.006 ~ 2.007. In addition, metal ions which contain unpaired electrons have a huge different g-factors compared to organic radicals. Such as the g factor of Cu^{2+} can be as large as 2.3 (the value largely depend on the geometry of complex). Hence, g factor can directly provide information of chemical structure, just like a fingerprint of the radical sample.

$$E_{\alpha} = +\frac{1}{2}g \mu_B B_0 \quad (2-1)$$

$$E_{\beta} = -\frac{1}{2}g \mu_B B_0 \quad (2-2)$$

$$\Delta E = E_{\alpha} - E_{\beta} = g \mu_B B_0 \Delta m_s = g \mu_B B_0 \quad (2-3)$$

$$\Delta E = h\nu = g \mu_B B_0 \quad (2-4)$$

$$g = h\nu / \mu_B B_0 \quad (2-5)$$

$$\mu_B = g_e \beta / 2 \quad (2-6)$$

$$h\nu = g_e \beta (B_e + \delta B) \quad (2-7)$$

$$h\nu = (g_e + \delta g)\beta B = g \beta B \quad (2-8)$$

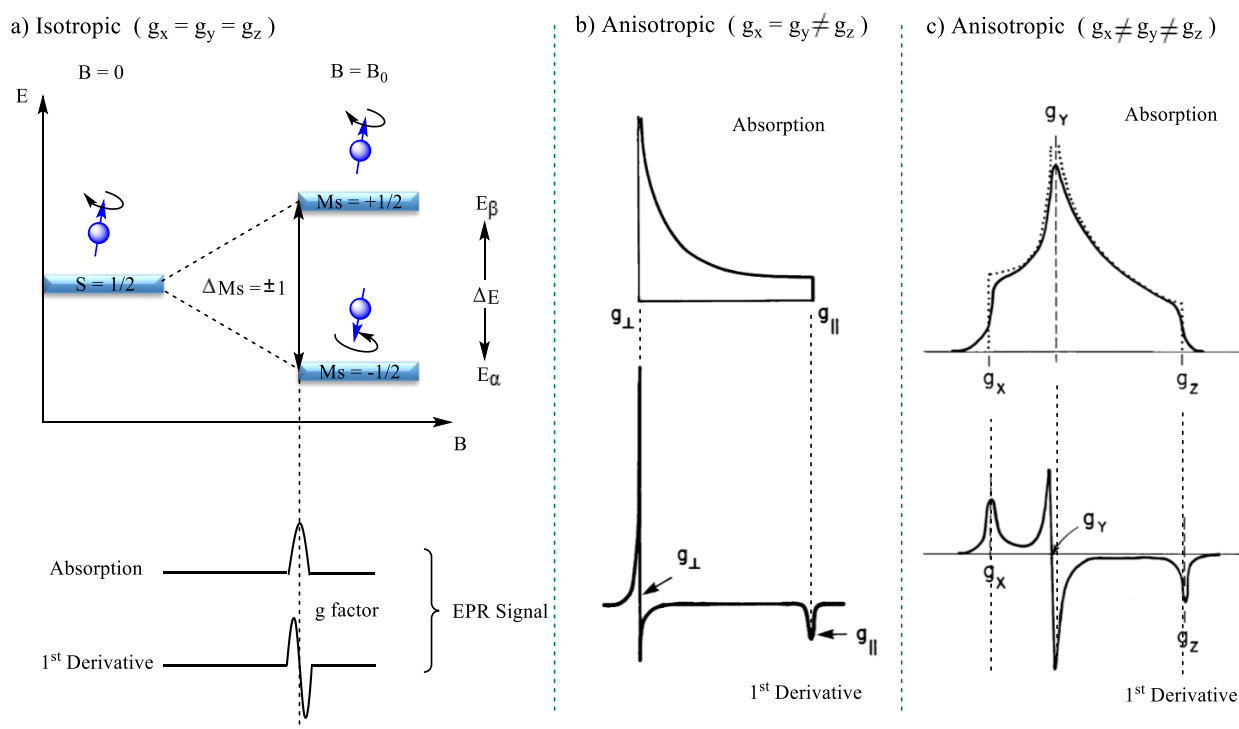


Figure 2-1. Zeeman effect in EPR measurements for isotropic and anisotropic cases.

Actually, for a specific spin species, the signal pattern of EPR absorption considerably depends on the direction of δg in (x, y, z) axis-three dimensional systems. For an isotropic system, which means $g_x = g_y = g_z$, the EPR absorption and first derivatives are symmetric, as shown in figure 2-1 (a). But in anisotropic system, there are two situations which are different from isotropic system. One situation is $g_x = g_y \neq g_z$. we could find that the EPR absorption and first derivatives are not symmetric like the situation (a). It comes two new concepts, $g_{//}$ and g_{\perp} which means $g_{//} = g_z$ and $g_{\perp} = g_{xy}$ respectively. The apparent value of g factor was presented by two different g factor: $g_{//}$ and g_{\perp} . The EPR absorption at the position of g_{\perp} is higher than the absorption at the position of $g_{//}$. The reason is the higher chance of B-vector in xy-plane than parallel to z-axis for every individual spin species in total anisotropic system (considering probability statistics). The other anisotropic situation possessed $g_x \neq g_y \neq g_z$ present an EPR absorption peak with two unsymmetrical shoulder peaks. It means the apparent value of g factor is presented by three different g factors: g_x , g_y and g_z , as shown in figure 2-1 (c). The first derivative of absorption is also completely different from isotropic system. For the normal cases which the samples are dissolved in liquid solution (isotropic system), the peaks of EPR signal is centrosymmetric. Here the concepts of isotropic samples and anisotropic samples for EPR measurements should be made clearly. The isotropic samples are e.g. in liquid solution where molecules rapid moving with Brownian motion, while the anisotropic samples are in the solid state, e.g. frozen solution, diluted powders or crystals and so on. The molecules in these systems are fixed and can not relatively move or rotate.

Table 2-1. The relationships between microwave frequency and magnitude of magnetic field in different microwave band regions.

Microwave Band	Microwave Frequency (MHz)	B_0 (Gauss) (for $g = 2$)
L	1000	357.2
S	3000	1071.7
X	9000	3215.0
K	24000	8573.4
Q	35000	12502.9
W	94000	33579.3

The microwave band for measurement of electron normally was divided into six different band based on the value of frequency, as shown in table 2-1 above. Microwave X

band which labeled in red box in table 2-1 generally was chosen for EPR measurements with the frequency around 9 ~ 10 GHz. The intensity range of magnetic field where the radical signal appeared is normally around 3000 ~ 3500 gauss, because most of the g factor of radical samples are close to 2.

2.3.2. Principle of Hyperfine Splitting

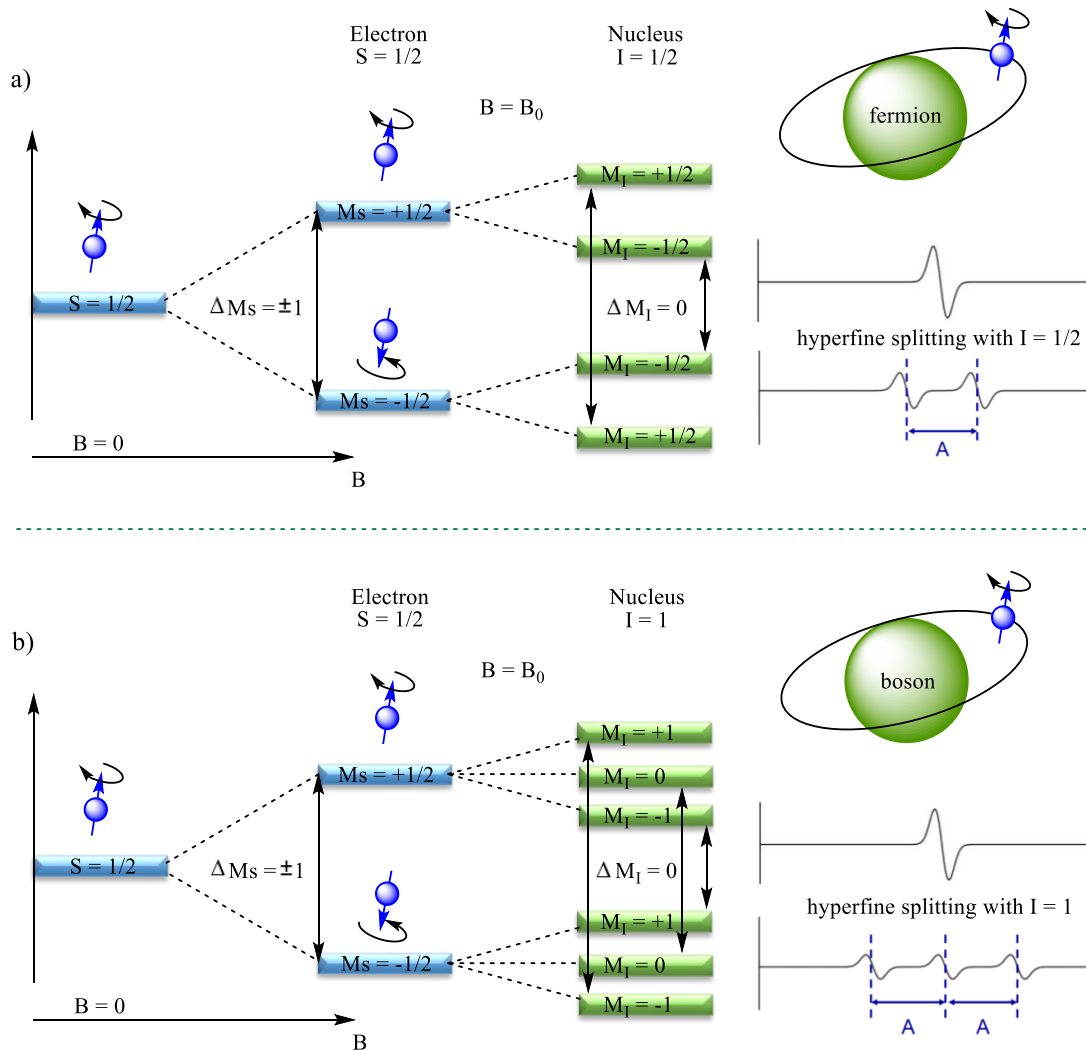


Figure 2-2. The hyperfine splitting of $I = 1/2$ nucleus and $I = 1$ nucleus in EPR measurements

Hyperfine splitting in EPR signal is derived from the interaction of unpaired electron spin with the nucleus spin around. The splitting principle is shown in the figure 2-2. Resonance signals, which are the transitions among several new quantization energy levels originated from nearby nucleus spin interactions, could be detected. This resonance transitions should obey the quantum selection rules that $|\Delta M_S| = 1$ and $|\Delta M_I| = 0$. The new energy level quantization from nucleus of $I = 1/2$ could split into two states $M_I = \pm 1/2$ for every electron spin state in magnetic field. So there are two transitions are allowed for $I = 1/2$ situation.

While three transitions are allowed for $I = 1$, because of three states are split by nuclear spin interactions for every electron spin state ($M_I = \pm 1$ and $M_I = 0$). Hence the EPR signal of the two situations are also split into double-peaks pattern and triple-peaks pattern respectively. The distance between two new splitting peaks is the hyperfine coupling constant A . The position of original non-splitting signal would be exactly in the middle of the two new hyperfine splitting peaks. (This rule is used for isotropic case in diluted solution.)

All the nucleus of atoms can be divided into two categories: Boson and Fermion by the mass number of nucleus. If the mass number is odd, the nucleus is Fermion. While the mass number is even, the nucleus belongs to Boson. The nucleus spin quantum number of Boson is integer, such as ^{12}C , ^{16}O ($I = 0$) and ^2D , ^{14}N ($I = 1$), while the number I of Fermion is half integer, such as ^1H , ^{13}C and ^{15}N ($I = 1/2$).

Table 2-2. The list of isotope (mass number), the nucleus spin quantum number (I) and the number EPR splitting peaks about non-metallic elements

Atom (Non-Metallic Element)	Isotope (Mass Number)	Nucleus Spin Number (I)	EPR Splitting Pattern
H	1 (99.9%)	1/2	2
C	13 (1.1%)	1/2	2
N	14 (99.6%)	1	3
N	15 (0.4%)	1/2	2
F	19	1/2	2
P	31	1/2	2
Cl	35 (75.8%)	3/2	4

Some selected nucleus isotope, the nucleus spin quantum number (I) and the number EPR splitting peaks of non-metallic elements are listed in table 2-2.

2.3.3. Analysis of the EPR Signal Splitting Pattern

For a single nucleus spin influenced electron spin species, the hyperfine splitting number of signal pattern obey the rule $2I + 1$. But when the influences of nucleus around are more than one, the situations become complicated. To the several equivalent spins of nuclei,

we can use the rule $2nI + 1$ to calculate the number of hyperfine splitting, n stands for the number of equivalent nuclei. While the nuclei nearby the electron spin species are inequivalent, or the hyperfine interactions arise from different nucleus. the number of splitting is much complicated (normally, the number of splitting is less than the number calculated by the rule $(2n_a I_a + 1) \times (2n_b I_b + 1) \times (2n_c I_c + 1) \times \dots$, a, b and c stand for different types of nucleus) and depend on the different values of A_i attributed to various nucleus.

The figure 2-3 below shows two situations of hyperfine splitting of equivalent $n \times$ nucleus for Fermion a) and Boson b), respectively. The numbers of hyperfine splitting and the relative intensities of each splitting peaks are obey Pascal triangle ratio distributions. The ratio of intensities of every splitting peaks to Fermion and Boson, and the peaks splitting number of them are both different.

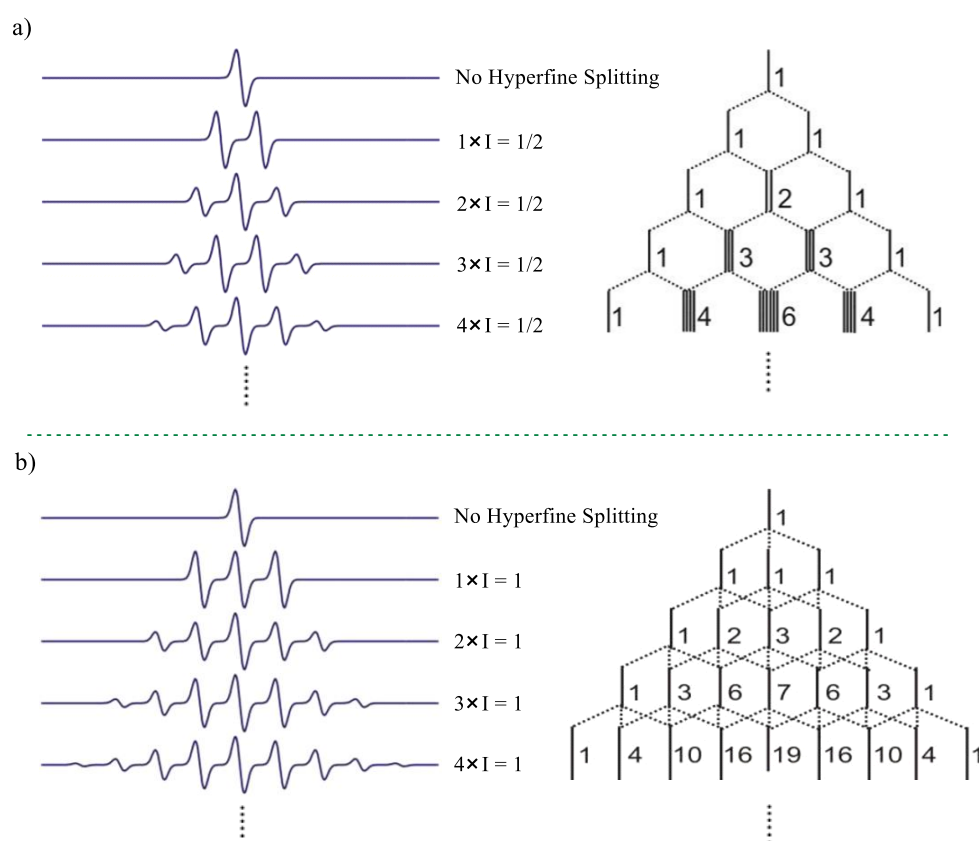


Figure 2-3. The splitting of EPR signals by equivalent nucleus effect from 0 nucleus to 4 nucleus for $I = 1/2$ and $I = 1$, respectively.

We show four typical hyperfine splitting patterns of organic radical species which could represent most cases in general situations in figure 2-4. The first example a) is *tert*-butyl

nitroxide which only contains one nucleus ($I = 1$) hyperfine interaction split a triplet lines pattern in EPR spectrum. The second radical species is radical trap PBN adduct which contains a nucleus ($I = 1$) and a nucleus ($I = 1/2$) hyperfine interactions split to three doublet signals. Two bottom examples of figure 2-4 c) and d) are both nitroxide radicals and both contain two nuclei hyperfine interactions. But the splitting is different, due to the two interaction nuclei are equivalent or not. For the equivalent case c), quintet lines pattern signals with ratio of $1 : 2 : 3 : 2 : 1$ acquired, while the inequivalent case d), heptet lines pattern with ratio of $1 : 1 : 2 : 1 : 2 : 1$ acquired (a_{N1} and a_{N2} are different).

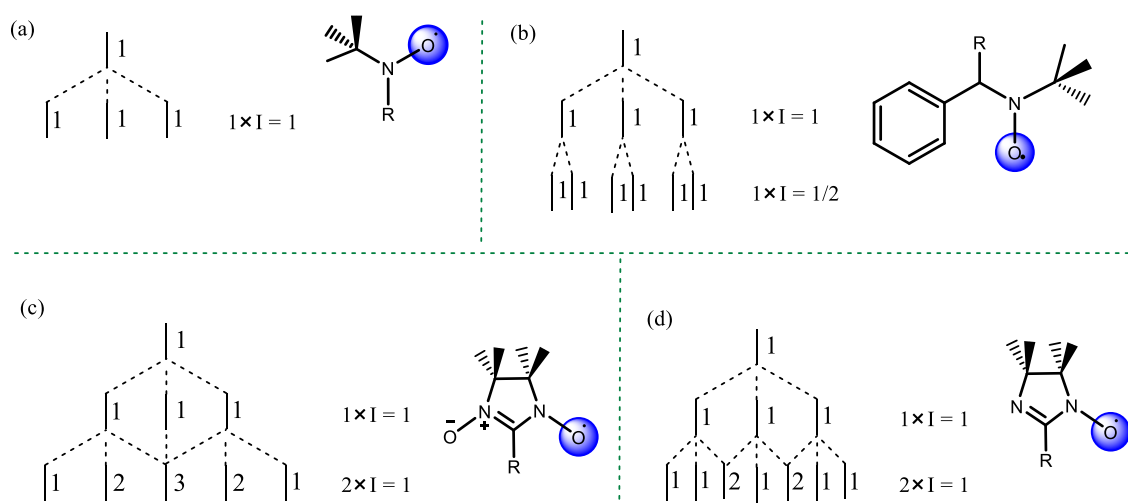


Figure 2-4. Four detailed hyperfine splitting patterns of organic radicals. a) *tert*-butyl nitroxide. b) PBN adduct. c) nitronyl nitroxide. d) imino nitroxide.

2.3.4. Spin Systems with More Than One Unpaired Electron ($S \geq 1$) and Zero Field Splitting (zfs)

The spin species or systems we discussed above all have only one unpaired electron ($S = 1/2$). But actually, most cases we encountered are more than one unpaired electron ($S \geq 1$). Two situations were divided in the cases of $S \geq 1$. One is a kind of systems with odd number of electrons which lead to the spin quantum number $S = 1/2, 3/2, 5/2$ and so on. These systems are called Kramers' systems or half-Integer spin systems. The other one is the systems with even number of electrons which lead to $S = 1, 2, 3$ and so on. These systems normally are called non-Kramers' systems or Integer spin systems.

Let's take the system with two unpaired electrons $S = 1$ as an example, then two different states of multiplicity exist in ground state: singlet state or triplet state. The degeneracy of triplet sub state is lifted and new quantization of spin state take place in frozen solution or powder state. This is called zero field interaction and the energy level spacing or

splitting is called zero field splitting (*zfs*), which the "zero field" means it is independent to any external field. The description of the anisotropic dipole-dipole interactions between the two spin centers are presented by *zfs* parameters D and E. The three components of D in (x, y, z) axis-three dimensional system are not independent, as the equation 2-9. *zfs* parameter D is a traceless symmetrical tensor and can be reduced to two scalar parameters, that is to say only two parameters exist (in the range of D_x , D_y and D_z). The relationships between D and E are shown in equation (2-10, 2-11). So vital information of geometrical shape of spin distribution could be obtain by *zfs* parameters D and E, which D can reflect the distance between two interacting spins, while the value of E can describe the deviation of electron density distribution from symmetry axis, when $x \neq y$. The relationships between the distance of two spin centers (d) and the *zfs* parameter D is shown in equation 2-12. The units of (d) and D are nm and cm^{-1} respectively. We could draw an important conclusion that the distance (d) between the two spin centers is inversely proportional to the *zfs* parameter D

$$D_x^2 + D_y^2 + D_z^2 = 0 \quad (2-9)$$

$$D = \frac{3D_z}{2} \quad (2-10)$$

$$E = \frac{D_x - D_y}{2} \quad (2-11)$$

$$d = 0.138 / |D|^{1/3} \quad (2-12)$$

2.3.5. The Signals of EPR Measurements Influenced by External Factors

A perfect EPR signal response or spectra depend on sample preparation and the selection of proper operation parameters. It is influenced by various intrinsic properties and external factors.⁴⁻¹¹ The former discussions are focused on the intrinsic physical and chemical properties. Here we present several external measurement factors on EPR signal that have to be considered. (1) The temperature of sample in measurement. The EPR signals especially the intensity of signals differ a lot in rt, high temperature or cryogenic temperatures respectively. (2) The microwave frequency ν and the applied magnetic field magnitude B. (3) The relative orientations of B. (4) The field modulation amplitude at the sample positions. (5) The exact position of sample in EPR cavity. (6) The overall spectrometer gain including conversion time, time constant and the times of multi-scanning.

So from another perspective, the spectra of EPR signal also reflect time-dependent properties. It is related to another concept of relaxation times for spin centers which could be

affected by various conditions. (Relaxation time is a relative time concept compare to the time of EPR scan and measurement) In some cases, the lifetime of every individual spin center no matter for the spin orientation states or for the distance of spin interactions would affect the linewidth. Then some kinetic information can be obtained from the lineshape (height or width of peaks or intensity ratio of peaks) and can reflect some properties of samples and conditions surrounded spin centers, such as the intermolecular electron exchange and transfer, intramolecular motions, conformations change, molecular tumbling in solutions or even chemical reactions in samples and so on. In some other cases, if the relaxation only depends on the concentration of the spin species, the signal intensity changes can directly reflect the kinetic information.

2.4. Application of Quantitative EPR

The applications of quantitative EPR measurements spread out in various aspects, from the chemistry, physics and biology applications to the material science, biomedical research and industry application.^{1,4,17,19} For the physics and chemistry applications, the quantitative EPR measurements can be used in investigating the reaction kinetics and mechanism of enzyme reactions photocatalysis reactions and redox reactions, the structure characterization of spin species and so on. The membrane proteins spin labelling, RNA and DNA oxidation and the aspect of metalloproteins are effectively detected or studied by quantitative EPR measurements for biology applications. In addition, for the application of materials, biomedicine and industry, the quantitative EPR measurements are widely used in study of degradation of polymer engineering products, the defects of solar cells or some other devices, the oxidative stability of foods and beverages in food science, antioxidant capacity, pharmaceutical analysis, radiation dosimetry and even in diamond quality evaluation.

2.5. Expectation of EPR

EPR measurements as a tool to detect the signal of electron resonance for different kind of samples. We can obtain many information from the spectra of EPR, such as the intensity, g factors, hyperfine splitting and so on, in a specific position of sample. In other words, the information are coming from one point in sample. If we could collect the EPR information from many points of a samples (in 2-dimensional regions or 3-dimensional regions), then we may create an imaging for a sample, called EPR imaging. The principle is similar like the magnetic resonance imaging. For example, the total integral of intensity of

EPR signal for every points in a specific 2-dimensional regions or 3-dimensional regions were collected, an imaging with different values of EPR signal intensity (gradient line) for a specific sample (the picture of changes of gradient) can be acquired. Some preliminary works about EPR imaging have been down recently.¹⁷⁻²⁰ This technique of imaging will become an unique imaging method of electron spin to samples and would be widely applied in biomedicine and clinical medicine in the future.

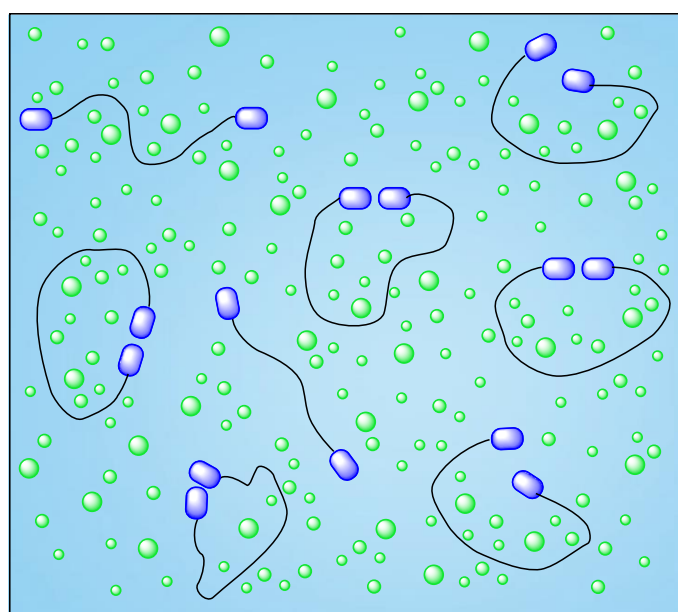
2.6. EPR-Related Books and References

- (1) Roessler, M. M.; Salvadori, E. Principles and Applications of EPR spectroscopy in the Chemical Sciences. *Chem. Soc. Rev.* **2018**, *47*, 2534-2553
- (2) Abragam, A. *The Principles of Nuclear Magnetism*. Oxford University Press, Oxford, 1961.
- (3) Van Vleck, J. H. *The Theory of Electric and Magnetic Susceptibilities*. Oxford University Press, London, 1932.
- (4) Alger, R.S. *Electron Paramagnetic Resonance: Techniques and Applications*. Wiley, New York, 1968.
- (5) Kochelaev, B. I.; Yablokov, Y. V. *The Beginning of Paramagnetic Resonance*. World Scientific, Singapore, 1995.
- (6) Pake, G. E.; Estle, T. L. *The Physical Principles of Electron Paramagnetic Resonance*. Second Edition, Benjamin, Reading, MA, 1973.
- (7) Trifunac, A. D.; Thurnauer, M. C. "Time-Resolved Electron Spin Resonance of Transient Radicals in Liquids", in *Time-Domain Electron Spin Resonance*. Wiley, New York, 1979.
- (8) Hagen, W. R. *Biomolecular EPR Spectroscopy*. CRC Press, 2009.
- (9) Rieger, P. H. *Electron Spin Resonance Analysis and Interpretation*. The Royal Society of Chemistry, Cambridge, 2007.
- (10) Atherton, N. M. *Principles of electron spin resonance*, Ellis Horwood Limited, PTR Prentice Hall, 1993.
- (11) Gerson, F.; Huber, W. *Electron Spin Resonance Spectroscopy of Organic Radicals*. WILEY-VCH Verlag GmbH & Co. KGaA, Weinheim, 2004.
- (12) Atkins, P. W.; Symons, M. C. R. *The Structure of Inorganic Radicals*. Elsevier, Amsterdam, 1967.
- (13) Baumgarten, M. "High Spin Molecules Directed Towards Molecular Magnets", In *EPR of Free Radicals in Solids II*. Springer, Netherlands, 2012.
- (14) Hagen, W. R. "g-Strain: Inhomogeneous Broadening in Metalloprotein EPR", in *Advanced EPR: Applications in Biology and Biochemistry*. Elsevier, Amsterdam, 1989.

- (15) Weil, J. A.; Bolton, J. R. *Electron Paramagnetic Resonance: Elementary Theory and Practical Applications*. Second Edition, John Wiley & Sons, Inc., New Jersey, 2006.
- (16) Gerloch, M. *Magnetism and Ligand-Field Analysis*. Cambridge University Press, Cambridge, 1983.
- (17) Naveed, K. R.; Wang, L.; Yu, H. J. Recent Progress in The Electron Paramagnetic Resonance Study of Polymers. *Polym. Chem.* **2018**, *9*, 3306-3335
- (18) Soule, B. P.; Hyodo, F.; Matsumoto, K. I.; Simone, N. L.; Cook, J. A.; Krishna, M. C.; Mitchell, J. B. The Chemistry and Biology of Nitroxide Compounds. *Free Radical Biology & Medicine* **2007**, *42*, 1632-1650
- (19) Kishimoto, S.; Matsumoto, K. I.; Krishna, M. C. Pulsed Electron Paramagnetic Resonance Imaging: Applications in the Studies of Tumor Physiology. *Antioxidants & Redox Signaling* **2018**, *28*, 1378-1393
- (20) Parekh, G.; Shi, Y. Y.; Zheng, J. J.; Zhang, X. C.; Leporatti, S. Nano-Carriers for Targeted Delivery and Biomedical Imaging Enhancement. *Ther. Deliv.* **2018**, *9*, 451-468

Chapter 3 Temperature Stimuli Responsive Spin Coupling Interactions of Nitronyl Nitroxide Diradicals

A biradical system with temperature stimuli responsive transition feature was investigated. It consisting of two nitronyl nitroxide (NN) radicals bridged by diphenyl- hexa ethylene glycol chain [phenyl-O-(CH₂CH₂O)₆-phenyl (GBN1)] was synthesized and investigated using electron paramagnetic resonance (EPR) spectroscopy in solution at different temperature. The reversible temperature dependence behavior of spin coupling exchange is comprehensively reflected by the different lifetime of conformations due to a tumbling motion of the flexible hexaethylene glycol chain. The influences of different solvent on the exchange interactions between the radical entities are described by a two-conformational model, which was first time applied for di-NN molecule and revealed the thermodynamic parameters enthalpy and entropy (ΔH and ΔS) of the conformational changes. The positive value of enthalpy indicates lower energy of the stretched form (as calculated) compared to the bent form. The transition enthalpy in polar MeCN is larger than in toluene and the positive entropy sign indicates more chain conformation options in the bent state. The magnetic properties of this molecule were investigated in solid state by magnetization studies and EPR spectroscopy. (large parts of this chapter originated from the publication: *J. Phys. Chem. A* **2018**, *122*, 574-581)



Schematic Diagram of Diradicals With Flexible Bridge in Solution

3.1 Introduction

For a long period of time, magnetic molecules have drawn a lot of attentions, because of fantastic charm and the spin magnetic properties.¹ Organic radicals² possessing unpaired electron spin residing in p-orbitals offer a wide molecular design where structural flexibility became a promising research field among magnetic molecules that can have potential applications in spintronics devices, charge transfer materials, quantum computer or memory devices, and biomacromolecular-based magnets.³⁻⁷ Among various organic high spin compounds^{2,8} especially those composed of two nitronyl nitroxide (NN) radicals attract more and more interests for inter- or intra-molecular magnetic exchange interactions. Investigations suggest that in NN radicals the unpaired electron spin-density is delocalized over the ONCNO fragment. For the NN biradicals, the exchange interaction J is described by the spin Hamiltonian (Heisenberg exchange) equation $H = -2JS_1S_2$ (S_1 , S_2 are spin quantum numbers of the two neighboring spin unit). Many studies have reported on tuning through bond exchange interactions J by different kinds of conjugated structures as bridges between two radicals,⁹⁻¹⁰ where the absolute value of J can decrease drastically from several hundred to several Kelvin upon changing the bridging length¹¹⁻¹² or the torsion in the conjugated backbone. Up to now mainly pure nitroxides as proxyl¹³ or TEMPO radicals¹⁴⁻¹⁹ were considered for their through space exchange coupling.¹⁵⁻¹⁷ In contrast non conjugated long chain flexibly connected NN biradicals were rarely studied. Only one article published recently mentioned a similar structure with a shorter flexible chain for use in batteries, but the spin exchange coupling was not discussed at all.¹⁸ Therefore the radical interaction in such biradicals deserves further attentions.¹⁹ Thus we consider nitronyl nitroxides connected via a flexible saturated hexa-ethylene glycol bridge to investigate the solution and solid state spin exchange coupling.

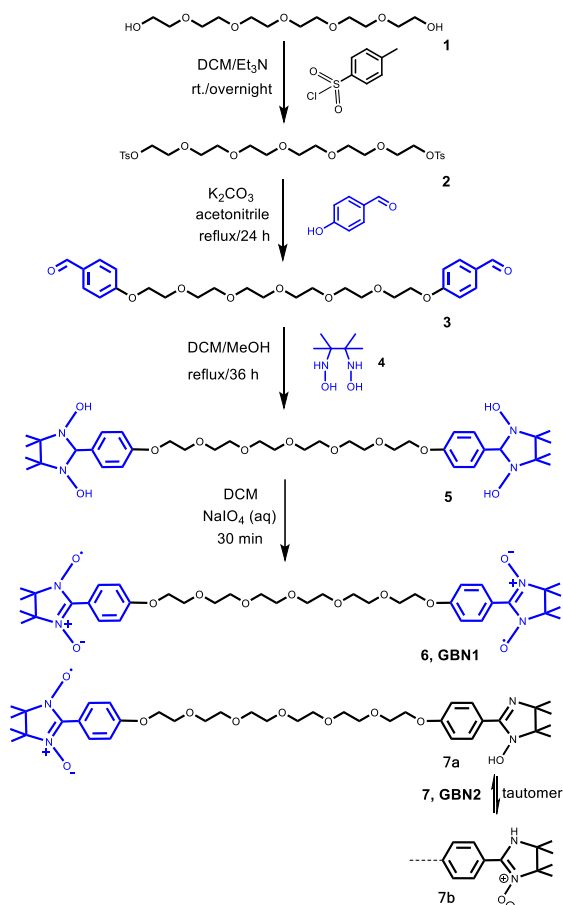
Among the characterizations of radicals, one of the most direct and efficient method to investigate the physical and chemical properties of radicals is EPR spectroscopy. For the case of a mono nitronyl nitroxide radical or NN biradicals without spin coupling exchange, J is zero. The signals of EPR spectra of NN in solution split into 5 lines with the intensity ratio 1 : 2 : 3 : 2 : 1, and would depart by the distance of a_N due to electron nuclear hyperfine splitting which is generated by the presence of two equivalent nitrogens.²⁰ For the situation of strong exchange coupling J between two radical units $|J/a_N| \gg 1$, each electron spin is coupled to four equivalent nitrogens such that a nonet line shape spectrum with a peak to peak separation

of $a_N/2$ and an intensity ratio 1 : 4 : 10 : 16 : 19: 16: 10 : 4 : 1 can be detected in EPR measurements. The number of lines in the spectra generally obeys the rule of $2(nI) + 1$, where 'n' refers to the number of equivalent fermion nitrogen nuclei and 'I' refers to the nuclear spin angular momentum ($I=1$ for ^{14}N). The total spectral width of signals of the biradical system is the same as for the corresponding mono NN radical.

The relative intensity of nine lines in EPR spectra changed drastically during the change of temperature in our case. So far as the intramolecular spin coupling exchange mechanism is considered,²¹ there are two main paths, through bond²²⁻²³ and through space.²⁴⁻²⁵ For our case, the bridge between two spin fragments is composed of a number of saturated C-C σ bonds and C-O σ bonds. These long and non-conjugated structures could not offer a pathway for radicals to couple each other through bond.¹³ That means only through space the intramolecular spin coupling exchange can be explained. In liquid solution different conformations can be adopted through the long flexible bridge between the radical entities where the polarity and viscosity of solvents influence the equilibrium between stretched and bent state. Thus we have chosen several different solvents, from non-polar solvents with low viscosity like toluene and dichloromethane to polar solvents with high viscosity as, acetonitrile, methanol, and even water. Mixtures of solvents with different ratios were also considered to investigate the influence of solvent molecules filling the bridged biradicals space. Different temperatures were discussed in this system from 330 K to the degree of freezing point of solvent and were found out playing the main role in affecting the spin exchange.

3.2 Synthesis of Temperature Stimuli Responsive Radicals

The synthesis of the bis-(nitronyl nitroxide) biradical with phenyl-O-(CH₂CH₂O)₆-phenyl bridge **GBN1**, started from commercially available hexa-ethylene glycol (**1**), which was tosylated to **2** in dichloromethane and trimethylamine as base at room temperature in a similar method as previously published.²⁶ All the synthesis steps are shown in Scheme 3-1. The transformation from the methylbenzenesulfonates to the corresponding dialdehydes **3** was achieved in acetonitrile and potassium carbonate (K₂CO₃) with Y. J. Ma, in yields around 55%.



Scheme 3-1. Synthesis of diradical **GBN1** and monoradical **GBN2** as tautomers **7a** and **7b**.

Due to the crucial dialdehydes precursor **3** for the whole synthesis of **GBN1**, we offer the NMR spectrum of the new precursor which is shown in figure 3-1 below, for analyzing the detail structure of **3**. Six groups of hydrogen characteristic peaks were clearly attributed to the dialdehydes derivatives. The proton labeled "a" in figure attributed to aldehyde group where the single peak position is at 9.77 ppm. Two groups of double peaks labeled "b" and "c" at 7.72-7.75 ppm and 6.94-6.97 ppm respectively, were attributed to aromatic protons belonging to two phenyl groups. Other protons which belong to ethylene glycol chain and labeled "d", "e" and "f" are shown in figure 3-1. The chemical shifts of four groups of proton which labeled "f" are very close around the region 3.51-3.61 ppm, due to the long distance with aldehyde groups and phenyl groups. The whole ratio of protons from "a" to "f" are nearly about 1 : 2 : 2 : 2 : 2 : 4, which fitted the theoretical value.

The condensation reaction of the dicarbaldehyde **3** with 2,3-diamino-*N,N'*-dihydroxy-2,3-dimethylbutane (**4**) according to a similar procedure²⁷ was realized in a mixture of solvents of absolute dry methanol and DCM (ratio is 1 : 4), which was degassed by argon bubbling before use, then the reaction mixture was heated to 65 °C and stirred for 36 h.

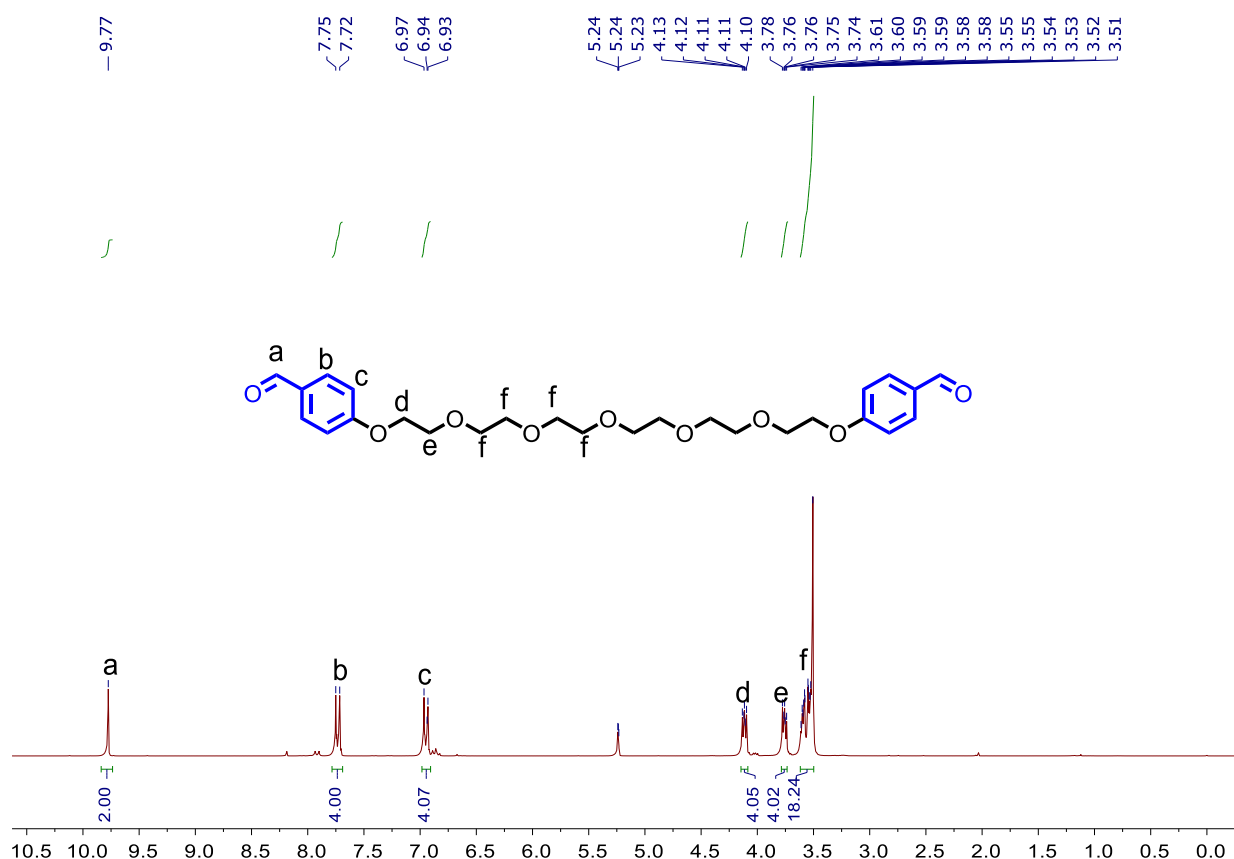


Figure 3-1. ¹H NMR spectrum (250.0 MHz) of **3** in CD₂Cl₂ at room temperature

The N,N'-dihydroxyimidalozidine **5** was finally oxidized to the biradical **6** with sodium periodate as oxidant in a two-phase solvent mixture of water and DCM, in an ice bath around 0-5 °C. The biradical product was separated by column chromatography providing a MS-FD MW= 745.5 g/mol fully consistent with the calculated mass for **GBN1**. Partially insufficient oxidation led to the mono NN radical **GBN2** which also could be isolated by column chromatography providing a mass of MS-FD MW= 729.4 g/mol consistent with the isomeric structure **7**.

3.3 Optical Properties

The UV-Vis spectrum provided characteristic absorptions at 370 nm and 617 nm (Fig. 3-2 a). The two main absorptions originated from the π - π^* transition of the substituted ethoxy-benzene-imidazolidine and the n- π^* transition of the nitronyl nitroxide, respectively. The broad absorption patterns in the visible range changed with the variation of solvents (Fig. 3-2 b). The whole UV-Vis spectra of **GBN1** in five different solvents are shown in figure 3-3. There occurred a clear hypsochromic shift with increasing solvent polarity, which is a clear

indication of negative solvatochromism.^{28,29} This is due to the dipolar structure of the nitronyl nitroxide, where the ethylene glycol helps to make it even soluble in water and is also an electron donor. Here mainly the n-p* transition of the radical is involved and responsible for the negative solvatochromism that was observed. Thus the apparent colours of solutions vary from blue to cyan and purple (Fig. 3-2 c). That is to say, the different polarity of solvents change a little bit the energy gap between the ground state and excited state.

The colour of the solution is blue (the same colour to the **GBN1** in solid state) when **GBN1** is dissolved in acetonitrile, methanol or DCM, as shown in Fig. 3-2 c left. The colour of solution turned to cyan (dark green), when **GBN1** was dissolved in toluene (Fig. 3-2 c middle) and it appeared purple when dissolved in water as shown in the Fig. 3-2 c right.

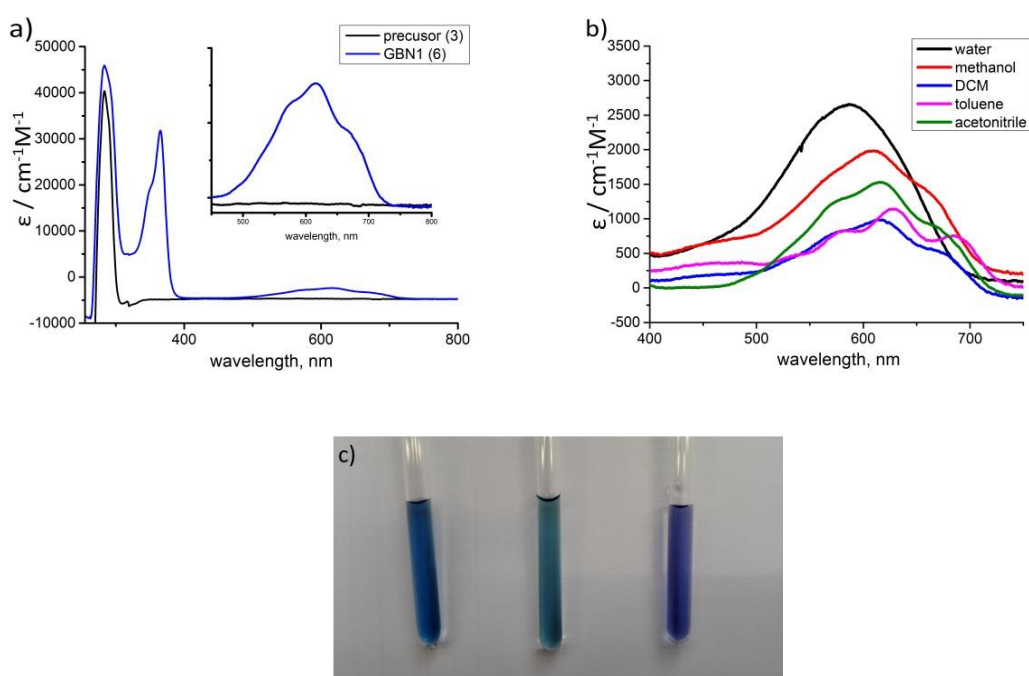


Figure 3-2. a) UV-Vis absorption spectra of nitronyl nitroxide diradicals **GBN1** (6, blue line) and precursor (3, black line) recorded in acetonitrile solutions at room temperature. Inset: amplification of optical absorption spectra in the visible range from 400 nm to 800 nm. b) UV-Vis spectra of visible range in different solvents. c) Apparent colour of **GBN1** in different solvents acetonitrile (left), toluene (middle), water (right).

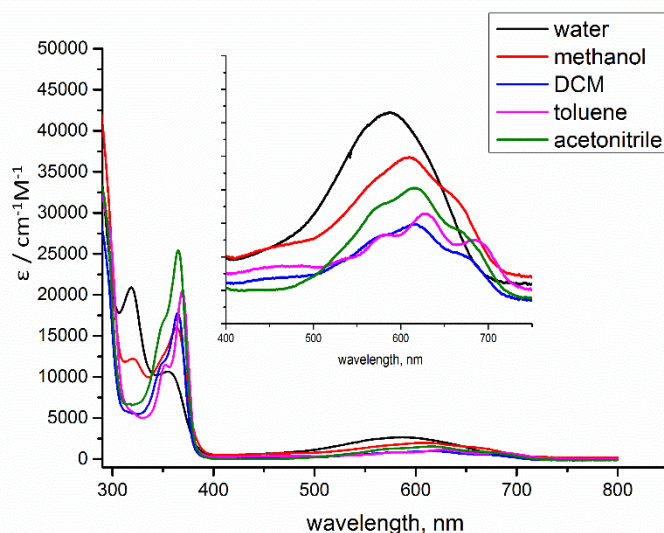


Figure 3-3. UV-Vis spectra of **GBN1**. Inset: amplification of optical absorption spectra from 400 nm to 800 nm.

3.4 EPR Measurements and Analysis

3.4.1. EPR spectra of **GBN1** and **GBN2** at room temperature

The EPR spectrum of **GBN1** in acetonitrile at room temperature showed a typical nine line spectrum centered at $g=2.0067$ with spacing of $a_N/2= 3.84$ G (Fig 3-4). The monoradical **GBN2** presented just a five line EPR spectrum in acetonitrile at room temperature (Fig. 3-5) with $g=2.0064$ and hyperfine interaction of $a_N= 7.67$ G for coupling with two equivalent nitrogens. Thus **GBN2** is an important reference sample for discussing the principle of intramolecular spin exchange coupling interaction through space found for **GBN1**.

We got a series of EPR spectra with nine lines pattern of bis(nitronyl nitroxide) radicals in different solvents at room temperature, as shown in the Fig. 3-4. They indicate a strong spin coupling exchange between two nitronyl nitroxide radicals in solution state. Among them, the diradical sample which dissolved in acetonitrile (the black one) presented the most homogenous nine line pattern of nitronyl nitroxide diradical, and also the most symmetrical one. The samples dissolved in toluene (red), methanol (green) dichloromethane (dark blue), and water (light blue) showed less homogenous EPR spectra where every 2nd line differed in relative intensity, which is

usually interpreted as a mixture of non interacting monoradicals and exchange coupled biradicals. One reason of the differences between these EPR spectra at room temperature is the consequence of different polarity and viscosity of the solvents, which influence the flexibility of the backbone leading to different amounts of conformations and therewith of partly strong exchange coupled radicals.

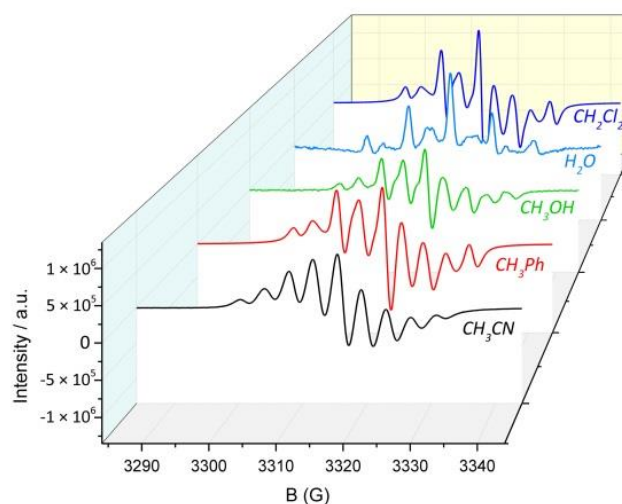


Figure 3-4. EPR spectra of **GBN1** in different solvents at $T= 293$ K.

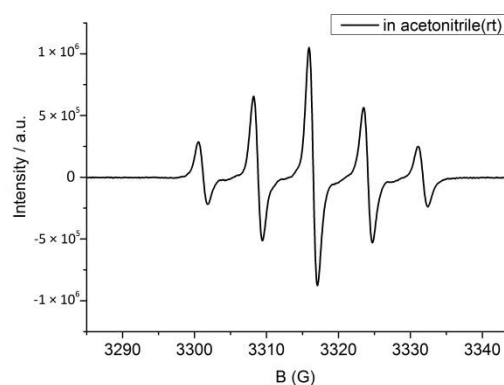
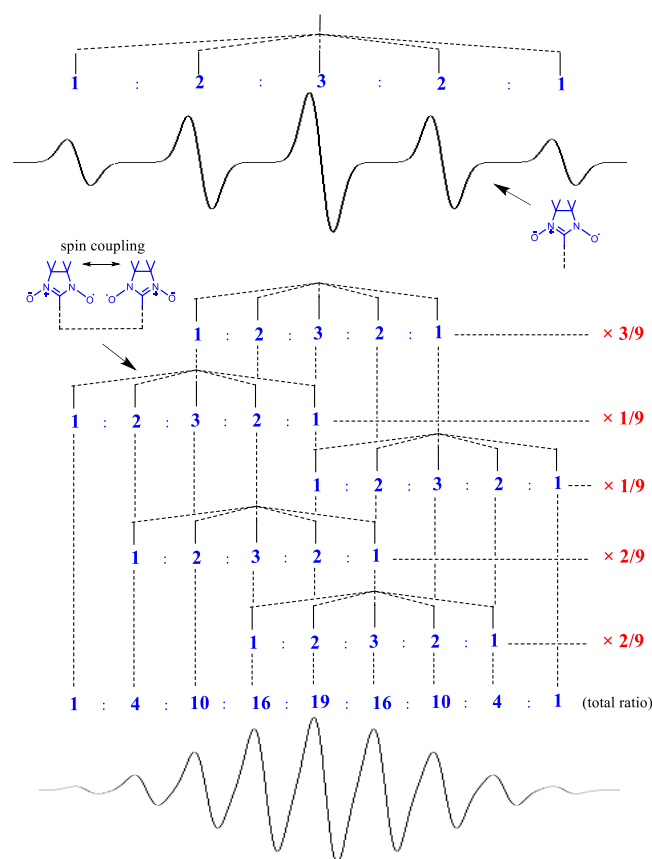


Figure 3-5. EPR spectrum of **GBN2** in acetonitrile at room temperature

3.4.2. The Deduction of EPR Spectrum of **GBN1** (The Relative Intensity of Every Splitting)

The mono-NN has two equivalent nitrogens, while di-NN has four equivalent nitrogens that lead to half of hyperfine splitting. The intensity ratio of nine lines could be deduced by the overlapping of five quintet line signals with every quintet line signal ratio of $1 : 2 : 3 : 2 : 1$ (from left to right with the statistical weights of every quintet line signal, $1/9$, $2/9$, $3/9$, $2/9$, $1/9$, respectively), which are shown in scheme 3-2. The red fractions in the right

of scheme are statistical weights of every quintet line signal, which were calculated from the intensity ratio of 5 lines pattern spectrum.^{30,31} The total spectral width of signals of the biradical system in the strong exchange limit is thus the same as for the corresponding mono NN radical.



Scheme 3-2. Relative intensity ratio of EPR spectral lines of a nitronyl nitroxide diradical with strong spin exchange coupling.

3.4.3. Temperature Dependent EPR Spectra of **GBN1** in Pure Solvents

We measured the temperature dependent EPR spectra of **GBN1** in acetonitrile, toluene, DCM, water, and methanol, respectively. Clear transitions from five lines splitting pattern for non-interacting spins at low temperature to a nine lines splitting pattern for strongly exchange coupled spins at high temperature was observed in all the five solvents (Fig. 3-7). The EPR spectra of **GBN1** in three solvents (acetonitrile, toluene and methanol) at three specific temperatures are depicted here for clarity (Fig. 3-6). The transition of splitting patterns changed by gradual increase of intensities of the second, fourth, sixth, and eighth peak between the original five lines EPR spectrum. (For the acetonitrile case, the transition of second peak appears at the dashed line which was marked with star * in Fig. 3-6 a) The spectrum is much more similar to

ideal nine lines spectrum ($|J| \gg a_N$) when the temperature increased to 300 K, and it changed to mono NN radical behavior without spin coupling when the temperature is close to the freezing point. When the temperature increase, the long chain bridge between two radicals become more flexible due to the much easier rotations around σ bonds along the long chain.³² This will also lead to more vigorous motions of radical end groups and increase the collisional frequencies of radicals³³ through more rapid reorientations of NN radicals. In addition, the **GBN1** system was also carried out in mixed solvents for characterizing temperature dependent EPR spectra (shown in Figure 3-10). The simulated EPR spectra of **GBN1** in solution state can also predict the spin interaction well (shown in Figure 3-8).

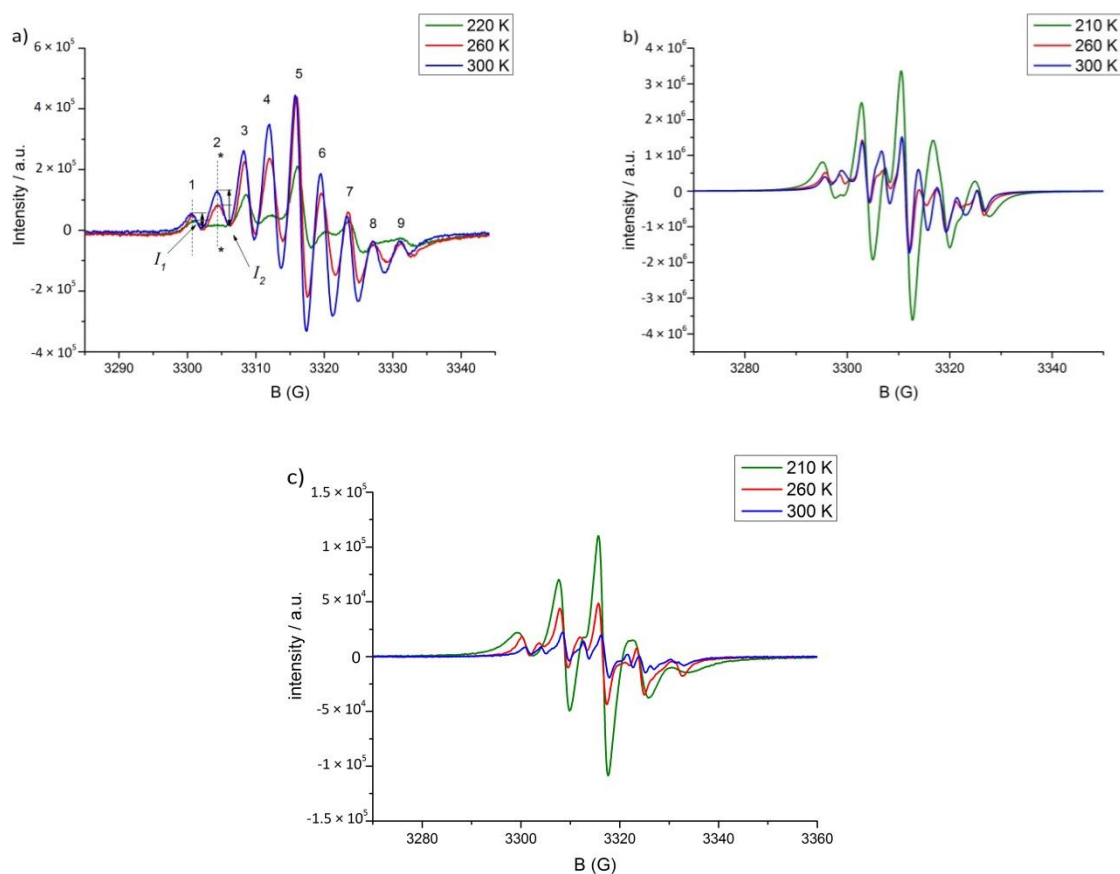


Figure 3-6. Temperature dependent EPR spectra of **GBN1** in different solvents a) in acetonitrile, b) in toluene, c) in methanol. I_1 and I_2 are the relative intensities of the first and second line in the spectra used for further analysis of their ratios.

The Fig. 3-7 which show temperature dependent EPR spectra of **GBN1** (from around 210 K to around 330 K, with 10 degree gradient) in acetonitrile, toluene, DCM, water, and methanol, respectively, all of them give clear trends of transitions from five

lines splitting pattern for non-interacting spins to a nine lines splitting pattern for strongly exchange coupled spins. But the EPR signal tendency of **GBN1** which was dissolved in acetonitrile is the most perfect and most symmetrical spectra which could fit the simulated spectra well among the different five solvents. The overall transition tendency of EPR spectra about **GBN1** in five solvents from low temperature to high temperature still clearly existed. (The transition tendency is a linear increase of intensity I_2 with temperature ascending)

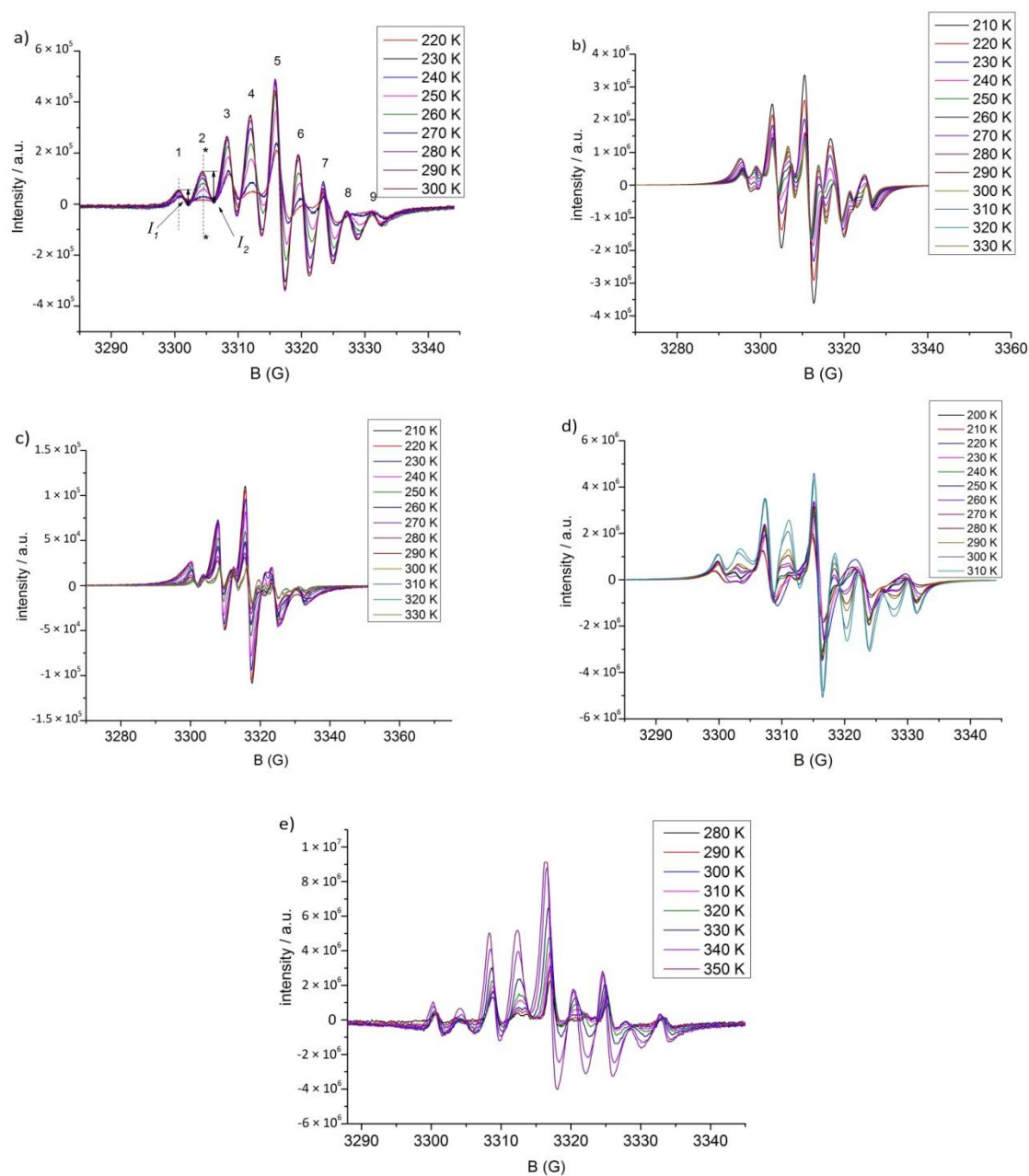


Figure 3-7. Temperature dependent EPR spectra of **GBN1** in a) acetonitrile, b) toluene, c) methanol, d) DCM and e) water. I_1 and I_2 are the relative intensities of the first and second line in the spectra a), which were used for further analysis of their ratios.

Two simulated EPR spectra of diradical and monoradical, with the parameters from the experimental spectra above were acquired and added in different portions of the two simulated EPR spectra. They represent different ratios of spin coupled and non-spin coupled radicals superimposed on each other as shown in Fig. 3-8 and well compare with the changed amount of spin coupled radicals upon temperature variation. As the portion of diradicals (which with spin coupling features) increased from 0% to 100%, the peaks pattern were changed from 5 lines mono radical features gradually to 9 lines diradical spectrum. Due to the overlap of peak position of the two situations, which the five peaks belong to mono NN radical are overlapped with five peaks (the first peak, third peak, fifth peak, seventh peak and ninth peak) belong to di-NN radicals. So at the intermediate mixture period, the intensity of the second peak, fourth peak, sixth peak and eighth peak seems weak in total spectra for the simulated EPR spectra. It is well fitted to the experimental EPR data of GBN1 in solution which were shown in front.

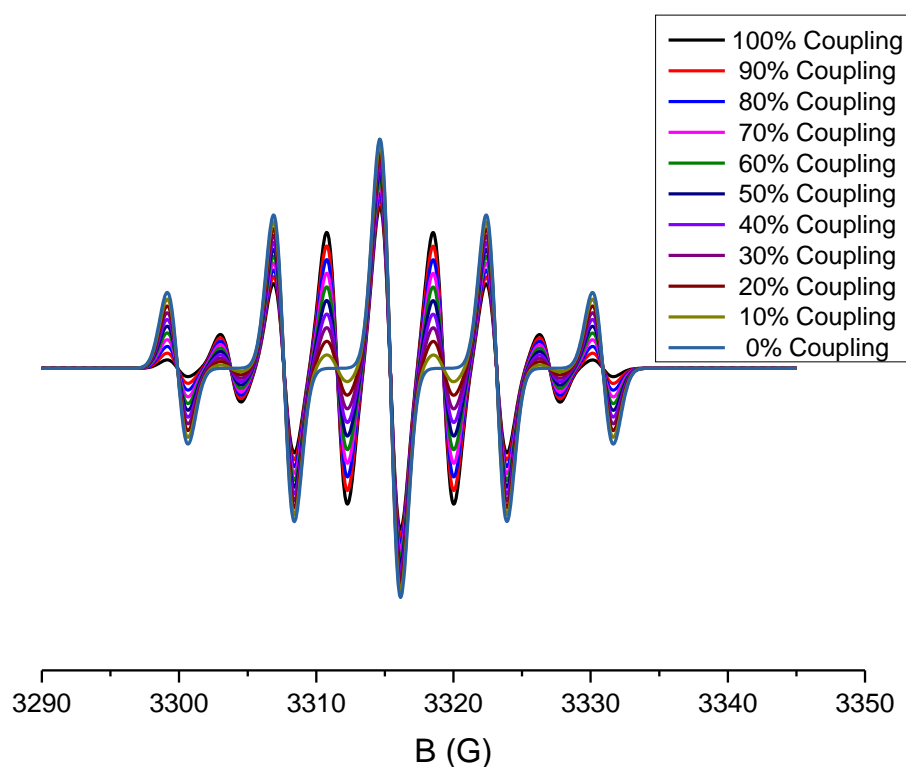


Figure 3-8. Simulated EPR spectra in acetonitrile (Frequency is 9.311586 MHz, $B_c = 3315$) by using the parameter of g factor is 2.0067 and a_{n1} is 7.75, a_{n2} is 3.875 with spin coupling interactions of diradicals from 0% to 100%

GBN2 was used as a control sample to exclude intermolecular interactions under the given concentrations ($c \sim 10^{-4}$ M). Only a five lines pattern in the EPR

spectrum of the mono nitronyl nitroxide was detected at different temperatures, as shown in Fig. 3-9. These EPR measurements of control sample (**GBN2**) proved the diradical NN features and spin interactions between two spin species derived from intramolecular interactions, rather than derived from intermolecular interactions.

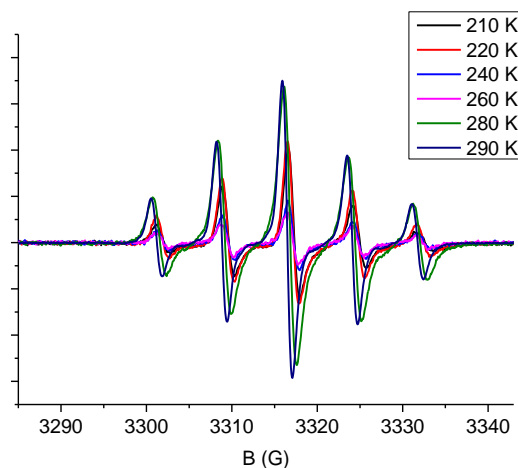


Figure 3-9. EPR spectra of monoradical **GBN2** in acetonitrile at different temperatures

3.4.4 EPR Spectra of **GBN1** in Mixed Solvents

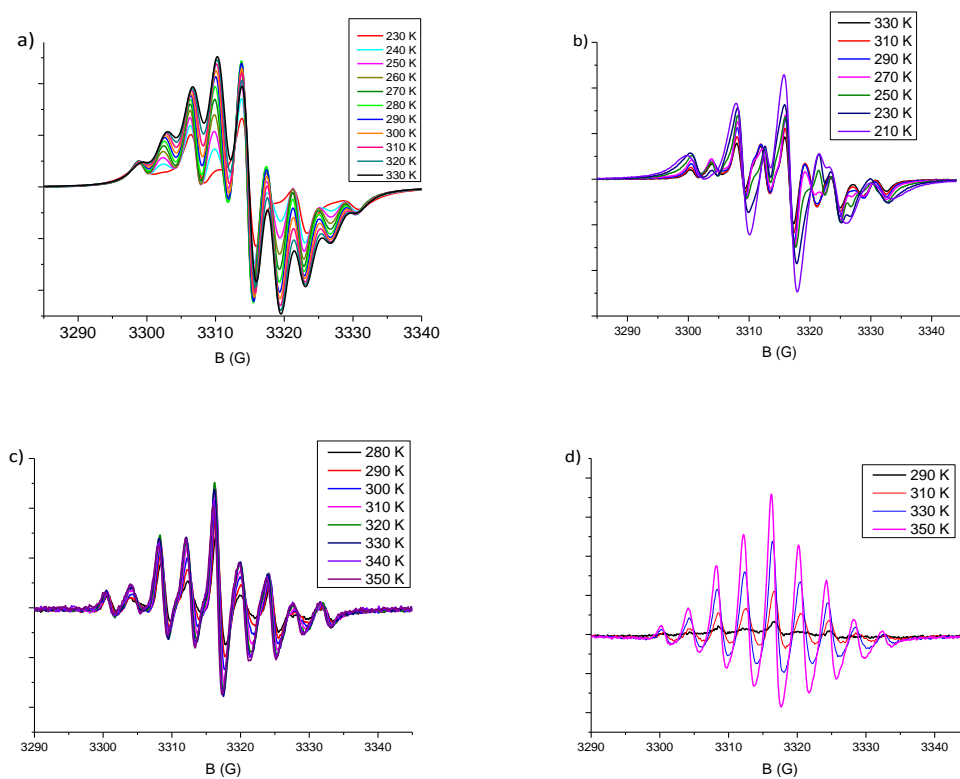


Figure 3-10. Temperature dependent EPR spectra of GBN1 in different mixed solvents a) the ratio of acetonitrile to toluene is 6 : 4, b) the ratio of toluene to methanol is 6 : 4, c) the ratio of acetonitrile to water is 1 : 9, d) the ratio of acetonitrile to water is 9 : 1.

The EPR measurements of different mixed solvents of sample **GBN1** could visually reflect some solvent polarity effect on spin interactions between radical species. As the depiction ahead about the pure solvent **GBN1**, the EPR spectra measured in acetonitrile present the most symmetrical signal patterns, during the switching tendency between high temperature and low temperature. But the EPR spectra measured in pure toluene and water showed worse signal regularity than the signal in acetonitrile at different temperature. Then we use toluene and water to mix with acetonitrile respectively, as shown in figure 3-10 a), c) and d). The results reflect that the mixture of toluene and acetonitrile as solvent could obtain much more linear change of intensity than pure toluene situation. The mixture of water and acetonitrile could also draw the same conclusion. The different ratio of water and acetonitrile from 9 : 1 to 1 : 9 reflected the change of signal pattern during the temperature shift, compared to pure solvents. The data b) is **GBN1** in the mixture of toluene and methanol as a control experiment.

3.4.5. EPR Spectrum of Solid State of **GBN1**

The EPR spectrum of **GBN1** in solid state at room temperature showed only one broadened line signal with $g=2.0068$ and no zero field splitting for **GBN1** was observed (Figure 3-11).

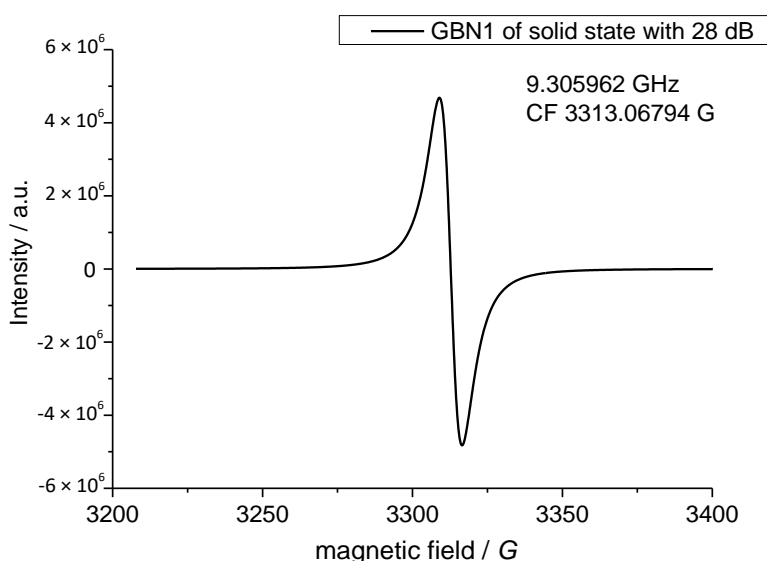
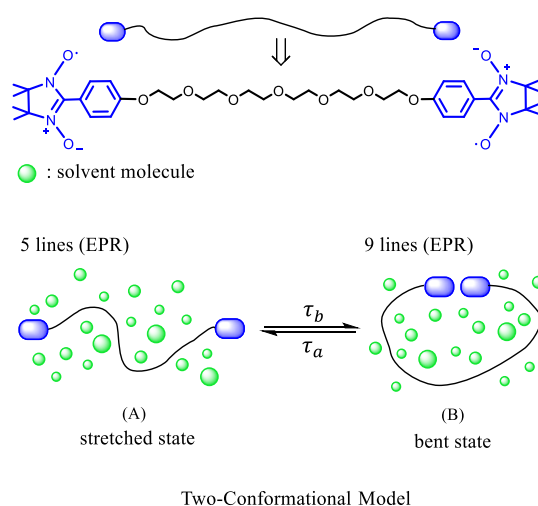


Figure 3-11. EPR spectrum of **GBN1** in solid state

3.5 Analysis and Deduction of New Model: Two-Conformational Model

3.5.1. Deduction of Two-Conformational Model

For a similar case of two nitroxide radicals (proxyl or TEMPOs)³⁴⁻³⁵ with long σ chain connected,³⁶ Parmon et al.³⁷⁻³⁹ gave a semi-quantitative analysis of temperature dependence of EPR spectra changing from 3 lines at low temperature to 5 lines at high temperature.⁴⁰⁻⁴¹ This three-conformational model was put forward and can explain the transition phenomenon of 3 to 5 lines well. Based on the non-conjugated bridge structure, we used this model³⁹ to describe the new bridged NN radicals. When the two nitronyl nitroxides move close enough to each other by rotation of σ bonds in the long flexible chain they can interact strongly (bent state) as shown in scheme 3-3. For the linear extended (stretched) conformation labeled 'A' the two end-capped radical groups are far apart from each other where they cannot undergo exchange ($J = 0$). The conformations labeled 'B' refer to the bent situation, that the two end-capped radical groups are very close and have a strong spin coupling interaction ($|J| \gg a_N$). Another possible bent conformation with less mutual exchange interaction to each ($|J| \sim a_N$) could not be detected by EPR and in the analysis we are restricted therefor to a two conformational model.



Scheme 3-3. Diagrammatic sketch of two-conformational model.

From this model also the average lifetimes of nitronyl nitroxide fragments in the bent state τ_b , and the stretched extended state τ_a can be derived. This is equal to the forward and backward reaction equilibrium provided by the Eyring-Polanyi equation³⁷,

$$K = \frac{k_1}{k_{-1}} = \exp\left(\frac{\Delta S}{R} - \frac{\Delta H}{RT}\right), \quad (1)$$

where k_1 and k_{-1} are the reaction rate constants for the forward reaction (from linear extended to bent state) and the backward reaction (conformation change from bent to extended) respectively. Thus with $k_1 / k_{-1} = \tau_b / \tau_a$.

$$\frac{\tau_b}{\tau_a} = \exp\left(\frac{\Delta S}{R} - \frac{\Delta H}{RT}\right). \quad (2)$$

We can acquire the ratio of life time by analysis of the EPR spectra from the intensity of first or second line and the temperature dependent change in designated solvent as I_2 / I_1 , as $I_1^{bn} = \tau_b I / 81(\tau_b + \tau_a)$, $I_2^{bn} = 4\tau_b I / 81(\tau_b + \tau_a)$, $I_1^{lin} = \tau_a I / 9(\tau_b + \tau_a)$ and $I_2^{lin} = 0$. The superscript 'bn' and 'lin' refers to case of bent situation and stretched situation. The above four equations about intensity ratio value of bent state and stretched state could be respectively acquired from scheme 3-2. Subscripts '1' '2' refer to the line number of EPR from left. So the observed intensities of line 1 and line 2, will be equal to: $I_1 = I_1^{lin} + I_1^{bn}$ and $I_2 = I_2^{lin} + I_2^{bn}$.

$$I_1 = (9\tau_a + \tau_b)I / 81(\tau_a + \tau_b). \quad (3)$$

$$I_2 = 4\tau_b I / 81(\tau_a + \tau_b). \quad (4)$$

$$\frac{I_2}{I_1} = \frac{4\frac{\tau_b}{\tau_a}}{(9 + \frac{\tau_b}{\tau_a})}. \quad (5)$$

$$\frac{\tau_b}{\tau_a} = \frac{9I_2}{4I_1 - I_2}. \quad (6)$$

From this intensity ratios result the relation to the change of thermodynamic parameters entropy and enthalpy ΔS and ΔH ,

$$\exp\left(\frac{\Delta S}{R} - \frac{\Delta H}{RT}\right) = 9 \frac{I_2}{I_1} / \left(4 - \frac{I_2}{I_1}\right). \quad (7)$$

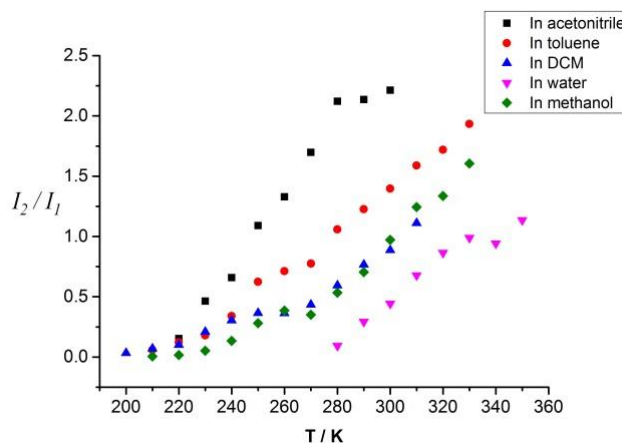
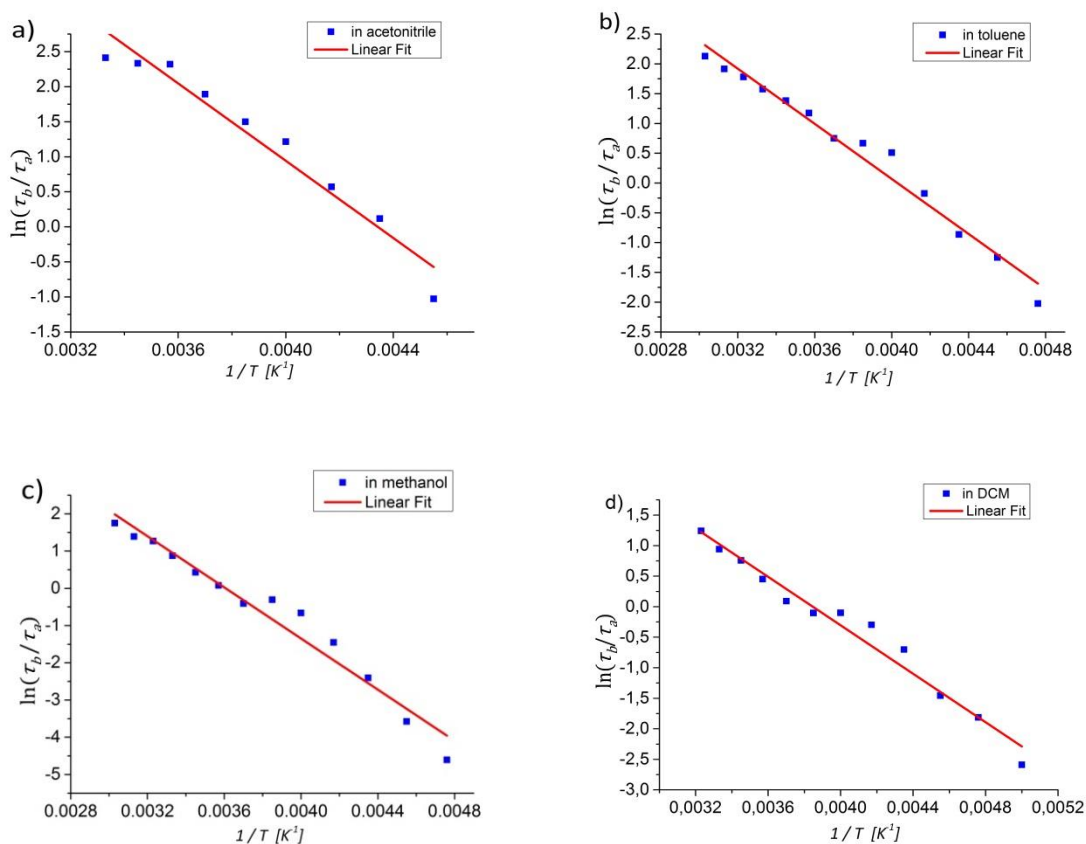


Figure 3-12. Relative ratios of intensities of EPR spectra of second line to first line at low field in different solvents, \square represent the solvent acetonitrile, \circ is in toluene, Δ is in DCM, \diamond is in methanol, the inverted triangle is in water.

We could clearly distinguish the increasing intensity of I_2 at the position of the second dashed line from the left marked with star * Fig. 3-6 a) and find the ratios for all solvents to differ with temperature (Fig. 3-12).

3.5.2. The Relationships Among Thermodynamic Parameters, Temperature and EPR Data

Equation (6) was used to calculate the relationship with relative lifetime ratio of bent conformations to linear extended conformations and the temperature. Then the logarithmic plot was acquired versus reciprocal temperature, and also the linear fit as shown in Fig. 3-13 for acetonitrile a), toluene b), methanol c), DCM d), and H₂O e), respectively. As the temperature increases, a longer lifetime of bent conformations is favored. From the linear fit, we can directly get the thermodynamic parameters according to the equation (2) deduced above.



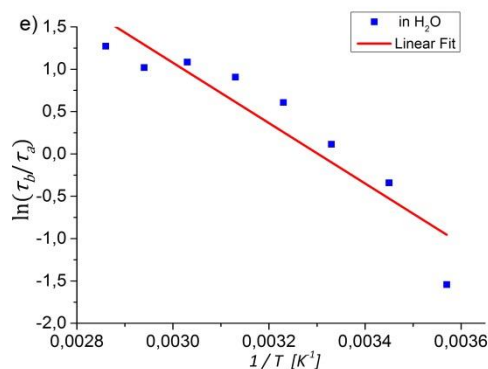


Figure 3-13. The logarithmic plots of relative lifetime ratio of the bent conformation with diradicals close to each other and the extended linear conformation where the radicals stay far away vs. reciprocal temperature and their linear fit of **GBN1** a) the solvent is acetonitrile, b) toluene, c) methanol, d) DCM and e) water.

Table 3-1. The EPR spectra and thermodynamic parameters for the **GBN1** in different solvents.

	$g^{[a]}$	$a_N[G]^{[b]}$	ΔH [kJmol ⁻¹] ^[c]	ΔS [Jmol ⁻¹ K ⁻¹] ^[d]	<i>Polarity</i> ^[e]	<i>Viscosity</i> $E_\eta^{[f]}$ [kJ/mol]
DCM	2.0066(5)	7.50	16.5 ± 1.7	63.4 ± 3.2	3.4	No record
Toluene	2.0066	7.50	19.2 ± 2.0	77.5 ± 3.9	2.4	9.1
Acetonitrile	2.0066	7.75	22.9 ± 2.3	99.5 ± 5.0	6.2	7.5
Methanol	2.0066	7.75	27.4 ± 2.7	100.6 ± 5.0	6.6	11.3
H ₂ O	2.0066	8.25	29.6 ± 3.0	97.8 ± 5.0	10.2	15.3

[a] g factor measured in different solvent. [b] Hyperfine splitting of diradical without spin coupling. [c] The enthalpy value calculated by the slope of linear fit from Fig. 6 and Fig. S6 according to equation (2). [d] The entropy value calculated by the intercept of linear fit from Fig. 6 and Fig. S6 according to equation (2). [e] The polarity index is a measure of the relative polarity of solvent.⁴² [f] Activation energy of viscosity”, E_η ⁴³

Thermodynamic parameters of ΔH and ΔS can reveal some tendency of conformational freedom by rotation around the saturated σ -bonds in these solution systems. Positive value of enthalpy indicates lower energy of stretched form and the

positive entropy sign indicates more chain conformation options in bent state and more opportunities to have an exchange spin coupling for the bent conformation. Temperature does not affect the value of ΔH and ΔS , as can be clearly seen from the Fig. 3-13 that nearly all the dots are close to the linear fit. They depend on the intrinsic properties of solvents. We ranked the table 3-1 by the sequence from small to large order of ΔH and found out the relative polarity has approximate sequence with ΔH . We (cooperate with Alexander I. Kokorin) tried to plot the following dependencies of ΔH vs. polarity units and activation energy of viscosity, E_η but no clear linear dependencies could be depicted just some tendencies for both relations are obvious as seen from the table, namely a general increase of ΔH with either polarity or activation energy of viscosity (Figure 3-15).

3.6 Magnetic Measurements

Using a SQUID magnetometer we determined the magnetic properties of two samples of GBN1 which differ in their age and masses. This experiment was done by Bernd Wolf in Frankfurt. Sample #1 which was newly synthesized has 18.4 mg and #2 which was synthesized half a year before has a mass of 9.86 mg. The material itself is very sticky and to handle it properly, it was dissolved in dichloromethane and then filled in suitable capsules. Before they are closed, the entire dichloromethane was evaporated as good as possible. All data have been corrected for the temperature-independent diamagnetic core contribution of the constituents, the magnetic contribution of the sample holder, and the contribution of the empty capsule. The data were taken in the temperature range $2 \text{ K} \leq T \leq 270 \text{ K}$ and a magnetic field of 1 T.

Figure 3-14 exhibits the $\chi_{\text{mol}}T$ data of samples #1 and #2 as a function of temperature. For both samples $\chi_{\text{mol}}T$ have no temperature dependence down to approximately 30 K. With a value of $0.59 \text{ cm}^3\text{Kmol}^{-1}$ for sample #1 and $0.58 \text{ cm}^3\text{Kmol}^{-1}$ at 250 K, both sample exhibit nearly the theoretical value of $0.75 \text{ cm}^3\text{Kmol}^{-1}$ expected for two uncoupled $S = 1/2$ units. So that only paramagnetic features exist for **GBN1**. It also indicate that every NN radical in this system was isolated from each other by the long flexible chain in condensed state and the orientations of all the radicals are isotropic. The small reduction of the $\chi_{\text{mol}}T$ value of #1 and #2 below 30 K is due to a very small antiferromagnetic interaction in the material. To determine its size we plot the inverse molar susceptibility as a function of temperature for $T < 60 \text{ K}$

in the inset of figure 3-14. Both samples strictly follow the Curie-Weis law. Fitting these data we obtained a very small Curie-Weis temperature of -0.5 ± 0.1 K reflecting the very small antiferromagnetic correlations only visible at low temperatures. The red solid line in the inset shows the Curie-Weis fit.

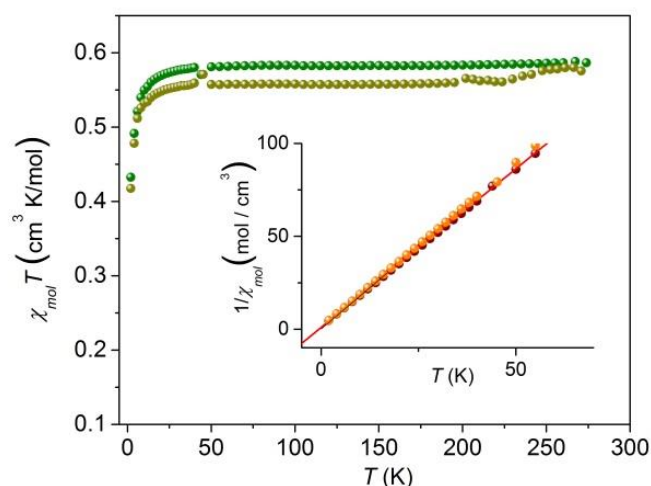


Figure 3-14. $\chi_{\text{mol}}T$ as a function of temperature of sample #1 (dark green circles) and sample #2 (dark yellow circles) of **GBN1**. Inset: Inverse molar susceptibility of #1 (brown circles) and #2 (orange circles) together with a Curie-Weis fit (red solid line).

3.7 Analysis of Additional Plots

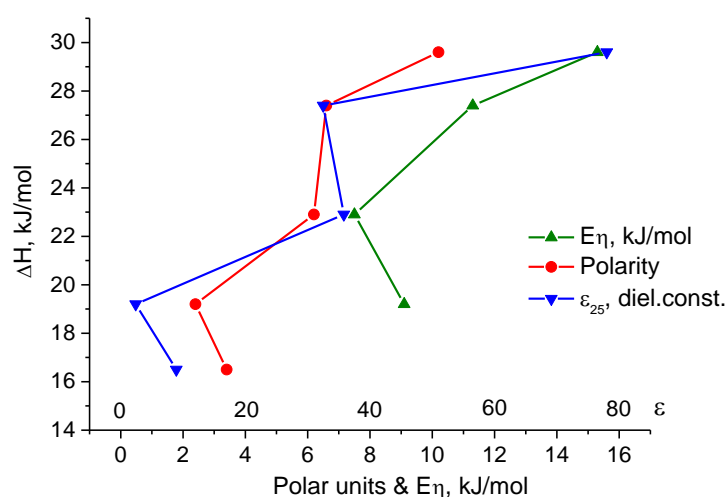


Figure 3-15. Plot of ΔH vs. activation energy of viscosity E_{η} , polarity and dielectric constant at 25°C

The additional plots here were done by Alexander I. Kokorin in Moscow. The Figure 3-15 visually show the relationships of enthalpy ΔH with activation energy of viscosity, polarity of solvents and dielectric constant. Except the lowest dot, most parts of the lines (blue and red) belong to ΔH vs. polarity and dielectric constant (ϵ) have the tendencies that ΔH increased with the value of polarity of solvents and dielectric constant of solvents increased. But the relationship between activation energy of viscosity E_η and ΔH has no clear dependencies.

Another method which using the intensity ratios of third and fourth line (d_1 and d_2 labeled in figure 3-16) acquired the same tendency with the former method which the intensity ratios of first and second line were used. The sample was dissolved in toluene and the intensity ratio of d_2 and d_1 increased as the dependence of the temperature increase. The highest ratio of d_2 and d_1 is 16 : 10 which is the ratio of pure diradical feature. We still use two-conformational model to interpret the whole process of spin transition.

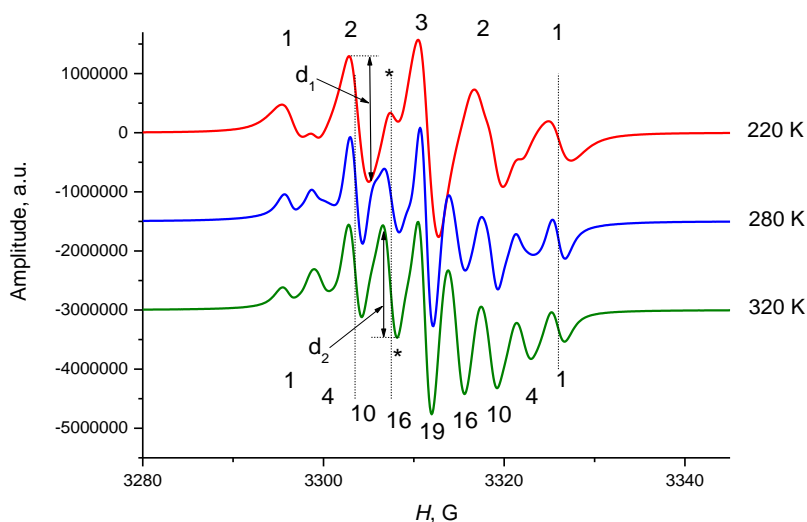


Figure 3-16. Analysis for third and fourth line intensity d_1 and d_2 for comparison in toluene solvent of GBN1.

The plot of relative life times of two conformations with temperature and a linear fit is shown in figure 3-17. Eight of the eleven dots in the figure is perfectly on the linear fit, which means all the dots could form an intercept and a gradient and would not change by the temperature change. The values of ΔH and ΔS were extracted from gradient and intercept of the linear fit respectively, which got a similar range of value compared to the method of using

intensity ratio of first and second line in EPR spectrum. They are: $\Delta H = 26.2 \pm 2$ kJ/mol, and $\Delta S = 93 \pm 8$ J/molK.

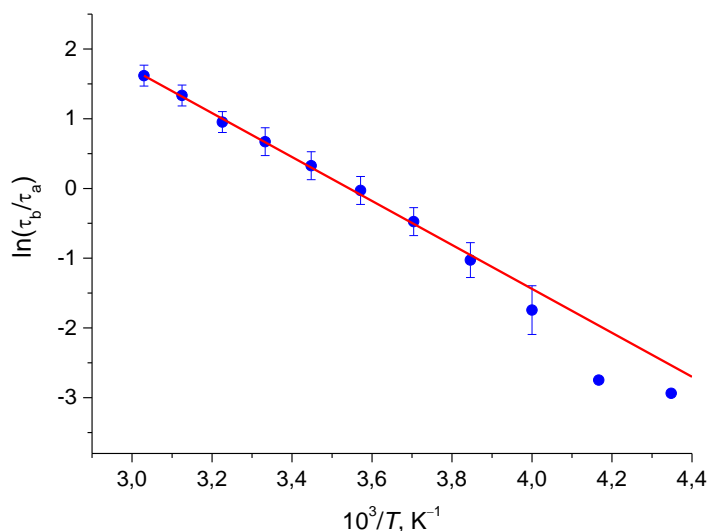


Figure 3-17. The logarithmic plots of relative lifetime ratio of the bent conformation with diradicals close to each other and the extended linear conformation where the radicals stay far away vs. reciprocal temperature and their linear fit of GBN1 in toluene.

3.8 Conclusions

We reported a nitronyl nitroxide diradical system bridged by phenyl-O-(CH₂CH₂O)₆-phenyl which exhibits temperature dependent exchange spin coupling interactions through space. The temperature external stimuli factor is successfully introduced to switch spin properties. The EPR spectra and SQUID measurement gave a clear presentation of magnetic behaviour of the long flexible chain bridged diradicals in solution state or solid state in different temperature. A two conformational model was applied to analyse the thermodynamic parameters to explain the phenomena to some extent. A new equation about the lifetime of bent state conformation and linear stretched state conformation to the relative intensity ratio of second peak and first peak from EPR spectra was first time deduced in a nitronyl nitroxide system to testify the spin exchange coupling. The thermodynamic parameters enthalpy and entropy (ΔH and ΔS) of the conformational changes and the relationships related to different solvents were used to depict the coupling process. The EPR spectra revealed that the polarity and viscosity of the solvents affects the biradical coupling interaction also derived through the thermodynamic parameters, but no linear dependency

could be found. In addition the diradical molecule also exhibits an interesting solvatochromism phenomenon which could be valuable for further research and application.

3.9 References

- (1) Miller, J. S. Magnetically Ordered Molecule-Based Materials. *Chem. Soc. Rev.* **2011**, *40*, 3266-3296.
- (2) Baumgarten, M.; Müllen, K. Radical Ions: Where Organic Chemistry Meets Materials Sciences. *Electron Transfer I*, Mattay, J., Ed. Springer Berlin-Heidelberg, 1994; pp 1-103.
- (3) Gryn'ova, G.; Marshall, D. L.; Blanksby, S. J.; Coote, M. L. Switching Radical Stability by Ph-Induced Orbital Conversion. *Nat. Chem.* **2013**, *5*, 474-481.
- (4) Ratera, I.; Veciana, J. Playing with Organic Radicals as Building Blocks for Functional Molecular Materials. *Chem. Soc. Rev.* **2012**, *41*, 303-349.
- (5) Terreno, E.; Castelli, D. D.; Viale, A.; Aime, S. Challenges for Molecular Magnetic Resonance Imaging. *Chem. Rev.* **2010**, *110*, 3019-3042.
- (6) Winter, S. M.; Hill, S.; Oakley, R. T. Magnetic Ordering and Anisotropy in Heavy Atom Radicals. *J. Am. Chem. Soc.* **2015**, *137*, 3720-3730.
- (7) Park, J. S.; Karnas, E.; Ohkubo, K.; Chen, P.; Kadish, K. M.; Fukuzumi, S.; Bielawski, C. W.; Hudnall, T. W.; Lynch, V. M.; Sessler, J. L. Ion-Mediated Electron Transfer in a Supramolecular Donor-Acceptor Ensemble. *Science* **2010**, *329*, 1324-1327.
- (8) Abe, M. Diradicals. *Chem. Rev.* **2013**, *113*, 7011-7088.
- (9) Coulaud, E.; Hagebaum-Reignier, D.; Siri, D.; Tordo, P.; Ferre, N. Magnetic Exchange Coupling in Bis-Nitroxides: A Theoretical Analysis of the Solvent Effects. *Phys. Chem. Chem. Phys.* **2012**, *14*, 5504-5511.
- (10) Nishizawa, S.; Hasegawa, J.-y.; Matsuda, K. Theoretical Investigation of the B Value of the Π -Conjugated Molecular Wires by Evaluating Exchange Interaction between Organic Radicals. *J. Phys. Chem. C* **2013**, *117*, 26280-26286.
- (11) Wolf, B.; Cong, P. T.; Remović-Langer, K.; Borozdina, Y. D.; Mostovich, E.; Baumgarten, M.; Lang, M. Coupled Spin $S = 1/2$ Dimer Systems Based on Nitronyl-Nitroxide Biradicals. *J. Phys.: Confer. Ser.* **2010**, *200*, 012225 p1-4.
- (12) Shinomiya, M.; Higashiguchi, K.; Matsuda, K. Evaluation of the B Value of the Phenylene Ethynylene Unit by Probing the Exchange Interaction between Two Nitronyl Nitroxides. *The J. Org. Chem.* **2013**, *78*, 9282-9290.

- (13) Fritscher, J.; Beyer, M.; Schiemann, O. Synthesis, Crystal Structure and Magnetic Properties of a Novel Nitroxide Biradical. Theoretical Investigation of the Exchange Mechanisms. *Chem. Phys. Lett.* **2002**, *364*, 393-401.
- (14) Liu, Y.; Villamena, F. A.; Rockenbauer, A.; Song, Y.; Zweier, J. L. Structural Factors Controlling the Spin-Spin Exchange Coupling: Epr Spectroscopic Studies of Highly Asymmetric Trityl-Nitroxide Biradicals. *J. Am. Chem. Soc.* **2013**, *135*, 2350-2356.
- (15) Wang, J.; Hou, L.; Browne, W. R.; Feringa, B. L. Photoswitchable Intramolecular through-Space Magnetic Interaction. *J. Am. Chem. Soc.* **2011**, *133*, 8162-8164.
- (16) Casati, C.; Franchi, P.; Pievo, R.; Mezzina, E.; Lucarini, M. Unraveling Unidirectional Threading of α -Cyclodextrin in a [2]Rotaxane through Spin Labeling Approach. *J. Am. Chem. Soc.* **2012**, *134*, 19108-19117.
- (17) Porel, M.; Ottaviani, M. F.; Jockusch, S.; Jayaraj, N.; Turro, N. J.; Ramamurthy, V. Suppression of Spin-Spin Coupling in Nitroxyl Biradicals by Supramolecular Host-Guest Interactions. *Chem. Commun.* **2010**, *46*, 7736-7738.
- (18) Hagemann, T.; Winsberg, J.; Haupler, B.; Janoschka, T.; Gruber, J. J.; Wild, A.; Schubert, U. S. A Bipolar Nitronyl Nitroxide Small Molecule for an All-Organic Symmetric Redox-Flow Battery. *NPG Asia Mater.* **2017**, *9*, e340 p1-8.
- (19) Nakabayashi, K.; Kawano, M.; Yoshizawa, M.; Ohkoshi, S.-i.; Fujita, M. Cavity-Induced Spin-Spin Interaction between Organic Radicals within a Self-Assembled Coordination Cage. *J. Am. Chem. Soc.* **2004**, *126*, 16694-16695.
- (20) Improta, R.; Barone, V. Interplay of Electronic, Environmental, and Vibrational Effects in Determining the Hyperfine Coupling Constants of Organic Free Radicals. *Chem. Rev.* **2004**, *104*, 1231-1254.
- (21) Chiarelli, R.; Novak, M. A.; Rassat, A.; Tholence, J. L. A Ferromagnetic Transition at 1.48 K in an Organic Nitroxide. *Nature* **1993**, *363*, 147-149.
- (22) Hu, X.; Yang, H.; Li, Y. Syntheses and Spin-Spin Exchange Interactions of Calix[4]Arene Biradicals. *Spec. Chim. Acta A: Mol. Biomol. Spec.* **2008**, *70*, 439-444.
- (23) Matsumoto, K.; Oda, M.; Kozaki, M.; Sato, K.; Takui, T.; Okada, K. Exchange Interaction of Bispyridinyl Diradicals Linked by σ -Frames. *Tetrahedron Lett.* **1998**, *39*, 6307-6310.
- (24) Goldberg, A. H.; Dougherty, D. A. Effects of through-Bond and through-Space Interactions on Singlet-Triplet Energy Gaps in Localized Biradicals. *J. Am. Chem. Soc.* **1983**, *105*, 284-290.

- (25) Barone, V.; di Matteo, A.; Mele, F.; Moreira, I. d. P. R.; Illas, F. Through-Bond and through-Space Effects in the Magnetic Properties of Nitroxide Biradicals by an Integrated Qm/Mm Approach Including Solvent Effects. *Chem. Phys. Lett.* **1999**, *302*, 240-248.
- (26) Ji, L.; Yang, Z.; Zhao, Y.; Sun, M.; Cao, L.; Yang, X.-J.; Wang, Y.-Y.; Wu, B. Sandwich Phosphate Complexes of Macrocyclic Tris(Urea) Ligands and Their Rotation around the Anion. *Chem. Commun.* **2016**, *52*, 7310-7313.
- (27) Ovcharenko, V. I.; Fokin, S. V.; Romanenko, G. V.; Korobkov, I. V.; Rey, P. Synthesis of Vicinal Bishydroxylamine. *Russ. Chem. Bull.* **1999**, *48*, 1519-1525.
- (28) Cha, S.; Choi, M. G.; Jeon, H. R.; Chang, S.-K. Negative Solvatochromism of Merocyanine Dyes: Application as Water Content Probes for Organic Solvents. *Sens. Actuat. B: Chem.* **2011**, *157*, 14-18.
- (29) Reichardt, C. Solvatochromic Dyes as Solvent Polarity Indicators. *Chem. Rev.* **1994**, *94*, 2319-2358.
- (30) Hagen, W. R. *Biomolecular EPR Spectroscopy*. CRC Press, 2009.
- (31) Atherton, N. M. *Principles of electron spin resonance*, Ellis Horwood Limited, PTR Prentice Hall, 1993.
- (32) Ionita, G.; Vorobieva, G. A.; Chechik, V.; Kokorin, A. I. Intramolecular Spin Exchange in Flexible Peg-Based Nitroxide Biradicals in Aqueous Solutions. *Appl. Magn. Res.* **2015**, *46*, 251-260.
- (33) Sankarapandi, S.; Sukumar, M.; Balaram, P.; Manoharan, P. T. Biradicals as ESR Probes of Conformations in Model Beta-Turn Peptides. *Bioche. Biophys. Res. Comm.* **1995**, *213*, 439-446.
- (34) Szydłowska, J.; Pietrasik, K.; Głaz, Ł.; Kaim, A. An ESR Study of Biradicals Formed from Two 4-Amino-TEMPOs Linked by $-(\text{CH}_2)_n-$, ($n = 2, 3, 4, 6$). *Chem. Phys. Lett.* **2008**, *460*, 245-252.
- (35) Komaguchi, K.; Iida, T.; Goh, Y.; Ohshita, J.; Kunai, A.; Shiotani, M. An ESR Study of Dynamic Biradicals of Two TEMPOs Bridged with $-(\text{SiMe}_2)_n-$ ($n=1-4$) in Liquid Solution. *Chem. Phys. Lett.* **2004**, *387*, 327-331.
- (36) Ionita, G.; Meltzer, V.; Pincu, E.; Chechik, V. Inclusion Complexes of Cyclodextrins with Biradicals Linked by a Polyether Chain-an EPR Study. *Org. & Biomol. Chem.* **2007**, *5*, 1910-1914.
- (37) Parmon, V. N.; Kokorin, A. I.; Zhidomirov, G. M.; Zamaraev, K. I. On the Mechanism of Spin Exchange in Long-Chain Nitroxide Biradicals. *Mol. Phys.* **1975**, *30*, 695-701.

- (38) Parmon, V. N.; Zhidomirov, G. M. Calculation of the E.S.R. Spectrum of a Dynamic Biradical System with More Than Two Conformations. *Mol. Phys.* **1976**, *32*, 613-619.
- (39) Parmon, V. N.; Kokorin, A. I.; Zhidomirov, G. M. Conformational Structure of Nitroxide Biradicals Use of Biradicals as Spin Probes. *J. Struct. Chem.* **1977**, *18*, 104-147.
- (40) Tran, V. A.; Rasmussen, K.; Grampp, G.; Kokorin, A. I. The Solvent Effect on Spin Exchange in Long-Chain Nitroxide Biradicals. *Appl. Magn. Res.* **2007**, *32*, 395-406.
- (41) Tran, V. A.; Kokorin, A. I.; Grampp, G.; Rasmussen, K. Features of Spin Exchange in Nitroxide Biradicals in the Ionic Liquid BmimPF₆. *Appl. Magn. Res.* **2009**, *35*, 389-398.
- (42) Smallwood, I. M. *Handbook of Organic Solvent Properties*, Butterworth-Heinemann: Oxford, 1996.
- (43) Gilmont, R. Liquid Viscosity Correlations for Flowmeter Calculations. *CEP magazine*, **2002**, *10*, 36-42.

Chapter 4 Redox Stimuli Spin Responsive Systems with the Formation of Cation-Radical Diradicals

External redox stimuli factor refers to utilizing oxidant or reductant to change a system by chemical reactions. During the process of stimuli, there are some spin units or magnetic properties changing.^{1,2} The redox stimuli factor is the only chemical way among all the external stimuli factors.³ In this chapter, we investigated four organic stable radicals for redox stimuli responsive properties to explain the spin switching process. We provide strong experimental evidences about the formation of spin molecules composed of stable radical and cation radical during the oxidation stimuli, and the spin coupling interaction between the two spin centers.

4.1 Introduction

Two typical organic radical groups nitronyl nitroxide (NN) and imino nitroxide (IN)^{4,5} were functionalized to phenothiazine and phenoxazin which form tertiary amine structures (could transform to cation radical^{6,7} when an electron lost). The four new structures are 10-phenyl-3,7-dithiophen-phenothiazine-NN, 10-phenyl-3,7-dithiophen-phenothiazine-IN, 10-phenyl-phenoxazine-NN, 10-phenyl-phenoxazine-IN, which were labeled as PDTN-NN, PDTNIN, PO-NN and PO-IN respectively, as shown in figure 4-1. An electron donor group is indispensable to a spin-polarized open shell structure.^{8,9} Phenothiazine and phenoxazine were taken into consideration as classical electron donors in recent two or three decades.¹⁰⁻¹⁴ Planar structures with ten atom π system which contain secondary amine are redox-active. The spin density distribution of nitrogen cation radical is delocalized on the whole phenothiazine or phenoxazine conjugated structures. K. Okada and coworkers synthesized a series of phenothiazine based radical cations and diradical dications¹⁵⁻¹⁷ which exhibited high spin intra or intermolecular coupling.^{18,19} But the questions about coexistence of the delocalized spin of tertiary amine cation radical and the localized spins of nitroxide radical group appeared and the spin interactions between them still lack of proper investigation.²⁰ For typical stable organic radical groups NN and IN, the spin distributions are localized on O-N=C-N-O \cdot and N=C-N-O \cdot fragments, respectively. They have become vital spin function groups in organic synthesis.^{4,21} The asymmetrical fragments O-N=C-N-O \cdot in NN are actually tautomers. The fragment O-N=C-N-O \cdot and \cdot O-N-C=N-O interconvert to each other in equilibrium.²²⁻²⁵ The spin density

distribution of NN and IN would also be influenced by the newly-formed delocalized cation radicals and the change of redox conditions in whole process.

Apparent color change of oxidization process:

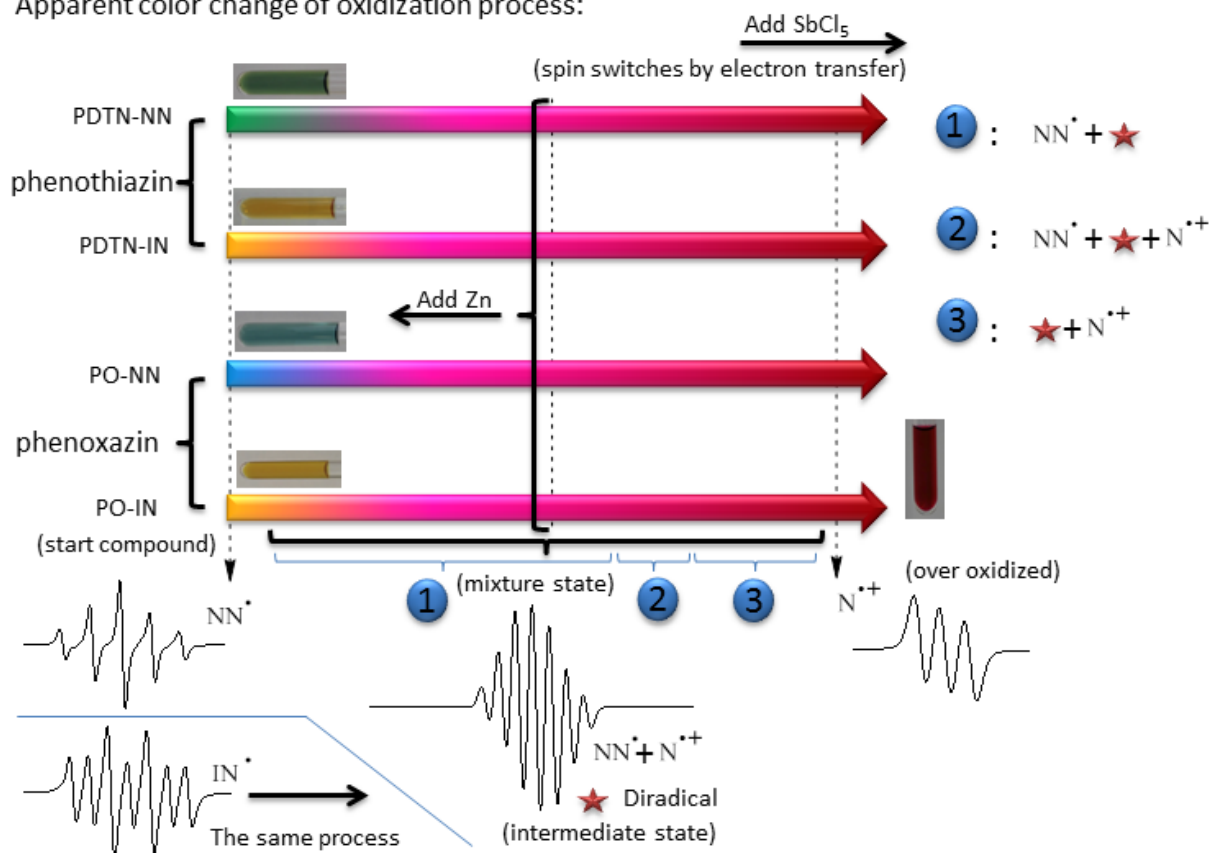


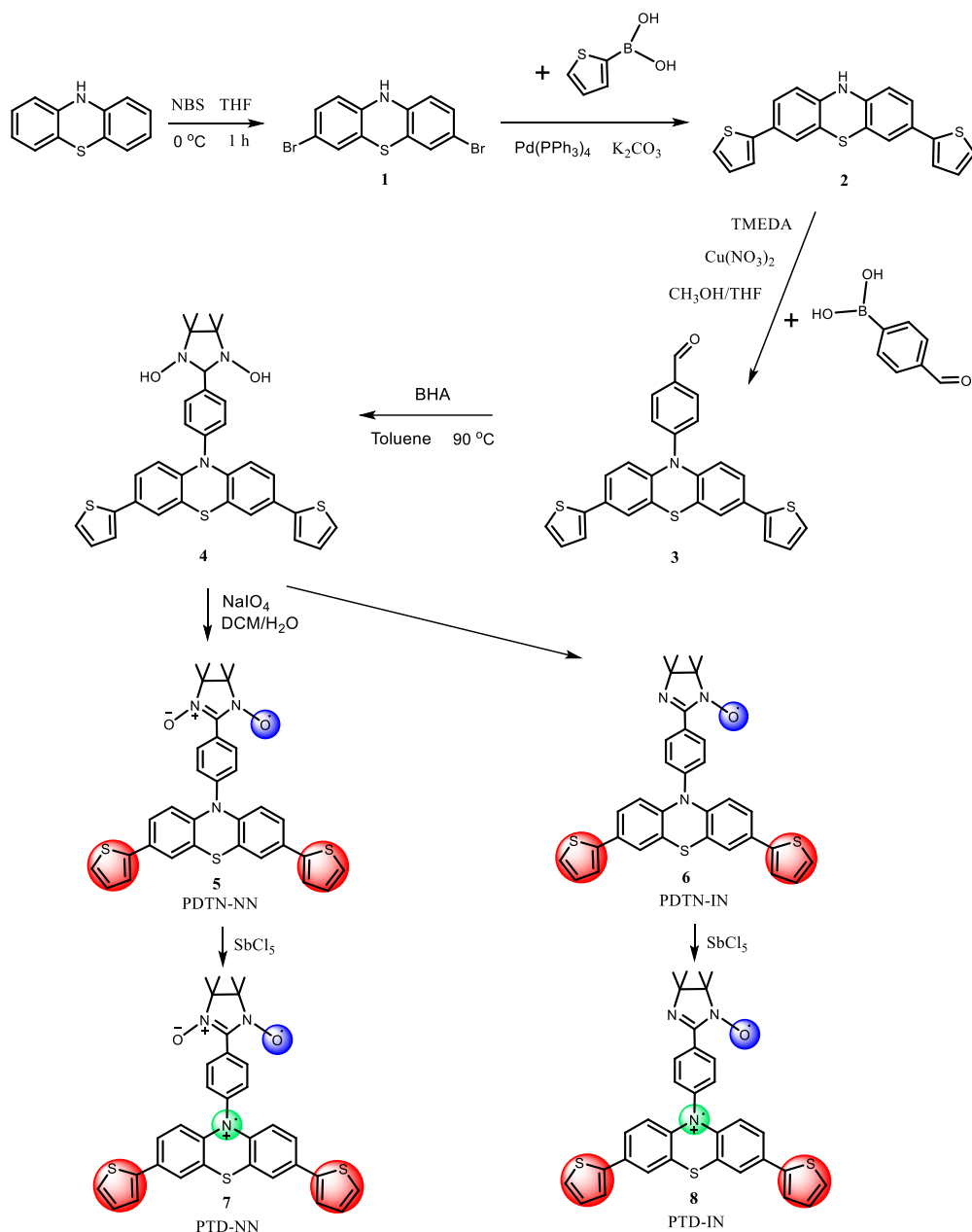
Figure 4-1. The apparent color and different oxidation stages of the four spin systems in the redox process

Till to now, the investigations of basic physical and chemical process about how does the new diradical composed of stable radical and cation radical form and the experimental evidences about intramolecular spin properties switch upon the change of oxidation and reduction conditions are still relatively scarce.²⁶⁻³³ Although most of interests and research efforts in the field of organic cation radical have focused on the synthesis and application of spintronics.⁸ This work provides four new radicals (PDTN-NN, PDTNIN, PO-NN and PO-IN). NN and IN are connected with donors phenothiazine combined with two thiophenes at 3,7 positions and phenoxazine through 1,4-phenylene spacer respectively.³⁴ Oxidations with SbCl_5 (with a series of ratios) were carried out by titration for the four structures in DCM.^{35,36} The apparent color of solutions suddenly changed to pink color then continuously deepen to red until the final dark red. Two different stages (mixed state and over oxidized state) successively appeared during the process of oxidation. The mixed state with pink color is the first stage which has a similar

EPR signal pattern with nitroxide radical at beginning. As the titration of oxidant SbCl_5 , the sample's EPR signals have the trend to be influenced by tertiary amine nuclei. The original quintet signal and heptet signal patterns were affected by hyperfine splitting from nitrogen nuclei which belongs to the new formed nitrogen cation radical (the nuclear spin angular momentum $I=1$ for ^{14}N), and the numbers of peaks incline to split more. Further oxidation would lead the mixed state close to over oxidized state. The EPR signal at this stage is also more and more similar with the typical nitrogen cation radical (3 lines pattern spectrum). So actually the mixed state can be divided into three stages with different components of radical species, due to the newly formed diradical molecules. The over oxidized state happened when the electric potential of oxidation is higher than the oxidation potential of nitroxide radical and most of nitroxide radical structures were destroyed at about more than 5 equivalents of oxidant. The g factor also changed slightly upon the whole different stages, due to the process of new spin center formed and the destruction of nitroxide radical. Normally, the apparent g factor which calculated from the equation $g = h\nu/\mu_B B_c$ is average value of g factors of all radicals which existed in whole molecule. For our case the apparent g factor g_{av} is average of the original nitroxide radical g_{or} and new formed nitrogen cation radical g_{ne} , which could be written as $g_{av} = (g_{or} + g_{ne}) / 2$.³⁷ We also observed a temperature dependent reversible feature in EPR that the spin features of mixed state switch between the spin intermediate and typical three line pattern signal of cation nitrogen radical in the temperature range from rt to around 200 K. Reversible redox features which lead to intramolecular spin properties change were also testified by oxidant AgSbF_6 and reductant Zn on the opposite direction to oxidation in mixed state.

The whole process of spin switches of the four synthesized structures (scheme 4-1, 4-2) were investigated by using electron paramagnetic resonance (EPR).^{38,39} The electronic interaction between donor (phenothiazine, phenoxazin) and nitroxide radical (NN, IN) was also confirmed by UV-Vis absorption spectroscopy and cyclic voltammetry (CV). Density functional theory (DFT) was used to calculate the electron spin density distributions of the four organic radicals in different valence states.⁴⁰⁻⁴² From the calculated J value, we found that the newly formed cation-radical diradical species own intramolecular ferromagnetic coupling interaction.

4.2 Synthesis of Cation-Radical Diradicals



Scheme 4-1. Synthesis of mono-radical PDTN-NN, PDTN-IN and cation-radical diradicals PTD-NN, PDT-IN

All the four new synthesized cation-radical diradicals are started from phenothiazine and phenoxazin which are commercial compounds. The routes of functionalization of aldehyde groups are according to a similar method as previously published.⁴³⁻⁴⁵ For the synthesis of PTD-NN, PTD-IN, as the scheme 4-1 of synthesis route shown above, the first step is dibromination of phenothiazine on 2 and 7 positions. The adding process of N-bromosuccinimide should be very carefully dropwise. The quantity of N-bromosuccinimide should be also controlled (the ratio to phenothiazine is 2 : 1) precisely to eliminate some other bromination byproducts of phenothiazine (the dots of mono-bromination byproduct to tri-

bromination byproduct on TLC board stay so close that is hard to separate). Compound 2,7-dibromo-10H-phenothiazine **1** which is green solid was acquired with the yield of 50% — 55%.

The second step of synthesizing 2,7-dithien-2-yl-10H-phenothiazine **2** from the compound **1** is using Suzuki coupling with 2-thienylboronic acid. The product **2** is yellow solid with metal-like gloss after purification, and the final yield of double thiophene substitution is around 70%. The third step 2,7-di(thiophen-2-yl)-10-(benzaldehyde-4-yl)phenothiazine **3**, where an aldehyde group was introduced to compound **2**, is the most important reaction to prepare stable radical precursor among the whole synthesis route. The secondary amine which belongs to phenothiazine was coupled with the boronic acid group by following Chan-lam coupling reaction.^{46,47} The same quantity of tetramethylethylenediamine (TMEDA) to copper nitrate was employed as a ligand for Cu ions. The complex ligand and metal ions could notably increase the reaction yield. In addition, air bubbling is necessary during the coupling reaction, due to the promotion effect of oxygen. The NMR spectrum of the new precursor (figure 4-2) is shown below. The proton labeled "a" in figure clearly attribute to aldehyde group with the peak position at 10.0 ppm. The ratio of integral of the proton "a" and the different protons belong to aromatic positions is about 1 : 16. The positions of all the protons belong to compound **3** are labeled clearly on the right top (magnification of spectrum from 7 ppm to 8 ppm) of the figure, and every ratio of aromatic protons to proton "a" is around ratio 2 : 1. In addition the calculated MW = 467.1; FD. Mass: 467.7. (the detail positions of ¹H NMR are described in chapter 6)

The synthesis of 2,7-di(thiophen-2-yl)-10-(benzimidazolidine-4-yl)phenothiazine **4** is an annelation reaction to form an intermediate structure *N,N'*-dihydroxyimidazolidines. The condensation reaction of aldehyde precursor **3** with 2,3-diamino-*N,N'*-dihydroxy-2,3-dimethylbutane (BHA) according to a similar procedure was realized in absolute dry toluene, which was degassed by argon bubbling before. Then the reaction mixture was heated to 90 °C and stirred for 36 h. The color of mixture turned to orange. The mixture was washed by MeOH for two times, and the solvent was evaporated. The product does not need further purification and directly used for next step.

The synthesis of radical structure PDTN-NN **5** and PDTN-IN **6** were performed through oxidation of **4** with sodium periodate as oxidizing agent in a two-phase solvent mixture of water and DCM, in ice bath with the temperature 0 °C. After 1 hour oxidation reaction, **5** and **6** were simultaneously acquired in the reaction. The reason is over oxidation

of **5** with sodium periodate would lead to the formation of **6**. So the reaction time is a key factor of this oxidation process. The longer time it takes, the more compound **6** obtained. The two products have different value of *r_f* on TLC board. **5** has a smaller *r_f* value and moved slower than **6** on TLC board. In addition the apparent color of **5**, which is green, and **6**, which is orange, also have a big difference that could easily be distinguished on the TLC board. The mixture products were separated by column chromatography providing a MS-FD MW= 594.1 g/mol fully consistent with the calculated mass for PDTN-NN. And partially over oxidized product PDTN-IN could also be isolated by column chromatography providing a mass of MS-FD MW= 577.9 g/mol. The products were also confirmed by UV-Vis absorption spectroscopy and EPR measurements.

The last step of formation of cation-radical diradicals PTD-NN **7** and PTD-IN **8** were performed by adding oxidant SbCl_5 to the solution of **5** and **6** respectively. The solution colors of both were changed to red. The whole reaction processes were monitored by UV-Vis absorption measurement and EPR measurements.

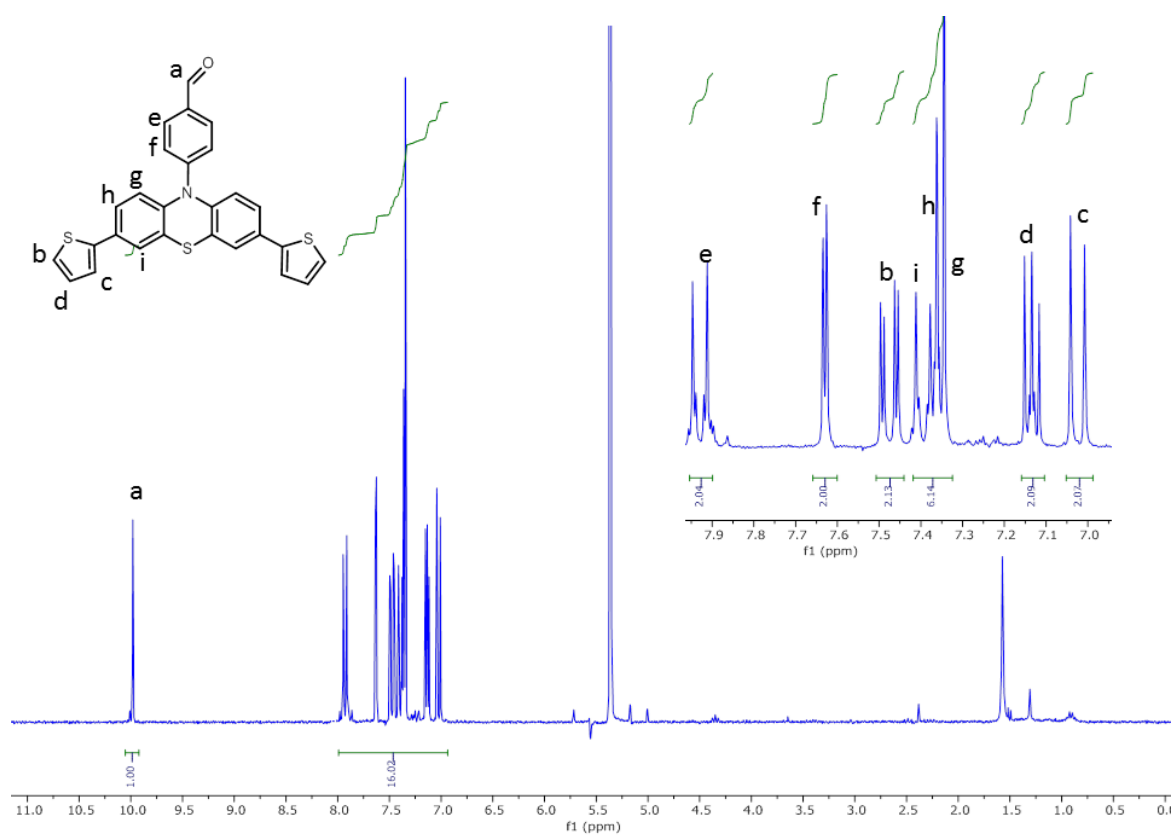
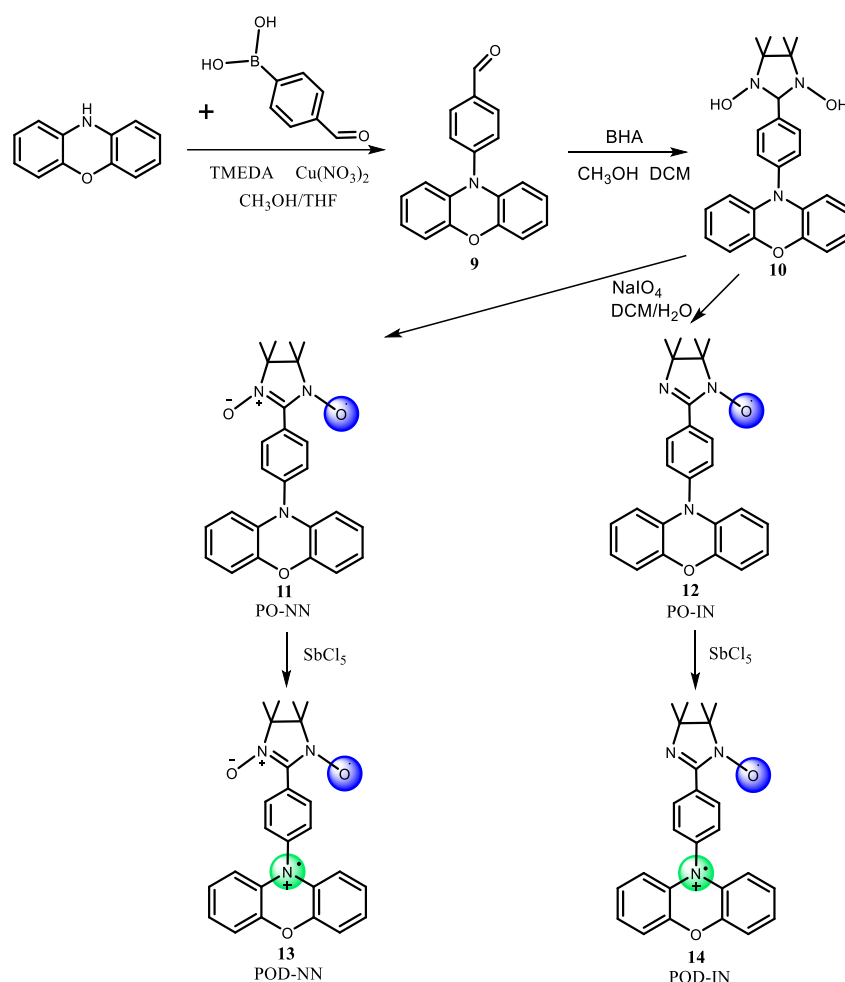


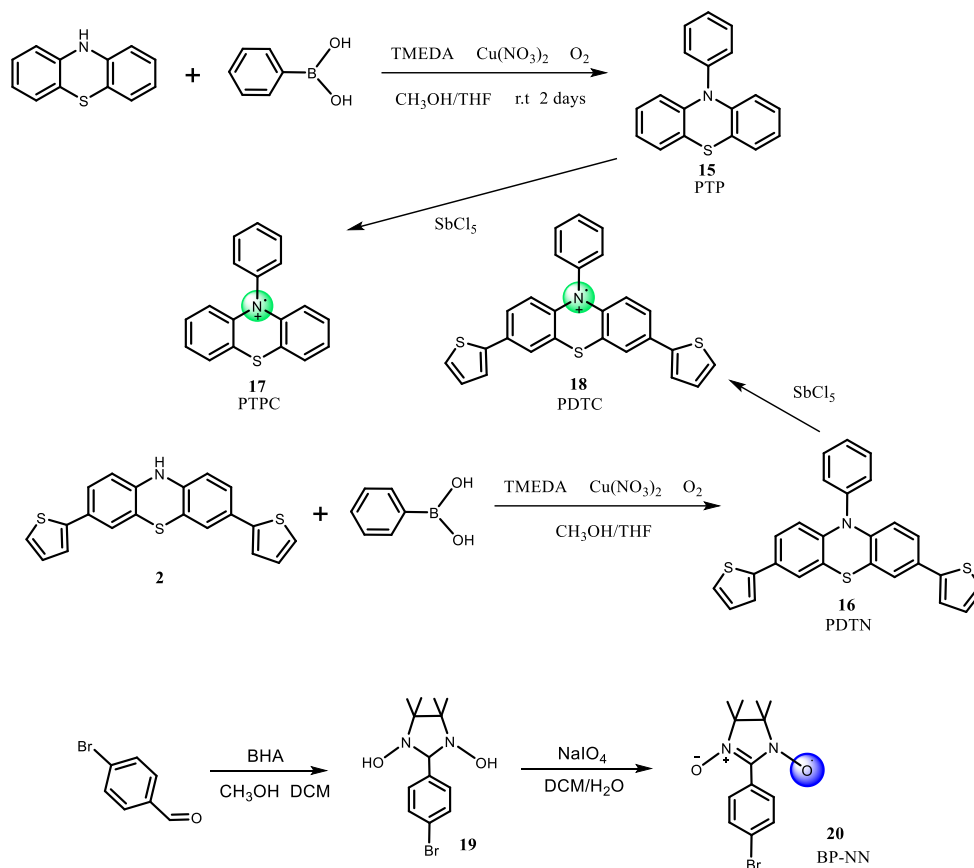
Figure 4-2. ^1H NMR spectrum (250.0 MHz) of **3** in CD_2Cl_2 at room temperature

For the synthesis of POD-NN **13**, POD-IN **14**, as the scheme 4-2 of synthesis route shown below, the most of steps are similar with the synthesis of **7** and **8**, which discussed above. The differences are the starting compound is phenoxazin, rather than 2,7-dithien-2-yl-10H-phenothiazine **2**, and the colors of PO-NN, PO-IN are light blue and orange respectively.



Scheme 4-2. Synthesis of mono-radical PO-NN, PO-IN and cation-radical diradicals POD-NN, POD-IN

For comparison with cation-radical diradicals, one stable radical with NN structure and two precursors which can be oxidized to cation radicals were synthesized, as shown in scheme 4-3. The same method Chan-lam coupling reaction was used to synthesize PTP **15** and PDTN **16** from phenothiazine and dithiophen-phenothiazine, respectively. The cation radical PTPC **17** and PDTN **18** were oxidized by SbCl_5 in the solution of DCM with the same procedure as **7** and **8**. A nitronyl nitroxide radical connected with bromobenzene, BP-NN **20** was synthesized for comparison. MS-FD and EPR measurements were used for structure characterization.



Scheme 4-3. Synthesis of mono-cation radical PTPC, PDTC and bromobenzene-NN

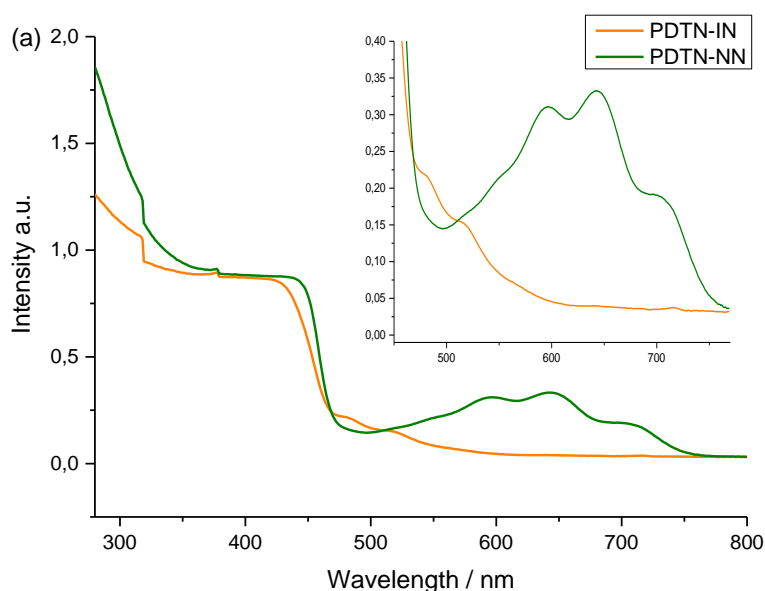
4.3. Optical Properties

4.3.1. UV-Vis Absorption Spectra of Radicals with Phenothiazine and Phenoxazin

The UV-Vis absorption measurements can provide not only clear characteristic absorptions of NN and IN radical, but also the calculation of energy of transition between SOMO and LUMO from absorption band. For our NN and IN functionalized with phenothiazine, the characteristic absorptions are shown in figure 4-3 (a). There are two distinctive districts on each absorption band. The absorption peaks between 330 nm to 450 nm originate from the p-p* transition of the substituted dithiophene-phenothiazine-imidazolidine. The other region of absorption peaks which are between 460 nm to 700 nm belong to the n-p* transition of two different nitronyl nitroxide and imino nitroxide respectively. So this absorption region is the main characteristic absorptions to distinguish NN and IN. for PDTN-NN, the main absorption of NN (originate from aminoxyl moieties) is from 580 nm to 700 nm, and the maximum peak is 640 nm, while a NN moiety (without other functional groups) has a maximum absorption around 610 nm ~ 620 nm. This difference is attributed to the influence

of dithiophene-phenothiazine groups. The electron donor groups, which have the ability for pushing electron, made the SOMO of molecule higher. It would shrink the energy gap between SOMO and LUMO of NN group. So this is also the reason of the PDTN-NN' color is green, while a NN group with phenyl is blue. The characteristic absorption of PDTN-IN originated from aminoxyl moiety (orange color) is around 470 nm to 520 nm. The maximum absorption is around 480 nm.

The same principle was used to interpret UV-Vis absorption spectra of PO-NN and PO-IN, as shown in figure 4-3 (b). We could clearly distinguish the different absorptions of $p-p^*$ transition region which belong to phenoxazin and phenothiazine. The interactions of the two conjugated donor structures also have different influence on the nitroxide radicals which they connected to, especially to NN radical. The characteristic absorptions of radicals to PO-NN are from 550 nm to 700 nm, and the maximum peaks are 590 nm and 625 nm. This also indicates that the electron donor ability of dithiophene-phenothiazine is stronger than phenoxazin group. The difference on structure led the apparent color of PO-NN to light blue. The characteristic absorption of PO-IN which also originated from aminoxyl moiety is from 460 nm to 520 nm. The maximum absorption is around 480 nm.



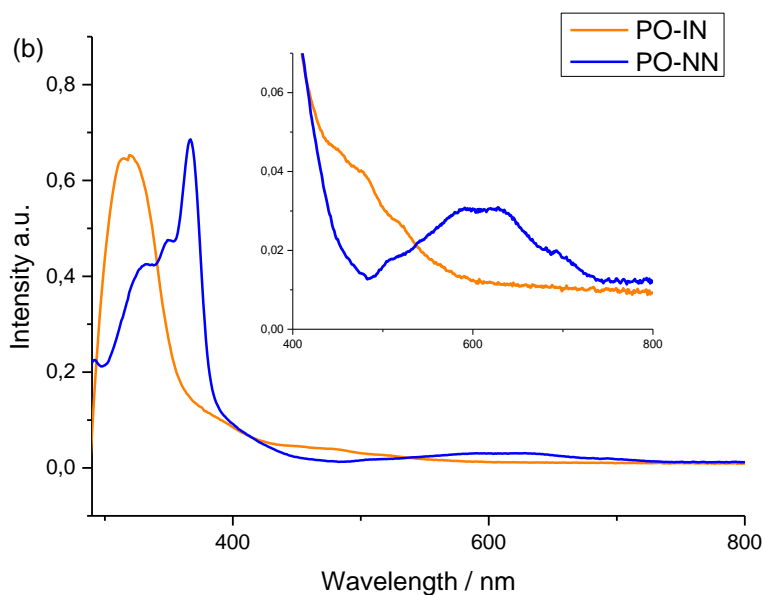


Figure 4-3. a) UV-Vis absorption spectra of PDTN-NN **5** and PDTN-IN **6** recorded in DCM solutions at room temperature. Inset: amplification of optical absorption spectra in the visible range from 400 nm to 800 nm. b) UV-Vis absorption spectra of PO-NN **11** and PO-IN **12** recorded in DCM at rt. Inset: amplification of optical absorption spectra in the visible range from 400 nm to 800 nm.

4.3.2. UV-Vis Absorption of Redox Stimuli Responsive Process and Cation Radicals

In order to investigate the whole process of the oxidation from mono nitroxide radicals to intermediate states, then to over oxidized radicals, we utilize UV-Vis absorption measurement to monitor the titration of the four structures (PDTN-NN, PDTNIN, PO-NN and PO-IN) with oxidant SbCl_5 in DCM by series ratios from 0.01 eq to 50 eq. The concentrations of substrates are 1.0×10^{-5} . (guarantee the total concentration of solutions are the same during the whole titration process) We got whole process change of UV-Vis absorption spectra of four molecules oxidation, as shown in figure 4-4 to 4-7 respectively below. The apparent color of the four sample solutions changed to pink no matter from green, orange or light blue of starting compounds. Then the color of samples continuously changed to red until the final dark red. All the characteristic absorptions belong to the four structures gradually changed during the series of oxidative titration.

Figure 4-4 (a) shows the spectrum change of whole titration process of PDTN-NN. Two main districts were detected characteristic absorptions enhancement, one is around 310 nm ~ 350 nm (the maximum absorption at 315 nm) and the other is around 450 nm ~ 580 nm (the maximum absorption at 555 nm), during the whole process of adding oxidant SbCl_5 .

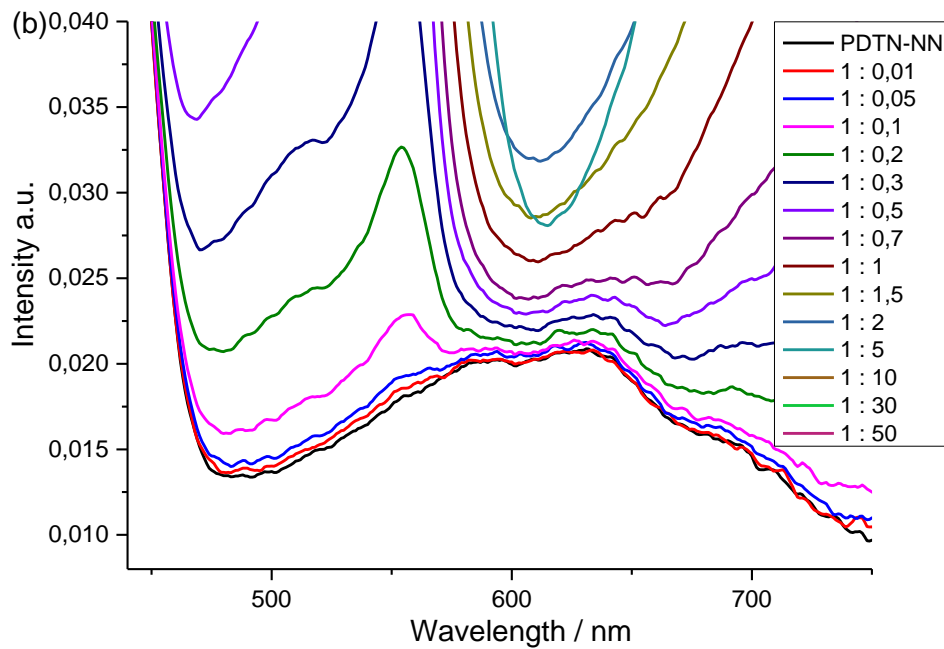
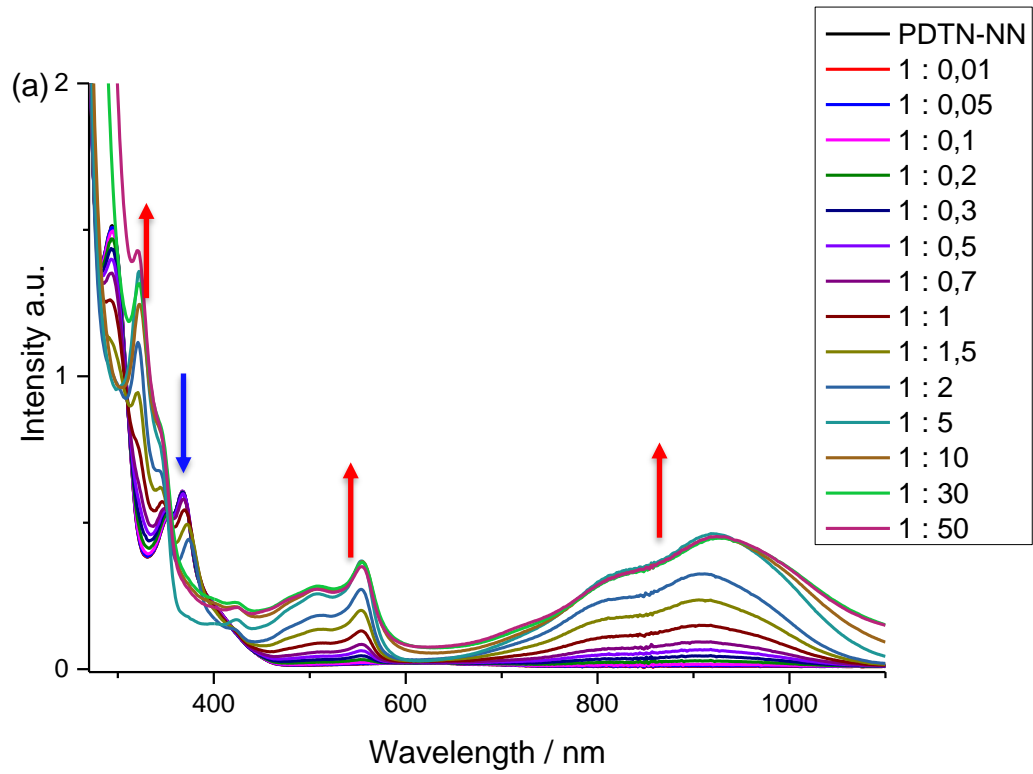


Figure 4-4. a) UV-Vis absorption spectra of the whole titration process of PDTN-NN by adding different ratios of oxidants SbCl_5 recorded in DCM at rt. b) Amplification of optical absorption spectra in the visible range from 400 nm to 800 nm.

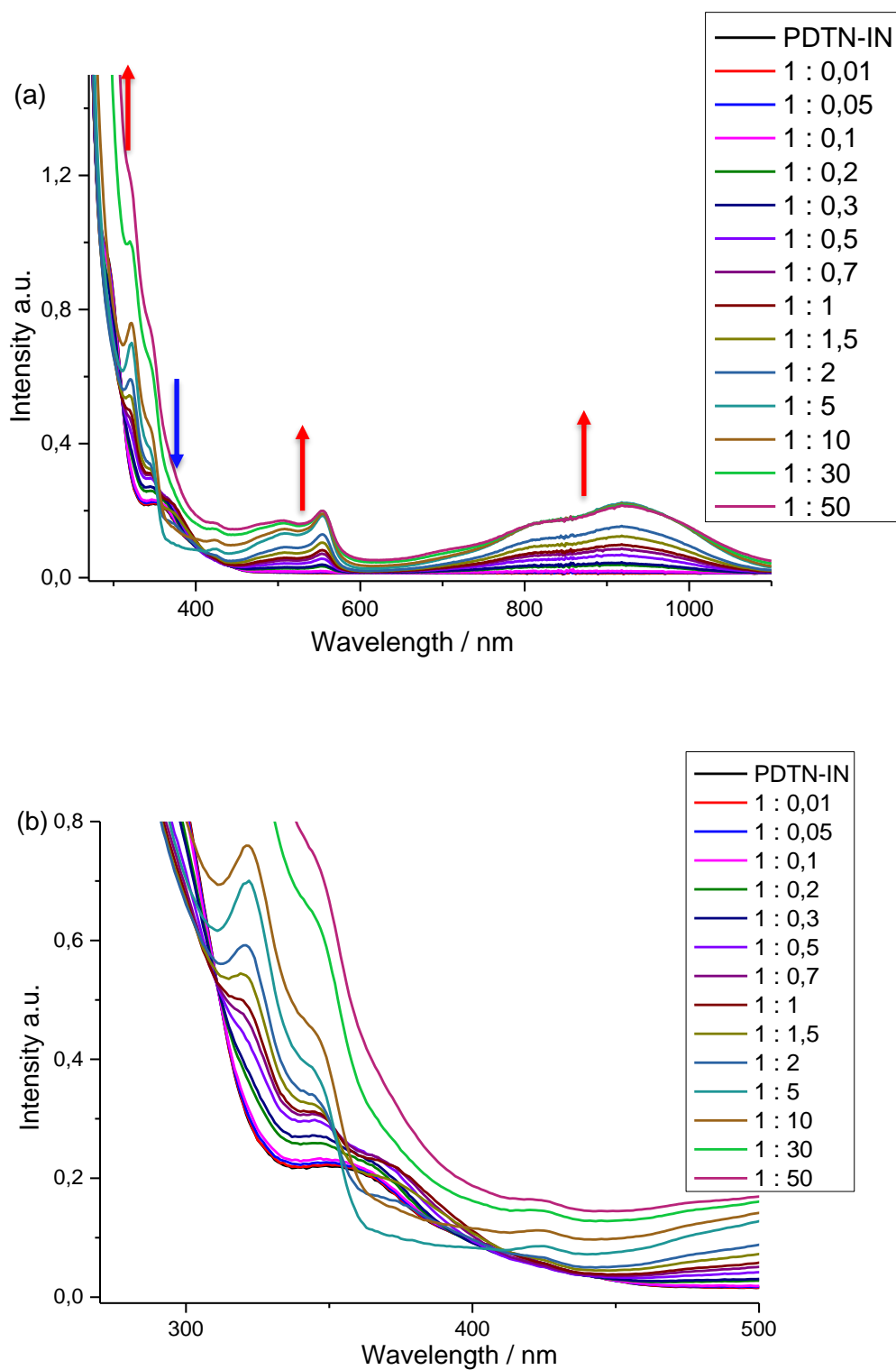


Figure 4-5. a) UV-Vis absorption spectra of the whole titration process of PDTN-IN by adding different ratios of oxidants SbCl_5 recorded in DCM at rt. b) Amplification of optical absorption spectra in the range from 300 nm to 500 nm.

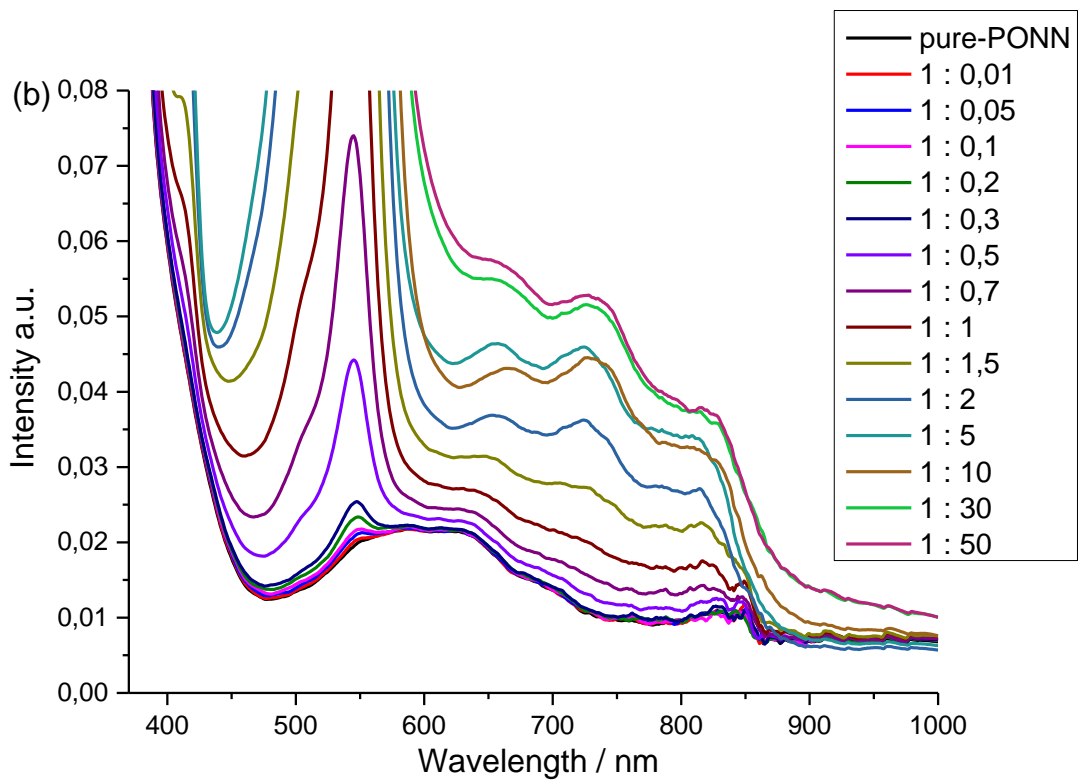
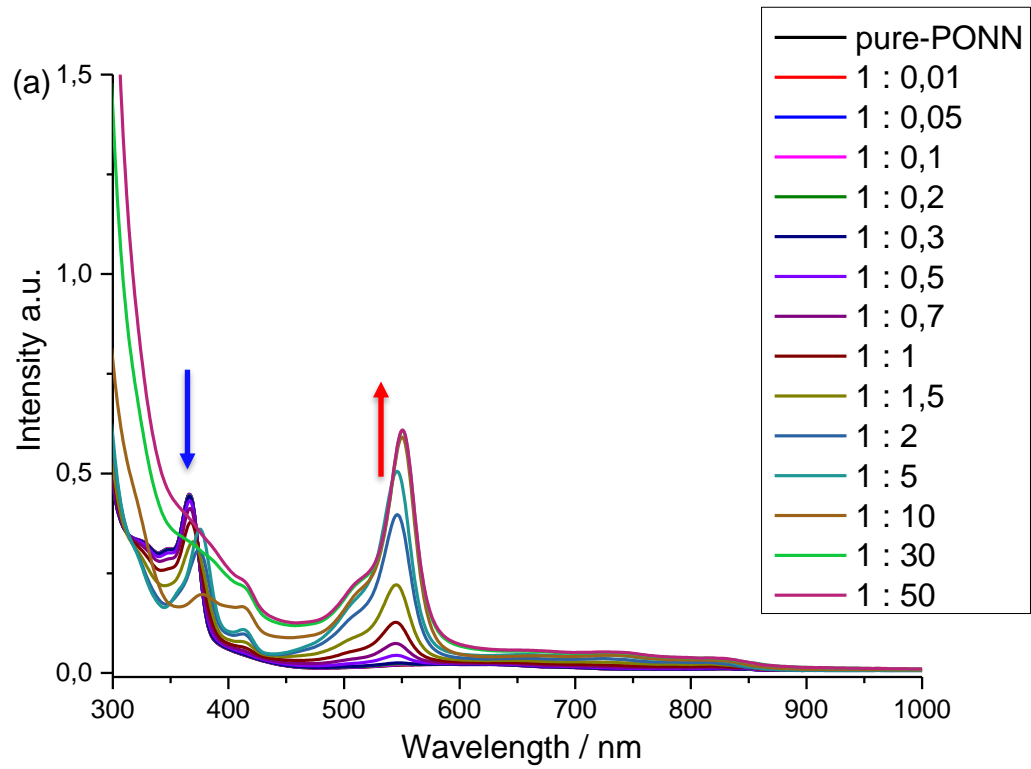


Figure 4-6. a) UV-Vis absorption spectra of the whole titration process of PO-NN by adding different ratios of oxidants SbCl_5 recorded in DCM at rt. b) Amplification of optical absorption spectra in the range from 400 nm to 1000 nm.

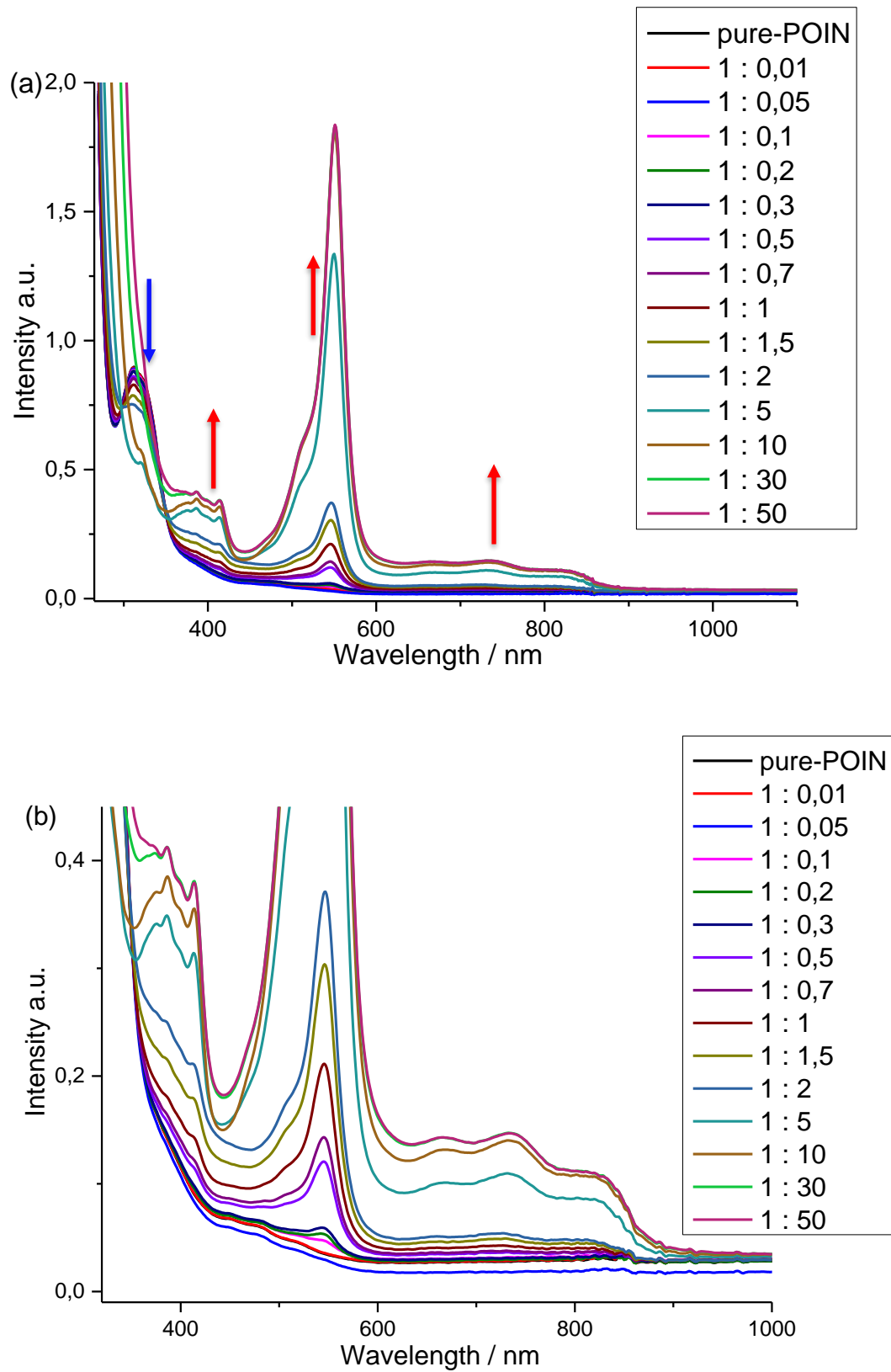


Figure 4-7. a) UV-Vis absorption spectra of the whole titration process of PO-IN by adding different ratios of oxidants SbCl_5 recorded in DCM at rt. b) Amplification of optical absorption spectra in the range from 320 nm to 1000 nm.

Figure 4-4 (b) can exactly prove the existence of NN groups in the condition of 1 oxidant equivalent. That means new structure formed during the electron transfer in the oxidation process, but the nitronyl nitroxide group is still stable under this situation. As the oxidation proceed to around the ratio of SbCl_5 to 5 eq, the absorption between 360 nm ~ 380 nm which belongs to imidazolidine (the maximum absorption at 370 nm) suddenly disappeared. Another characteristic absorption attributed to NN (originate from aminoxyl moieties from 580 nm to 670 nm, and the maximum peak is 640 nm,) is also changed at the same condition. The change of absorptions indicate that as the gradually increasing ability of oxidation to critical point, NN radical group could not bear the high concentration of SbCl_5 further, and was oxidized gradually as in CV experiments. These two characteristics can directly prove the nitronyl nitroxide radical was decomposed. The absorptions of new formed structure in the former stage continuously increase, till to a specific point (maximum value). The whole trend of absorption transition elucidate that the new formed structure started from the beginning of oxidation, and ended short before terminal point. But the decomposition of NN group started after the formation of large quantity of PTD-NN.

The general oxidation process and the critical point of structure transition of PDTN-IN, PO-NN and PO-IN are similar to PDTN-NN. Only the peak positions of absorptions have a little bit difference. For the case of PDTN-IN in oxidative titration experiment, as shown in figure 4-5, the spectra presented two regions of characteristic absorptions enhancement: one is around 310 nm ~ 355 nm (the maximum absorption at 320 nm), the other region is the same with PDTN-NN around 450 nm ~ 580 nm (the maximum absorption at 555 nm). As the oxidation proceed to around the ratio of SbCl_5 to 5 eq, the absorptions between 350 nm ~ 400 nm which belong to imidazolidine (the maximum absorption at 370 nm) and characteristic absorption peak of IN aminoxyl moiety (480 nm) suddenly disappeared. These phenomena indicate the imino nitroxide radical was decomposed at this oxidation condition. For the case of PO-NN as shown in figure 4-6, two districts of absorptions increase, one is around 400 nm ~ 430 nm (the maximum absorption at 415 nm) and the other region is around 460 nm ~ 590 nm (the maximum absorption at 545 nm), during the whole process of adding oxidant SbCl_5 . As the oxidation proceed to around the ratio of SbCl_5 to 5 eq, the absorptions between 320 nm ~ 380 nm which belongs to imidazolidine (the maximum absorption at 370 nm) and

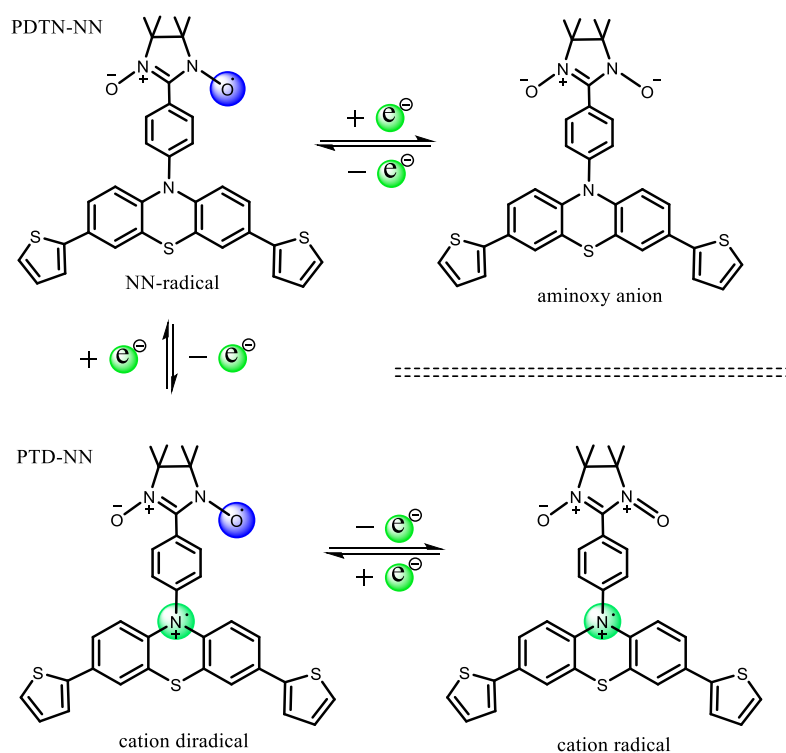
characteristic absorption to NN aminoxy moieties (580 nm ~ 620 nm) were gradually reduced. These decreases of absorptions indicate the NN radical was oxidized in the period of oxidation condition. For the case of PO-IN as shown in figure 4-7. two districts of absorptions increase, one is around 350 nm ~ 425 nm (the maximum absorption at 385 nm) and the other region is around 480 nm ~ 590 nm (the maximum absorption at 545 nm), during the whole process of adding oxidant SbCl_5 . As the oxidation proceeded to around the ratio of SbCl_5 to 5 eq, the absorptions between 300 nm ~ 345 nm which belongs to imidazolidine (the maximum absorption at 315 nm) and characteristic absorption peak to IN aminoxy moiety (470 nm ~ 520 nm) were gradually reduced. These decreases of absorptions indicate the IN radical was decomposed at this oxidation condition.

4.4. Cyclic Voltammetry Measurements

In order to investigate the electrochemical properties and the oxidation process of the four new molecules PDTN-NN, PDTNIN, PO-NN and PO-IN with PTP, PDTN and BP-NN for comparison, Cyclic Voltammetry (CV) measurements were carried out. The CV experiments were performed by using a three-electrode cell in CH_2Cl_2 solution of tetrabutylammonium tetrafluoroborate ($n\text{-C}_4\text{H}_9$) $_4\text{NPF}_6$ (0.1 M) with a scan rate of 100 mV/s at room temperature. Three electrodes, which are platinum (Pt) electrode, silver (Ag) electrode, and glassy carbon electrode, respectively were used as the counter electrode, reference electrode, and the working electrode. Ferrocene which has a formal potential at 0.46 V in DCM with ($n\text{-C}_4\text{H}_9$) $_4\text{NPF}_6$ (0.1 M) was used as an internal standard, and the difference between experimental value of oxidation potential and 0.46 V should be deducted from spectra. All the final CV curves reported in this part were calibrated by Fc/Fc^+ couple at 0.46 V with the experimental potential value of Fc/Fc^+ , and the experimental value of potentials ($E_{1/2}$, half wave potential, the central point between the maximum point and minimum point) were against with Ag/AgCl (0 V).

For a general case of mono nitronyl nitroxide radical, there is only one oxidation and reduction peak in CV measurements. When an electron is lost in oxidation cycle, the NN moiety became oxoammonium cation moiety without unpaired electron anymore. While an electron acquired in reduction cycle, the NN moiety became aminoxy anion moiety and also without unpaired electron. Both of the processes are reversible in CV measurement condition. Imino nitroxide radical has a similar reduction cycle as NN moiety, while the oxidation cycle

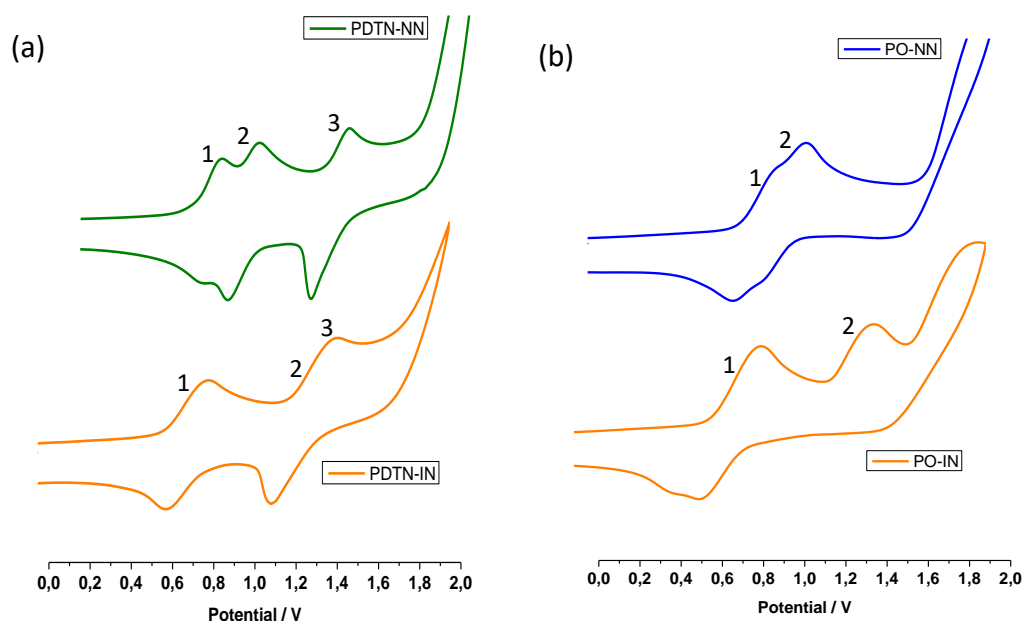
of IN is non-reversible cycle, and about 0.32 V higher than the oxidation potential of NN, without a complete oxidation cycle peak. When nitroxide radical is connected with other conjugated structures which could be oxidized to cation radical, the CV spectrum becomes complicated. We took PDTN-NN structure as predicted sample, shown in scheme 4-4. The reduction process has no difference to mono NN radical while the oxidation has three steps which mean three oxidation potential peaks in the CV spectrum, as shown in figure 4-8 (a) the green spectrum. The first oxidation peak occurred at $E_{\text{oxi-1}} = 0.78$ V which means one electron is lost at tertiary amino, meanwhile a new nitrogen cation radical formed. The whole molecule PDTN-NN became a cation diradical (PTD-NN). The next oxidation with the potential at $E_{\text{oxi-2}} = 0.93$ V led the NN group lose an electron and change to oxoammonium cation. The whole molecule PTD-NN changed to mono cation radical. The third oxidation peak which $E_{\text{oxi-1}} = 1.37$ V led the molecule change to dication without any unpaired electron on the molecule skeleton. Actually the oxidation potential of phenothiazine labeled "1" is smaller than the oxidation potential of NN and IN labeled "2". This oxidation sequence gives precondition to get cation diradical.



Scheme 4-4. The electron transfer among four redox states in CV measurements

We also measured the CV of PDTN-IN, as shown in figure 4-8 (a) the orange spectrum. The positions of first and the third peaks which labeled "1" and "3" are nearly same with PDTN-NN. The potential of second peak which labeled "2" increased to $E_{\text{oxi-2}} = 1.25$ V.

This is because of the higher oxidation potential of IN. The CV spectra of PO-NN and PO-IN are shown in figure 4-8 (b). The potential of first and second oxidation peaks which labeled



"1" and "2" are also shown in table 4-1. The reason for the two structures that do not have third peak in the spectra is that the second electron-oxidation potential of phenoxazin is more than $E_{\text{oxi}} = 1.9 \text{ V}$ which exceed the range of measurement.

Figure 4-8. The cyclic voltammetry curves (the oxidation part) of a) PDTN-NN, PDTN-IN, and b) PO-NN, PO-IN recorded in DCM at rt, respectively. (Bu_4NPF_6 , 0.1 M, the scan rate is 100 mV/s)

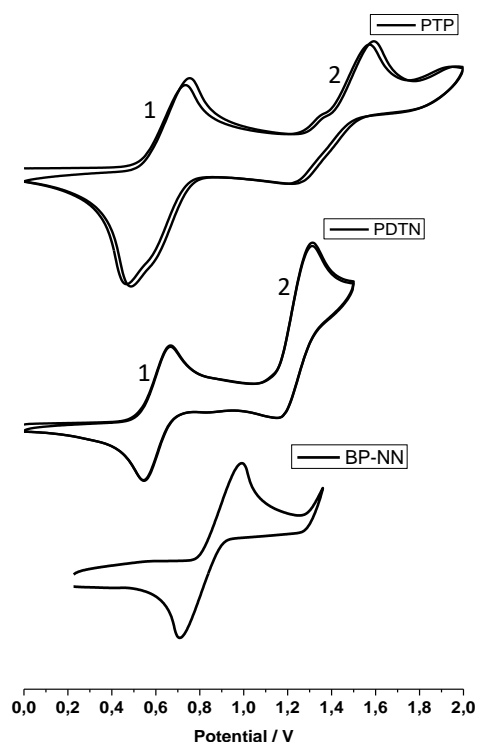
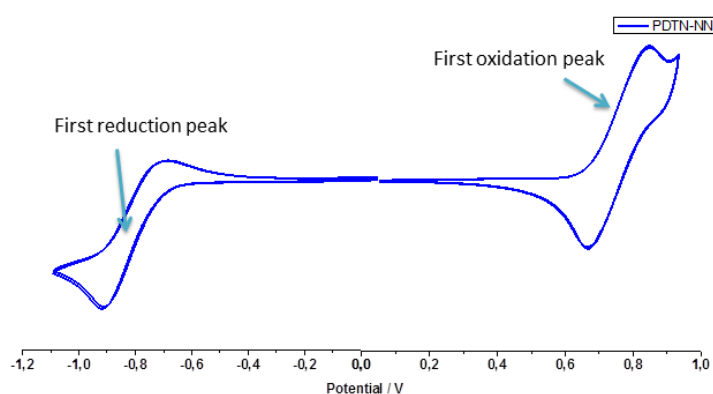


Figure 4-9. The cyclic voltammetry curves (the oxidation part) of PTP, PDTN, and BP-NN recorded in DCM at rt, respectively. (Bu_4NPF_6 , 0.1 M, the scan rate is 100 mV/s)

Table 4-1. The different oxidation potentials of the chemicals which mentioned in figure 4-8 and 4-9. (Every oxidation potentials correspond to an $E_{1/2}$ of oxidation peak in CV curves.)

Potential [V]	PTP	PDTN	BP-NN	PDTN-NN	PDTN-IN	PO-NN	PO-IN
$E_{\text{Oxi-1}}$	0.63	0.61	0.91	0.78	0.68	0.77	0.62
$E_{\text{Oxi-2}}$	1.42	1.25	—	0.93	1.25	0.91	1.23
$E_{\text{Oxi-3}}$	—	—	—	1.37	1.28	—	—

Figure 4-9 shows some contrast samples PTP, PDTN and BP-NN with all over oxidation potential values were also shown in table 4-1. The oxidation potential labeled "1" is attributed to the first electron loss from tertiary amino of phenothiazine which became a cation radical. The other oxidation potential labeled "2" is attributed to the second electron from the same nitrogen of phenothiazine which then became dication. The values $E_{\text{Oxi-1}}$ and $E_{\text{Oxi-2}}$ of PTP are larger than the values of PDTN showing an electron donor ability from thiophene which make the structure PDTN easier to oxidize.



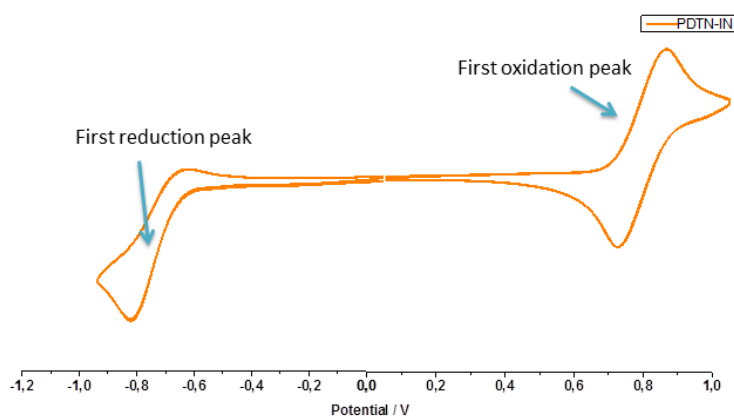


Figure 4-10. The first oxidation and reduction of cyclic voltammety curves of PDTN-NN and PDTN-IN recorded in DCM at rt, respectively. (Bu_4NPF_6 , 0.1 M, the scan rate is 100 mV/s)

We checked the CV of PDTN-NN and PDTN-IN with full cycle of oxidation and reduction. The first oxidation potential peak and first reduction potential peak were carried out from figure 4-10 for calculating SOMO, LUMO energy levels and energy gap between them by following the equations (a) and (b) listed in table 4-2.

$$E_{\text{SOMO}} = -(E_{\text{Ox-1}} - E_{\text{Fc/Fc}}^{(1/2)} + 4.8) \text{ eV} \quad (\text{a})$$

$$E_{\text{LUMO}} = -(E_{\text{Red-1}} - E_{\text{Fc/Fc}}^{(1/2)} + 4.8) \text{ eV} \quad (\text{b})$$

Table 4-2. The optical and electrochemical energy levels of PDTN-NN and PDTN-IN

	E_{Ox} , V	E_{Red} , V	E_{SOMO} , eV	E_{LUMO} , eV	ΔE_{g} , eV	E_{opt} , eV
PDTN- NN	0.78	-0.80	-5.12	-3.54	1.58	1.61
PDTN-IN	0.80	-0.75	-5.14	-3.59	1.55	2.14

4.5. EPR Measurements and Properties

EPR measurement is an important and direct method to investigate the radicals or cation radicals and to characterize newly formed radicals in the oxidation process. By analysing Zeeman splitting, hyperfine splitting, zero field splitting and also the comparison between the experimental spectra and simulation EPR spectra, the radical and spin properties could be interpret from the patterns, numbers, positions and the relative intensity of EPR peaks.

4.5.1. EPR Spectra of Control Radicals and the Oxidation Process

Figure 4-11 present the EPR spectra of pure BP-NN and the oxidation process with different ratio of oxidant SbCl_5 in DCM, (the ratio of BP-NN to SbCl_5 are 1 : 1, 1 : 2 and 1 : 4). The spectrum shows a clear mono-nitronyl nitroxide with five lines patterns signals (g factor is 2.0070) on the left top of figure 4-11. There are no difference of EPR spectra between the pure BP-NN sample and the oxidation sample with the SbCl_5 ratio 1 : 1 and 1 : 2. That means the radical NN is stable at least in the oxidation condition of 2 eq SbCl_5 . But contrast sample mono-NN was nearly all decomposed at the oxidation condition of 4 eq SbCl_5 . The signal peak almost disappeared which indicate the unpaired electron in NN moiety has been destroyed, as shown in the spectrum right bottom of figure 4-11.

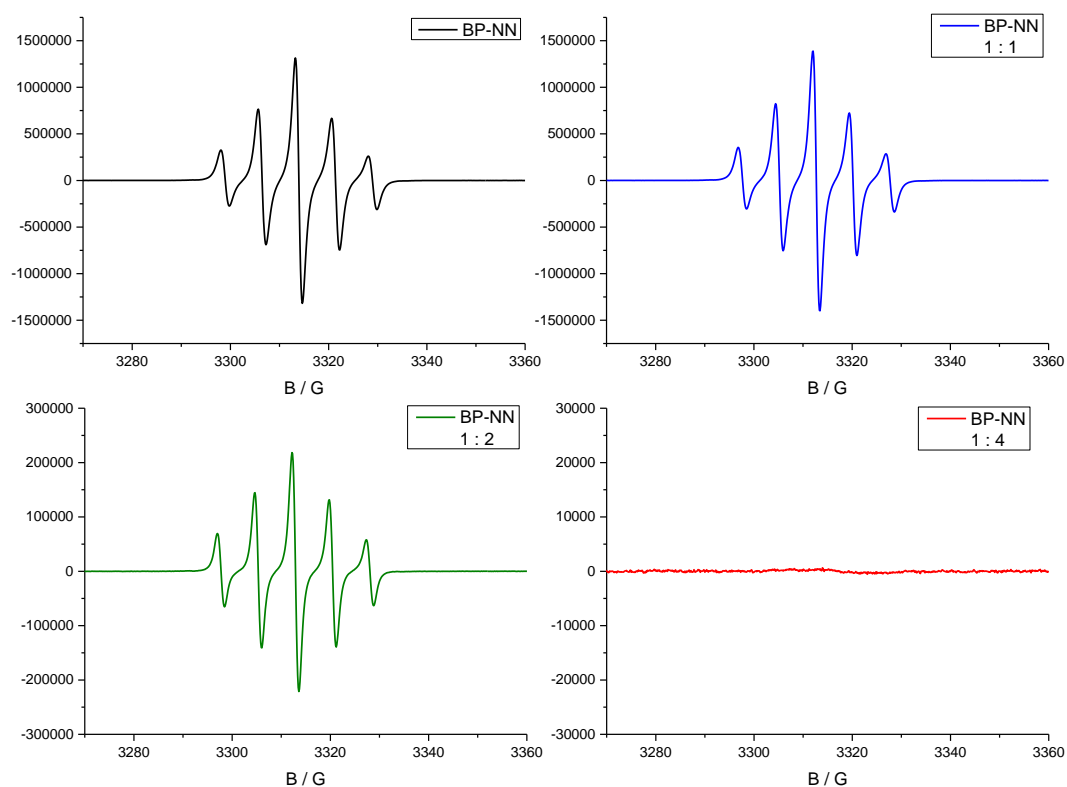


Figure 4-11. X-band EPR spectra of BP-NN with different ratios of oxidant SbCl_5 in DCM ($c \sim 10^{-4}$ M) at rt.

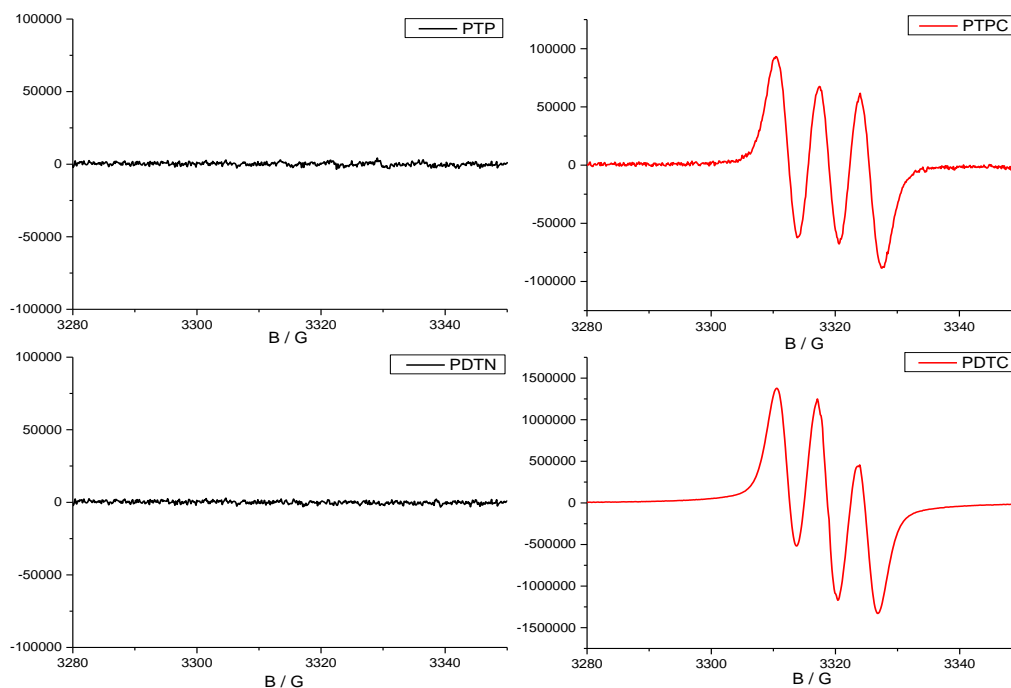


Figure 4-12. X-band EPR spectra of PTP, PDTN and the oxidized cation radical PTPC and PDTC in DCM ($c \sim 10^{-4}$ M) at rt (the oxidant is SbCl_5).

Figure 4-12 presents the EPR spectra of neutral close shell molecule PTP and PDTN in left two spectra, while another two spectra of oxidized state are shown in the right. The three lines pattern signal indicates the spin bearing nitrogen which means that the cation radicals (PTPC and PDTC with the g factor 2.0052 and $a_N \approx 6.74$) were formed in the two cases during the oxidation.

4.5.2. EPR Spectra of Redox Stimuli Responsive Process

Figure 4-13 shows representative spectra for every oxidation stage about the four radical molecules PDTN-NN, PDTNIN, PO-NN and PO-IN during the whole oxidation process. The first column of EPR spectra are the starting compounds, while the second column present one oxidation stage situation of mixture state for every sample. The last column of EPR spectra show the over oxidized state of every sample which only nitrogen cation radical spin center left in structures. Due to the newly formed cation diradical molecules in the process of oxidation, actually the mixed state can be divided into three stages with different components of radical species. The first stage is the mixture of new formed cation diradical and the starting neutral radical. Let's take PDTN-NN sample as an example. The newly formed cation diradical PTD-NN should be 7 line pattern (in simulated EPR spectrum) which mixed with 5 line-pattern signal of NN would give a 9

line-like pattern signal on EPR experimental spectrum. This indicates the sample is composed of mixture of PDTN-NN and PTD-NN. The second stage of the mixture state is composed of three molecules PDTN-NN, PTD-NN and over oxidized compound (nitrogen cation radical). This is due to some quantity of NN moiety remains, which coupled with the appearance of over oxidized compound. And the third stage of mixture is composed of PTD-NN and over oxidized compound. Depending on the data and analysis of UV-Vis Absorption, CV and EPR, all the four oxidation stimuli responsive molecules have radical structures change and spin switch for several times in the oxidation process. The g factor of spectra for every situation are listed in table 4-3.

We made a detailed titration experiment of PDTN-NN for EPR measurement with a series ratio of oxidant SbCl_5 . Some special point of oxidation titration as representative of different oxidation states were chosen and listed in figure 4-14. The line pattern of spectrum changed from 5 lines gradually to around 9 lines, due to the plus of 5 lines signal and the formation of cation diradical which is 7 lines pattern signal (the nuclear spin angular momentum $I=1$ for ^{14}N). As the oxidation proceeds, the spectrum of 9 lines pattern gradually change to 3 lines pattern (typical mono-nitrogen cation radical). The reason is more and more NN radicals were over oxidized from a specific point of oxidation potential, which is controlled by the quantity of SbCl_5 . We also did reduction experiments which are contrary to oxidation titration with the reductant Zn to check the stimuli responsive process is reversible. The system could be reduced back to PDTN-NN with 5 lines EPR signal pattern before the point of ratio with 2 eq oxidant. Although the radical system is not reversible in whole process, but before the formation of over oxidized compound (nitrogen cation radical), the mixture of PDTN-NN and PTD-NN could be reversibly reduced back to pure PDTN-NN radical. The mono nitrogen cation radical which is over oxidized could not be reduced to PDTN-NN radical.

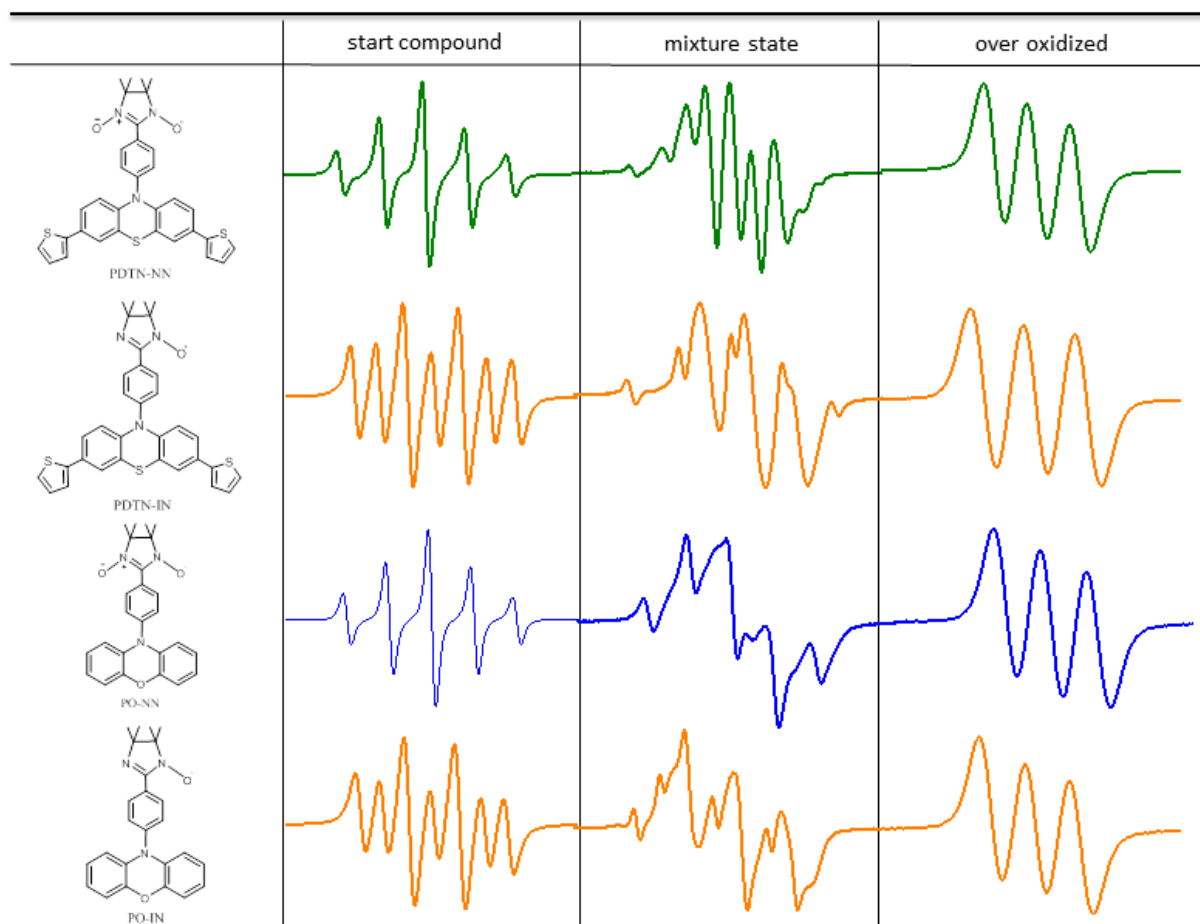


Figure 4-13. EPR spectra curves of PDTN-NN, PDTNIN, PO-NN and PO-IN with different oxidation states (representative EPR spectra curves which contain biradical features were chosen for mixture state) in DCM ($c \sim 10^{-4}$ M) at rt.

Table 4-3. The corresponding g factor of PDTN-NN, PDTNIN, PO-NN and PO-IN in different oxidation states. (The g factors of four new cation diradical were calculated from the following EPR spectra analysis.)

g factor	start compound	mixture state	over oxidized	cation diradical
PDTN-NN	2.0071	2.0067	2.0053	2.0063
PDTN-IN	2.0064	2.0062	2.0052	2.0059
PO-NN	2.0071	2.0064	2.0034	2.0056
PO-IN	2.0063	2.0058	2.0035	2.0052

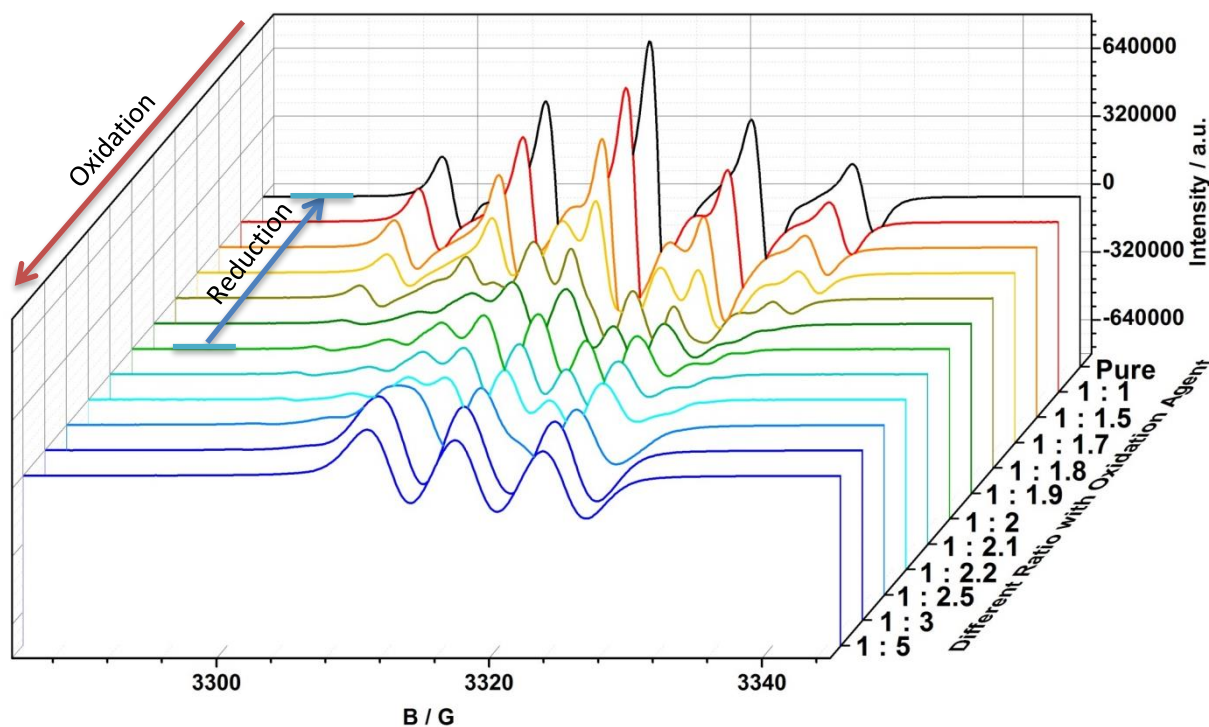


Figure 4-14. X-band EPR spectra of PDTN-NN with different ratios of oxidant SbCl_5 (during the titration of oxidation process) in DCM ($c \sim 10^{-4}$ M) at rt.

4.5.3. Fitting of Simulated EPR with New Signal Pattern of Experimental EPR Spectra

We simulated the EPR spectra of starting compound of PDTN-NN and its over oxidized state, as shown in figure 4-15 (a), (b). They both perfectly fitted to the experimental data which show above. We chose an EPR spectrum of mixed state at the ratio of oxidant to starting compound equals 2 : 1, as a representative to analyze the intermediate cation-radical diradical species. It has a nine lines pattern signal. We plus EPR spectra of two pure states (starting state and over oxidized state) with proportion of 1 : 1, and obtain a new spectrum which is show in figure 4-15 (c). It completely doesn't fit the experimental spectrum of mixed state, no matter the number of peak splitting and the position (gauss value) of the signal. So it must be a new signal pattern exist which belongs to an intermediate radical species in the mixed state during the process of oxidation. We simulated a diradical species (PTD-NN) with g factor 2.0063 and septet splitting peaks with ($a_{N1} = 3.76$, $a_{N2} = 3.25$), as shown in figure 4-15 (d). This simulated spectrum would be checked whether it fitted the experimental spectrum of intermediate radical species PTD-NN we expected.

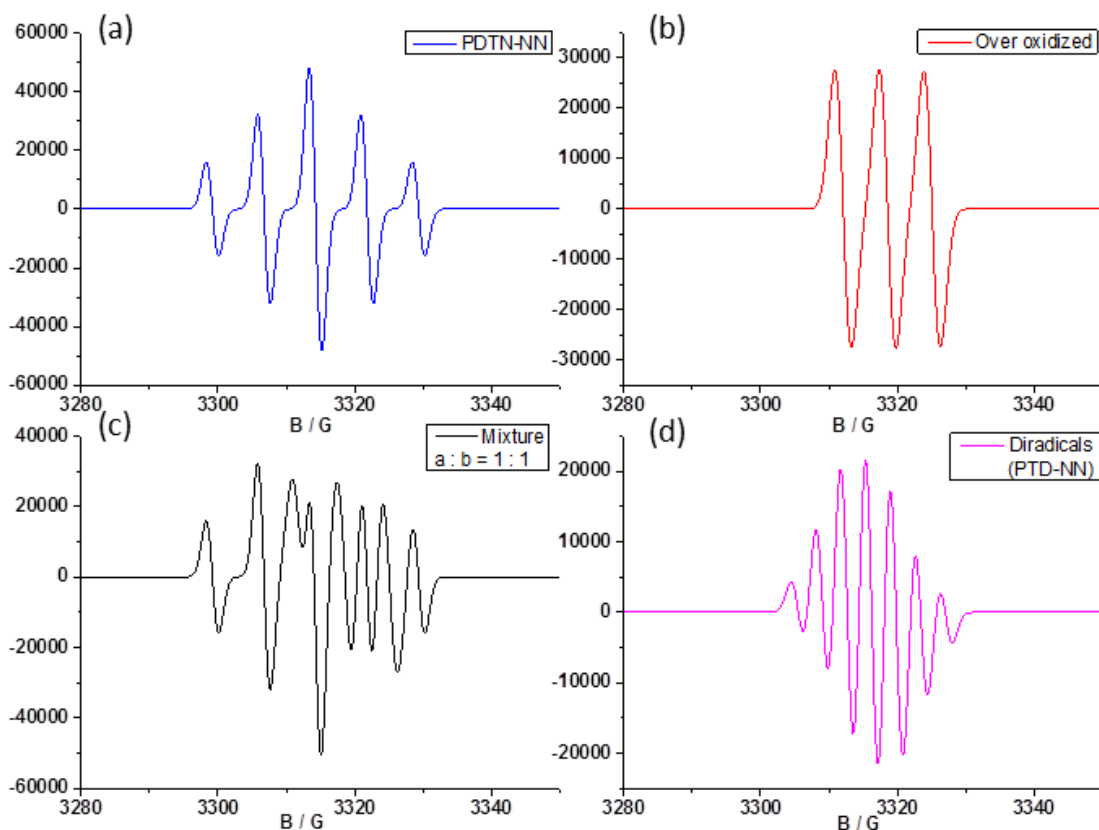


Figure 4-15. The simulation EPR spectra of (a) PDTN-NN, (b) the over oxidized state, (c) the mixture of (a) and (b) with the ratio 1 : 1, (d) cation-radical diradical PTD-NN.

We made comparison of experimental spectra with different stages of mixture states (the deduced spectrum was obtained by the subtraction of PDTN-NN spectrum or the spectrum of over oxidized state from the spectrum of mixed state). Seven lines pattern and the relative positions of each splitting peaks are fitted the simulation spectrum of PTD-NN. The comparisons is shown in figure 4-16 and figure 4-17. It provided a convincing EPR proofs that cation-radical diradical species existed during the oxidation process. The figure 4-16 shows the first stage of mixture in the oxidation process with the situation of oxidant SbCl_5 at left and oxidant AgSbF_6 at right, respectively. The figure 4-17 left shows the spectra of second stage of mixture with the components of PDTN-NN, PTD-NN, over oxidized monocation radical and the comparison consequence of experimental PTD-NN spectrum to simulated diradical species, while the right shows the spectra of third stage of mixture with the components of PTD-NN, over oxidized monocation radical and the comparison consequence.

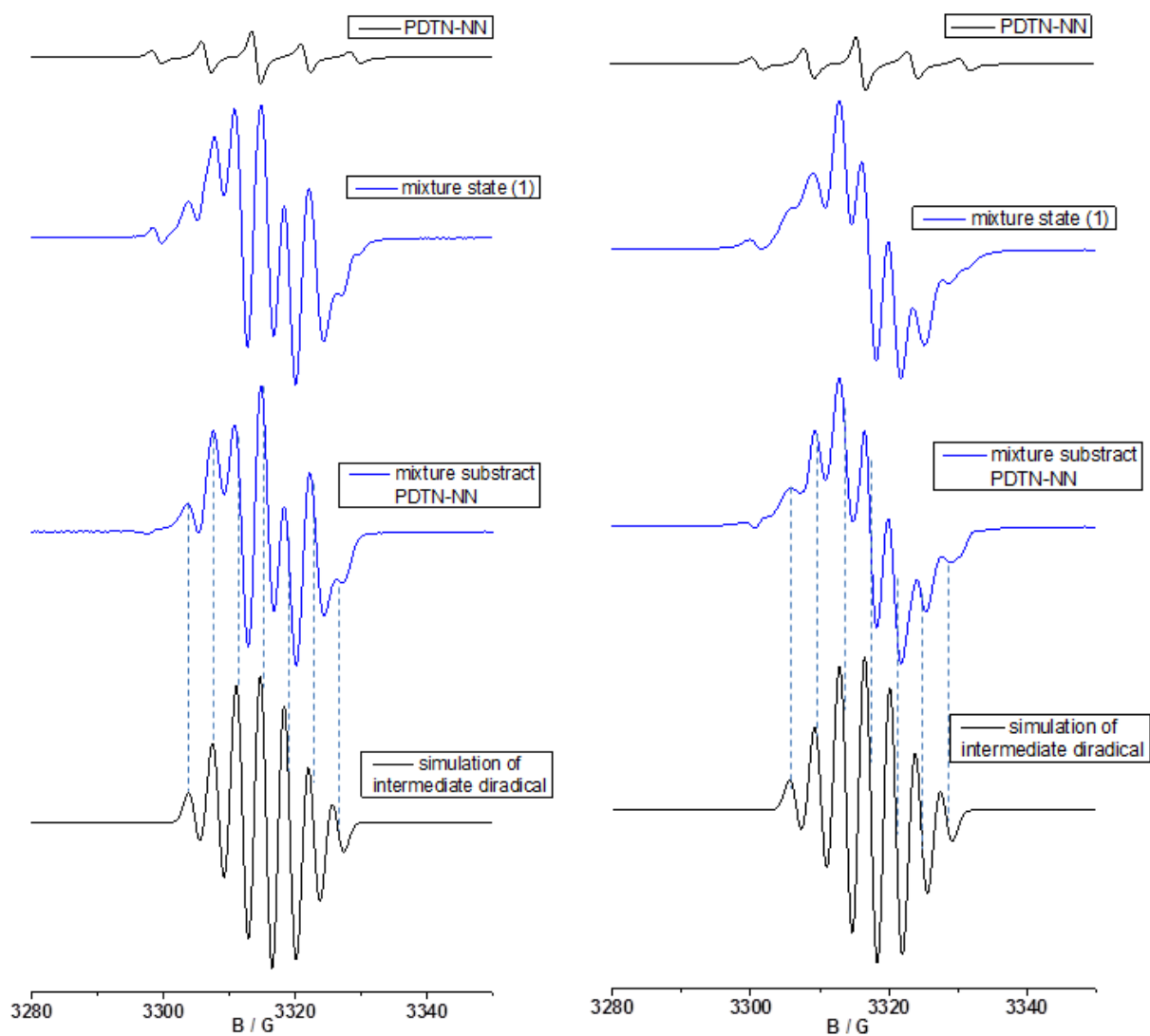


Figure 4-16. EPR spectra and the analysis of the first mixture state for PDTN-NN by the situation of oxidant SbCl_5 (left), and the situation of oxidant AgSbF_6 (right).

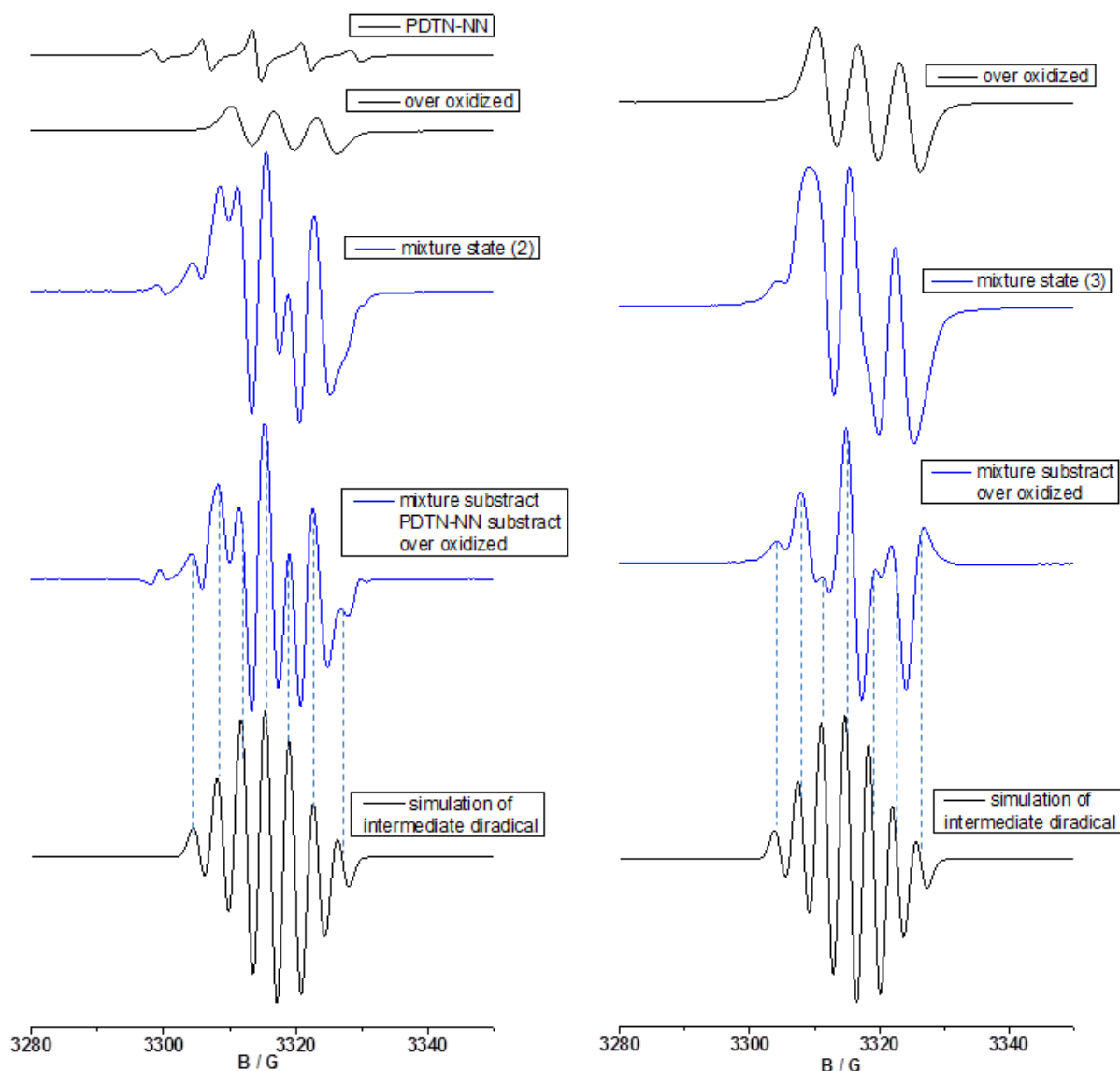


Figure 4-17. EPR spectra and the analysis of the second mixture state for PDTN-NN (left), the third mixture state for PDTN-NN (right).

4.5.4. EPR Spectra of Bidirectional Oxidation-Reduction Process (Reversibly Stimuli Responsive System)

We checked the redox stimuli responsive radical system by two oxidant SbCl_5 AgSbF_6 and one reducer Zn powder. The figure 4-18 shows a circular transform of redox process by oxidation and reduction. The signal pattern of EPR spectrum switched from PDTN-NN quintet peaks pattern to a nine lines signal pattern of mixed state which contains cation diradical PTD-NN with septet splitting peaks signal, and then switched back to pure PDTN-NN with quintet peaks pattern. In addition, the color also reversibly changed from green to red corresponding with each states. Then it returns to green fulfilling with a complete cycle. So depending on the EPR spectra of

bidirectional switch, we can draw a conclusion that the transform of redox stimuli responsive radical system is a reversible and repeatable process.

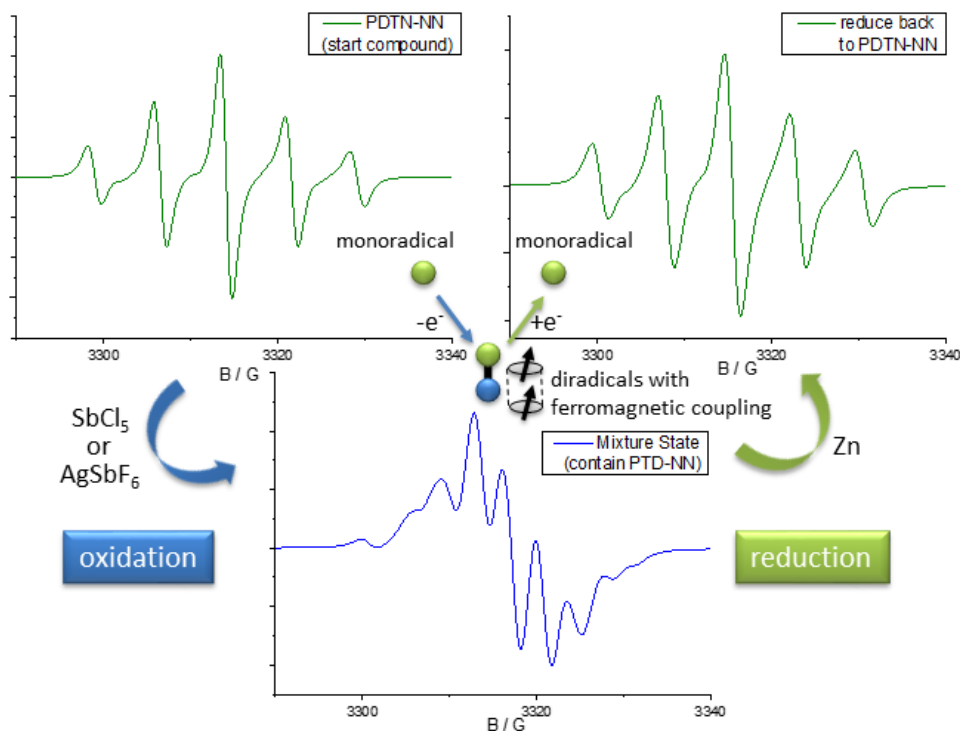


Figure 4-18. The EPR spectra of reversible transition of bidirectional oxidation-reduction process for PDTN-NN.

4.6 DFT Calculations of Redox Stimuli Responsive System (Spin Distribution and Orbital Energy Level)

DFT (density functional theory) Gaussian 09W was used to calculate the spin density distribution for PDTN-NN and PO-NN with three different redox states which means three different radical species, and the orbitals energy levels for PDTN-NN case through the condition of method (Optimization Plus Frequency) and the basis set UBLYP/6-31G(d). The front view and side view of spin density distribution corresponding to the three different radical species of PDTN-NN and PO-NN, respectively, are shown in figure 4-19, 4-20. We observed that the spin distributions of PDTN-NN and PO-NN concentrate at the range of NN group, while the the spin distributions of PTD-NN and POD-NN delocalized in whole molecules. The spin distributions of over oxidized states concentrate at the range of phenothiazine group and phenoxazine group. The changes of spin distribution by the electron transfer in redox reactions analogy to the streaming of spin distribution flowed on the molecular backbone on redox stimuli conditions. In addition, the broken symmetry method was used to calculate the energy of singlet state and triplet state and value of interaction

coupling constants ($J = \Delta E_{BS-T}$) of cation diradicals species. For the case of PTD-NN, the results of singlet is $HF=-2625.463149|S2=0.937689|S2-1=0.|S2A=0.000051|$ and the triplet is $HF=-2625.4684608|S2=2.020318|S2-1=0.|S2A=2.000117|$. The interaction coupling constants of PTD-NN $J = 1168,596 \text{ cm}^{-1}$. For the case of POD-NN, the results of singlet is $HF=-1199.0315485|S2=2.020864|S2-1=0.|S2A=2.000122|$ and the triplet is $HF=-1199.0330987|S2=0.855647|S2-1=0.|S2A=0.00007|$. The interaction coupling constants of POD-NN $J = 340.22957 \text{ cm}^{-1}$. The positive value of interaction coupling constants means both of the two cation diradicals own intramolecular ferromagnetic coupling interactions.

The Streaming of Spin Distribution by Electron Transfer

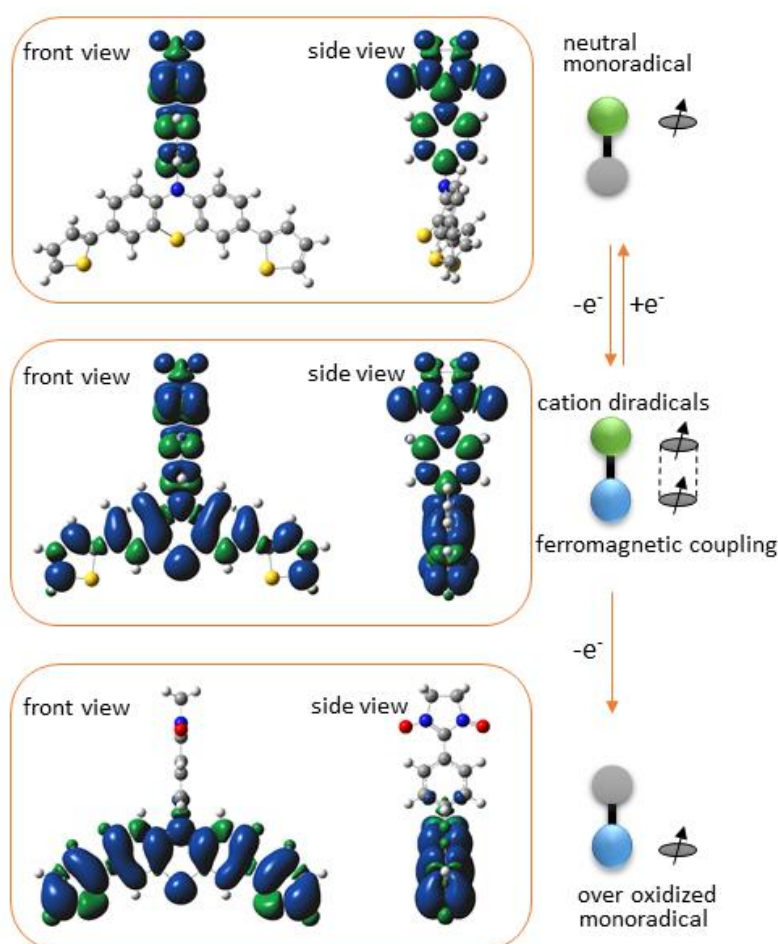


Figure 4-19. The spin density distribution of PDTN-NN among different states (neutral monoradicals, cation-radical diradicals and over oxidized dication monoradicals) calculated by DFT (Gaussian 09 W).

The Streaming of Spin Distribution by Electron Transfer

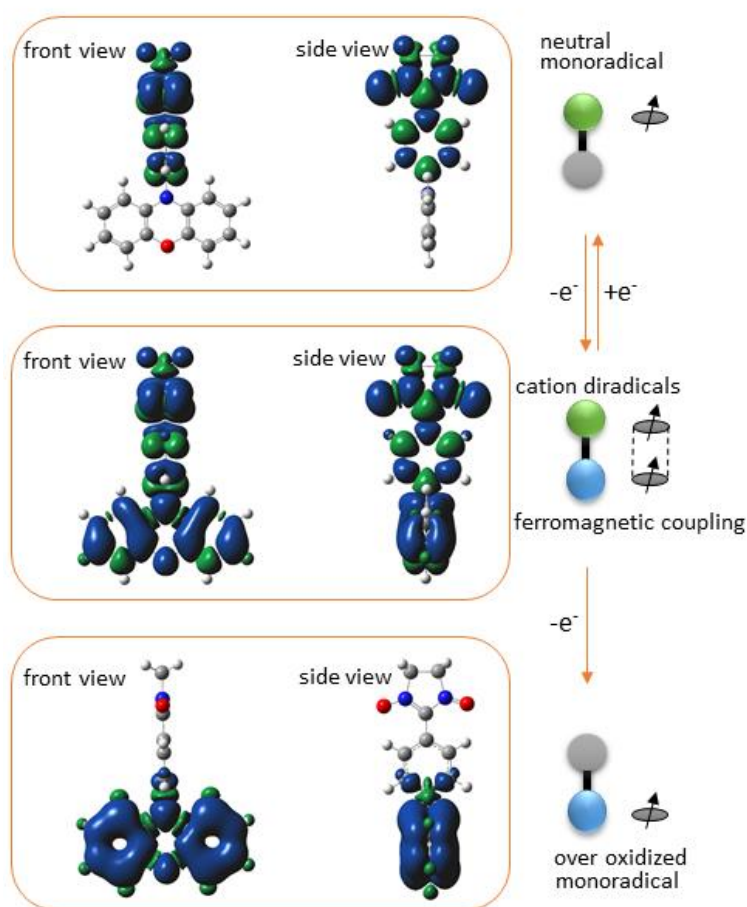


Figure 4-20. The spin density distribution of PO-NN among different states (neutral monoradicals, cation-radical diradicals and over oxidized dication monoradicals) calculated by DFT (Gaussian 09 W).

Figure 4-21 shows the SOMO and HOMO energy levels and electrons distributions for different oxidation states of PDTN-NN, including the orbitals energy levels of two structure components phenyl-NN and dithiophen-phenothiazine. We could clearly observe that the energy of α electron on SOMO, the β and α electrons on HOMO-1 of PDTN-NN are -0.1811 Hartrees, -0.1811 Hartrees and -0.2129 Hartrees, respectively. It means the next electron lost (oxidation) would happen on the β electron on HOMO-1. So the one electron transferred structure PTD-NN possess a intramolecular ferromagnetic coupling interaction, as the two unpaired electrons (α) occupied in SOMO and SOMO-1 respectively shown. The streaming of spin distributions transferred through whole molecule backbone.

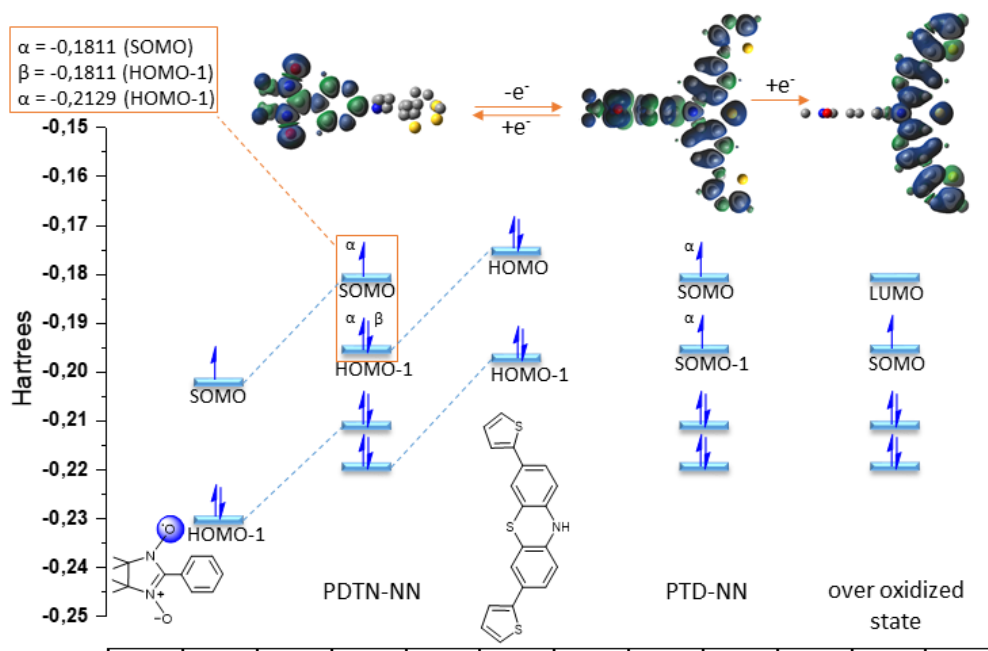


Figure 4-21. The SOMO, HOMO energy levels and electrons distributions for different oxidation states of PDTN-NN combining phenyl-NN and dithiophen-phenothiazine.

4.7. Conclusions

We successfully synthesized four nitroxide radical species PDTN-NN, PDTNIN, PO-NN and PO-IN that contain electron donor groups phenothiazine or phenoxazine. They are new precursors which can be oxidized to cation-radical diradical species. It provides the possibility to use redox stimuli conditions to switch the spin species or spin properties. UV, CV and EPR spectroscopic methods were used to analyze and characterize the oxidation process. Several different spin species were detected during the different corresponding oxidation states. One of the most important target, the intermediate cation-radical diradical species were found and verified. The diradicals were also confirmed to have intramolecular ferromagnetic coupling interactions (owns triplet ground state). The flow of spin distribution streaming throughout the whole molecule was clearly displayed by DFT calculations of spin density distribution. In addition, the redox stimuli-responsive process of spin species is testified to be reversibly and repeatable. These characteristics of spin systems would have prosperous potentials in application of spintronics.

4.8. References

- (1) Sato, O.; Tao, J.; Zhang, Y. Z. Control of Magnetic Properties through External Stimuli. *Angew. Chem. Int. Ed.* **2007**, *46*, 2152-2187
- (2) Nakatsuji, S. Recent Progress toward the Exploitation of Organic Radical Compounds with Photo-Responsive Magnetic Properties. *Chem. Soc. Rev.* **2004**, *33*, 348-353
- (3) Ali, M. E.; Staemmler, V.; Illas, F.; Oppeneer, P. M. Designing the Redox-Driven Switching of Ferro- to Antiferromagnetic Couplings in Organic Diradicals *J. Chem. Theory Comput.* **2013**, *9*, 5216–5220
- (4) Tretyakov, E. V.; Ovcharenko V. I. The Chemistry of Nitroxide Radicals in the Molecular Design of Magnets. *Rus. Chem. Rev.* **2009**, *78*, 971-1012
- (5) Ionita, P.; Whitwood, A. C.; Gilbert, B. C. Synthesis and Characterization of Some Novel Hetero-diradicals Containing Linked Hydrazyl and Aminoxyl (Nitroxide) Moieties. *J. Chem. Soc., Perkin Trans.* **2001**, *2*, 1453-1462
- (6) Zheng, X.; Wang, S. Y.; Qiu, Y. F.; Li, Y. T.; Zhou, C. K.; Sui, Y. X.; Ma, J.; Wang, X. P. One-Electron Oxidation of an Organic Molecule by $B(C_6F_5)_3$; Isolation and Structures of Stable Non-*para*-Substituted Triarylamine Cation Radical and Bis(triarylamine) Dication Diradicaloid. *J. Am. Chem. Soc.* **2013**, *135*, 14912-14915
- (7) Oka, H. Synthesis and Magnetic Properties of Orthogonally Linked Phenothiazine Cation Radical Dimer and Tetramer. *Org. Lett.* **2010**, *12*, 448-451
- (8) Sugawara, T.; Komatsu, H.; Suzuki, K. Interplay Between Magnetism and Conductivity Derived from Spin-Polarized Donor Radicals. *Chem. Soc. Rev.* **2011**, *40*, 3105-3118
- (9) Kuratsu, M.; Suzuki, S.; Kozaki, M.; Shiomi, D.; Sato, K.; Takui, T.; Kanzawa, T.; Hosokoshi, Y.; Lan, X. Z.; Miyazaki, Y.; Inaba, A.; Okada, K. (Nitronyl Nitroxide)-Substituted Trioxyltriphenylamine Radical Cation Tetrachlorogallate Salt: A 2p-Electron-Based Weak Ferromagnet Composed of a Triplet Diradical Cation. *Chem. Asian J.* **2012**, *7*, 1604-1609
- (10) Luo, J. S.; Wan, Z. Q.; Jia, C. Y. Recent advances in phenothiazine-based dyes for dye-sensitized solar cells. *Chinese chemical letters.* **2016**, *27*, 1304-1318
- (11) Wainwright, M. Tricyclic Cationic Chromophores as Models for New Photoantimicrobials. *J. Braz. Chem. Soc.* **2015**, *26*, 2390-2404
- (12) Massie, S. P. The Chemistry of Phenothiazine. *Chem. Rev.* **1954**, *54*, 797-883
- (13) Opperman, K. A.; Mecklenburg, S. L.; Meyer, T. J. Intramolecular, Photoinduced Electron Transfer in Ruthenium(II) Bipyridine—Quinone Complexes. *Inorg. Chem.* **1994**, *33*, 5295-5301

- (14) Shruti,; Dwivedi, J.; Kishore, D.; Sain, S. Recent Advancement in The Synthesis of Phenoxazine Derivatives and Their Analogues. *Synthetic Communications*. **2018**, *48*, 1377-1402
- (15) Okada, K.; Imakura, T.; Oda, M.; Murai, H. 10,10'-(*m*- and *p*-Phenylene)diphenothiazine Dications: Violation of a Topology Rule in Heterocyclic High-Spin π -Systems. *J. Am. Chem. Soc.* **1996**, *118*, 3047-3048
- (16) Okamoto, T.; Kuratsu, M.; Kozaki, M.; Okada, K. Remarkable Structure Deformation in Phenothiazine Trimer Radical Cation. *Org. Lett.* **2004**, *6*, 3493-3496
- (17) Kuratsu, M.; Kozaki, M.; Okada, K. 2,2':6'2'':6'',6-Trioxotriphenylamine: Synthesis and Properties of the Radical Cation and Neutral Species. *Angew. Chem. Int. Ed.* **2005**, *44*, 4056-4058
- (18) Kuratsu, M.; Suzuki, S.; Kozaki, M.; Shiomi, D.; Sato, K.; Takui, T.; Okada, K. Magnetic Interaction of Tri- and Di-oxytriphenylamine Radical Cation FeCl₄ Salts. *Inorg. Chem.* **2007**, *46*, 10153–10157
- (19) Suzuki, S.; Nagata, A.; Kuratsu, M.; Kozaki, M.; Tanaka, R.; Shiomi, D.; Sugisaki, K.; Toyota, K.; Sato, K.; Takui, T.; Okada, K. Trinitroxide-Trioxotriphenylamine: Spin-State Conversion from Triradical Doublet to Diradical Cation Triplet by Oxidative Modulation of a *p*-Conjugated System. *Angew. Chem. Int. Ed.* **2012**, *51*, 3193–3197
- (20) Ito, A.; Kurata, R.; Sakamaki, D.; Yano, S.; Kono, Y.; Nakano, Y.; Furukawa, K.; Kato, T.; Tanaka, K. Redox Modulation of *para*-Phenylenediamine by Substituted Nitronyl Nitroxide Groups and Their Spin States. *J. Phys. Chem. A* **2013**, *117*, 12858-12867
- (21) Ratera, I.; Veciana, J. Playing with Organic Radicals as Building Blocks for Functional Molecular Materials. *Chem. Soc. Rev.* **2012**, *41*, 303-349
- (22) Dupeyre, E. M.; Lemaire, H.; Rassat, A. A Stable Biradical in the Nitroxide Series. *J. Am. Chem. Soc.* **1965**, *87*, 3771-3772
- (23) Blundell, S. J.; Pratt, F. L. Organic and Molecular Magnets. *J. Phys. Condens. Matter* **2004**, *16*, 771-828
- (24) Caneschi, A.; Gatteschi, D.; Rey, P. The Chemistry and Magnetic-Properties of Metal Nitronyl Nitroxide Complexes. *Prog. Inorg. Chem.* **1991**, *39*, 331-429
- (25) Miller, J. S. Magnetically Ordered Molecule-Based Materials. *Chem. Soc. Rev.* **2011**, *40*, 3266-3296
- (26) Jalilov, A. S.; Han, L.; Nelsen, S. F.; Guzei, I. A. Oxidation Products of Doubly Trimethylene-Bridged Tetrabenzyl *p*-Phenylenediamine Paracyclophane. *J. Org. Chem.* **2013**, *78*, 11373–11381

- (27) Nelsen, S. F.; Ismagilov, R. F.; Teki, Y. Comparison of the Singlet, Triplet Energy Gap of a Symmetrical Diradical Dication with ET Parameters Derived from Its Optical Spectrum. *J. Am. Chem. Soc.* **1998**, *120*, 2200-2201
- (28) Barlow, S.; Risko, C.; Odom, S. A.; Zheng, S. J.; Coropceanu, V.; Beverina, L.; Brédas, J. L.; Marder, S. R.; Tuning Delocalization in the Radical Cations of 1,4-Bis[4(diarylamino)styryl]benzenes, 2,5-Bis[4(diarylamino)styryl]thiophenes, and 2,5-Bis[4(diarylamino)styryl]pyrroles through Substituent Effects. *J. Am. Chem. Soc.* **2012**, *134*, 10146–10155
- (29) Sato, K.; Yano, M.; Furuichi, M.; Shiomi, D.; Takui, T.; Abe, K.; Itoh, K.; Higuchi, A.; Katsuma, K.; Shirota, Y. Polycationic High-Spin States of One- and Two-Dimensional (Diarylamino)benzenes, Prototypical Model Units for Purely Organic Ferromagnetic Metals As Studied by Pulsed ESR/ Electron Spin Transient Nutation Spectroscopy. *J. Am. Chem. Soc.* **1997**, *119*, 6607-6613
- (30) Stickley, K. R.; and Blackstock, S. C.; Triplet Dication and Quartet Trication of a Triaminobenzene. *J. Am. Chem. Soc.* **1994**, *116*, 11576-11577
- (31) Bushby, R. J.; McGill, D. R.; Ng K. M.; Taylor, N. Disjoint and coextensive diradical diions. *J. Chem. Soc., Perkin Trans.* **1997**, *2*, 1405-1414
- (32) Yokoyama, Y.; Sakamaki, D.; Ito, A.; Tanaka, K.; Shiro, M. A Triphenylamine Double-Decker: From a Delocalized Radical Cation to a Diradical Dication with an Excited Triplet State. *Angew. Chem. Int. Ed.* **2012**, *51*, 9403–9406
- (33) Fatila, E. M.; Clérac, R.; Rouzières, M.; Soldatov, D. V.; Jennings, M.; Preuss, K. E. High-Spin Ribbons and Antiferromagnetic Ordering of a MnIIBiradical-MnII Complex. *J. Am. Chem. Soc.* **2013**, *135*, 13298–13301
- (34) Karpinska, J.; Starczewska B.; Tarasiewicz, H. P. Analytical Properties of 2- and 10-Disubstituted Phenothiazine Derivatives. *Anal. Sci.* **1996**, *12*, 161-170
- (35) Baumgarten, M.; Gügel, A. EPR and Optical Absorption Spectra of Reduced Buckminsterfullerene. *Adv. Mater.* **1993**, *5*, 458-461
- (36) Rathore, R.; Burns, C. L. A Practical One-Pot Synthesis of Soluble Hexa-peri-hexabenzocoronene and Isolation of Its Cation-Radical Salt. *J. Org. Chem.* **2003**, *68*, 4071-4074
- (37) Nishinaga, T.; Kanzaki, Y.; Shiomi, D.; Matsuda, K.; Suzuki, S.; Okada, K.; Radical Cation p-Dimers of Conjugated Oligomers as Molecular Wires: An Analysis Based on Nitronyl Nitroxide Spin Labels. *Chem. Eur. J.* **2018**, *24*, 11717–11728

- (38) Rosspeintner, A.; Griesser, M.; Matsumoto, I.; Teki, Y.; Li, G. Q.; Nelsen, S. F.; Gescheidt, G. EPR and ENDOR Studies of Dimeric Paracyclophane Radical Cations and Dications Containing Tri- and Pentamethylene-Bridged p-Phenylene Diamine Units. *J. Phys. Chem. A* **2010**, *114*, 6487–6492
- (39) Nelsen, S. F.; Ismagilov, R. F.; Powell, D. R. Charge-Localized p-Phenylenedihydrazine Radical Cations: ESR and Optical Studies of Intramolecular Electron Transfer Rates. *J. Am. Chem. Soc.* **1997**, *119*, 10213-10222
- (40) Maurel, V.; Skorka, L.; Onofrio, N.; Szewczyk, E.; Djurado, D.; Dubois, L.; Mouesca, J. M.; Kulszewicz-Bajer, I. Ferromagnetic Spin Coupling through the 3,4'-Biphenyl Moiety in Arylamine Oligomers Experimental and Computational Study. *J. Phys. Chem. B* **2014**, *118*, 7657–7667
- (41) Fang, S.; Lee, M. S.; Hrovat, D. A.; Borden, W. T. Ab Initio Calculations Show Why m-Phenylene Is Not Always a Ferromagnetic Coupler. *J. Am. Chem. Soc.* **1995**, *117*, 6727-6731
- (42) Mañeru, D. R.; Pal, A. K.; Moreira, I. P. R.; Datta, S. N.; Illas, F. The Triplet–Singlet Gap in the m-Xylylene Radical: A Not So Simple One. *J. Chem. Theory Comput.* **2014**, *10*, 335–345
- (43) Hemgesberg, M.; Bayarmagnai, B.; Thiel, W. R. Structurally Stressed PT09SBA: A Close Look at The Properties of Large Pore Photoluminescent, Redox Active Mesoporous Hybrid Silica. *RSC Adv.* **2013**, *3*, 8242-8253
- (44) Rao, K. S.; Wu, T. S. Chan-Lam Coupling Reactions: Synthesis of Heterocycles. *Tetrahedron.* **2012**, *68*, 7735-7754
- (45) Chan, D. M. T.; Monaco, K. L.; Wang, R. P.; Winters, M. P. New N- and O-Arylations with Phenylboronic Acids and Cupric Acetate. *Tetrahedron Letters.* **1998**, *39* 2933-2936
- (46) Rao, K. S.; Wu, T. S. Chan-Lam Coupling Reactions: Synthesis of Heterocycles. *Tetrahedron.* **2012**, *68*, 7735-7754
- (47) Chan, D. M. T.; Monaco, K. L.; Wang, R. P.; Winters, M. P. New N- and O-Arylations with Phenylboronic Acids and Cupric Acetate. *Tetrahedron Letters.* **1998**, *39* 2933-2936

Chapter 5 Photo Induced Spin Responsive Systems Studied by EPR

5.1 Introduction

In this chapter, we study the process of photo induced activated radical or spin species where EPR measurements were used to characterize and analyze the newly formed radical or spin species in miscellaneous photo-active systems^{1,2}. Four photo induced reactions that contain radical intermediate species during the process of reactions are mentioned in major, namely photo oxidation³, [2 + 2] cycloaddition reactions about styrene derivatives⁴, α -alkylation of aldehyde derivatives⁵ and cycloaddition of diphenylphosphine oxide and alkynes derivatives⁶. The works were cooperated with Kai Zhang's research group in Mainz. By the analysis of EPR spectra, the different intensities, g factors and the hyperfine splitting patterns of signals, we could investigate the detailed structure of the radical intermediates and get to know in which stage in reaction the radical species are formed. The mechanisms of photo induced reactions are triggered by radical intermediate species, i.e. radical mechanism^{7,8}.

5.2 Photo Induced Radical or Spin Species Activated Systems in Photocatalysis Reaction

Photo induced intermediate species such as radicals were considered as the most plausible mechanism in many photochemical catalysis reactions. The radicals or some other intermediate species which were produced with the interaction of photocatalyst in photo illumination can activate the reaction proceeding, which could not be carried forward in illumination without photocatalyst. The radical trap adducts give EPR a possibility to "catch" and measure it.⁹ So EPR is an excellent and convenient method to investigate photo induced reactions for radical mechanism. Due to the instability and the short life time of most intermediate radical species, some are low to several nano second, it is hard to find the radical signal if we directly check or monitor the reaction by EPR measurement. So radical traps like 2,2,6,6-tetramethylpiperidine (TEMP), N-tert-butyl- σ -phenylnitron (PBN) and 5,5-dimethylpyrroline N-oxide (DMPO) were used to capture intermediate radical species and provide a better proof for the existence of radical species.^{10,11} The principle is that the radical trap would react with the unstable intermediate radical species and quickly form a new radical species during the photochemical reactions. The new formed radical is much more stable and have much longer life time than the first formed radicals which were quickly quenched. EPR measurements and the analysis method of EPR spectra were applied to investigate following

four photo induced reaction systems. The main goals are to verify the most plausible mechanism and interpret some structure information about intermediate radical species.

Molecular O_2 is at triplet state ($^3\Sigma_g^-$) in general surroundings because of the unique properties of ground triplet state.¹² There are two unpaired electrons on two anti-bonding orbitals ($2p\pi_x^*$, $2p\pi_y^*$) respectively with the same spin direction in every gas molecule of oxygen, as shown in figure 5-1. There also another two singlet states ($^1\Delta_g$, $^1\Sigma_g^+$) of oxygen molecule, which are also called first excited state and second excited state respectively, have higher energy with 92.0 kJ/mol and 154.8 kJ/mol more than triplet state.^{13,14} The quantum spin of the two singlet states of oxygen are both zero and it is kinetically unstable at ambient temperature. The difference between $^1\Delta_g$, $^1\Sigma_g^+$ of oxygen molecule is the different arrangements of two valence electron on $2p\pi_x^*$, $2p\pi_y^*$. For $^1\Delta_g$, the two electron paired with opposite directions on one anti-bonding orbital $2p\pi_x^*$, while the two electron of $^1\Sigma_g^+$ are distributed on two anti-bonding orbitals $2p\pi_x^*$, $2p\pi_y^*$ also with opposite spin directions.

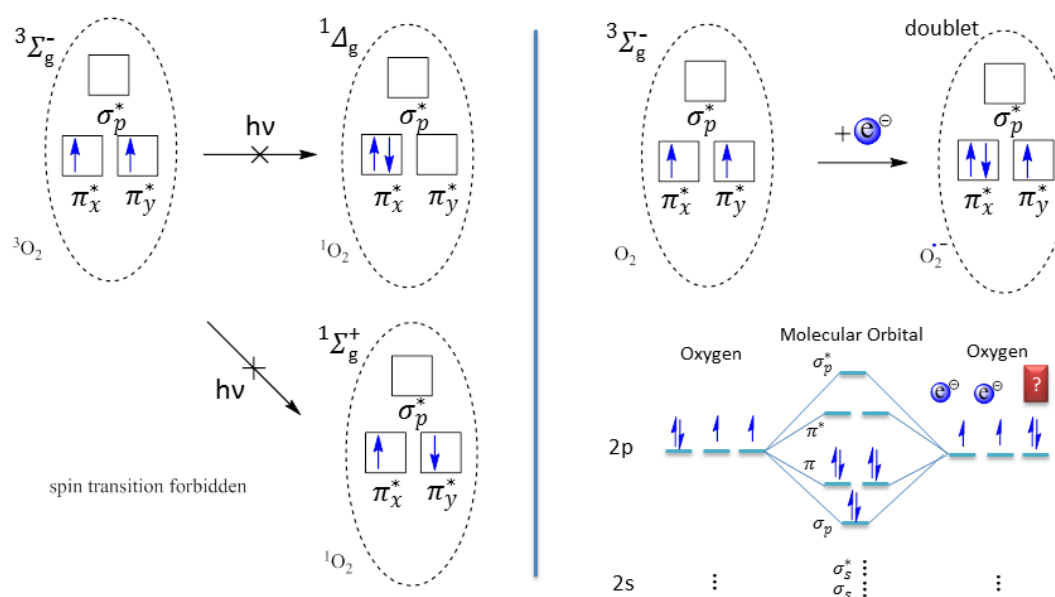


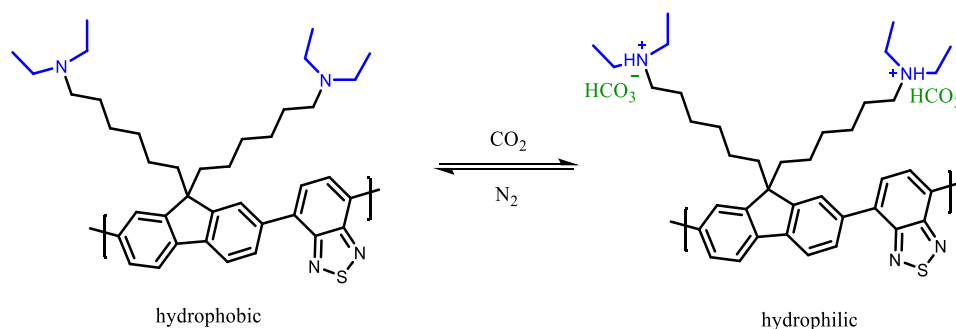
Figure 5-1. Illustration of distribution of orbitals and electrons for different states of oxygen and the transitions of them

The transition between singlet and triplet oxygen (the two quantum states) is forbidden, because of the spin selection rule $\Delta S = 0$ and the parity (Laporte) rule that g-g transitions are forbidden. That means triplet oxygen molecule could not directly transform to either of two singlet oxygen molecule by direct absorption of light energy. But the transition can be achieved by the activation of photocatalyst under illumination. Some specific photocatalyst

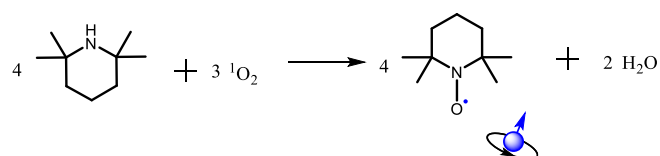
can be excited by light and interact with triplet oxygen. Thereby the oxygen molecule would be excited to singlet oxygen molecule, while the photocatalyst lose the energy and relax back to the ground state.

5.2.1 Radical and Spin Analysis of Photo Induced Reaction through Hydrophobic-Hydrophilic Switchable Photocatalyst

For this part, we discuss a switchable hydrophilicity of conjugated polymer photocatalyst which can be triggered by carbon dioxide. The work was cooperated with Jeehye Byun in Mainz. The polymer (PF-BT) was copolymerized with monomer fluorene and monomer benzothiadiazole. Every fluorene monomer was functionalized with two tertiary amines groups. Carbon dioxide can change the solubility of the polymer photocatalyst from hydrophobic to hydrophilic by reversible combination with tertiary amine terminal in every units as shown in scheme 5-1. Quaternary amine salts were gradually formed (PF-BT-CO₂) when the mixture of polymer and water was under CO₂ bubbling. At first the polymercatalyst is not soluble in water, but then gradually dissolved in water after more and more quaternary amine salts which are hydrophilic functional groups were formed. The catalytic activity could be enhanced in water. And water compatibility of photocatalyst is a crucial point for energy and environmental application that has been pursued intensively.



Scheme 5-1. Diagrammatic sketch of structure change of PF-BT with hydrophobic-hydrophilic switch property through CO₂ and N₂ exchange



Scheme 5-2. The reaction equation of singlet oxygen which was trapped by TEMP and TEMPO formed.

The photo induced reactions which interacted with the hydrophilic-hydrophobic switchable polymer were speculated by the activation of intermediate singlet oxygen. We designed a route to verify the mechanism of this photochemical reaction.

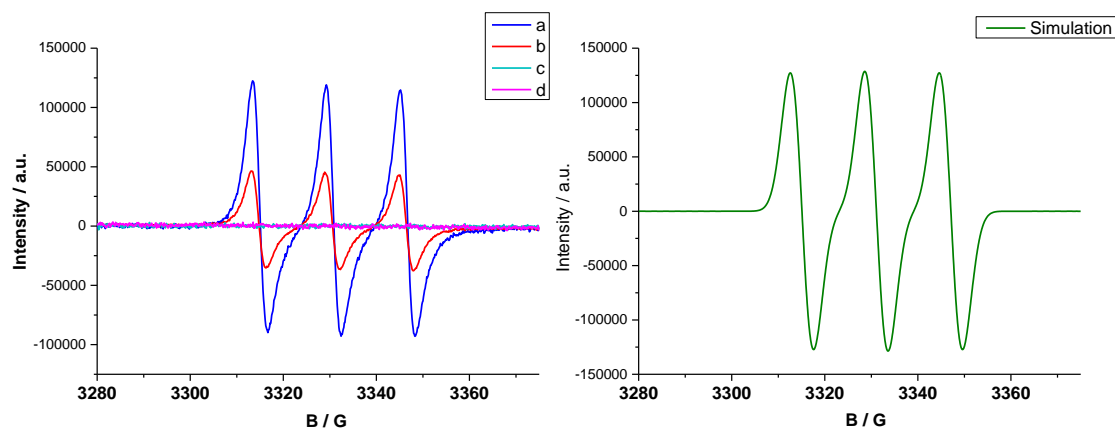


Figure 5-2. EPR spectra, a) photocatalyst PF-BT-CO₂, TEMP (0.1 M), and O₂. b) photocatalyst PF-BT, TEMP (0.1 M), and O₂. c) photocatalyst PF-BT and TEMP (0.1 M). d) TEMP (0.1 M) and O₂ on the left. Simulation EPR spectrum on the right.

We used 2,2,6,6-tetramethylpiperidine (TEMP) as the radical trap which can "catch" the singlet oxygen (if the photocatalyst system can produce intermediate singlet oxygen) and transform it to a much more stable radical (TEMPO) which can be detected by EPR measurement, as shown in scheme 5-2. The EPR signal should split from one line pattern to three lines pattern by hyperfine coupling with nitrogen nucleus with spin quantum number (¹⁴N, I = 1) in nitroxide group. We carried out four tests which differ in the photochemical catalysis (PF-BT-CO₂ or PF-BT) system in order to compare what are the effects due to these different conditions, as shown in figure 5-2. The four groups of experiments are (a) photocatalyst PF-BT-CO₂ (1 mg/ml, which acquired from PF-BT with CO₂ bubbling for 1 h at room temperature under stirring) was used to activate the reaction, TEMP (0.1 M), and O₂. (b) hydrophobic photocatalyst PF-BT was used to induce the photochemical reaction, TEMP (0.1 M), and O₂ for control. (c) photocatalyst PF-BT, TEMP (0.1 M) and without O₂. (d) TEMP (0.1 M) and O₂, respectively labeled in the left picture of figure 5-2. All the four samples were dissolved in dry acetonitrile and were irradiated under white LED for one hour. Then all the samples were sealed in EPR quartz tube with the same volume in specific positions of EPR cavity. We observed the peaks intensities of the TEMPO is up to 1.25×10^5 (arbitrary units) in sample (a) with g factor 2.00623 and hyperfine splitting of nitrogen nucleus $a_N = 15.8$ G. The intensity value in sample (b) is only half of the former with 5×10^4 (a. u.) with the same hyperfine splitting $a_N = 15.8$ G. For conditions c) and d) no radical formation was detected.

The intensity of the signal peak corresponds to direct proportion of radical concentration. That means the photochemical reaction in condition (a) had higher efficiency of photocatalysis and would produce more radical intermediate than in condition (b). The right picture of figure is the EPR simulation of nitroxide radical in our case (it suit the EPR experimental date with the same splitting patterns and linewidth).

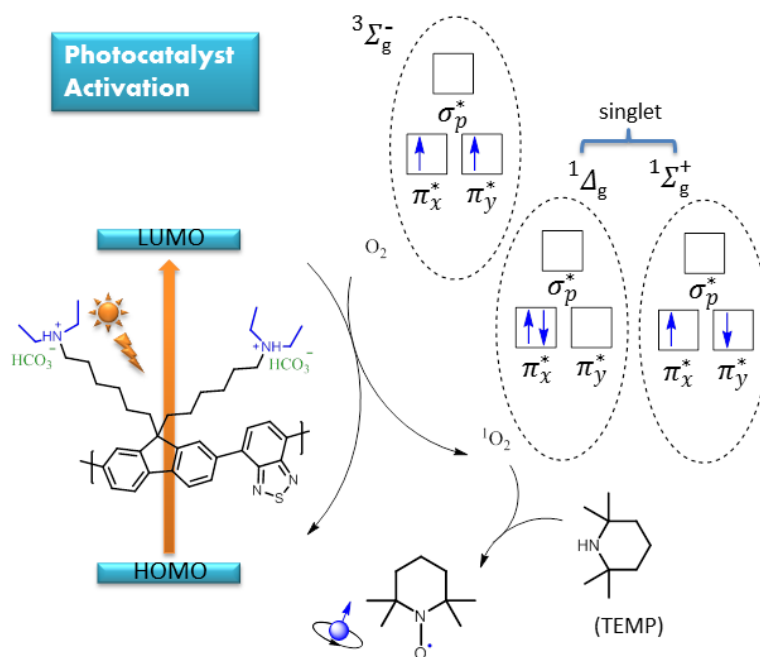
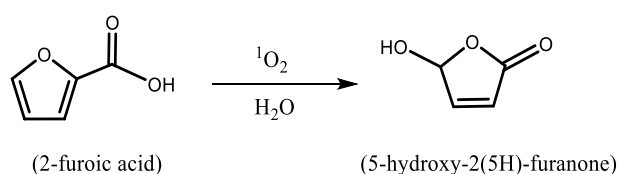


Figure 5-3. Mechanism of photo reaction of catalyst PF-BT-CO₂ (with radical trap TEMP).



Scheme 5-3. The reaction equation of oxidation in PF-BT-CO₂ photo induced reaction.

We conclude that the transition of oxygen molecule from ground triplet state to excited singlet state can be achieved by the activation of switchable hydrophilicity of conjugated polymer under illumination, as shown in figure 5-3. The new formed intermediate singlet oxygen was quickly trapped by TEMP and transformed to stable radical that can be detected by EPR. So the mechanism of photochemical reactions which were carried out in the same conditions with the existence of polymer (PF-BT-CO₂ or PF-BT) and oxygen was proved to be an intermediate radical mechanism. For example, 2-furoic acid was carried out in this photochemical condition, and 5-hydroxy-2(5H)-furanone was formed. Generally, 5-hydroxy-2(5H)-furanone was regarded to be oxidized from furoic acid only through the existence of

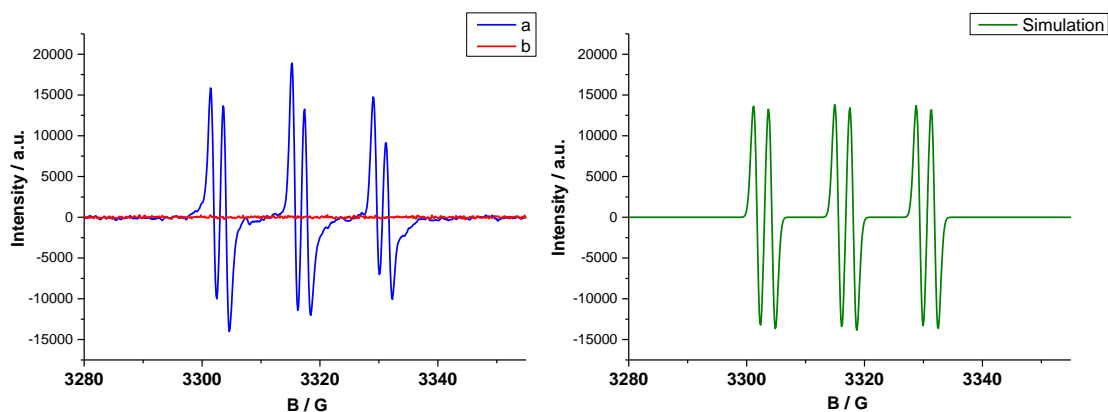


Figure 5-4. EPR spectra, a) Photocatalyst PBT (1 mg/ml), PBN (0.1 M) and trans-anethole, 0.1 M. b) PBN (0.1 M) and trans-anethole (0.1 M) on the left. Computer simulated EPR spectrum on the right.

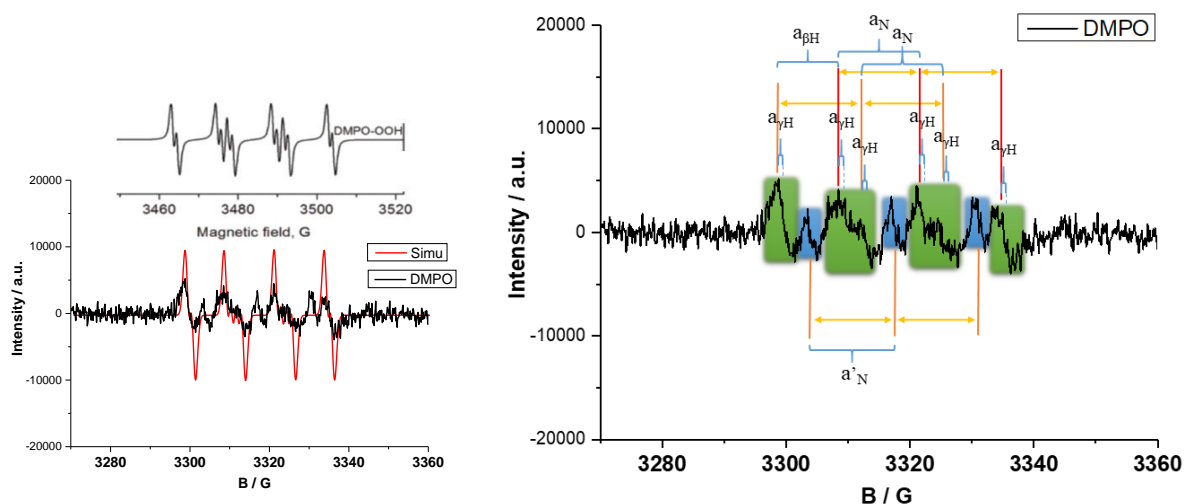


Figure 5-5. EPR spectra, black). photocatalyst PBT (1 mg/ml), DMPO (0.1 M) dissolved in CH_3NO_2 with O_2 bubbling, red). The simulation EPR spectrum (at the left bottom). Referenced EPR spectra of DMPO/ $\cdot\text{OOH}$ adduct which were reported before for comparison¹⁵ (at the left top). The detailed analysis of EPR spectrum of DMPO radical adducts (in the right).

Two samples were prepared to measure EPR for comparison which is shown in the figure 5-4 left (a) photocatalyst PBT (1 mg/ml), PBN (0.1 M) and styrene derivate (trans-anethole, 0.1 M), (b) PBN (0.1 M) and trans-anethole (0.1 M). Both of the two samples were dissolved in dry CH_3NO_2 and were irradiated under visible light for 2 hours. Then both samples are sealed in EPR quartz tube with the same volume and the same position of EPR cavity. As anticipated by using the PBN trap, a spectrum sample (a) with 3 groups of doublet peaks (sextet pattern) were detected with g factor 2.0060. The intensity of signal peak is around 15000. The sextet signal pattern was derived from double hyperfine splitting of hydrogen nucleus $a_{\text{H}} = 2.5$ G (from the position of α carbon of nitroxide) and triplet hyperfine

splitting of nitrogen nucleus $a_N = 14.0$ G. The hydrogen nuclei from the position of β carbon of nitroxide are far away from the spin center, and the number of this kind of hydrogen nuclei is 10. So we didn't find hyperfine splitting from these hydrogen nuclei in EPR spectrum, or resolved inside the spectrum. The sample (b) under the same condition as (a) only without photocatalyst PBT gives no signal at all in EPR measurement. That means no intermediate radical species existed in the sample (b) under the light illumination. The PBT networks play an important role which can initiate the intermediate radical in the irradiation of visible light. As shown in the mechanism figure 5-6, PBT was excited by visible light under these conditions. One electron in HOMO was excited and transfer to LUMO. The electron cavity (cation) formed and will trigger one electron transfer from trans-anethole. A mono cation radical of anethole was formed. Then it would undergo [2 + 2] cycloaddition with another styrene derivate molecule. The right picture of figure 5-4 is the EPR simulation of nitroxide radical which was trapped by PBN in our case (it suit the EPR experimental data with the same splitting patterns and linewidth).

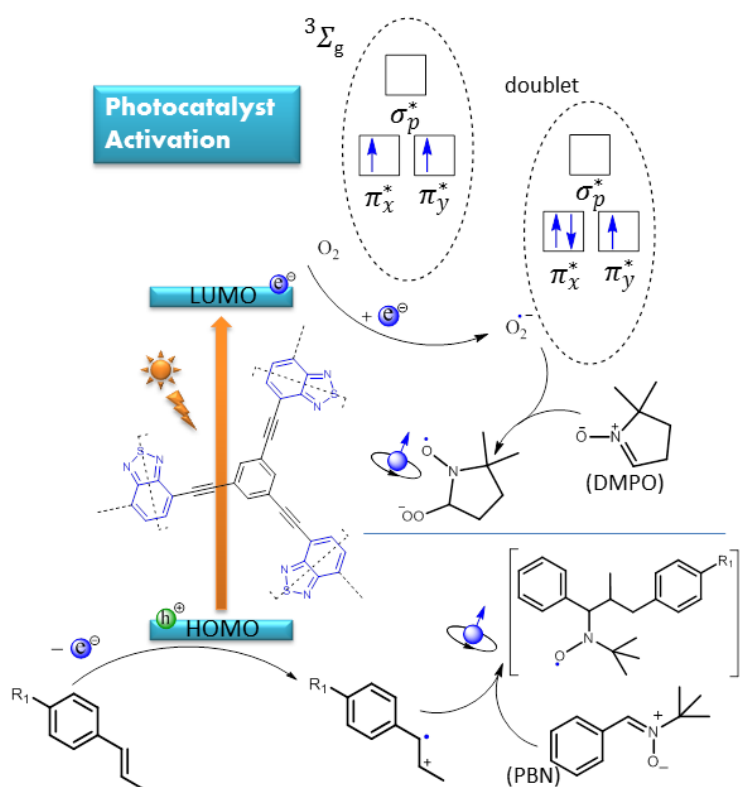
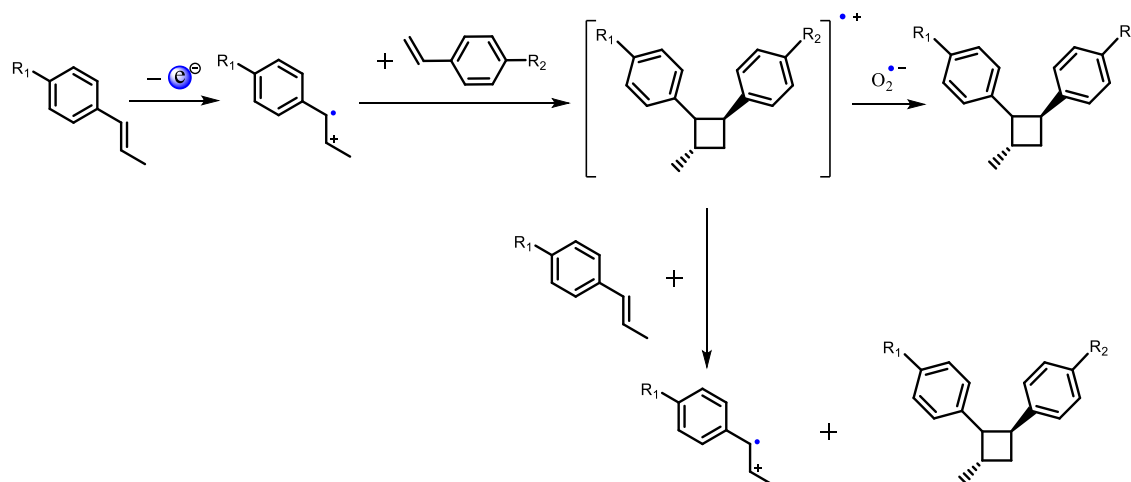


Figure 5-6. Mechanism of photo reaction of catalyst PBT (with radical trap PBN and DMPO).

DMPO radical trap was used to investigate the mode of the transfer or suspension about the intermediate radicals after the formation of cyclobutane in [2 + 2] cycloaddition reaction. DMPO was known to have the ability to trap superoxide radical and hydroxyl radical,

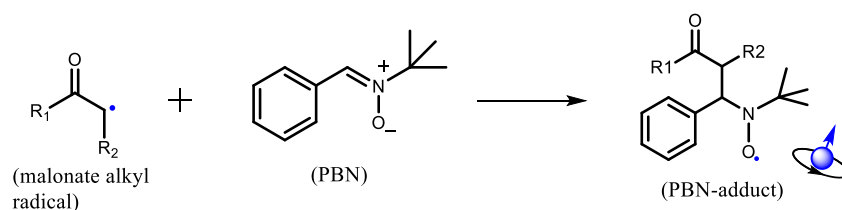
as shown in the scheme 5-4. The half-life time of DMPO/ \cdot OOH ($t_{1/2}$) is still very short, although it can be detected by EPR spectroscopy. We designed an experiment where the sample was composed of photocatalyst PBT (1 mg/ml), DMPO (0.1 M) dissolved in CH_3NO_2 with O_2 bubbling and was irradiated under visible light for 2 hours. The right spectrum of figure 5-5 shows very weak EPR signals with several hyperfine splitting in four groups. Because the DMPO trapped superoxide radical is still very unstable, the concentration of DMPO/ \cdot OOH in the system is too low which lead to low intensity of EPR signal. Comparing to the reference EPR signal pattern¹⁵ of DMPO/ \cdot OOH with the total width of 47 ~ 48 G and $a_N = 14.2$ G, $a_{\beta\text{H}} = 11.7$ G and $a_{\gamma\text{H}} = 1.3$ G (shown at the left top of figure 5-5), the DMPO/ \cdot OOH spectrum has the same total width of signal 47 ~ 48 G and the same hyperfine splitting pattern with $a_N = 12.7$ G, $a_{\beta\text{H}} = 9.8$ G and $a_{\gamma\text{H}} = 1.3$ G, respectively, as shown in the green parts of right spectrum. The blue parts of right spectrum figure out there are radical mixture which have triplet singlet patterns with $a_N = 12.7$ G existing in the system. It might be another radical species decomposed from the unstable radical DMPO/ \cdot OOH which lost a H_2O molecule per radical. The red spectrum of figure 5-5 is the EPR simulation of DMPO/ \cdot OOH case (it suit the EPR experimental data with the same splitting patterns and linewidth). The typical EPR spectrum with four clear peaks-signal from hydroxyl radical can be excluded (without $a_{\gamma\text{H}}$ hyperfine splitting). We could make sure the superoxide radical existed during the photo reaction and joined the cycle of electron transfer. Another possible route may be the new formed cyclobutane cation could continuously get one electron from another unreacted trans-anethole. The final product neutral cyclobutane acquired and the new formed intermediate cation radical would continuously trigger the [2 + 2] cycloaddition reaction. So the intermediate radical initiated cycloaddition could continuously pass on, as shown in scheme 5-5.



Scheme 5-5. The reaction of [2 + 2] cycloaddition reaction in PBT photo induced reaction.

5.2.3 Radical and Spin Analysis of Photo Induced Reaction about α -Alkylation of Aldehyde Derivatives

A reaction of α -bromocarbonyl compound and aldehydes (the α -alkylation of aldehyde derivatives, as shown in scheme 5-7) can be performed by using the same organic conjugated hyperbranched poly(benzothiadiazole) photocatalyst (PBT) in visible light, where the synthesis of catalyst was previously reported. Generally, this kind of α -alkylation reaction with aldehydes can be performed in transition metal based photocatalyst. But by using metal free heterogeneous polymer catalyst PBT, the reaction could be performed in an environmental way and can be regarded as molecular backbone coupling with R₁, R₂ to R₃. (R₁, R₂ to R₃ represent alkyl group or aryl group, and this work was cooperated with Wei Huang in Mainz.) For this part, we use EPR measurement to investigate the mechanism and process of the visible light induced reaction which is possibly intermediate radical mechanism. PBN was used as radical trap method to analysis the potential intermediate radical species α -bromocarbonyl compound where a C-Br bond in the molecule may be broken and a bromine atom was released in the photo chemical reaction. The possible radical structures which are trapped by PBN are shown in the scheme 5-6.



Scheme 5-6. The reaction of malonate alkyl radical which was trapped by PBN.

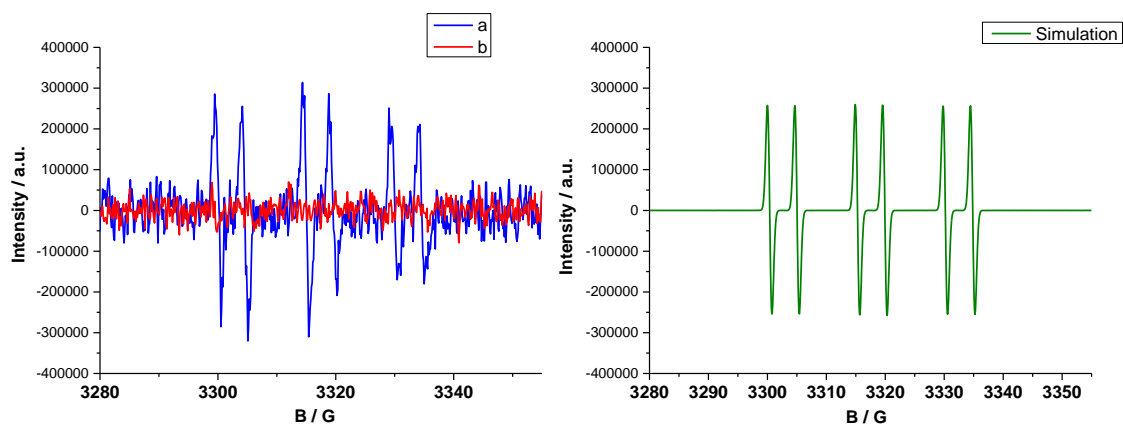


Figure 5-7. EPR spectra, a) Photocatalyst PBT (1 mg/ml), PBN (0.1 M) and α -bromomalonate (0.5 M). b) PBN (0.1 M) and α -bromomalonate (0.1 M) on the left. Simulation EPR spectrum on the right.

Two samples for comparison were prepared to measure EPR which is shown in the figure 5-7 left (a) photocatalyst PBT (1 mg/ml), PBN (0.1 M) and α -bromocarbonyl compound (α -bromomalonate, 0.5 M), (b) PBN (0.1 M) and α -bromomalonate (0.1 M). Both of the two samples were dissolved in dry DMF and were irradiated under visible light for 5 hours. Then both samples were sealed in EPR quartz tube with the same volume and the same position of EPR cavity. A typical PBN adduct malonate alkyl radical signal of EPR spectrum with 3 groups of doublet peaks (sextet pattern) presented about sample (a) with g factor 2.0061. Although the background noisy has a little bit somehow, the EPR spectrum with sextet signal pattern could be obviously observed. The sextet signal pattern was derived from double hyperfine splitting of hydrogen nucleus $a_H = 4.7$ G (from the position of α carbon of nitroxide) and triplet hyperfine splitting of nitrogen nucleus $a_N = 14.9$ G. The hydrogen nuclei from the position of β carbon of nitroxide are far away from the spin center, and the number of this kind of hydrogen nuclei is 10. So we didn't find hyperfine splitting from these hydrogen nuclei in EPR spectrum, or resolved inside the spectrum. The sample (b) with the same condition as (a) only without photocatalyst PBT gives no signal at all in EPR measurements. That means no intermediate radical species produced in the sample (b) during the photo reaction. So the heterogeneous polymer catalyst PBT plays a determinate role which can initiate the intermediate radical in the irradiation of visible light. As shown in the mechanism figure 5-8, PBT was excited by visible light to excited state which would interact with α -bromomalonate. A bromine atom was released with a C-Br bond broken in the molecule, meanwhile the malonate intermediate radical formed and the catalyst PBT returned back to ground state for undergoing the next excitation cycle. The right picture of figure 5-7 is the EPR simulation of malonate alkyl radical in our case which obey a typical EPR signal pattern of PBN adduct radical species (it suit the EPR experimental data with the same splitting patterns and linewidth). If the intermediate radical scavenger (PBN radical trap) does not exist in the system, intermediate malonate radical would attack α -carbon position of aldehyde and the α -alkylation of aldehyde reaction performed, as shown in scheme 5-7.

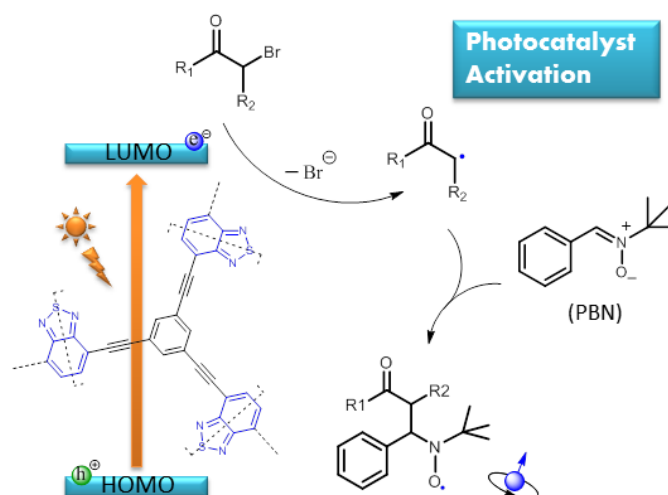
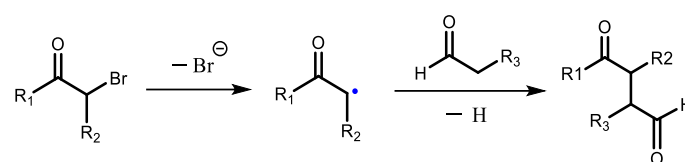


Figure 5-8. Mechanism of photo reaction of catalyst PBT (with radical trap PBN)



R1, R2 and R3 : alkyl or aryl

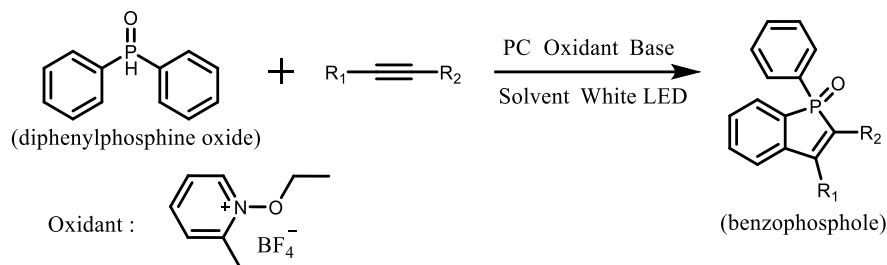
Reaction Conditions: PC, Base and White Light

Scheme 5-7. The reaction equation of α -alkylation of aldehyde reaction in PBT photo induced reaction

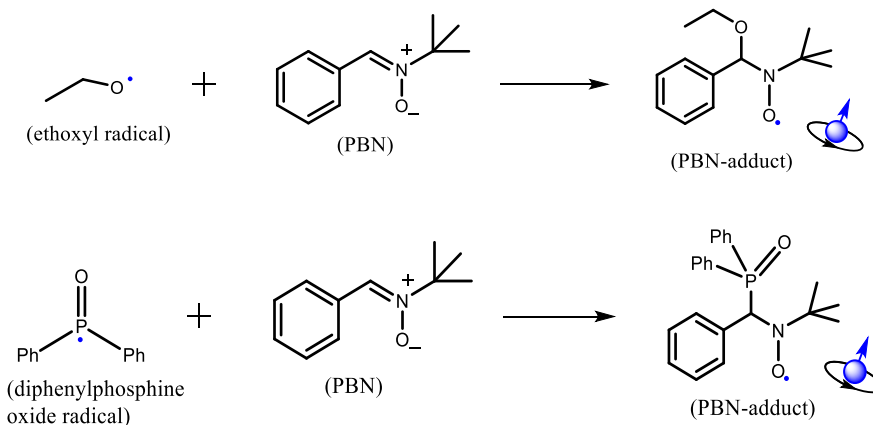
5.2.4 Radical and Spin Analysis of Photo Induced Reaction about Cycloaddition of Diphenylphosphine Oxide Derivatives and Alkynes Derivatives

A newly designed asymmetric covalent triazine polymercatalyst (PTTP) was synthesized via trimerization of monomer 5-(4-cyanophenyl)thiophene-2-carbonitrile. The polymerization proceeded in solid state (dispersed with SiO₂), which can acquire porous polymer framework for photochemical reaction. Benzophosphole oxide derivatives which owns unique electronic properties were synthesized through cycloaddition of diphenylphosphine oxide and alkynes derivatives (symmetric alkynes or asymmetric alkynes) by catalyst PTTP in visible light, as shown in scheme 5-8. This work was cooperated with Wei Huang in Mainz. For this part, EPR measurements were used to investigate the mechanism and process of the visible light induced cycloaddition reaction between diphenylphosphine oxide and alkynes derivatives. Due to *N*-ethoxy-2-methylpyridinium tetrafluoroborate was predicted as an oxidant which forms intermediate ethoxyl radical would release out by the interaction with photocatalyst PTTP in visible light. It would possibly participate in the photocatalytic cycle by reacting with diphenylphosphine oxide derivatives. New radical intermediate species may be performed in this stage. So we predicted the

photochemical reaction is activated by intermediate radical mechanism and we also designed a PBN radical trap method in two stages to analyse the detail about the potential intermediate radical species to initiate cycloaddition reaction.



Scheme 5-8. The equation of cycloaddition of diphenylphosphine oxide and alkyne reactions



Scheme 5-9. Two reaction equations of ethoxyl radical which was trapped by PBN (upper) and diphenylphosphine oxide intermediate radical which was trapped by PBN (lower), respectively.

Two samples where the radical trap PBN was added in different stages for comparison were prepared. The possible procedure of radical trapping is shown in scheme 5-9. One is the PBN added at beginning with *N*-ethoxy-2-methylpyridinium tetrafluoroborate, photocatalyst PTPP. The other one is the PBN added with not only oxidant and photocatalyst PTPP, but also starting compound diphenylphosphine oxide. Both of the samples which are labeled (a) and (b) respectively in the following EPR measurements were dissolved in *tert*-butylbenzene. The two samples were both irradiated with white LED lamp ($\lambda > 420$ nm) for 2 hours and bubbled with inert gas before measurement. As the EPR figure 5-9 shown below, a typical PBN adduct radical signal of EPR spectrum with 3 groups of doublet peaks (sextet pattern) was presented with *g* factor 2.00620 for sample (a). The sextet signal pattern was derived from double hyperfine splitting of hydrogen nucleus $a_H = 2.1$ G and triplet hyperfine splitting of nitrogen nucleus $a_N = 14.7$ G. That means the intermediate radical species (ethoxyl radical) existed under these conditions of photo chemical reaction. (successfully released out from

oxidant) Meanwhile, the sample (b) which contains diphenylphosphine oxide gives an unique spectrum twelve quartet-patten signals (which is actually double sextet peaks signal) in EPR measurement with g factor 2.0062. The special spectrum of radical sample (b) which split by three different groups of nucleus was derived from double hyperfine splitting of hydrogen nucleus $a_H = 3.2$ G, triplet hyperfine splitting of nitrogen nucleus $a_N = 14.1$ G and another double hyperfine splitting of hydrogen nucleus $a_P = 19.0$ G respectively. This special EPR features are different from ones of sample (a) and illustrate that new radicals intermediate species based on diphenylphosphine oxide formed at current stage of reaction by the interaction with the ethoxyl radical. The right pictures of figure 5-9 are the EPR simulations of different radical species in our case which obey the signal pattern of PBN adduct radicals and hyperfine splitting rules (it suit the EPR experimental date with the same splitting patterns and linewidth).

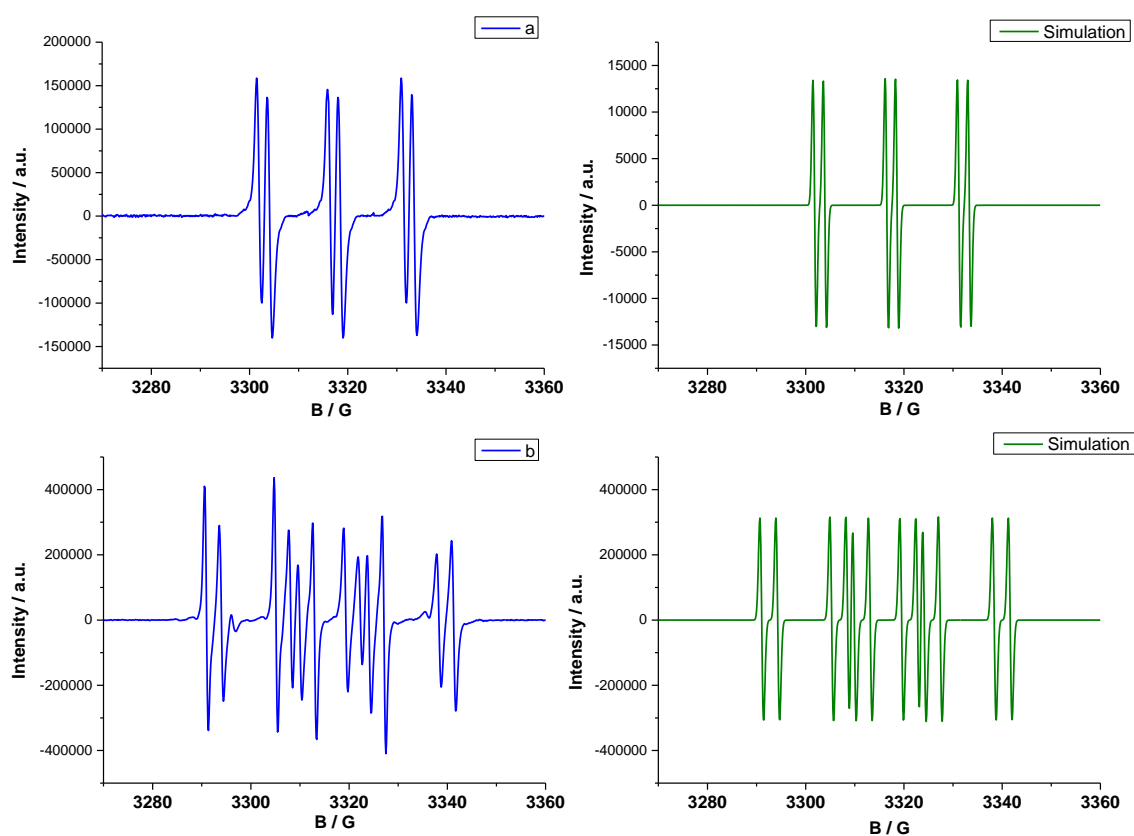


Figure 5-9. EPR spectra, a) Photocatalyst PTPP (5 mg), *N*-ethoxy-2-methylpyridinium tetrafluoroborate (0.15 mmol) and PBN (0.15 mmol) were dissolved in tert-butylbenzene (5 ml). b) Photocatalyst PTPP (5 mg), *N*-ethoxy-2-methylpyridinium tetrafluoroborate (0.15 mmol), diphenylphosphine oxide (0.15 mmol) and PBN (0.15 mmol) were dissolved in tert-butylbenzene (5 ml) on the left. Simulation EPR spectra on the right two pictures.

The detailed analysis of the unique EPR spectrum is shown in figure 5-10. Triplet hyperfine splitting of ^{14}N lead to three signal groups which are framed up by pink, green and orange square (dashed line) respectively are shown,. Due to the diphenylphosphine oxide intermediate radical trapped by PBN, phosphorus which the nucleus with spin quantum number ($I = 1/2$) appeared at β position of nitroxide spin center. The hyperfine splitting of phosphorus nucleus $a_{\text{P}} = 19.0$ G is larger than for the nitrogen nucleus $a_{\text{N}} = 14.1$ G in this case. So the peak splitting pattern looks like axial symmetry at the axis $B = 3316$ G, rather than a typical signal pattern with triplet individual groups of peaks in nitroxide radicals. The hyperfine splitting of hydrogen nucleus $a_{\text{H}} = 3.2$ G which is at normal range is derived from H at the α -carbon position.

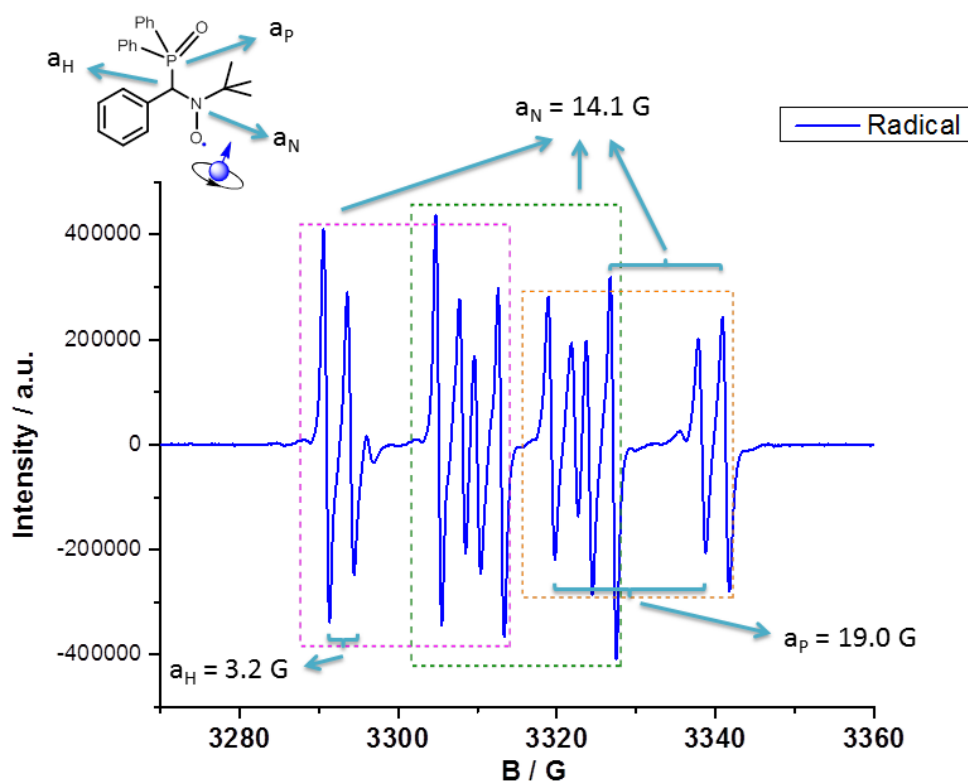


Figure 5-10. Detail analysis of EPR spectrum of diphenylphosphine oxide intermediate radical

Depending on the radical trap method and the EPR measurements, the mechanism of the photo catalysis reaction of whole process is clarified. It is initiated by intermediate radical species in two stages. As shown in figure 5-11 below, newly synthesized triazine polymercatalyst (PTTP) was activated by visible light and interacted with oxidant to release ethoxyl radical species in the first stage. Then the radical species continuously trigger starting compound to diphenylphosphine oxide intermediate radical in the second stage. If alkynes

derivatives exist in this system, the carbon carbon triple bonds would be attacked by the diphenylphosphine oxide radical and perform a cycloaddition reaction to final compound benzophosphole oxide derivatives in alkaline conditions. The reaction mechanism is shown in scheme 5-10.

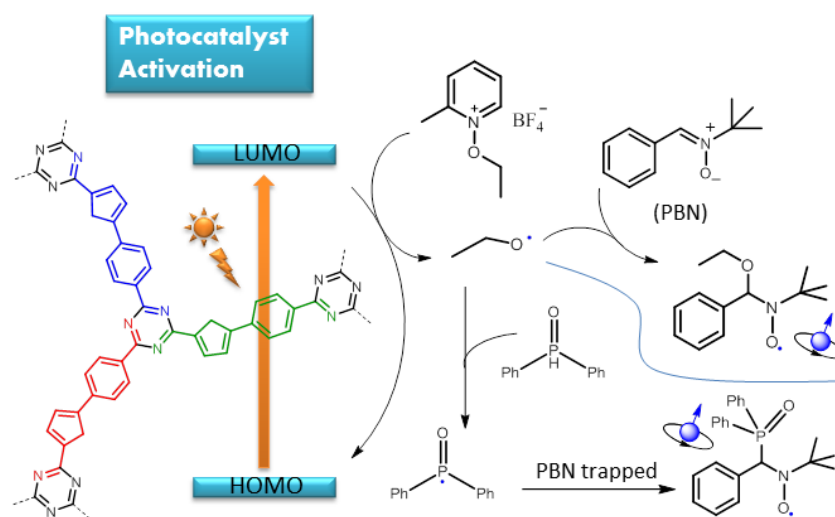
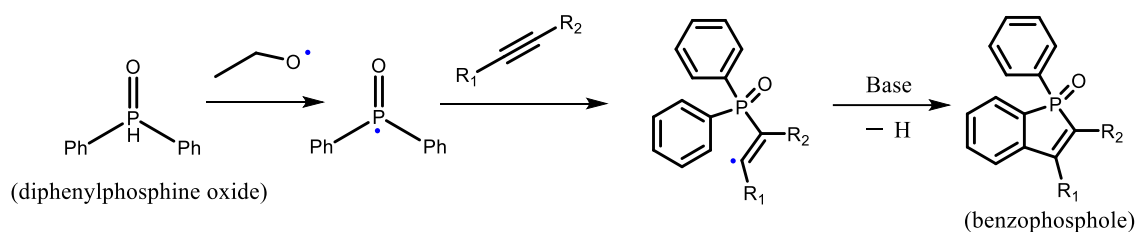


Figure 5-11. Mechanism of photo reaction of catalyst PTTP (with radical trap PBN)



Scheme 5-10. The reaction of cycloaddition of diphenylphosphine oxide and alkynes reaction in PTTP photo induced reaction.

5.3 Conclusions

For this chapter, we used EPR spectroscopy measurements to investigate the systems which may have radical species or spin centers. The four photo induced chemical reactions activate spin species during the processes of reactions. Radical intermediate species which play an important role in the preceding of these reactions were predicted. EPR spectroscopy is successfully used to investigate the mechanism of the whole photo induced reaction by trap and analysis the radical intermediate species existed during the whole processes. Different radical trap compound were used to find radical species and various radical trap adducts were acquired, like TEMPO radical adducts, PBN radical adducts and DMPO radical adducts.

Some of these specific radical trap adducts were first found and published. Their radical features are well characterized and interpreted.

5.4 Reference

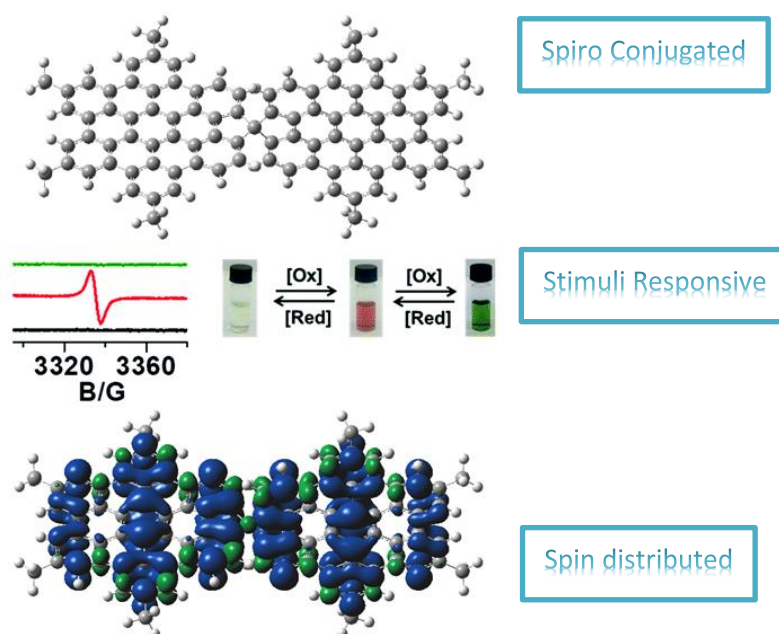
- (1) Li, R.; Byun, J.; Huang, W.; Ayed, C.; Wang, L.; and Zhang, K. A. I. Poly(benzothiadiazoles) and Their Derivatives as Heterogeneous Photocatalysts for Visible-Light-Driven Chemical Transformations. *ACS Catal.* **2018**, *8*, 4735-4750
- (2) Nicewicz, D. A.; MacMillan, D. W. C. Merging Photoredox Catalysis with Organocatalysis: The Direct Asymmetric Alkylation of Aldehydes. *Science* **2008**, *322*, 77-80
- (3) Byun, J.; Huang, W.; Wang, D.; Li, R.; Zhang, K. A. I. CO₂-Triggered Switchable Hydrophilicity of a Heterogeneous Conjugated Polymer Photocatalyst for Enhanced Catalytic Activity in Water. *Angew. Chem. Int. Ed.* **2018**, *57*, 2967-2971
- (4) Li, R.; Ma, B. C.; Huang, W.; Wang, L.; Wang, D.; Lu, H.; Landfester, K.; Zhang, K. A. I. Photocatalytic Regioselective and Stereoselective [2 + 2] Cycloaddition of Styrene Derivatives Using a Heterogeneous Organic Photocatalyst. *ACS Catal.* **2017**, *7*, 3097-3101
- (5) Huang, W.; Ma, B. C.; Wang, D.; Wang, Z. J.; Li, R.; Wang, L.; Landfester, K.; Zhang, K. A. I. A fixed-bed photoreactor using conjugated nanoporous polymer-coated glass fibers for visible light-promoted continuous photoredox reactions. *J. Mater. Chem. A* **2017**, *5*, 3792-3797
- (6) Huang, W.; Byun, J.; Rçrich, I.; Ramanan, C.; Blom, P. W. M.; Lu, H.; Wang, D.; Silva, L. C.; Li, R.; Wang, L.; Landfester, K.; Zhang, K. A. I. Asymmetric Covalent Triazine Framework for Enhanced Visible-Light Photoredox Catalysis via Energy Transfer Cascade. *Angew. Chem. Int. Ed.* **2018**, *57*, 8316-8320
- (7) Ghosh, I.; Marzo, L.; Das, A.; Shaikh, R.; König, B. Visible Light Mediated Photoredox Catalytic Arylation Reactions. *Acc. Chem. Res.* **2016**, *49*, 1566-1577.
- (8) Yoon, U. C.; Mariano, P. S. Mechanistic and Synthetic Aspects of Amine-Enone Single Electron Transfer Photochemistry. *Acc. Chem. Res.* **1992**, *25*, 233-240.
- (9) Buettner, G. R. Spin Trapping: ESR parameters of spin adducts. *Free Radical Biology and Medicine* **1987**, *3*, 259-303
- (10) Lagercrantz, C. Spin Trapping of Some Short-Lived Radicals by the Nitroxide Method. *J. Phy. Chem.* **1971**, *75*, 3466-3475
- (11) Janzen, E. G. Spin Trapping. *Accounts of Chemical Research* **1971**, *4*, 31-40

- (12) Borden, W. T.; Hoffmann, R.; Stuyver, T.; Chen, B. Dioxygen: What Makes This Triplet Diradical Kinetically Persistent? *J. Am. Chem. Soc.* **2017**, *139*, 9010–9018
- (13) Wayne, R. P.; Pitts, J. N.; Hammond, G. S.; Noyes, W. A. Singlet Molecular Oxygen. *Advances in Photochemistry* **1969**, *7*, 311–371
- (14) Schweitzer C.; Schmidt, R. Physical Mechanisms of Generation and Deactivation of Singlet Oxygen. *Chem. Rev.* **2003**, *103*, 1685–1757
- (15) Finkelstein, E.; Rosen, G. M.; Rauckman, E. J. Spin trapping of superoxide and hydroxyl radical: Practical aspects. *Archives of Biochemistry and Biophysics* **1980**, *200*, 1-16

Chapter 6 Redox Spin Active Systems of Aromatic Hydrocarbons Studied by EPR

6.1 Introduction

In this chapter, redox spin active systems discussed here is reversibly radical or spin species switched system with large aromatic conjugated hydrocarbons structures. They are both hexabenzocoronene (HBC) derivatives, with one is single HBC structure and the other one is spiro-fused HBC structure. The works were cooperated with Yunbin Hu. Three different states which were formed by electron transfer with different radical features were verified by EPR measurements and the simulation of the experimental spectra. In addition, DFT calculations were used to simulate the orbital energy levels of various states, the spin density distributions and the situations of orbital degeneracy for neutral spiro-HBC and neutral mono-HBC. The spin properties of HBC contained polycyclic aromatic hydrocarbons at closed-shell or open-shell structures are well presented here. (some parts of this chapter originated from the publication: *Chem. Commun.* **2018**, Accepted Manuscript DOI: 10.1039/C8CC07405D)

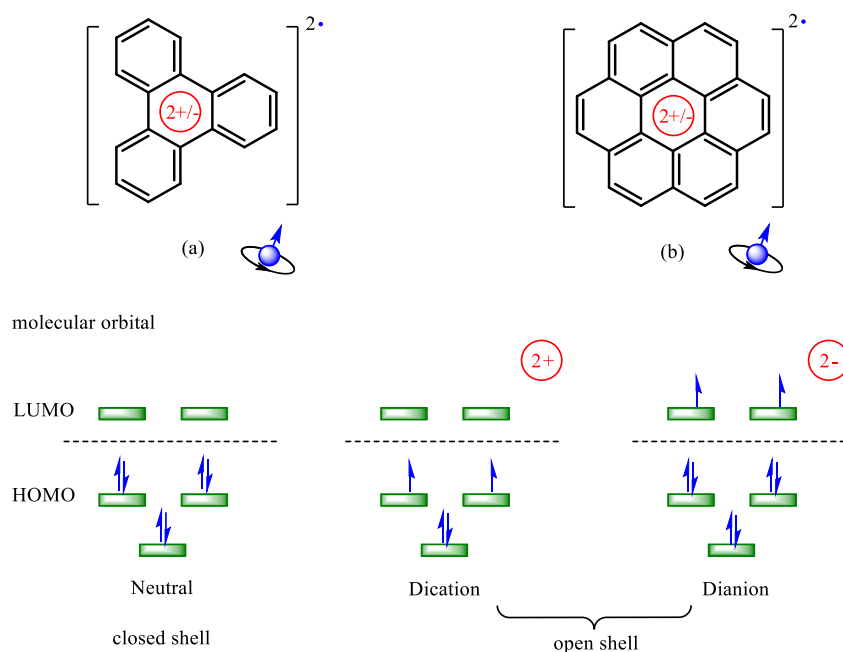


Schematic Diagram of Spiro-HBC Structure and Spin Density Distribution of Cation Radical, the EPR Spectra and Color Change through Redox Stimuli

6.2 Redox Spin Switch of Aromatic Hydrocarbons

Aromatic hydrocarbons from small fused structures, like triphenylene derivatives¹ or coronene derivatives^{2,3} to much more complicated fused structures, including hexabenocoronene derivatives⁴ or even fullerenes (C_{60})⁵ have been investigated for many years. But most of the studies focused on their neutral state. When the aromatic hydrocarbons undergo electrons transfer, and form radical cation or radical anion molecules, the spin properties may emerge as the unpaired electron exist on frontier orbital in response at different valence state of aromatic hydrocarbon derivatives. The relationships between the spin multiplicity and properties and the different valence state about the cations/anions in aromatic hydrocarbons systems still need further investigation.

6.2.1 Back Ground Knowledge about Redox Processes in Triphenylene and Coronene



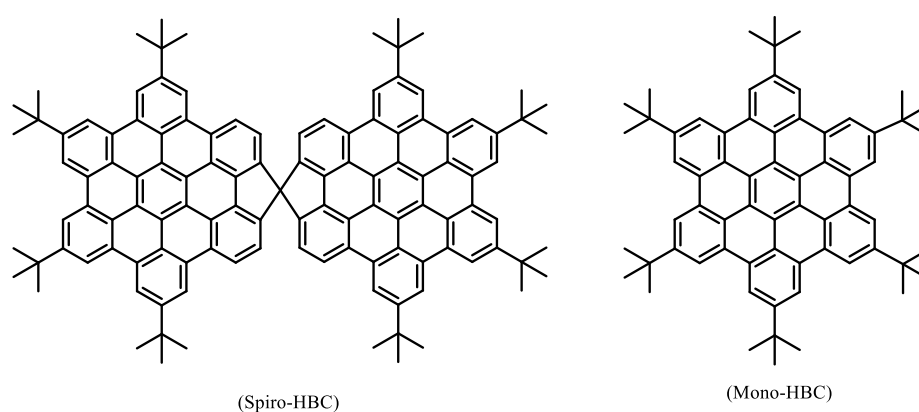
Scheme 6-1. The structure of triphenylene and coronene in the charge state of dication/dianion (upper), The HOMO, LUMO and electrons distribution in closed shell and open shell structure (lower)

The cyclic annulenes, like as triphenylene and coronene are famous examples to depict the aromatic carbon skeleton radical and spin properties in the situation of open shell structures. The neutral state of triphenylene and coronene with closed shell structure has no spin or radical in the hydrocarbon skeleton. If these molecules are oxidized or reduced, the charged cyclic annulenes would switch to open-shell structure and own radicals and spin properties. The dianion of triphenylene which means two electrons transfer to the hydrocarbon structure in reduction conditions owns a triplet ground state.¹ For coronene,

however the biradical dication and dianions with an open shell structure could be evidenced by EPR spectroscopy, but they possess singlet ground state,^{2,3} as shown in scheme 6-1. The reason for these hydrocarbon structures with two electron loss or acquisition carrying radicals or spin center is that the degeneracy of HOMO and LUMO which can provide diradicals upon two electrons charging. The degenerate orbitals of HOMO and LUMO which are due to the high symmetry of these molecular structure made the orbital energy levels identical, two unpaired electrons were singly occupied in every degenerate orbital according to Hund's rule (the total energy of molecule is the lowest at this situation).

6.2.2 EPR Measurement of Spiro-HBC and Mono-HBC in Different Valence State

5,5',8,8',11,11',14,14'-octa-*tert*-butyl-1,1'-spirobi-(tetrabenzo[*ef,hi,kl,no*] fluoreno[3,4,5,6-*qrabc*]coronene) (spiro-HBC) was newly synthesized by Y. Hu, et al.⁶ while hexa-*peri*-hexabenzocoronene (mono-HBC) is a well known molecule first reported in 1958,⁷ which was used here for comparison (Scheme 6-2)⁸⁻¹⁶. For the closed shell structure of polycyclic aromatic hydrocarbons, the large π -system offers these kinds of structures many peculiar and intriguing properties, just as self-assembly and high intrinsic charge-carrier mobility.¹⁷⁻⁴³ It is also very interesting and valuable to study these cyclic aromatic hydrocarbons when they are transferred to open shell structures. We investigated the radical and spin properties of the two HBC containing structures in different oxidation and reduction conditions by EPR measurements and density functional theory (DFT) calculations with Gaussian 09W program suite.⁴⁴



Scheme 6-2. The structure of spiro-HBC and mono-HBC

A certain concentration of spiro-HBC and mono-HBC solution (1.0×10^{-5} mol L⁻¹ in DCM) was prepared. Oxidant antimony pentachloride (SbCl₅) and reductant stannous chloride (SnCl₂) or Zn were used to start redox reaction with them.^{3,4,45,46} Three different valence states

including the original neutral compounds were acquired upon different treatments of oxidant and reductant. Both of spiro-HBC and mono-HBC in solutions undergo obvious color change for their three valence states. The colorless starting neutral compounds changed to red in the first stage of oxidation. And then further oxidation in second stage would lead to the apparent green color. The switching processes among the different states upon specific redox conditions are reversible. The reductant SnCl_2 or Zn which added into the systems could induce a reverse transfer from the second oxidized stage to the neutral compound. We labeled the three different valence states A, B and C state which refers to the original neutral compound, the first stage of oxidized compound and the second stage of oxidized compound, respectively. All the redox reactions were carried out under argon bubbling. The samples transferred to EPR tube, as soon as the color of solution became. The EPR spectra below display the radical features of different states to spiro-HBC and mono-HBC, as shown in figure 6-1 and figure 6-2.

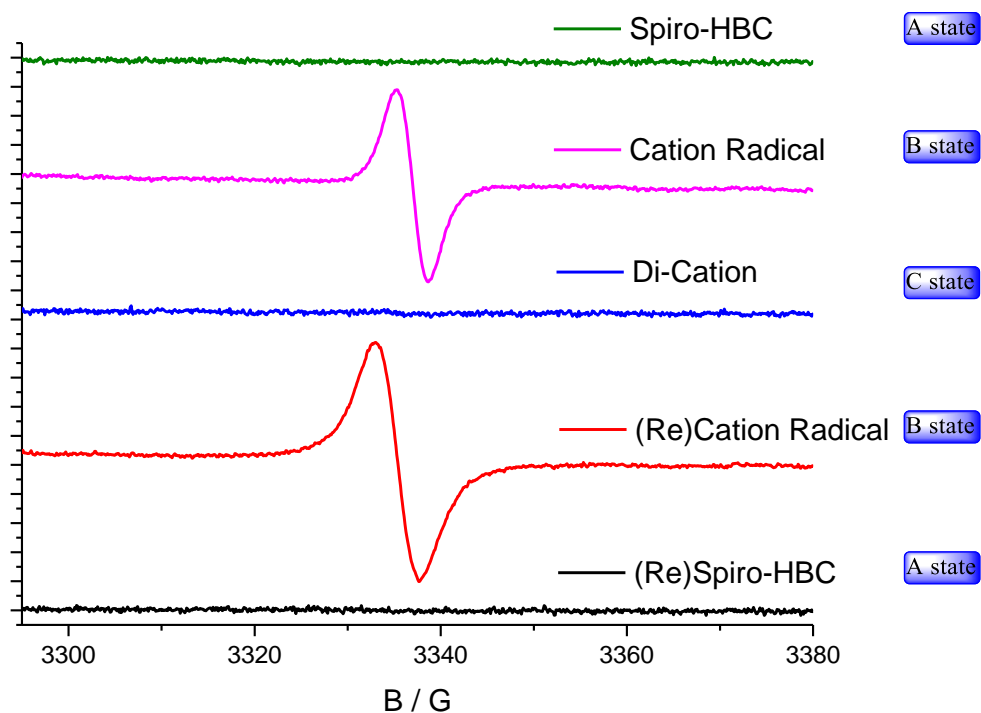


Figure 6-1. EPR spectra of spiro-HBC in three states in two processes of oxidation and reduction respectively

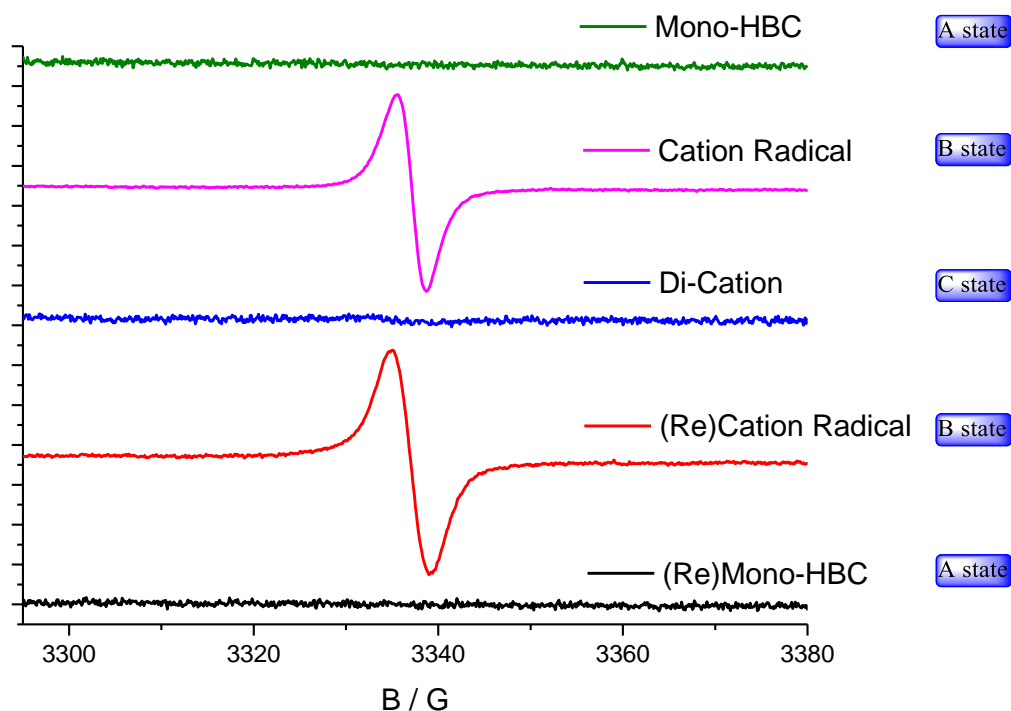


Figure 6-2. EPR spectra of mono-HBC in three states in two processes of oxidation and reduction respectively

No matter for the A state of spiro-HBC or mono-HBC, there are no EPR signals found for these closed shell structures. When oxidant SbCl_5 was added to the systems to get the first stage of oxidation, a single peak signal with the g factor 2.0033 for spiro-HBC appeared in EPR spectra. The g factor for mono-HBC is 2.0032 at the first stage of oxidation. That means the structure has become open shell with unpaired electron occupied in orbital. The B state should be cation radical species. Due to the hydrogen (fermion) in this hydrocarbon structure could split the EPR signal (hydrogen nucleus with spin quantum number $I = \frac{1}{2}$), the radical position should locate on the large π -conjugated skeleton which no hydrogen atom exist on α carbon position of the radical species. No hyperfine coupling with the protons on the conjugated carbon structures or the interactions are resolved, depending on the EPR spectra signal. Further amount of oxidant SbCl_5 adding would lead to C state. The EPR signal disappeared again compared to former B state. It refers to the termination of radical by further oxidation process. The loss of the unpaired electron made HBC became a pure dication species without any spin properties. Excessive SnCl_2 or Zn as reductant to check if the former oxidation process could reversibly switch back from C state to A state, and the whole process was monitored by EPR measurements. We observed the green solution (C state) quickly change to red again in 30 second after adding of excessive SnCl_2 reductant. EPR measurement

was carried out immediately to seek radical signal of the red solution. A same EPR signal spectrum with B states was acquired in this condition. Further reaction time about 5-10 min with the excessive reductant for this system would lead to colorless solution with no signal in EPR spectrum. This state has the same apparent color and spin properties with starting compound A state. This reverse reduction process certified the whole redox procedure, which the procedure is from no-spin to spin then to no-spin again, is reversible. The whole redox process is repeatable for multiple times. All the EPR measurements were carried out in room temperature with the same conditions of EPR measurements, modulation amplitude = 0.5 G, modulation frequency = 100 kHz, microwave power = 2 mW, conversion time = 320.00 ms and time constant = 327.680 ms.

The following two EPR spectra, as shown in figure 6-3 belong to the cation radical of mono-HBC and spiro-HBC. The black spectra are EPR experimental data, while the red spectra are EPR simulation spectra. (The simulation suit the EPR experimental data with the same g factor and linewidth).

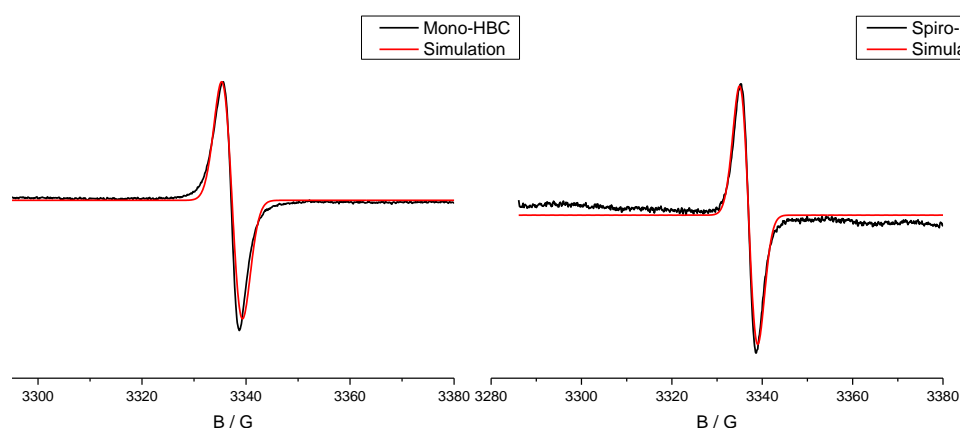
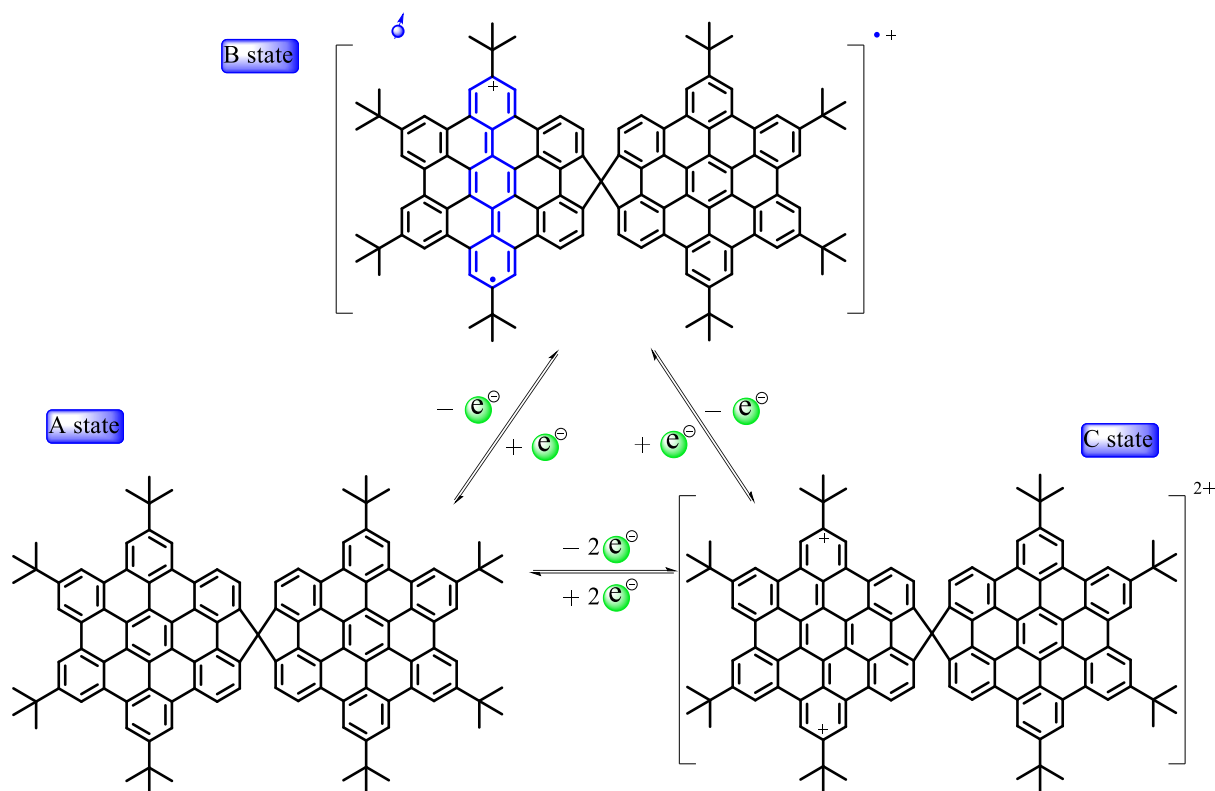
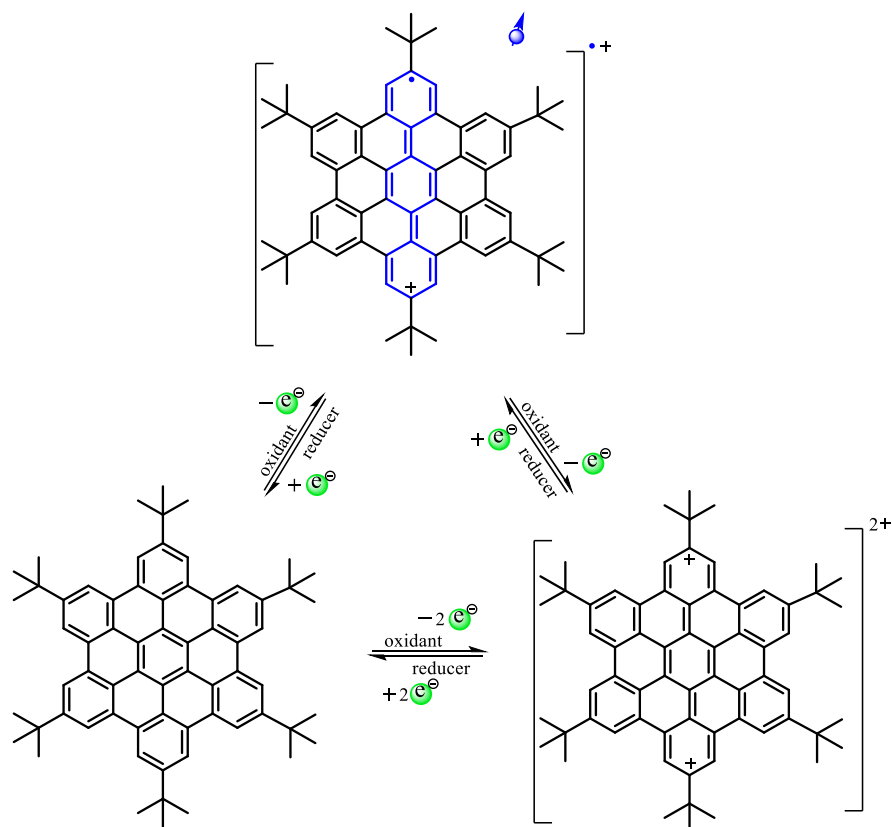


Figure 6-3. EPR spectra of spiro-HBC and mono-HBC in B state (black line) and simulation spectra of the two cases (red line)

The following two diagrammatic sketches, as shown in scheme 6-3 and 6-4, display the conversion processes of spiro-HBC and mono-HBC among the three different valence states by electron transfer in various redox conditions. The EPR spectra which are shown in figure 6-4 presents the radical features of B and C state of spiro-HBC and also the signal feature of an intermediate state which mix with the two states of compounds, during the conversion from B state to C state. The signal intensity of the intermediate state is smaller than the pure B state.



Scheme 6-3. Structure sketch of reversible transform among three different states by electron transfer about spiro-HBC



Scheme 6-4. Structure sketch of reversible transform among three different states by electron transfer about mono-HBC

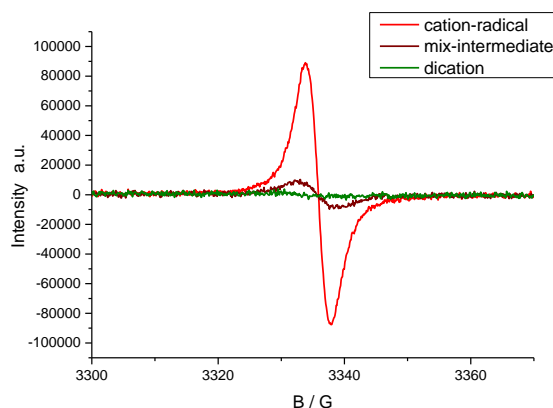


Figure 6-4. EPR spectra of spiro-HBC in B state (red line), C state (green line) and the intermediate state with the mixture of B and C (brown line)

6.2.3 DFT Calculations about Spiro-HBC and Mono-HBC in Different Valence State

Density functional calculations (DFT) (Gaussian 09W) was used to calculate the orbital energy levels for spiro-HBC and mono-HBC in different valence state and simulate the electron probability density distribution by the method of Optimization Plus Frequency. Due to the tert-butyl group would cost too much DFT calculation time, a methyl substituent was considered with the same conjugated backbone to simulate the systems. Three different charges and multiplicity sets which simulated the three valence state were chose for each cyclic aromatic structure, that are 0 charge singlet, 1 charge doublet and 2 charge singlet respectively, with the basis set 6-31G. Due to the high structure symmetric properties, it exist high possibility of orbital energy levels degeneration in the aromatic hydrocarbons. The figure 6-5, 6-7 and table 6-1 show the calculation results of spiro-HBC in the situations of neutral state and dication state. Orbital degeneration occurred in two places: one is the degeneracy of LUMO+2 and LUMO+3, and the other one is at HOMO-1 and HOMO-2 in the neutral state of Spiro-HBC (0 charge singlet). But the HOMO and LUMO are single orbital levels without degeneration. For the dication state of spiro-HBC (2 charge singlet), the orbital energy levels changed and the degeneracy orbitals are LUMO+1, LUMO+2 and HOMO-1, HOMO-2. The orbitals HOMO, LUMO are still single orbital energy level without degeneration. This means the two electrons were both transferred from the same HOMO. No radical or spin species exist in dication. It is completely different to the orbital degeneration of annulenes triphenylene and coronene, which the orbital degenerations happened in LUMO, LUMO+1 and HOMO, HOMO-1 respectively, which gives the possibility to acquire open shell singlet or triplet dication charging situation with two unpaired electrons singly occupied in two HOMO degeneration orbitals, respectively. The spin density distribution of spiro-HBC in the

situation of 1 charge doublet is delocalized on the whole π -system structure by spiro conjugation (figure 6-6). The table 6-2 lists the characters of spiro-HBC cation radical.

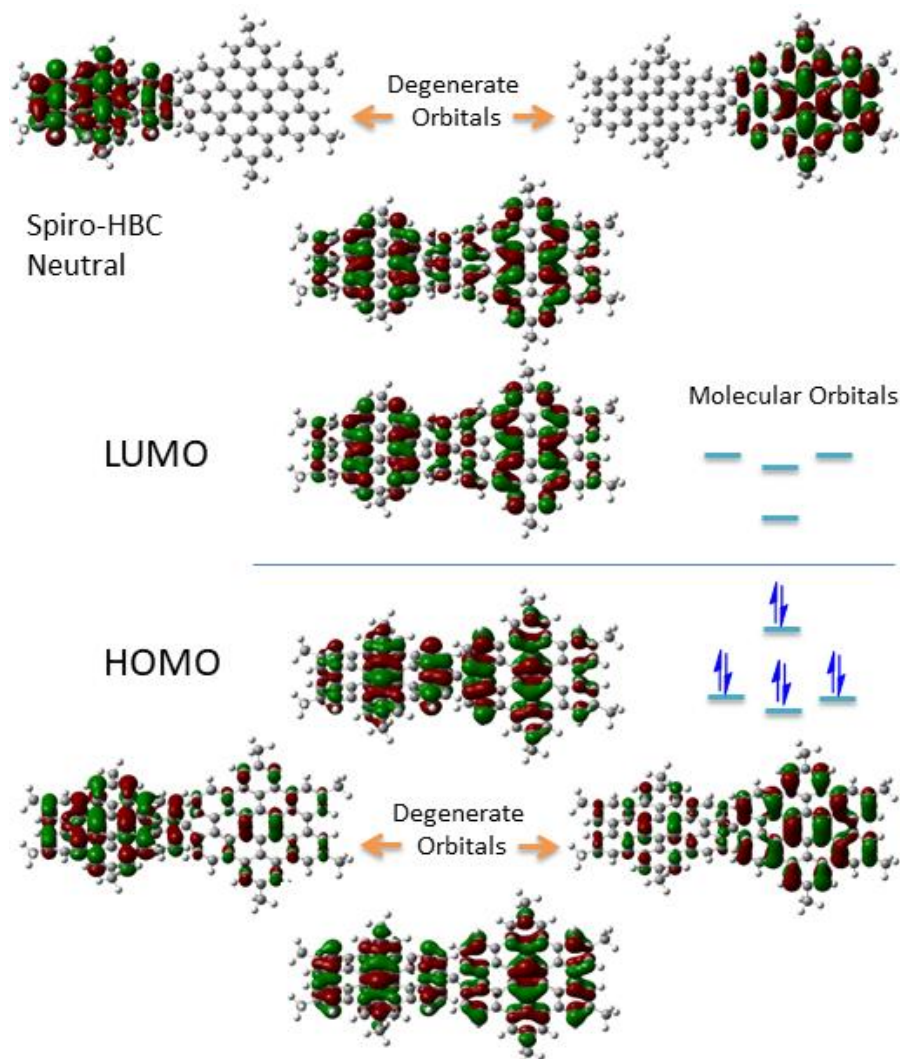


Figure 6-5. Degenerate orbitals, relative energy levels and electron density distribution of spiro HBC for neutral

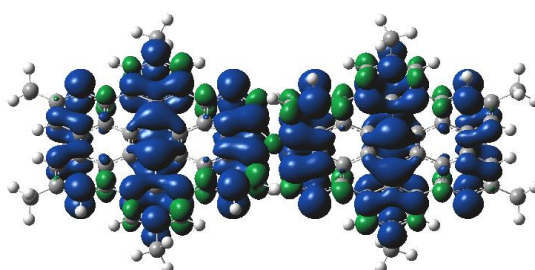


Figure 6-6. Spin density distribution of spiro HBC for mono cation radical (doublet)

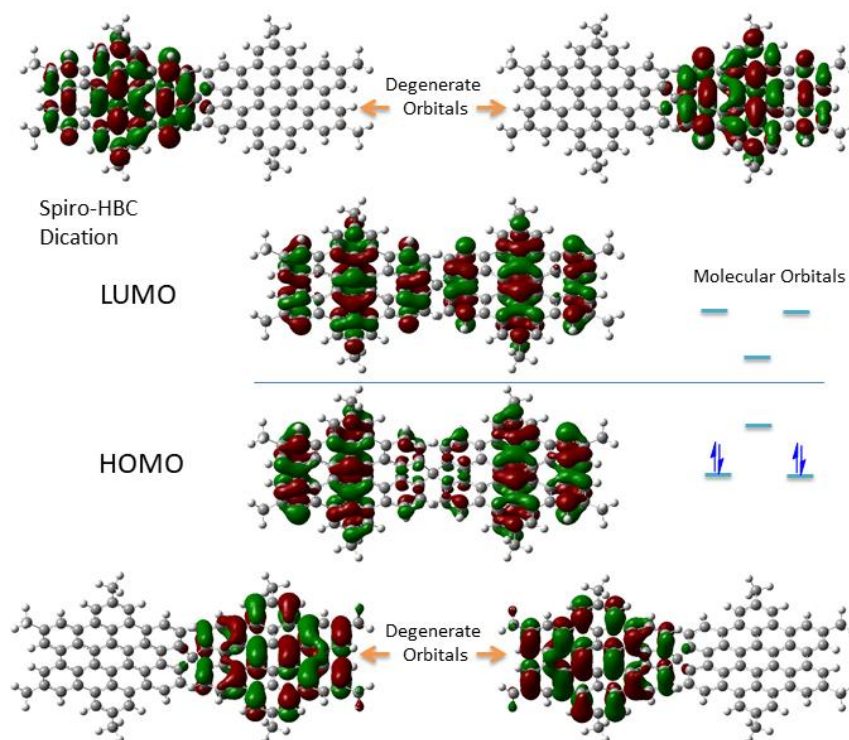


Figure 6-7. Degenerate orbitals, relative energy levels and electron density distribution of spiro HBC for dication

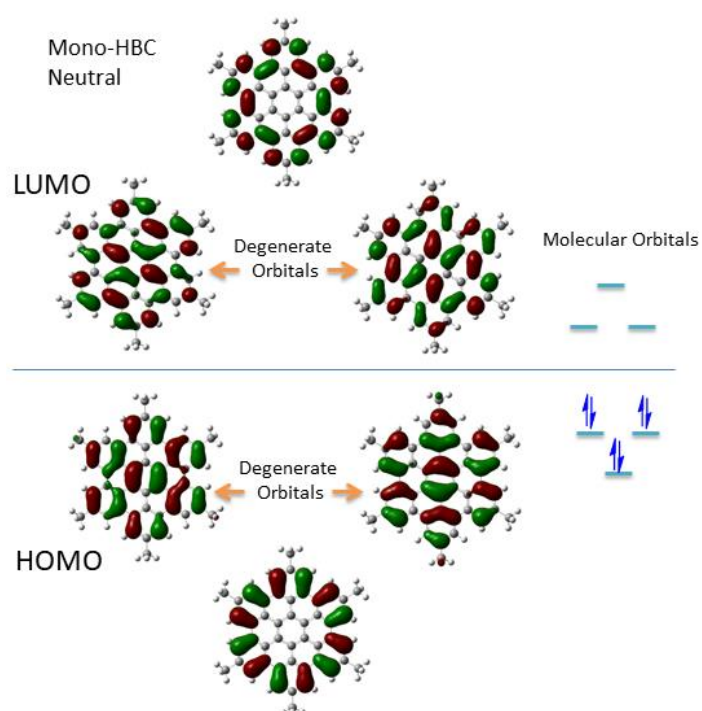


Figure 6-8. Degenerate orbitals, relative energy levels and electron density distribution of mono HBC for neutral

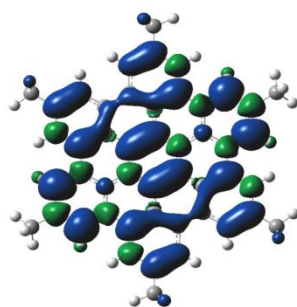


Figure 6-9. Spin density distribution of Mono HBC for mono cation radical (doublet)

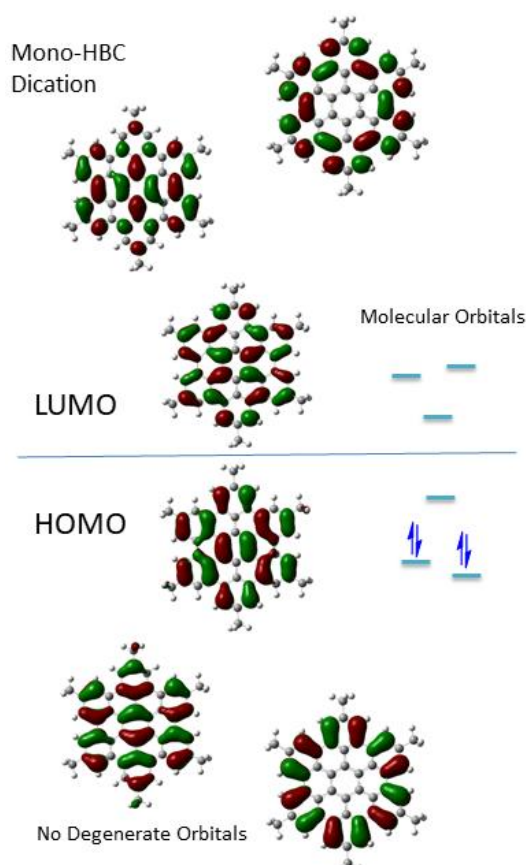


Figure 6-10. Degenerate orbitals, relative energy levels and electron density distribution of mono HBC for dication

The figure 6-8, 6-10 and table 6-1 show the calculation results of mono-HBC in the situations of neutral state and dication state. But the orbital degeneracy is totally different, it occurred in two places which are in LUMO and HOMO in the neutral state (0 charge singlet). The orbital degeneracy is similar like the cases of triphenylene and coronene. While for the dication state of mono-HBC (2 charge singlet), the orbital energy levels changed and the orbital degeneracy totally lose no matter in LUMO or HOMO. This can explain the data in EPR why there is no signal of EPR spectra in the situations of dication state. The figure 6-9 shows the spin density distribution of mono-HBC in the situation of 1 charge doublet which

was delocalized on the whole π -system structure. The table 6-2 shows the characters of mono-HBC cation radical.

Table 6-1. Energy level of orbitals about spiro-HBC and mono-HBC in neutral and dication state respectively

Energy Level of Orbital / eV	S-HBC (Neutral)	S-HBC (Dication)	M-HBC (Neutral)	M-HBC (Dication)
LUMO+3	-1.48	—	—	—
LUMO+2	-1.48	-5.72	-1.30	-6.91
LUMO+1	-1.49	-5.72	-1.46	-7.05
LUMO	-1.56	-8.62	-1.46	-7.44
HOMO	-5.03	-8.93	-5.05	-10.00
HOMO-1	-5.12	-9.22	-5.05	-10.82
HOMO-2	-5.12	-9.22	-5.52	-11.08
HOMO-3	-5.13	—	—	—
Multiplicity	Singlet State	Singlet State	Singlet State	Singlet State

— did not check (the energy levels of LUMO+3 and HOMO-3 here are meaningless for the discussion of degenerate orbitals).

Table 6-2. Features of spiro-HBC and mono-HBC in mono cation radical state

Mono-cation Mono-radical	Total Energy / Hartrees	LUMO / eV	SOMO / eV	Dipole Moment	Multiplicity
S-HBC	-3572.23749267	-3.68	-7.14	0.0009	Doublet State
M-HBC	-1846.78303179	-4.60	-7.95	0.1186	Doublet State

6.2.4 The DFT Calculations about Spiro-HBC and Mono-HBC in Dication State through Broken Symmetry Method

We used broken symmetry approach which is according to L. Noodleman, and K. Yamaguchi etc.⁴⁷⁻⁵⁰ to simulate spiro-HBC and mono-HBC in dication state by using. This method is engaged in compare the energy level among singlet state with closed shell structure (non-spin), triplet state (spin activated) and single state with open shell structure (spin active).

For the sets of calculation, the condition of method is Energy with the basis set 6-31G. For the calculation of single state with open shell structure (broken symmetry singlet), the option of guess method: mix HOMO and LUMO orbitals should be chosen. The molecular energy of the three different states for the two structures are shown in table 6-3. In addition, the coupling constant J which is energy between the open-shell singlet state (broken symmetry) and triplet ($J = \Delta E_{BS-T}$) was also provided. The figure 6-11 and 6-12 show the spin density distribution of triplet state and the case of singlet state with the open shell for spiro-HBC and mono-HBC. And the electron density distribution of alpha and beta belong to the two electrons which are singly occupied on SOMO with opposite spin directions in the case of singlet state with open shell structure.

Table 6-3. Total molecular energy, ΔE and coupling constant J of spiro-HBC and mono-HBC in different multiplicity states

Dication Diradical	OS-Singlet State ^a	Triplet State	CS-Singlet State ^b	$\Delta E^c / cm^{-1}$	J^d / cm^{-1}
S-HBC	-3571.9578145	-3571.9577491	-3571.9478466	-2187.70	-14.35
M-HBC	-1846.4526801	-1846.4483937	-1846.4523016	-83.07	-940.76

a) Open shell singlet state which calculated by broken symmetry method. b) Closed shell singlet state. c) ΔE is the energy value difference between open shell singlet and closed shell singlet. d) Coupling constant J (the energy value difference between open shell singlet and triplet)

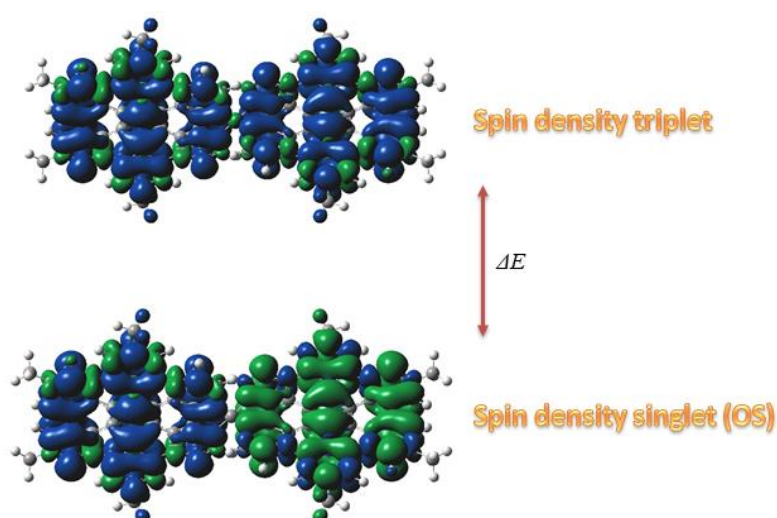


Figure 6-11. Spin density distribution of triplet and singlet (open shell structure) of spiro-HBC dication diradical (upper and lower).

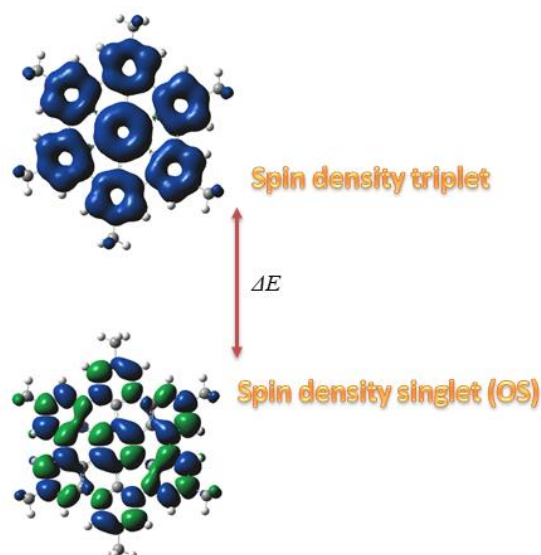


Figure 6-12. Spin density distribution of triplet and singlet (open shell structure) of mono-HBC dication diradical (upper and lower).

6.3 Conclusions

For this chapter, we discussed about the radical and spin situations of spiro-HBC and mono-HBC in different valence states by the method of redox reactions. Electron transfer which gives three different states could be reversibly switched between each other. EPR spectroscopy was used to monitor the three different states and different spin characters were found which were attributed to the three states. The neutral species and dication species of spiro-HBC and mono-HBC have no radical features exist, while radical features appeared in the monocation case. In addition, DFT calculations were used to simulate the orbital energy levels of various states, the situations of orbital degeneracy (the degeneracy happened at different orbitals level for neutral spiro-HBC and neutral mono-HBC), electron and spin density distributions, and gave a good explanation about spin properties of HBC contained polycyclic aromatic hydrocarbons at closed-shell or open-shell structures. The orbital degeneracy of spiro-HBC occurred in HOMO-1 and HOMO-2 in the neutral state, while the orbital degeneracy of mono-HBC occurred in HOMO in the neutral state. This is the reason why mono-HBC can be oxidized to dication diradicals species, whereas the spiro-HBC can only be oxidized to monocation monoradical species.

6.4 Reference

- (1) Vanwilligen, H.; Vanbroek, J.; and Deboer, E. An E.S.R. Study of the Mono and Dinegative Ions of Triphenylene. Evidence for the Jahn-Teller Instability of the Triplet Dianion. *Mol. Phys.* **1967**, *12*, 533-548
- (2) Glasbeek, M.; VanVoorst, J. D.; Hoijtink, G. J. Coronene Dinegative Ion. A Thermally EXcited Triplet State. *J. Chem. Phys.* **1966**, *45*, 1852-1853
- (3) Krusic, P. J.; Wasserman, E. Coronene Dication: a Thermally Accessible Triplet. *J. Am. Chem. Soc.* **1991**, *113*, 2322-2323
- (4) Pal, S. K.; Bag, P.; Itkis, M. E.; Tham, F. S.; Haddon, R. C. Enhanced Electrical Conductivity in a Substitutionally Doped Spiro-bis(phenalenyl)boron Radical Molecular Solid. *J. Am. Chem. Soc.* **2014**, *136*, 14738-14741
- (5) Baumgarten, M.; Gügel, A. EPR and Optical Absorption Spectra of Reduced Buckminsterfullerene. *Adv. Mater.* **1993**, *5*, 458-461
- (6) Hu, Y.; Wang, D.; Baumgarten, M.; Schollmeyer, D.; Muellen, K.; Narita, A. Spiro-Fused Bis-Hexa-peri-hexabenzocoronene. *Chem. Commun.* **2018**, Accepted Manuscript
- (7) Halleux, A.; Martin, R. H.; King, G. S. D. Synthèses dans la série des dérivés polycycliques aromatiques hautement condensés. L'hexabenzocoronène, le tétrabenzocoronène, le tétrabenzopéryrène et le tétrabenzobisanthène. *Helvetica Chimica Acta* **1958**, *41*, 1177-1183
- (8) Wöhrle, T.; Wurzbach, I.; Kirres, J.; Kostidou, A.; Kapernaum, N.; Litterscheidt, J.; Haenle, J. C.; Staffeld, P.; Baro, A.; Giesselmann, F.; Laschat, S. Discotic Liquid Crystals. *Chem. Rev.* **2016**, *116*, 1139-1241
- (9) Smith, J. N.; Hook, J. M.; Lucas, N. T. Superphenylphosphines: Nanographene-Based Ligands That Control Coordination Geometry and Drive Supramolecular Assembly. *J. Am. Chem. Soc.* **2018**, *140*, 1131-1141
- (10) Yen, H. J.; Tsai, H.; Zhou, M.; Holby, E. F.; Choudhury, S.; Chen, A.; Adamska, L.; Tretiak, S.; Sanchez, T.; Iyer, S.; Zhang, H.; Zhu, L.; Lin, H.; Dai, L.; Wu, G.; Wang, H. L. Structurally Defined 3D Nanographene Assemblies via Bottom-Up Chemical Synthesis for Highly Efficient Lithium Storage. *Adv. Mater.* **2016**, *28*, 10250-10256
- (11) Zhang, C.; Liu, Y.; Xiong, X. Q.; Peng, L. H.; Gan, L.; Chen, C. F.; Xu, H. B. Three-Dimensional Nanographene Based on Triptycene: Synthesis and Its Application in Fluorescence Imaging. *Org. Lett.* **2012**, *14*, 5912-5915
- (12) Fujikawa, T.; Preda, D. V.; Segawa, Y.; Itami, K.; Scott, L. T. Corannulene–Helicene Hybrids: Chiral π -Systems Comprising Both Bowl and Helical Motifs. *Org. Lett.* **2016**, *18*, 3992-3995

- (13) Kato, K.; Segawa, Y.; Scott, L. T.; Itami, K. A Quintuple [6]Helicene with a Corannulene Core as a C₅-Symmetric Propeller-Shaped π -System. *Angew. Chem. Int. Ed.* **2018**, *57*, 1337-1341
- (14) Hilton, C. L.; Jamison, R.; Zane, H. K.; King, B. T. A Triphenylene-Based Triptycene with Large Free Volume Synthesized by Zirconium-Mediated Biphenylation. *J. Org. Chem.* **2009**, *74*, 405-407
- (15) Long, T. M.; Swager, T. M. Minimization of Free Volume: Alignment of Triptycenes in Liquid Crystals and Stretched Polymers. *Adv. Mater.* **2001**, *13*, 601-604
- (16) Yamaguchi, R.; Ito, S.; Lee, B. S.; Hiroto, S.; Kim, D.; Shinokubo, H. Functionalization of Hexa-peri-hexabenzocoronenes: Investigation of the Substituent Effects on a Superbenzene. *Chem. Asian J.* **2013**, *8*, 178-190
- (17) Saragi, T. P. I.; Spehr, T.; Siebert, A.; Fuhrmann-Lieker, T.; Salbeck, J. Spiro Compounds for Organic Optoelectronics. *Chem. Rev.* **2007**, *107*, 1011-1065
- (18) Poriel, C.; Rault-Berthelot, J. Structure–property Relationship of 4-Substituted-spirobifluorenes as Hosts for Phosphorescent Organic Light Emitting Diodes: an Overview. *J. Mater. Chem. C* **2017**, *5*, 3869-3897
- (19) Quinton, C.; Thiery, S.; Jeannin, O.; Tondelier, D.; Geffroy, B.; Jacques, E.; Rault-Berthelot, J.; Poriel, C. Electron-Rich 4-Substituted Spirobifluorenes: Toward a New Family of High Triplet Energy Host Materials for High-Efficiency Green and Sky Blue Phosphorescent OLEDs. *ACS Appl. Mater. Inter.* **2017**, *9*, 6194-6206
- (20) Jiang, Z.; Yao, H.; Zhang, Z.; Yang, C.; Liu, Z.; Tao, Y.; Qin, J.; Ma, D. Novel Oligo-9,9'-spirobifluorenes through ortho-Linkage as Full Hydrocarbon Host for Highly Efficient Phosphorescent OLEDs. *Org. Lett.* **2009**, *11*, 2607-2610
- (21) Thiery, S.; Tondelier, D.; Dedairieux, C.; Geffroy, B.; Jeannin, O.; Metivier, R.; Rault-Berthelot, J.; Poriel, C. J. 4-Pyridyl-9,9'-spirobifluorenes as Host Materials for Green and Sky-Blue Phosphorescent OLEDs. *Phys. Chem. C* **2015**, *119*, 5790-5805
- (22) Liao, Y. L.; Hung, W. Y.; Hou, T. H.; Lin, C. Y.; Wong, K. T. Hole Mobilities of 2,7- and 2,2'-Disubstituted 9,9'-Spirobifluorene-Based Triaryldiamines and Their Application as Hole Transport Materials in OLEDs. *Chem. Mater.* **2007**, *19*, 6350-6357
- (23) Saragi, T. P. I.; Pudzich, R.; Fuhrmann, T.; Salbeck, J. Organic Phototransistor Based on Intramolecular Charge Transfer in a Bifunctional Spiro Compound. *Appl. Phys. Lett.* **2004**, *84*, 2334-2336

- (24) Osedach, T. P.; Geyer, S. M.; Ho, J. C.; Arango, A. C.; Bawendi, M. G.; Bulović, V. Lateral Heterojunction Photodetector Consisting of Molecular Organic and Colloidal Quantum Dot Thin Films. *Appl. Phys. Lett.* **2009**, *94*, 043307
- (25) Saragi, T. P. I.; Pudzich, R.; Fuhrmann-Lieker, T.; Salbeck, J. Light Responsive Amorphous Organic Field-effect Transistor Based on Spiro-linked Compound. *Opt. Mater.* **2007**, *29*, 879-884
- (26) Wu, X. F.; Fu, W. F.; Xu, Z.; Shi, M.; Liu, F.; Chen, H. Z.; Wan, J. H.; Russell, T. P. Spiro Linkage as an Alternative Strategy for Promising Nonfullerene Acceptors in Organic Solar Cells. *Adv. Funct. Mater.* **2015**, *25*, 5954-5966
- (27) Nguyen, W. H.; Bailie, C. D.; Unger, E. L.; McGehee, M. D. Enhancing the Hole-Conductivity of Spiro-OMeTAD without Oxygen or Lithium Salts by Using Spiro(TFSI)₂ in Perovskite and Dye-Sensitized Solar Cells. *J. Am. Chem. Soc.* **2014**, *136*, 10996-11001
- (28) Bach, U.; Lupo, D.; Comte, P.; Moser, J. E.; Weissörtel, F.; Salbeck, J.; Spreitzer, H.; Grätzel, M. Solid-state Dye-sensitized Mesoporous TiO₂ Solar Cells with High Photon-to-electron Conversion Efficiencies. *Nature* **1998**, *395*, 583-585
- (29) Fournier, J. H.; Maris, T.; Wuest, J. D. Molecular Tectonics. Porous Hydrogen-Bonded Networks Built from Derivatives of 9,9'-Spirobifluorene. *J. Org. Chem.* **2004**, *69*, 1762-1775
- (30) Song, K. C.; Singh, R.; Lee, J.; Sin, D. H.; Lee, H.; Cho, K. Propeller-shaped Small Molecule Acceptors Containing a 9,9'-Spirobifluorene Core with Imide-linked Perylene Diimides for Non-fullerene Organic Solar Cells. *J. Mater. Chem. C* **2016**, *4*, 10610-10615
- (31) Jeon, N. J.; Lee, H. G.; Kim, Y. C.; Seo, J.; Noh, J. H.; Lee, J.; Seok, S. I. o-Methoxy Substituents in Spiro-OMeTAD for Efficient Inorganic–Organic Hybrid Perovskite Solar Cells. *J. Am. Chem. Soc.* **2014**, *136*, 7837-7840
- (32) Polander, L. E.; Pahner, P.; Schwarze, M.; Saalfrank, M.; Koerner, C.; Leo, K. Hole-transport Material Variation in Fully Vacuum Deposited Perovskite Solar Cells. *APL Mater* **2014**, *2*, 081503
- (33) Pop, L.; Dumitru, F.; Hadade, N. D.; Legrand, Y. M.; Lee, A.; Barboiu, M.; Grosu, I. Exclusive Hydrophobic Self-Assembly of Adaptive Solid-State Networks of Octasubstituted 9,9'-Spirobifluorenes. *Org. Lett.* **2015**, *17*, 3494-3497
- (34) Nakagawa, T.; Ku, S. Y.; Wong, K. T.; Adachi, C. Electroluminescence Based on Thermally Activated Delayed Fluorescence Generated by a Spirobifluorene Donor–acceptor Structure. *Chem. Commun.* **2012**, *48*, 9580-9582
- (35) Poriel, C.; Barrière, F.; Thirion, D.; Rault-Berthelot, J. Encumbered DiSpiro [Fluorene–IndenoFluorene]: Mechanistic Insights. *Chem. Eur. J.* **2009**, *15*, 13304-13307

- (36) Romain, M.; Tondelier, D.; Vanel, J. C.; Geffroy, B.; Jeannin, O.; Rault-Berthelot, J.; Métivier, R.; Poriel, C. Dependence of the Properties of Dihydroindenofluorene Derivatives on Positional Isomerism: Influence of the Ring Bridging. *Angew. Chem., In. Ed.* **2013**, *52*, 14147-14151
- (37) Wu, Y.; Zhang, J.; Fei, Z.; Bo, Z. Spiro-Bridged Ladder-Type Poly(p-phenylene)s: Towards Structurally Perfect Light-Emitting Materials. *J. Am. Chem. Soc.* **2008**, *130*, 7192-7193
- (38) Harada, N.; Ono, H.; Nishiwaki, T.; Uda, H. Synthesis, Circular Dichroism and Absolute Stereochemistry of Chiral Spiroaromatic Compounds. 9,9'-Spirobifluorene Derivatives. *J. Chem. Soc., Chem. Commun.* **1991**, *0*, 1753-1755
- (39) Ramakrishna, J.; Venkatakrishnan, P. Bigger and Brighter Fluorenes: Facile π -Expansion, Brilliant Emission and Sensing of Nitroaromatics. *Chem. Asian J.* **2017**, *12*, 181-189
- (40) Gao, G.; Liang, N.; Geng, H.; Jiang, W.; Fu, H.; Feng, J.; Hou, J.; Feng, X.; Wang, Z. Spiro-Fused Perylene Diimide Arrays. *J. Am. Chem. Soc.* **2017**, *139*, 15914-15920
- (41) Fan, C.; Chen, Y.; Gan, P.; Yang, C.; Zhong, C.; Qin, J.; Ma, D. Tri-, Tetra- and Pentamers of 9,9'-Spirobifluorenes through Full ortho-Linkage: High Triplet-Energy Pure Hydrocarbon Host for Blue Phosphorescent Emitter. *Org. Lett.* **2010**, *12*, 5648-5651
- (42) Pal, S. K.; Itkis, M. E.; Tham, F. S.; Reed, R. W.; Oakley, R. T.; Donnadiou, B.; Haddon, R. C. Phenalenyl-Based Neutral Radical Molecular Conductors: Substituent Effects on Solid-State Structures and Properties. *J. Am. Chem. Soc.* **2007**, *129*, 7163-7174
- (43) Kastler, M.; Schmidt, J.; Pisula, W.; Sebastiani, D.; Müllen, K. From Armchair to Zigzag Peripheries in Nanographenes. *J. Am. Chem. Soc.* **2006**, *128*, 9526-9534
- (44) Ducasse, L.; Fritsch, A. Theoretical design of a new, high spin, organic molecule. *Synthetic Metals* **1997**, *86*, 2229-2230
- (45) Herwig, P. T.; Enkelmann, V.; Schmelz, O.; Müllen, K. Synthesis and Structural Characterization of Hexa-tert-butyl- hexa-peri-hexabenzocoronene, Its Radical Cation Salt and Its Tricarbonylchromium Complex. *Chem. Eur. J.* **2000**, *6*, 1834-1839
- (46) Rathore, R.; Burns, C. L. A Practical One-Pot Synthesis of Soluble Hexa-peri-hexabenzocoronene and Isolation of Its Cation-Radical Salt. *J. Org. Chem.* **2003**, *68*, 4071-4074.
- (47) Noodleman, L. Valence bond description of antiferromagnetic coupling in transition metal dimers. *J. Chem. Phys.* **1981**, *74*, 5737
- (48) Sinnecker, S.; Neese, F.; Noodleman, L.; Lubitz, W. Calculating the Electron Paramagnetic Resonance Parameters of Exchange Coupled Transition Metal Complexes

Using Broken Symmetry Density Functional Theory: Application to a Mn^{III}/Mn^{IV} Model Compound. *J. Am. Chem. Soc.* **2004**, *126*, 2613-2622

(49) Neese, F. Definition of corresponding orbitals and the diradical character in broken symmetry DFT calculations on spin coupled system. *J. Phy. Chem. Sol.* **2004**, *65*, 781-785

(50) Soda, T.; Kitagawa, Y.; Onishi, T.; Takano, Y.; Shigeta, Y.; Nagao, H.; Yoshioka, Y.; Yamaguchi, K. Ab initio computations of effective exchange integrals for H–H, H–He–H and Mn₂O₂ complex: comparison of broken-symmetry approaches. *Chem. Phy. Let.* **2000**, *319*, 223-230

Chapter 7 Experimental Section

Materials

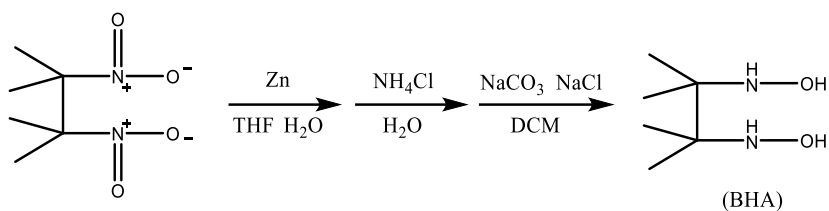
Hexaethylene glycol, *p*-toluenesulfonyl chloride, 4-hydroxybenzaldehyde, 2,3-dimethyl-2,3-dinitrobutane were purchased from Aldrich and Alfa Aesar without further purification. All other chemicals were used as received. Hexane was distilled from technical pure before use and kept dry by molecular sieves; other solvents which are all absolute dry were purchased from Aldrich.

Measurement Remarks

ESR spectra were recorded in dilute, oxygen-free solutions of distilled water, methanol, acetonitrile, dichloromethane and toluene, (concentration is 10^{-4} M), by using a Bruker EMX-plus spectrometer equipped with an NMR gauss meter (Bruker ER035), a frequency counter (Bruker ER041XK) and a variable temperature control continuous flow N₂ cryostat (Bruker B-VT 2000). These solutions were placed in ESR quartz tubes with outer diameter ~ 4 mm, and degassed in repeated pump-freeze-thaw cycles, then sealed in argon atmosphere. The measurements were performed with every 10 K temperature step and the upper temperature limit was determined by the point of stability of radical sample. The *g*-factor corrections were obtained by using the DPPH (*g* = 2.0037) as standard. Proton nuclear magnetic resonance (¹H NMR) spectra were recorded on a Bruker AMX 250/300 NMR instrument in deuterated DCM (5 mg / 0.6 mL for each NMR tubes). UV/ Vis spectra were recorded in distilled water, methanol, acetonitrile, dichloromethane and toluene solutions ($\sim 10^{-5}$ M) with a Perkin-Elmer spectrometer (UV/Vis/NIR Lambda 900) using a 1 cm optical path quartz cell at room temperature. IR spectra were recorded in solid state (Nicolet 730 FT-IR spectrometer) at room temperature. Mass spectra were obtained on FDMS, VG Instruments ZAB-2 mass spectrometer.

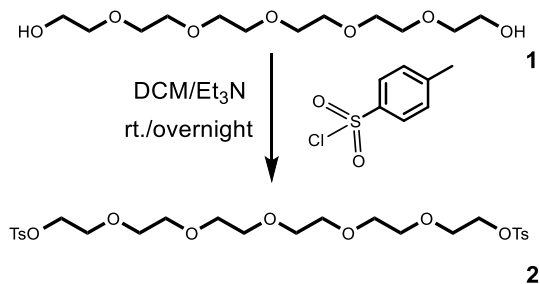
Detail Synthetic Procedures

Synthesis of 2,3-Dimethyl-2,3-bis(hydroxylamino)butane (4) the compound labeled in chapter 3.



The procedure was followed a similar method that previously published.¹ 11.7 g 2,3-dimethyl-2,3-dinitrobutane and 18.0 g of Zn (dust) in 200 mL THF and 40 mL H₂O was filled into a 1000 mL three-neck flask, and cooled down around 0 °C in an ice bath under argon. Then the solution of 28.7 g NH₄Cl in 150 mL distilled H₂O was added slowly dropwise (2 hours) under vigorous (mechanical) stirring, meanwhile keep the temperature of whole system not more than 5 °C. After addition was completed, the reaction was kept stirring for another 1.5 h at the same temperature, and an additional 0.5 h at room temperature. Then the white-gray precipitate of Zn slurry was filtered off, and was washed with THF (30 mL ×3). Filtrate was evaporated to viscous residue, cooled to -15°C (the mixture was kept in the freezer for 2 h). After that the flask was filled with argon and a mixture of 35 g Na₂CO₃ and 20 g NaCl salts was added at once. The flask was vigorously shaken for 15 min to guarantee homogeneous of whole mixture, and after homogenization the white solid was charged into a Soxhlet apparatus, protected under argon atmosphere, then refluxed and extracted with 300 mL of dichloromethane (72-96 h). There is white precipitate gradually appearing in DCM in the bottom flask, and the white precipitate was filtered off by Büchner funnel, washed with dichloromethane (3×30 mL), hexane (3×30 mL) and dried on air. Yield = 3.5 g (30%). **M.p.** 160 -161°C. **FT-IR** (powder, v/cm⁻¹): 3257 (vs and broad, ν_{OH}), 2987 (vs, ν_{C-H}), 1479-1374 (vs, several bands), 1261 (s), 1178 (vs), 1145 (vs), 1080 (s), 1035 (vs), 989 (m), 952 (vs), 904 (vs), 852 (m), 790 (m), 690 (m).

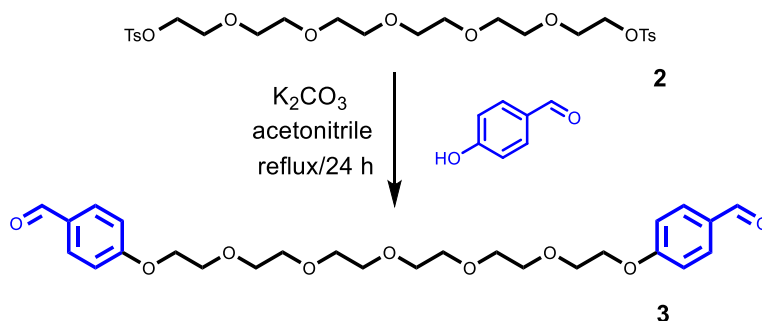
Synthesis of 3,6,9,12,15-Pentaoxaheptadecane-1,17-diyl(bis(4-methylbenzenesulfonate)) (2) the compound labeled in chapter 3.



The procedure was followed a similar method that previously published.² A mixture of hexaethylene glycol (4.0 g, 14.15 mmol), *p*-toluenesulfonyl chloride (6.0 g, 31.20 mmol) and

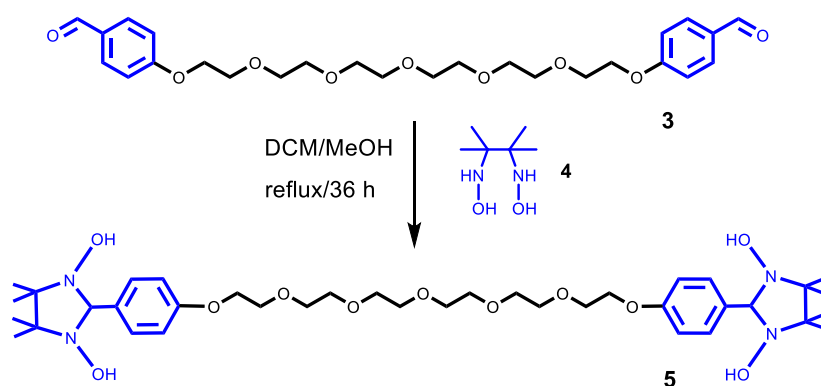
dry triethylamine (18.0 mL, 130 mmol) were dissolved in absolute dry DCM (60 mL) under argon atmosphere. The reaction was stirred at room temperature overnight. Then water (100 mL) was added and the crude product was extracted into DCM (100 mL, three times). The organic layer was combined and dried over anhydrous MgSO_4 . Afterwards the solvent was evaporated and compound **2** was acquired as white glutinous solid. The product was passed through a short silica gel column and does not need further purification, then directly used for further synthesis of compound **3**. Yield = 6.2 g (72%). Calculated MW = 590.70; **FD. Mass:** 591.5.

Synthesis of 4,4'-(3,6,9,12,15-Pentaoxaheptadecane-1,17-diyl)bis(oxy)dibenzaldehyde (3) the compound labeled in chapter 3.



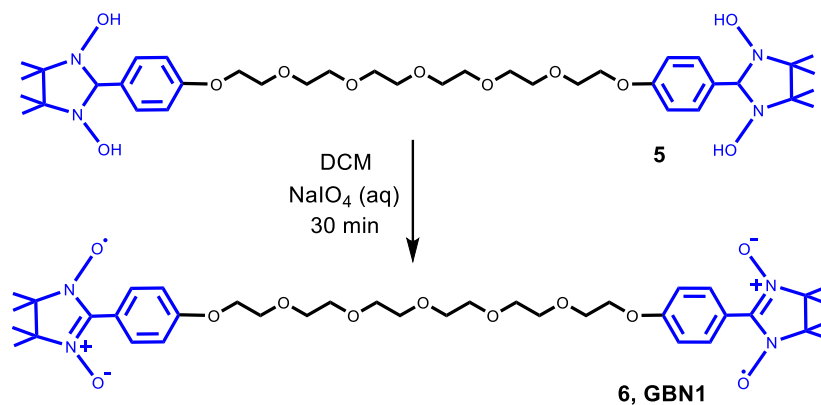
Compound **2** (1.2 g, 2.0 mmol), anhydrous K_2CO_3 (1.4 g, 10.0 mmol) and 4-hydroxybenzaldehyde (0.61 g, 5.0 mmol) were dissolved in dry acetonitrile (30 mL). Then the solution was refluxed under argon atmosphere for 2 days at 80 °C. After reaction, the mixture was poured into distilled water and extracted by DCM (100 mL, three times). Organic layer was combined and dried over anhydrous MgSO_4 . The crude product was purified by silica gel column using eluent with the ratio of ethyl acetate and hexane (1 : 4). Compound **3** was acquired as white glutinous fluid (become white solid in refrage). $^1\text{H NMR}$ (DCM_{d2} , 250.0 MHz), δ ppm: 9.77 δ (s, 2H, Ar-CHO), 7.72-7.75 δ (d, 4H, Ar-H), 6.94-6.97 δ (d, 4H, Ar-H), 4.10-4.13 δ (t, 4H, Ar-OCH₂CH₂), 3.74-3.78 δ (t, 4H, Ar-OCH₂CH₂), 3.51-3.61 δ (m, 16H, Ar-OCH₂CH₂-OCH₂CH₂-OCH₂CH₂). Yield = 560 mg (55%). Calculated MW = 490.22; **FD. Mass:** 490.5.

Synthesis of 4,4'-(3,6,9,12,15-Pentaoxaheptadecane-1,17-diyl)bis(4,4,5,5-tetramethylimidazolidine-1,3-diol) (5) the compound labeled in chapter 3.



Compound **3** (120 mg, 0.24 mmol) and 2.5 equiv 2,3-Dimethyl-2,3-bis(hydroxylamino)butane **4** (89 mg, 0.61 mmol) were charged into a flask, evacuated and kept under argon. Mixed solvent with DCM (20 mL) and methanol (5 mL) were added into the flask from syringes and was kept argon bubbling for 20 mins. Then the system was heated to 65 °C and refluxed for 40 hours. The color of the reaction mixture turned pale yellow. Then the solvent was evaporated and the white with a little light yellow solid does not need further purification for synthesis of next step.

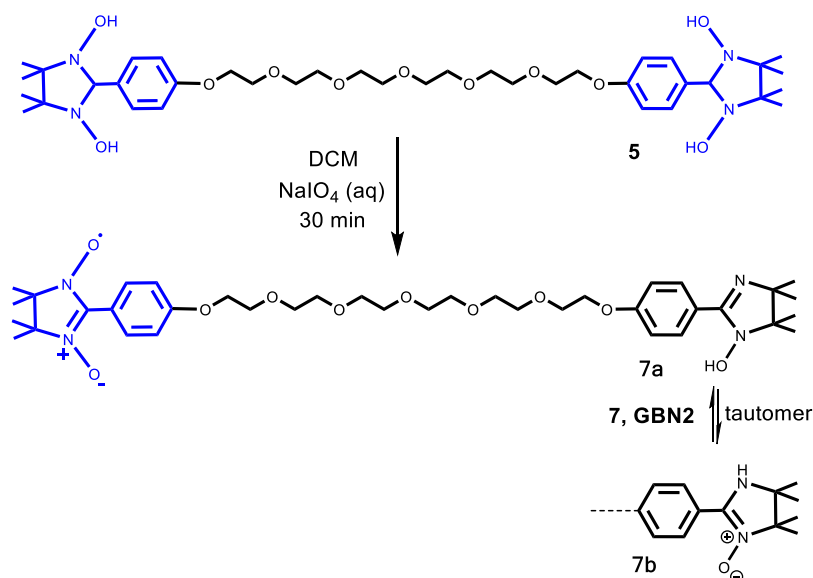
Synthesis of 4,4'-(3,6,9,12,15-Pentaoxaheptadecane-1,17-diyl)bis(1-oxyl-3-oxo-4,4,5,5-tetramethyl-4H,5H-imidazoline) (6, GBN1) the compound labeled in chapter 3.



Compound **5** was dissolved in 15 mL DCM and charged into a flask. Then the solution was slowly added with 2.2 equiv NaIO_4 dissolved in mixture of 10 mL distilled water and 10 mL DCM. The reaction was kept in ice bath for about 30 mins. When the color of mixture turned from pale yellow to dark blue, the proceeding of reaction could be stopped and a flash-column was used to purification. A blue sticky solid was separated and collected. UV-Vis (measured in acetonitrile) $\lambda_{\text{max}} = 617 \text{ nm}$ (specific UV-Vis absorption of nitronyl nitroxide from 480 nm to 740 nm). Yield = 40 mg (22%). Calculated MW = 744.39; **FD. Mass** (70 eV, CH_2Cl_2):

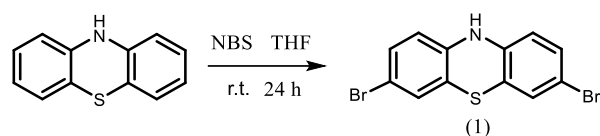
745.5. **EPR** spectrum (measured in acetonitrile) present the radical g factor 2.0066(5) and hyperfine coupling a_N is 7.75 G.

Synthesis of 4,4'-(3,6,9,12,15-Pentaoxaheptadecane-1,17-diyl)(1-oxyl-3-oxy-4,4,5,5-tetramethyl-4H,5H-imidazoline)(1-ol-4,4,5,5-tetramethyl-4H,5H-imidazoline) (7a or 7b) the compound labeled in chapter 3.



The same method used as the synthesis of GBN1 from the compound **5**. When the separation was undertaken, another blue sticky solid was separated and collected. Calculated MW = 729.41; **FD. Mass** (70 eV, CH_2Cl_2): 729.4. **EPR** spectrum (measured in acetonitrile) provides the radical g factor 2.0064 and $a_N = 7.67$ G.

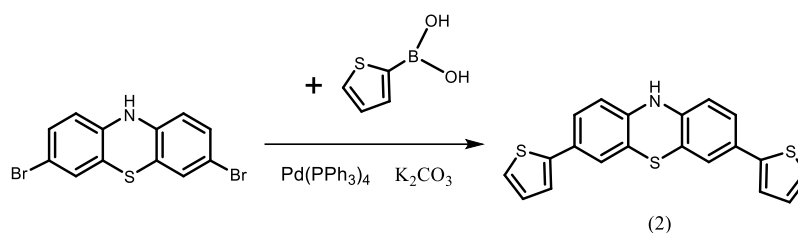
Synthesis of 2,7-dibromo-10H-phenothiazine (1) the compound labeled in chapter 4.



10H-phenothiazine (4.0 g, 20 mmol) was dissolved in THF (20 mL) at 0 °C and the resulting yellow solution was treated dropwise with a solution of N-bromosuccinimide (NBS, 7.5 g, 42 mmol) in THF (100 mL) under vigorous stirring over a period of 1 h. The resulting dark green solution was allowed to warm to r.t. and then stirred for a further 24 h. Two thirds of the solvent were then removed under reduced pressure and the mixture was rereduced by adding a solution of ascorbic acid (1.37 g, 10 mmol) in ethanol/water (1:1, 20 mL). The resulting clear yellow to light orange solution was treated with water (200 mL) to afford the crude product as an amorphous precipitate, which was filtered over a Buechner funnel and recrystallized from

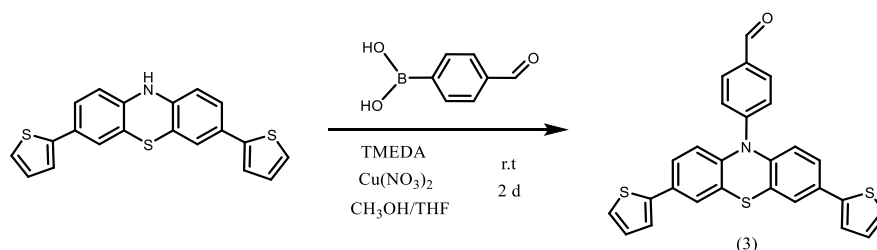
acetone/DCM (1:1, 100 mL), giving the product as light green crystals after some days of slow crystallization. The product was filtered, washed with cold acetone, and dried in vacuo. The combined yield was 2.5 g, 35%. $^1\text{H NMR}$ (DMSO-d_6 , 250.0 MHz), δ ppm: 8.87 δ (s, 1H), 7.16 δ (d, 2H), 7.14 δ (s, 2H), 6.62 δ (d, 2H). **MS** : m/z 357.4 (M^+).

Synthesis of 2,7-dithiophen-2-yl-10H-phenothiazine (2) the compound labeled in chapter 4.



The procedure was followed a similar method that previously published.³ 2,7-dibromo-10H-phenothiazine (500 mg, 1.4 mmol) was dissolved in a mixture of THF and water (10:1, 25 mL). To the resulting green solution, a finely ground mixture of thiophene-2-boronic acid (500 mg, 3.9 mmol), K_2CO_3 (1.0 mg, 7.2 mmol) and $\text{Pd}(\text{PPh}_3)_4$ (40 mg, 2%) was added immediately under vigorous stirring. Argon bobbling for 20 mins. Then the reaction mixture was kept under reflux conditions at for 5 h and then was allowed to cool to room temperature. The product precipitated during cooling. The suspension was diluted with deionized water (100 mL) to increase precipitation. The crude product was filtered over a Buechner funnel, washed with hexane and air dried. 300 mg, 60% product acquired. **MS** : m/z 363.2 (M^+).

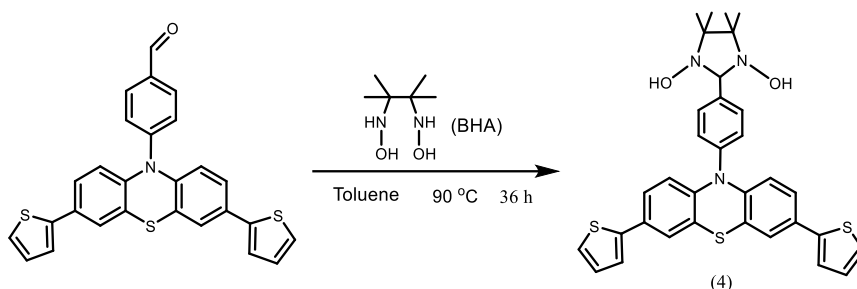
Synthesis of 2,7-di(thiophen-2-yl)-10-(benzaldehyde-4-yl)phenothiazine (3) the compound labeled in chapter 4.



The reaction was carried out, according to Chan-Lam coupling method previously published.^{4,5} 2,7-dithiophen-10H-phenothiazine (200 mg, 0.55 mmol), TMEDA (14.9 mg, 5%) and $\text{Cu}(\text{NO}_3)_2$ (31.2 mg, 10%) were dissolved in mixture of THF and methanol (10:1, 20 mL). Then benzaldehyde-4-boronic acid (165 mg, 1.1 mmol) which was dissolved in methanol was added to the flask dropwise. Air was used to bubble the solution. Keep the reaction at r.t. for 48

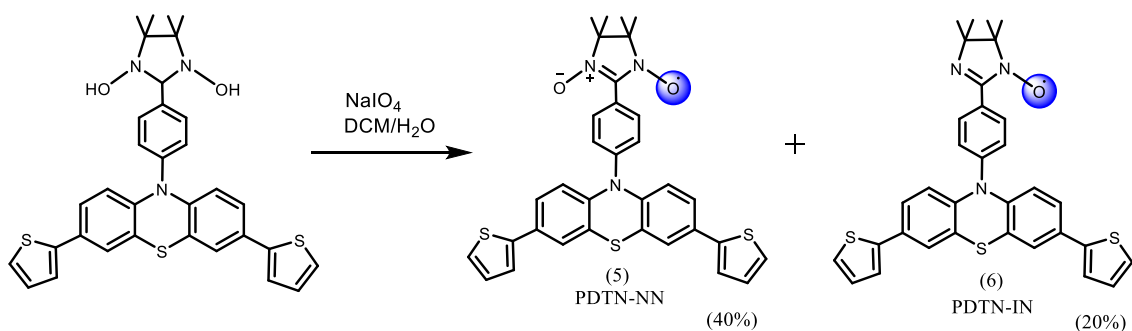
h. The reaction mixture was diluted with water (100 mL), extracted with dichloromethane for several times, washed with brine (100 mL), dried over anhydrous MgSO_4 , filtered, and concentrated under reduced pressure and then was purified by column chromatography. (hexane / toluene = 1 : 1). (yield, 206 mg, 80%). The product **3** is yellow crystal. $^1\text{H NMR}$ (DCM_{d2} , 250.0 MHz), δ ppm: 9.99 δ (s, 1H, Ar-CHO), 7.90-7.95 δ (d, 2H, Ar-H), 7.61-7.64 δ (d, 2H, Ar-H), 7.44-7.49 δ (d, 2H, Thiophene-H), 7.41-7.42 δ (s, 2H, Ar-H), 7.35-7.38 δ (d, 2H, Ar-H), 7.32-7.35 δ (d, 2H, Ar-H), 7.11-7.16 δ (t, 2H, Thiophene-H), 7.00-7.04 δ (d, 2H, Thiophene-H). Calculated MW = 467.1 ; **FD. Mass**: 467.7.

Synthesis of 2,7-di(thiophen-2-yl)-10-(benzimidazolidine-4-yl)phenothiazine (4) the compound labeled in chapter 4.



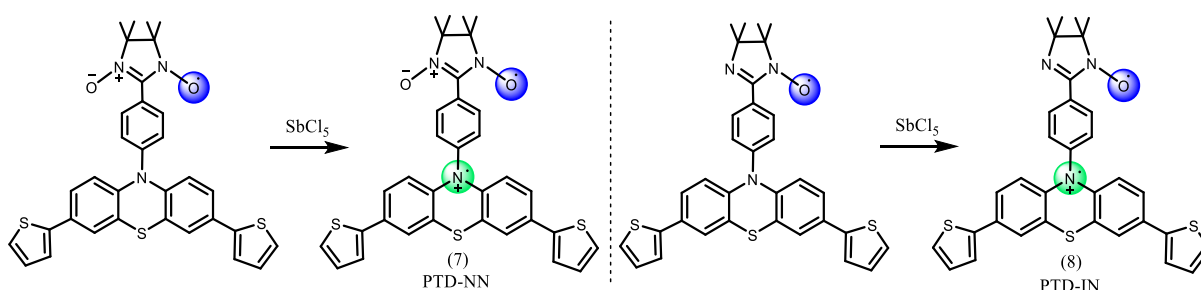
Precursor **3** (50 mg, 0.1 mmol) and 3 equiv 2,3-dimethyl-2,3-bis(hydroxylamino)butane (BHA, 45 mg) were charged into a flask, evacuated and kept under argon. Toluene (10 mL) was added to the flask from syringes and was kept argon bubbling for 20 mins. Then the system was heated to 90°C for 36 h. The color of mixture turned to orange. The mixture was washed by MeOH for two times. Then the solvent was evaporated and the orange solid does not need further purification for synthesis of next step.

Synthesis of 2,7-di(thiophen-2-yl)-10-(1-oxyl-3-oxy-4,4,5,5-tetramethylimidazoline-4-yl)phenothiazine (5, PDTN-NN) and 2,7-di(thiophen-2-yl)-10-(1-oxyl-4,4,5,5-tetramethylimidazoline-4-yl)phenothiazine (6, PDTN-IN) the compound labeled in chapter 4.



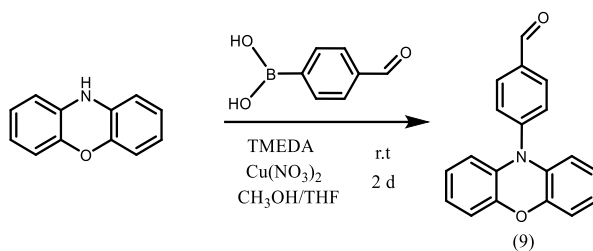
Compound **4** was dissolved in 15 mL DCM and charged into a flask. Then the solution was slowly added with 1.1 equiv NaIO_4 dissolved in mixture of 10 mL distilled water and 10 mL DCM. The reaction was kept in ice bath for about 1 hour. **5** and **6** were acquired simultaneously as mixture products. When the color of mixture turned from orange to dark green, the proceeding of oxidation could be stopped. **5** has a smaller r_f value and moved slower than **6** on TLC board. In addition the apparent color of **5**, which is green, and **6**, which is orange, also have a big difference that could easily distinguished on the TLC board. The mixture products were separated by column chromatography providing a MS-FD MW= 594.1 g/mol PDTN-NN, the yield is 55%. And over oxidized product PDTN-IN could also isolated by column chromatography providing a mass of MS-FD MW= 577.9 g/mol, the yield is 20%.. UV-Vis (measured in DCM) results: **5**, $\lambda_{\text{max}} = 640$ nm (specific UV-Vis absorption of NN from 550 nm to 700 nm). **6**, $\lambda_{\text{max}} = 480$ nm (specific UV-Vis absorption of IN from 470 nm to 520 nm). EPR spectrum (measured in DCM) present the radical **5** g factor 2.00709 and hyperfine coupling a_N is 7.67 G, and the radical **6** g factor 2.00644 and hyperfine coupling a_{N1} is 4.51 G, a_{N2} is 9.02 G.

The formation of cation-radical diradicals (7, PDT-NN) and (8, PDT-IN) the compound labeled in chapter 4.



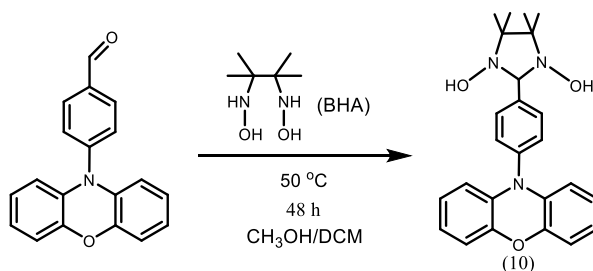
The last step of formation of cation-radical diradicals **PDT-NN 7** and **PDT-IN 8** were performed by adding oxidant SbCl_5 (10^{-3} M/L in DCM) to the solution of **5** (10^{-4} M/L in DCM) and **6** (10^{-4} M/L in DCM), respectively by microinjector. The solution colors of both are change to red. The highest conversions of cation-radical diradicals in the reactions are approximate at the ratio 2:1 of oxidant SbCl_5 to **5** and **6**. The whole reaction processes were monitored by UV-Vis absorption measurement and EPR measurements.

Synthesis of 10-(benzaldehyde-4-yl)phenoxazine (9) the compound labeled in chapter 4.



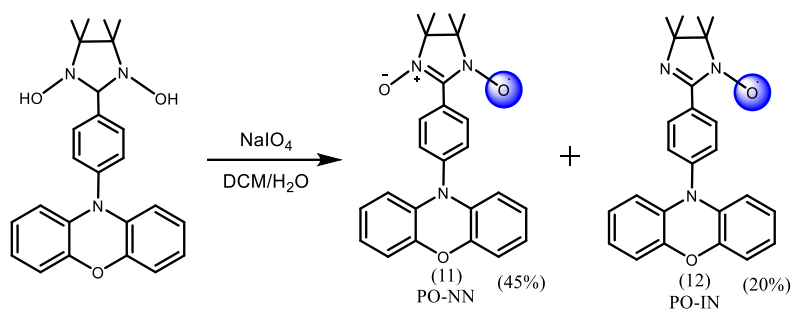
The procedure was followed a previously similar method of synthesis of **3**. 10H-phenoxazine (180 mg, 0.98 mmol), TMEDA (14.9 mg, 5%) and $\text{Cu}(\text{NO}_3)_2$ (31.2 mg, 10%) were dissolved in mixture of THF and methanol (10:1, 20 mL). Then benzaldehyde-4-boronic acid (165 mg, 1.1 mmol) which was dissolved in methanol was added to the flask dropwise. Air was used to bubble the solution. Keep the reaction at r.t. for 48 h. The reaction mixture was diluted with water (100 mL), extracted with dichloromethane for several times, washed with brine (100 mL), dried over anhydrous MgSO_4 , filtered, and concentrated under reduced pressure and then was purified by column chromatography. (hexane / toluene = 1 : 1). (yield, 240 mg, 85%). The product is yellow crystal. $^1\text{H NMR}$ (DCM_{d2} , 250.0 MHz), δ ppm: 9.98 δ (s, 1H), 7.91-7.93 δ (d, 2H), 7.46-7.51 δ (d, 2H), 6.68-6.72 δ (d, 2H), 6.55-6.65 δ (m, 4H), 5.95-5.98 δ (d, 2H). Calculated MW = 287.3 ; **FD. Mass**: 287.7.

Synthesis of 10-(benzimidazolidine-4-yl)phenoxazine (10) the compound labeled in chapter 4.



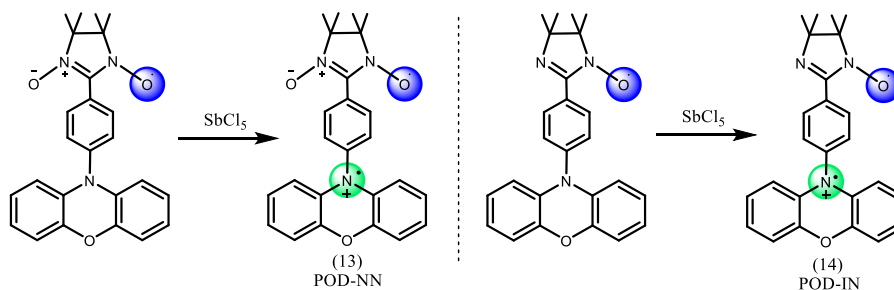
Precursor **9** (50 mg, 0.17 mmol) and 2 equiv 2,3-dimethyl-2,3-bis(hydroxylamino)butane (BHA, 50 mg) were charged into a flask, evacuated and kept under argon. Toluene (10 mL) was added to the flask from syringes and was kept argon bubbling for 20 mins. Then the system was heated to 90°C for 36 h. The color of mix turned to orange. The mixture was washed by MeOH for several times. Then the solvent was evaporated and the orange solid does not need further purification for synthesis of next step.

Synthesis of 10-(1-oxyl-3-oxy-4,4,5,5-tetramethylimidazoline-4-yl)phenoxazine (11, PO-NN) and 10-(1-oxyl-4,4,5,5-tetramethylimidazoline-4-yl)phenoxazine (12, PO-IN) the compound labeled in chapter 4.



Compound **10** was dissolved in 15 mL DCM and charged into a flask. Then the solution was slowly added with 1.1 equiv NaIO_4 dissolved in mixture of 10 mL distilled water and 10 mL DCM. The reaction was kept in ice bath for about 1 hour. **11** and **12** were acquired simultaneously as mixture products. When the color of mixture turned from orange to dark green, the proceeding of oxidation could be stopped. **11** has a smaller *rf* value and moved slower than **12** on TLC board. In addition the apparent color of **11**, which is light blue, and **12**, which is orange, also have a big difference that could easily distinguished on the TLC board. The mixture products were separated by column chromatography providing a MS-FD MW= 414.5 g/mol PDTN-NN, the yield is 45%. And over oxidized product PDTN-IN could also isolated by column chromatography providing a mass of MS-FD MW= 398.5 g/mol, the yield is 20%. UV-Vis (measured in DCM) results: **11**, $\lambda_{\text{max}} = 617$ nm (specific UV-Vis absorption of NN from 550 nm to 700 nm). **12**, $\lambda_{\text{max}} = 480$ nm (specific UV-Vis absorption of IN from 470 nm to 520 nm). EPR spectrum (measured in DCM) present the radical **11** g factor 2.00707 and hyperfine coupling a_{N} is 7.72 G, and the radical **12** g factor 2.00634 and hyperfine coupling $a_{\text{N}1}$ is 4.25 G, $a_{\text{N}2}$ is 8.51 G.

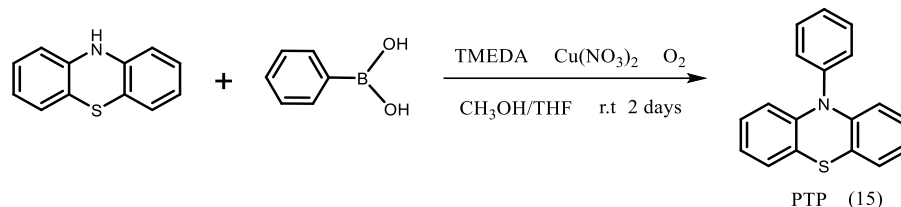
The formation of cation-radical diradicals (**13**, POD-NN) and (**14**, POD-IN) the compound labeled in chapter 4.



The last step of formation of cation-radical diradicals **POD-NN 13** and **POD-IN 14** were performed by adding oxidant SbCl_5 (10^{-3} M/L in DCM) to the solution of **11** (10^{-4} M/L in DCM) and **12** (10^{-4} M/L in DCM), respectively by microinjector. The solution colors of both are change to red. The highest conversions of cation-radical diradicals in the reactions are

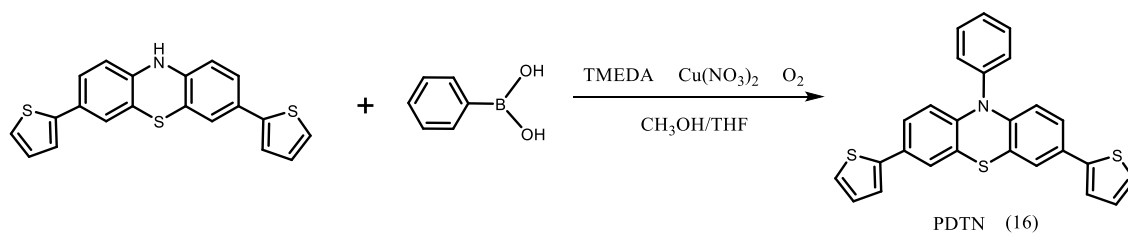
approximate at the ratio 2:1 of oxidant SbCl_5 to **11** and **12**. The whole reaction processes were monitored by **UV-Vis** absorption measurement and **EPR** measurements.

Synthesis of 10-phenyl-10H-phenothiazine (15) the compound labeled in chapter 4.



The procedure was followed a previously similar method of synthesis of **3**. 10H-phenothiazine (200 mg, 1.01 mmol), TMEDA (11.6 mg, 5%) and $\text{Cu}(\text{NO}_3)_2$ (24.2 mg, 10%) were dissolved in mixture of THF and methanol (10:1, 20 mL). Then phenylboronic acid (122 mg, 1.1 mmol) which was dissolved in methanol was added to the flask dropwise. Air was used to bubble the solution. Keep the reaction at r.t. for 24 h. The reaction mixture was diluted with water (100 mL), extracted with dichloromethane for several times, washed with brine (100 mL), dried over anhydrous MgSO_4 , filtered, and concentrated under reduced pressure and then was purified by column chromatography. (hexane / toluene = 1 : 1). $^1\text{H NMR}$ (DCM_{d2} , 250.0 MHz), δ ppm: 7.58-7.62 δ (t, 2H), 7.50 δ (t, 1H), 7.38-7.43 δ (d, 2H), 7.00-7.05 δ (d, 2H), 6.82-6.88 δ (m, 4H), 6.18-6.22 δ (d, 2H). (yield, 151 mg, 55%). The product is light yellow crystal. **MS** : m/z 275 (M⁺).

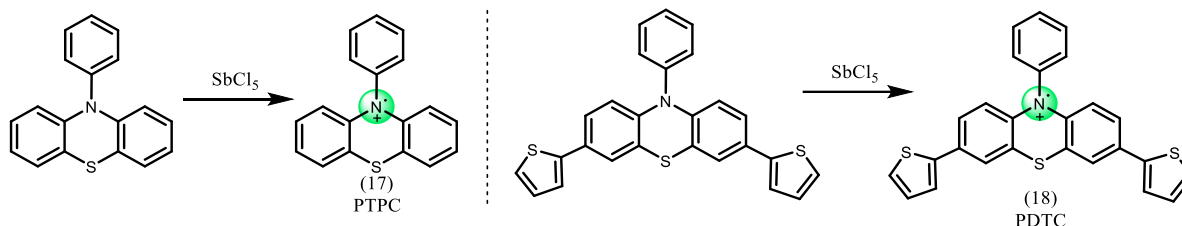
Synthesis of 2,7-di(thiophen-2-yl)-10-(phenyl-4-yl)phenothiazine (16) the compound labeled in chapter 4.



The procedure was followed a previously similar method of synthesis of **3**. 2,7-dithiophene-10H-phenothiazine **2** (150 mg, 0.41 mmol), TMEDA (11.6 mg, 8%) and $\text{Cu}(\text{NO}_3)_2$ (15.2 mg, 10%) were dissolved in mixture of THF and methanol (10:1, 20 mL). Then phenylboronic acid (60 mg, 0.55 mmol) which was dissolved in methanol was added to the flask dropwise. Air was used to bubble the solution. Keep the reaction at r.t. for 24 h. The reaction mixture was diluted with water (100 mL), extracted with dichloromethane for several times, washed with brine (100 mL), dried over anhydrous MgSO_4 , filtered, and concentrated under reduced

pressure and then was purified by column chromatography. (hexane / toluene = 1 : 1). ^1H NMR ($\text{DCM}_{\text{d}2}$, 250.0 MHz), δ ppm: 7.55-7.60 δ (t, 2H), 7.52 δ (t, 1H), 7.48-7.51 δ (d, 2H), 7.31-7.41 δ (m, 6H), 7.15-7.05 δ (m, 4H), 6.18-6.22 δ (d, 2H). (yield, 100 mg, 56%). The product is light yellow crystal. MS : m/z 440.7 (M^+).

The formation of cation radicals (**17**, PTPC) and (**18**, PDTC) the compound labeled in chapter 4.



The last step of formation of cation radicals **PTPC 17** and **PDTC 18** were performed by adding oxidant SbCl_5 (10^{-3} M/L in DCM) to the solution of **15** (10^{-4} M/L in DCM) and **16** (10^{-4} M/L in DCM), respectively by microinjector. The solution colors of both are change to red. The final ratio of oxidant SbCl_5 to **15** and **16** is 5:1. The whole reaction processes were monitored by EPR measurements. EPR spectrum (measured in DCM) present the radical **17** g factor = 2.0052 and hyperfine coupling a_{N} is 6.52 G, and the radical **18** g factor = 2.0052 and hyperfine coupling a_{N} is 6.55 G.

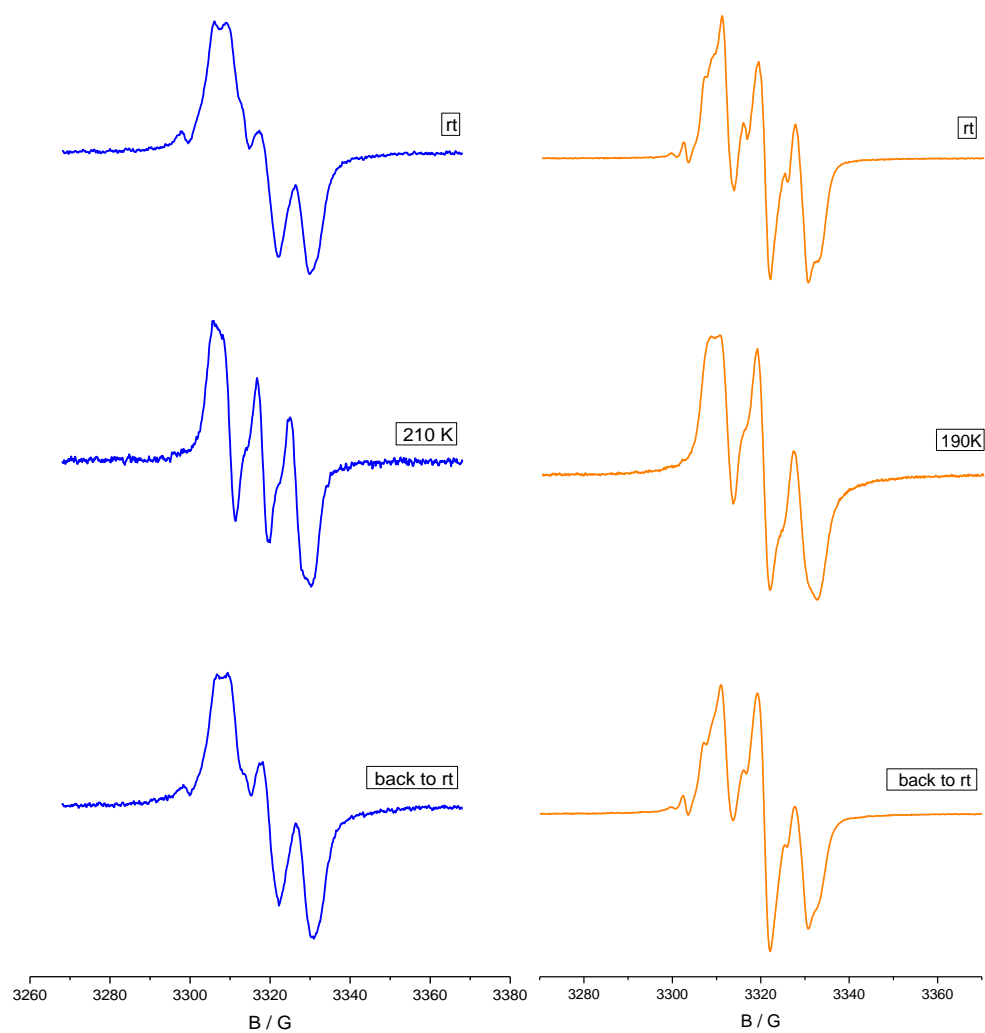
Supporting EPR Data

Figure 1. EPR Spectra of Intermediate states of PO-NN and PO-IN with temperature dependent reversible features in DCM.

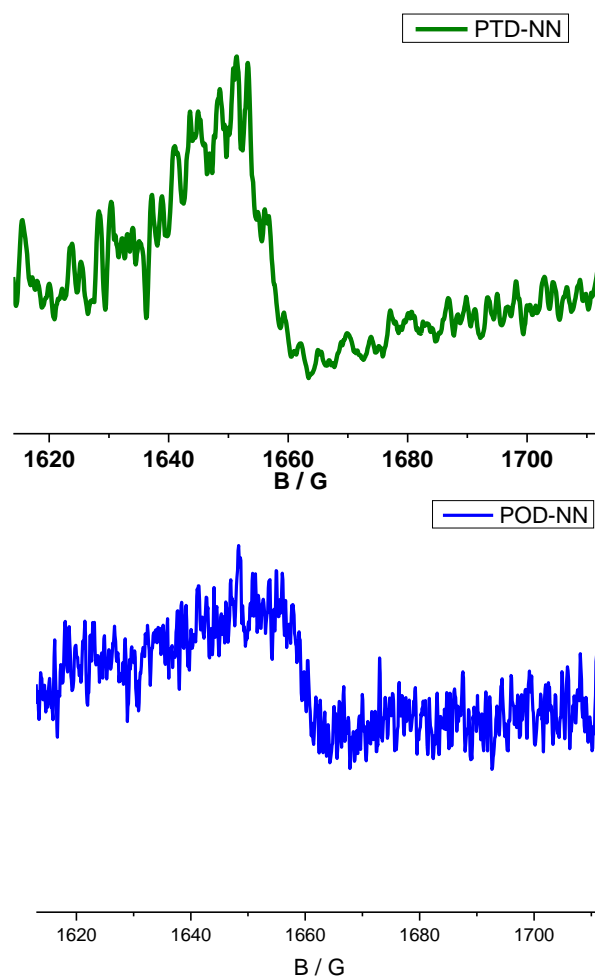


Figure 2. the peak signal appears both in PTD-NN sample (upper) and POD-NN sample (lower) in the forbidden transition ($\Delta_{ms} = 2$) around $g \approx 4$ region, measured at 120 K in DCM.

References

- (1) Ovcharenko, V. I.; Fokin, S. V.; Romanenko, G. V.; Korobkov, I. V.; Rey, P. Synthesis of Vicinal Bishydroxylamine. *Russ. Chem. Bull.* **1999**, *48*, 1519-1525.
- (2) Ji, L.; Yang, Z.; Zhao, Y.; Sun, M.; Cao, L.; Yang, X.-J.; Wang, Y.-Y.; Wu, B. Sandwich Phosphate Complexes of Macrocyclic Tris(Urea) Ligands and Their Rotation around the Anion. *Chem. Commun.* **2016**, *52*, 7310-7313.
- (3) Hemgesberg, M.; Bayarmagnai, B.; Thiel, W. R. Structurally Stressed PT09SBA: A Close Look at The Properties of Large Pore Photoluminescent, Redox Active Mesoporous Hybrid Silica. *RSC Adv.* **2013**, *3*, 8242-8253

- (4) Rao, K. S.; Wu, T. S. Chan-Lam Coupling Reactions: Synthesis of Heterocycles. *Tetrahedron*. **2012**, *68*, 7735-7754
- (5) Chan, D. M. T.; Monaco, K. L.; Wang, R. P.; Winters, M. P. New N- and O-Arylations with Phenylboronic Acids and Cupric Acetate. *Tetrahedron Letters*. **1998**, *39* 2933-2936

List of Publications

- (13) **Wang, D.;** Baumgarten, M. Synthesis and Characterization of Cation-Radical Diradicals in Redox Stimuli Responsive Systems. (Prepare to submit)
- (12) **Wang, D.;** Ma, Y. J.; Wolf, B.; Kokorin, A. I.; Baumgarten, M. Temperature-Dependent Intramolecular Spin Coupling Interactions of a Flexible Bridged Nitronyl Nitroxide Biradical in Solution. *J. Phys. Chem. A* **2018**, *122*, 574-581
- (11) Hu, Y.; **Wang, D.;** Baumgarten, M.; Schollmeyer, D.; Muellen, K.; Narita, A. Spiro-Fused Bis-Hexa-peri-hexabenzocoronene. *Chem. Commun.* **2018**, Accepted Manuscript DOI: 10.1039/C8CC07405D
- (10) Byun, J.; Huang, W.; **Wang, D.;** Li, R.; Zhang, K. A. I. CO₂-Triggered Switchable Hydrophilicity of a Heterogeneous Conjugated Polymer Photocatalyst for Enhanced Catalytic Activity in Water. *Angew. Chem. Int. Ed.* **2018**, *57*, 2967-2971
- (9) Ayed, C.; Silva, L. C.; **Wang, D.;** Zhang, K. A. I. Designing Conjugated Microporous Polymers for Visible Light-promoted Photocatalytic Carbon-carbon Double Bond Cleavage in Aqueous Medium. *J. Mater. Chem. A* **2018**, Advance Article DOI: 10.1039/C8TA05772A
- (8) Huang, W.; Byun, J.; Rçrich, I.; Ramanan, C.; Blom, P. W. M.; **Wang, D.;** Silva, L. C.; Landfester, K.; Zhang, K. A. I. Asymmetric Covalent Triazine Framework for Enhanced Visible-Light Photoredox Catalysis via Energy Transfer Cascade. *Angew. Chem. Int. Ed.* **2018**, *57*, 8316-8320
- (7) Ayed, C.; Huang, W.; Li, R.; Silva, L. C.; **Wang, D.;** Suraeva, O.; Najjar, W.; Zhang, K. A. I. Conjugated Microporous Polymers with Immobilized TiO₂ Nanoparticles for Enhanced Visible Light Photocatalysis. *Part. Part. Syst. Charact.* **2018**, *35*, 1700234
- (6) Huang, W.; Ma, B. C.; **Wang, D.;** Wang, Z. J.; Li, R.; Wang, L.; Landfester, K.; Zhang, K. A. I. A fixed-bed photoreactor using conjugated nanoporous polymer-coated glass fibers for visible light-promoted continuous photoredox reactions. *J. Mater. Chem. A* **2017**, *5*, 3792-3797

(5) Li, R.; Ma, B. C.; Huang, W.; Wang, L.; **Wang, D.**; Lu, H.; Landfester, K.; Zhang, K. A. I. Photocatalytic Regioselective and Stereoselective [2 + 2] Cycloaddition of Styrene Derivatives Using a Heterogeneous Organic Photocatalyst. *ACS Catal.* **2017**, *7*, 3097-3101

——During the Period of Master

(4) **Wang, D.**; Yu, Z. Q.; Hong, C. Y.; You, Y. Z. Strong Fluorescence emission from PEGylated Hyperbranched Poly(amido amine). *European Polymer Journal* **2013**, *49*, 4189-4194,

(3) Yan, J.; **Wang, D.**; Wu, D. C.; You, Y. Z. Synthesis of sequence-ordered polymers via sequential addition of monomers in one pot. *Chem. Comm.* **2013**, *49*, 6057

(2) Wang, Z. K.; **Wang, D.**; Wang, H.; You, Y. Z.; Wang Z. G. Preparation of Biocompatible Nanocapsules with temperature-responsive and Bioreducible Properties. *J. Mater. Chem.* **2011**, *20*, 15950-15956

(1) Tian, H. Y.; Yan, J.; **Wang, D.**; Gu, C.; You, Y. Z.; Chen, X. S. Preparation of Thermo-responsive Polymers with Both Tunable UCST and LCST via RAFT Polymerization. *Macromol. Rapid Commun.* **2011**, *32*, 660-664

Acknowledgement

At this very moment, with the accomplishment of my PhD dissertation, the five years PhD career has been coming to the final completion. All kinds of scenes about every aspect of my PhD student life are flashing through my brain like a camera quick-release show. They are full of joys and sorrows, excitement and harvest. But the most emotion for me is appreciation. I learned not only the professional ability of scientific research, but also all the knowledge and philosophy about life. I sincerely appreciate to all the people who helped me in any aspects of my life.

First of all, I deeply and sincerely appreciate to my supervisor Prof. Dr. Martin Baumgarten. He provided the precious opportunity to me to fulfill my PhD dream and gave me all the supports and inspirations during the whole PhD time. He kindly guide me on my scientific road and frankly supervise me in my research works. Martin, a man who always works diligently, tirelessly and with full of wisdom, he always has precise and serious attitude towards science. He is a perfect scientific model to me. Meanwhile, he gave me more than enough freedom to choose scientific research topic, which I am interested in, and encourage me all the time. So I want to say: “if without your passionate and tremendous help, I could not well finish my PhD works.” I appreciate again to my supervisor and also be the first German friend Martin.

Many thanks to two directors of MPIP, Prof. Dr. Klaus Müllen and Prof. Dr. Mischa Bonn, who provided so much convenient to me for the laborotary works and also some good suggestions about quarterly reports.

Many thanks to Dr. Kai Zhang and Prof. Dr. Katharina Landfester for the happy and precious scientific cooperation, and Dr. Jeehye Byun, Dr. Wei Huang, Dr. Run Li and Cyrine Ayed for extensive scientific discussions.

Many thanks to Dr. Yingjie Ma, Dr. Yunbin Hu for the scientific cooperation, and Dr. Benlin Hu, Kubandiran Kolanji for kindly accompany at office, and all the colleagues and friends in MPIP. There are so many happy and memorable moments to me with you guys, during my whole PhD period of time.

In addition, many thanks to Prof. Dr. Alexander I Kokorin for the kind discussions about new radicals spin systems, and Prof. Dr. Bernd Wolf for the measurements of SQUID. I also thank to Prof. Dr. Evgeny Tretyakov for some instructions about synthesis, and Prof. Dr. Anela Ivanova for the help of DFT calculations of spin systems.

Finally, I must appreciate to all the members of my family. Your love and care always made me feel warm and full of power and encourage me to keep moving no matter what happens.

The accomplishment of PhD means the new opportunity and also new challenge in the future career. Herein, I sincerely and frankly wish all of you happy, longevial and healthy lives forever. Thank you all.

Di Wang

November, Mainz



JOHANNES GUTENBERG
UNIVERSITÄT MAINZ





DiWang

Address: App.124 Richard-Schirrmann-Str.10
55122 Mainz Germany
E-mail: wangdi@mpip-mainz.mpg.de



Personal Information:

Chinese Name: 王帝
Marital Status: Single
Date of Birth: 09/02/1989

Gender: Male
Nationality: Chinese

Education:

Enrollment: Oct. 2013 — Nov. 2018 Max Planck Institute for Polymer Research (MPIP)
Major: Chemistry
Degree: Doctor of Science

Enrollment: Sep. 2010 — May. 2013 University of Science and Technology of China (USTC)
Major: Polymer Science and Engineering
Degree: Master of Science

Enrollment: Sep. 2006 — Jun. 2010 Hefei University of Technology (HFUT)
Major: Polymer Materials and Engineering
Degree: Bachelor of Science
Major GPA: 3.63/4.3 (3.57/4.0)

Academic Work Experience:

Oct. 2013 — Present: PhD student in Prof. Dr. Martin Baumgarten Research Group in Max Planck Institute for Polymer Research, (MPIP).

- Synthesis of organic radicals with external stimuli-responsive properties.
- Characterization and analysis of spin and magnetic properties.
- Operation and analysis of the measurements of electron paramagnetic resonance (EPR).
- Density functional calculations (DFT) (Gaussian 09W) of radicals or open-shell spin species.

Sep. 2010 — Jun. 2013: Graduate Research Assistant in Prof. Dr. Yezi You Research Group, Dept. of Polymer Science and Engineering, (USTC).

- I did research about a novel class of extraordinarily photoluminescent polymer which is synthesized through RAFT living polymerization. The study of new fluorescent materials and their derivants for the use of cell image.
- I found and discussed about a new sequential reaction combining Ring-Opening reaction and Thiol-Ene “Click” to get polymers with various topological structure under special condition.
- Synthesis and application of silica nanoparticles.
- Synthesis and modification about Grapheme Quantum Dots, and also some cell culture

experiments and cell cytotoxicity test.

Feb. 2010 — Jun. 2010: Undergraduate thesis project in Prof. Dr. Yezi You Research Group, Dept. of Polymer Science and Engineering, (USTC).

- I did research in the area of composite material of Quantum Dots and polymers and synthesize reversible and multisensitive Quantum Dots gel.

Sep. 2008 — Jun. 2009: Undergraduate innovative experiment in Prof. Dr. Wenping Wang Research Group, School of Chemical Engineering, (HFUT).

- Explore the synthesis and application of polymer-memory materials. (composite materials of organometallic complex and polymers)

Awards and Honors:

Jun. 2010 Outstanding Undergraduate Thesis Project (Grade 4 HFUT)

Dec. 2008 The Second Prize of Undergraduate Innovation Experiment Competition (Grade 3 HFUT) (Title: The Synthesis and Application of Polymer-Memory Materials)

Sep. 2013 The scholarship of CSC (China Scholarship Council) (Grade 3 USTC)

Languages:

Chinese (Native Language)

English (Passed National College English Test Band 4 and Band 6, and Graduate Record Examination.)

German (Easy Communication, Learning and Improving Now)

Hobbies and Specialities:

Football, Badminton, Vocal Music, Computer, Economics, Finance and Banking

Cell Phone: 0049-15210341997

Office: 0049-6131379288

